INTEGRAL AND COUPLED INTEGRAL-VOLUME METHODS FOR TRANSIENT PROBLEMS IN WAVE-STRUCTURE INTERACTION

by

Tonatiuh Sánchez-Vizuet

A dissertation submitted to the Faculty of the University of Delaware in partial fulfillment of the requirements for the degree of Doctor of Philosophy in Applied Mathematics

Summer, 2016

INTEGRAL AND COUPLED INTEGRAL-VOLUME METHODS FOR TRANSIENT PROBLEMS IN WAVE-STRUCTURE INTERACTION

by

Tonatiuh Sánchez-Vizuet

Approved: _____
Louis Rossi, Ph.D.
Chair of the Department of Mathematical Sciences

Approved: _____
George H. Watson, Ph.D.
Dean of the College of Arts and Sciences

Approved: _____
Ann L. Ardis, Ph.D.
Senior Vice Provost for Graduate and Professional Education

I certify that I have read this dissertation and that in my opinion it meets the academic and professional standard required by the University as a dissertation for the degree of Doctor of Philosophy.

Signed: _____

Francisco-Javier Sayas, Ph.D.
Professor in charge of dissertation

I certify that I have read this dissertation and that in my opinion it meets the academic and professional standard required by the University as a dissertation for the degree of Doctor of Philosophy.

Signed: _____

Constantin Bacuta , Ph.D.
Member of dissertation committee

I certify that I have read this dissertation and that in my opinion it meets the academic and professional standard required by the University as a dissertation for the degree of Doctor of Philosophy.

Signed: _____

Fioralba Cakoni, Ph.D.
Member of dissertation committee

I certify that I have read this dissertation and that in my opinion it meets the academic and professional standard required by the University as a dissertation for the degree of Doctor of Philosophy.

Signed: _____

Peter Monk, Ph.D.
Member of dissertation committee

ACKNOWLEDGEMENTS

None of the work in this dissertation (and even work not in this dissertation) would have been possible without the guidance of Prof. Francisco-Javier Sayas; who bravely undertook the task of bringing a physicist several steps closer to becoming a mathematician. For the knowledge and the moments shared, for the evenings in Pamplona, or Concepción, or the Summer barbecues, thank you.

I'm grateful to Professors Constantin Bacuta, Fioralba Cakoni and Peter Monk, for agreeing to be part of my dissertation committee, but I'm even more thankful for their constant advice, counsel and invaluable support over my years as a student and specially during the final stages of my doctoral studies. I sincerely thank them for contributing to my growth as an aspiring mathematician and as a person.

I would also like to thank Professors Víctor Domínguez and George Hsiao for the privilege of working and co-authoring with them, for the many things I learned along the way and their words both of wisdom and encouragement.

I'm particularly thankful to Matt Hassell for the thrust and the countless hours of fun, chat, and free therapy. To Michael DePersio for keeping us being on average good TA's and for all those random conversations. To all the friends who have made the Delaware experience unforgettable: Jake Rezak, Isaac Harris, Allan Hungria, Thomas Brown, Mike Stapf, Ryan Evans, Christine Rakowski, Tianyu Qiu, Shixu Meng, Irene de Teresa, Klajdi Qirko...

I must mention Professor Antonio Capella Kort who hooked me back into math and set me on the right track, encouraging me to pursue studies abroad, and my brother Guillermo Rosales Vizzuett who has always been my example to follow and has set the bar very high, making it hard (and fun) to keep up with him.

This work is dedicated to the three most important people in my life. My parents, Teresita Vizuet Martínez and Antonio Sánchez Ávila, for their unconditional love and support, for all those years of efforts and hardships and all the sacrifices they made for the sake of my education. And to my fiancée, Lise-Marie Imbert-Gérard, for her endless love, for keeping me on my toes, for guarding my sanity and encouraging my craziness, for the future... I would have never made it to this point without you.

... it is also dedicated to Cuchara, my friend and guardian, who came with me all the way from México and still sits on my shoulders, purring while I type mathematical nonsense.

TABLE OF CONTENTS

Appendix

LIST OF TABLES

LIST OF FIGURES

ABSTRACT

We study the discretization of the equations describing the propagation of elastic waves through a homogeneous medium and the transient interaction between acoustic waves traveling on free space and interacting with scatterers with different sorts of elastic properties.

In the case of plane elastodynamic waves a simple and efficient method based on `deltaBEM` is developed for scatterers with smooth boundaries. We provide mathematical and numerical evidence that the proposed discretization is the only choice of the one-parameter family of discretizations proposed in [31] that provides third order consistency for the operators of linear elasticity.

The remaining chapters of the thesis study the scattering of acoustic waves by obstacles with linearly elastic, piezoelectric, and thermoelastic behavior. The proposed formulations use a boundary potential representation of the scattered acoustic wave, resulting in systems of boundary integral equations, in the case of a homogeneous elastic scatterer, or coupled integro-differential systems for non homogeneous solids. The analysis is done in the Laplace domain, following [6, 82] where the systems are semi-discretized in space and the well-posedness of the continuous and semidiscrete problems is proven simultaneously.

The equations are fully discretized using second order multi-step Convolution Quadrature [91] for time evolution. We prove that the resulting fully discrete methods obtained with BDF2-CQ are of second order and provide explicit dependence of the error constants with respect to time. Numerical evidence is given to show that Trapezoidal Rule Convolution Quadrature yields a second order method as well.

Chapter 1

INTRODUCTION

This work deals with the analysis and implementation of numerical schemes for the solution of a class of time domain problems arising from either the study of elastic waves propagating on a medium containing bounded rigid inclusions that act as scatterers, or the interaction between an acoustic wave impinging on a bounded elastic body.

These situations result in systems of partial differential equations (PDEs) posed on unbounded domains with boundary conditions prescribed on a bounded hypersurface that divides the space into disjoint regions. In this context, and when the coefficients of the PDE are constant, the linearity of the problem and the knowledge of the fundamental solution can be used advantageously to transfer the problem into an integral equation posed only on the dividing hypersurface.

In many applications, though, the coefficients of the PDEs reflect varying physical properties and are therefore not constant throughout the entire space. For linear problems it would still be possible to treat such a system in terms of integral relations, but the resulting equations would now be posed on the entire space and would require also the approximation of the fundamental solution. These drawbacks would hinder the integral equation approach to the point of it not being competitive with other methods available.

There are situations of interest, however, where a wave propagating through a homogeneous medium interacts with a bounded obstacle with varying physical properties. In such cases, the homogeneity of the unbounded medium allows for an integral representation of the impinging wave, whereas the behavior of the bounded inhomogeneous region can be dealt with non-integral methods. This treatment leads to coupled

integro-differential systems and the largest part of this work is devoted to the study of the discretization and analysis of such kinds of problems.

The use of integral equation techniques in frequency domain scattering has a long and rich history, but the development of efficient tools for the analysis and discretization of time domain integral equations is recent and less extensive. The fundamental steps for the analysis of transient integral problems were laid out by Bamberger and Ha-Duong in their 1986 foundational papers [6, 7]. Their technique, which involves the passage through the Laplace domain, provides an elegant and unified approach and will be heavily used through this work.

Almost simultaneously, Christian Lubich developed Convolution Quadrature (CQ) as a tool to solve discrete convolution equations [56, 89, 90], and a few years later applied it to the solution of evolutionary PDEs [93, 92, 91]. CQ constitutes a powerful tool for the discretization of time domain integral equations which, in combination with the Laplace domain analysis, provides a clean way to establish stability bounds, convergence estimates, and regularity requirements for the problem data. In the current work we will focus on the usage of second order multi step CQ methods and their combined use with standard time-stepping techniques for our time discretizations.

The most frequently used techniques for space discretization of integral equations are Nyström methods, collocation methods, and Galerkin methods. The Nyström methods are relatively simple to understand conceptually and lend themselves easily to computational implementation but require the careful handling of singular integrals and specialized quadrature formulas that change with the equation under consideration. The Galerkin approach, while considered slightly more demanding computationally speaking, is robust and lends itself more easily to rigorous mathematical analysis. In the present work we study briefly a Nyström-like technique for the discretization of the integral operators of 2D linear elasticity based on the ideas behind `deltaBEM` developed in [31]. For the analysis of the coupled problems in the later parts of the text, however, we rely on Galerkin discretizations.

The thesis is structured as follows. Chapter 2 serves as a starting point providing

a very quick refresher of the main concepts that are used throughout the rest of the work fixing notation and terminology along the way. A reader familiar with the concepts and results summarized here is well prepared to follow the flow of the remaining chapters.

Chapter 3 deals with the aforementioned Nyström-like discretization of the integral operators of the 2D elastodynamic Calderón calculus for a smooth parameterizable curve in the plane. The method relies on the usage of symmetricaly staggered grids on the scatterer and exploits symmetry to yield third order accuracy. We provide numerical evidence supporting the convergence rate and give mathematical evidence that for elastodynamics this is the only method of the `deltaBEM` family that achives third order accuracy. This was done jointly with Víctor Domínguez and Francisco-Javier Sayas and was published in the paper [34].

In the remaining chapters we focus on the study of wave structure interactions of different sorts. Chapter 4 considers an acoustic wave interacting with a linearly elastic solid. In the first part the object is considered to be homogeneous, leading to a purely boundary integral equation treatment. The second part considers the more general case of an inhomogeneous anisotropic body and results in the discretization of an integro-differential system. We prove well-posedness of the semi-discrete and continuous problems simultaneously and provide a full discretization of order two with Convolution Quadrature. This chapter was the result of work done in collaboration with George Hsiao and Francisco-Javier Sayas that appeared in [66].

We next study the interaction between an acoustic wave and a piezoelectric scatterer in Chapter 5. The piezoelectric effect breaks the isotropy of the elastic medium and introduces a new variable into the sytem, namely the electric potential on the dielectric, wich couples with the elastic displacement through a constitutive relation that generalizes the elastic stress tensor. The resulting PDE system includes two hyperbolic equations (for the acoustic potential and elastic displacement) and one elliptic equation for the electric potential. The proposed formulation deals with the acoustic scattered wave with boundary integral equations and with the displacement and electric potentials variationally. We prove the well-posedness of the coupled discretization in the

Laplace domain and show that the BDF2-based CQ discretization is stable and second order accurate for smooth enough problem data. This part of the work was done with Francisco-Javier Sayas and has been submitted for publication [110].

When the thermodynamics of elastic deformation are considered, the resulting constitutive relation includes the effect of temperature gradients as sources of mechanical stress and introduces the temperature variations as an additional unknown. The final Chapter 6 considers the scattering of acoustic waves by thermoelsastic obstacles of this sort. The new system now includes two hyperbolic equations and one parabolic. The acoustic unknown is treated with integral equations and the thermal and elastic variables are discretized variationally aiming for a coupled BEM-FEM numerical treatment. Trapezoidal rule and BDF2 CQ are used for time discretization and we provide numerical evidence supporting a global second order discrete scheme. The work on this chapter is still in progress in collaboration with George Hsiao, Francisco Javier Sayas and Richard Weinacht [67].

The thesis concludes with two short appendices with the basic results we borrow from the theory of Banach space-valued time domain tempered distributions and their Laplace transforms (Appendix A) and a brief introduction to the ideas behind Convolution Quadrature and a terse summary of the main theorems we applied to the time discretizations on the main body of the thesis (Appendix B).

Chapter 2

NOTATION AND BACKGROUND MATERIAL

This chapter serves the purpose of fixing the notation, terminology, and geometric assumptions that that will be used throughout the thesis. It is a brief reminder of the basic results from Sobolev spaces, linear elasticity and boundary integral equations that are considered the starting point for the work and it is in now way intended to be exhaustive.

For a thorough treatment of Sobolev spaces we refer to the books by Adams and Fournier [1], and Haroske [58]. A concise treatment of the theory of elasticity from the point of view of theoretical physics can be found in the work of Landau and Lifschitz [84] while the books by Marsden [98], and Valent [122] provide a mathematically rigorous treatment. The books by Hsiao and Wendland [69], and McLean [102] are very complete references for the basic results on boundary integral equations on non-smooth domains.

2.1 Sobolev Space Notation

Consider an open domain $\mathcal{O} \subset \mathbb{R}^d$ with boundary $\partial\mathcal{O}$. For scalar, vector, and matrix-valued $L^2(\mathcal{O})$ inner products we will use respectively the brackets

$$(a, b)_{\mathcal{O}} := \int_{\mathcal{O}} a\, b, \qquad (\mathbf{a}, \mathbf{b})_{\mathcal{O}} := \int_{\mathcal{O}} \mathbf{a} \cdot \mathbf{b}, \qquad (\mathbf{A}, \mathbf{B})_{\mathcal{O}} := \int_{\mathcal{O}} \mathbf{A} : \mathbf{B},$$

where in the latter the colon denotes the Frobenius inner product of matrices. We will retain the same notation even in the case when the functions take complex values and will conjugate quantities explicitly whenever needed. When boldface is used instead of italic to denote a Sobolev or Lebesgue space it should be interpreted as the product space of d copies of the italicized space. For example, $\mathbf{L}^2(\Omega) := L^2(\Omega)^d$.

Let n be a non negative integer. We will denote

$$\|u\|^2_{n,\mathcal{O}} := \sum_{|\alpha|\leq n} \int_{\mathcal{O}} |\partial^\alpha u|^2,$$

where the sum is defined over the multi-index $\alpha \in \mathbb{Z}^d_+$. We also define the spaces

$$\begin{aligned} H^n(\mathcal{O}) &:= \{u : \mathcal{O} \longrightarrow \mathbb{R} : \|u\|_{n,\mathcal{O}} < \infty\}, \\ H^n_0(\mathcal{O}) &:= \overline{\mathcal{D}(\mathcal{O})}, \end{aligned}$$

where differentiation is taken in the sense of distributions, and the closure is taken with respect to the norm $\|\cdot\|_{n,\mathcal{O}}$. The space $\mathcal{D}(\mathcal{O})$ of smooth compactly supported test functions is defined by

$$\mathcal{D}(\mathcal{O}) := \{\phi : \mathcal{O} \longrightarrow \mathbb{R} : \phi \in \mathcal{C}^\infty(\mathcal{O}) \text{ and } supp\, \phi \subset\subset \mathcal{O}\}.$$

For functions in $H^1(\mathcal{O})$ we can define the *trace operator* $\gamma : H^1(\mathcal{O}) \longrightarrow L^2(\partial\mathcal{O})$ which is linear and bounded [1]. To represent the space of all functions $\varphi \in L^2(\partial\mathcal{O})$ such that $\varphi = \gamma u$ for some $u \in H^1(\mathcal{O})$ and its dual we will write

$$H^{1/2}(\partial\mathcal{O}) \qquad \text{and} \qquad H^{-1/2}(\partial\mathcal{O})$$

respectively and will denote with the angled brackets $\langle \lambda, \varphi \rangle_{\partial\mathcal{O}}$ the duality pairing of $\lambda \in H^{-1/2}(\partial\mathcal{O})$ and $\varphi \in H^{1/2}(\partial\mathcal{O})$ – similarly for $\boldsymbol{\lambda} \in \mathbf{H}^{-1/2}(\partial\mathcal{O})$ and $\boldsymbol{\varphi} \in \mathbf{H}^{1/2}(\partial\mathcal{O})$.

2.2 Geometric Set Up

Throughout the text, we will consider a solid body which, in the absence of any external stimulus, adopts a fixed *reference configuration* described by an open, bounded, not necessarily simply connected region $\Omega_- \subset \mathbb{R}^d$ with Lipschitz boundary $\partial\Omega_- := \Gamma$. Surrounding the solid body and filling the unbounded region $\Omega_+ := \mathbb{R}^d \setminus \overline{\Omega}_-$ we will consider a barotropic and irrotational flow of a homogeneous, inviscid and compressible fluid.

The *outward normal vector* defined on Γ will be denoted by $\boldsymbol{\nu}$. The mass density of the body will be given by the function $\rho_\Sigma \in L^2(\Omega_-)$ which will be assumed to be

strictly positive almost everywhere in Ω_-. A schematic representation of the geometric setup is found in Figure 2.1. Unless explicitly stated otherwise, in the analysis d will remain an arbitrary positive integer.

Given $u \in H^1(\mathbb{R}^d \setminus \Gamma)$, we consider its interior, exterior, averaged, and difference traces:

$$\gamma^- u, \quad \gamma^+ u, \quad \{\!\{\gamma u\}\!\} := \tfrac{1}{2}(\gamma^- u + \gamma^+ u), \quad [\![\gamma u]\!] := \gamma^- u - \gamma^+ u.$$

We will define the space

$$H^1_\Delta(\mathbb{R}^d \setminus \Gamma) := \left\{ u \in H^1(\mathbb{R}^d \setminus \Gamma) : \Delta u \in L^2(\mathbb{R}^d \setminus \Gamma) \right\},$$

that becomes a Hilbert space when equipped with the norm

$$\|u\|^2_\Delta := \|u\|^2_{\mathbb{R}^d} + \|\nabla u\|^2_{\mathbb{R}^d \setminus \Gamma} + \|\Delta u\|^2_{\mathbb{R}^d \setminus \Gamma}.$$

For functions $u \in H^1_\Delta(\mathbb{R}^d \setminus \Gamma)$ we define the interior and exterior normal derivatives $\partial^\pm_\nu : H^1_\Delta(\mathbb{R}^d \setminus \Gamma) \longrightarrow H^{-1/2}(\Gamma)$ using Green's formula

$$\langle \partial^\mp_\nu u, \gamma v \rangle_\Gamma := \pm(\Delta u, v)_{\Omega_\mp} \pm (\nabla u, \nabla v)_{\Omega_\mp} \qquad \forall v \in H^1(\mathbb{R}^d).$$

The following two operators related to the normal vector field

$$\begin{array}{rcl} \mathrm{N} : \mathbf{H}^{1/2}(\Gamma) & \longrightarrow & H^{-1/2}(\Gamma) \\ \boldsymbol{\phi} & \longmapsto & \boldsymbol{\phi} \cdot \boldsymbol{\nu}, \end{array} \qquad \begin{array}{rcl} \mathrm{N}^t : H^{1/2}(\Gamma) & \longrightarrow & \mathbf{H}^{-1/2}(\Gamma) \\ \phi & \longmapsto & \phi\, \boldsymbol{\nu}, \end{array}$$

will be used to give rigorous meaning to some elements appearing in the transmission conditions the we will be dealing with later on. Averaged normal derivatives and jumps are defined just as the traces; analogously two-sided traces and conormal derivatives will be defined for vector-valued functions.

2.3 Deformation, Motion, and Displacement

A *deformation* of the reference configuration is a $\mathcal{C}^1$ injection

$$\phi : \overline{\Omega}_- \longrightarrow \mathbb{R}^d$$

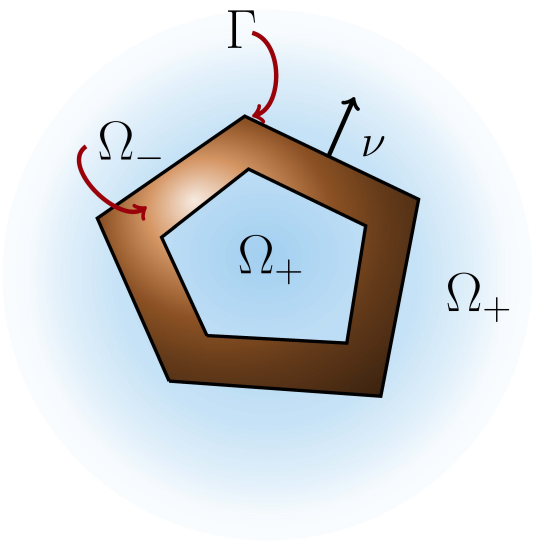

Figure 2.1: Schematic of the geometric setting, the elastic body is contained on a bounded region Ω_- not necesarily simply connected; the unbounded region Ω_+ is filled with a homogeneous fluid. It is assumed that the exterior normal $\boldsymbol{\nu}$ exists almost everywhere along the boundary Γ.

such that $det\ \nabla\phi > 0$. We will denote by $\widehat{\Omega}_-$ the image of Ω_- under ϕ and will refer to it as the *deformed configuration*. From the assumptions made on ϕ and as a consequence of the invariance of domain theorem and the inverse function theorem, it follows that ϕ is in fact a $\mathcal{C}^1$ orientation-preserving diffeomorphism of $\overline{\Omega}_-$ onto $\overline{\widehat{\Omega}}_-$ [122]. In particular

$$\phi(\partial\Omega_-) = \partial\widehat{\Omega}_-\,, \qquad \text{and} \qquad \phi(\overline{\Omega}_-) = \overline{\widehat{\Omega}}_-.$$

These facts together with the differentiability of ϕ^{-1} will allow us to carry out most of the computations on the reference domain Ω_-.

A deformation is said to be *rigid* if

$$\|\phi(\mathbf{x}) - \phi(\mathbf{y})\|_{\mathbb{R}^d} = \|\mathbf{x} - \mathbf{y}\|_{\mathbb{R}^d} \quad \forall\, \mathbf{x}, \mathbf{y} \in \Omega_-.$$

It can be shown that a deformation is rigid if and only if it can be expressed as

$$\phi(\mathbf{x}) = \mathbf{M}\,\mathbf{x} + \mathbf{b} \quad \forall \mathbf{x} \in\ \Omega_-\,,$$

for some $\mathbf{b} \in \mathbb{R}^d$ and some matrix $\mathbf{M} \in \mathbb{R}^{d\times d}$ such that

$$det\, \mathbf{M} > 0 \;\text{ and }\; \mathbf{M}^\top = \mathbf{M}^{-1}.$$

For any given a deformation, the points of the reference configuration undergo a *displacement* described by the function

$$\mathbf{u} := \phi - \mathrm{I}_{\overline{\Omega}_-} ,$$

where $\mathrm{I}_{\overline{\Omega}_-}$ is the restriction of the identity function to the closure of the reference configuration.

A *motion* of Ω_- is a mapping ϕ_t from the real line to the set of deformations of Ω_-. For every $\mathbf{x} \in \Omega_-$ we will consider that $\phi_t(\mathbf{x})$ is of class $\mathcal{C}^1$ and will say that ϕ_t is a *rigid motion* if it is a rigid deformation for every $t \in \mathbb{R}$.

2.4 Strain and Linearized Strain Tensors

To keep the notation as compact as possible, in what follows we will use the index summation convention

$$x_i x_i := \sum_{i=1}^{d} x_i x_i.$$

Following the treatment of Landau and Lifschitz [84], consider a pair of points $\mathbf{p}_1$ and $\mathbf{p}_2$ infinitesimally close in a reference configuration Ω_-. If their location is represented by their coordinates in a Cartesian coordinate system, and we let $\mathbf{x} = (x_1, \ldots, x_d)$

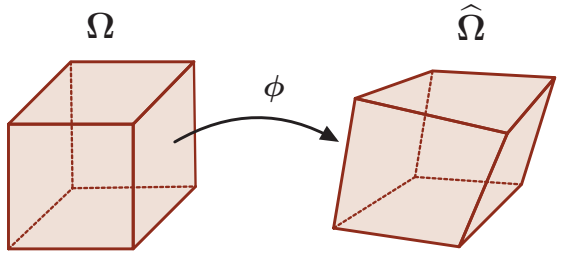

Figure 2.2: Under the action of a deformation the control volume Ω_- is mapped to a deformed configuration $\widehat{\Omega}_-$.

denote the vector connecting them, then length $dl = \|\mathbf{x}\|_{\mathbb{R}^d}$ can be given in terms of its components by

$$dl^2 = dx_i\, dx_i, \qquad i = 1, \ldots, d,$$

where we have used Einstein's summation convention. In a similar fashion, if the solid undergoes a deformation ϕ, the points will be mapped to new locations $\phi(\mathbf{p}_1)$ and $\phi(\mathbf{p}_2)$ and the length of the vector connecting the images $\widehat{dl} = \|\phi(\mathbf{p}_2) - \phi(\mathbf{p}_1)\|_{\mathbb{R}^d}$ is connected to its components by

$$\widehat{dl}^2 = d\widehat{x}_i\, d\widehat{x}_i, \qquad i = 1, \ldots, d.$$

Since the deformed coordinates are connected to the reference coordinates through the displacement

$$\widehat{\mathbf{x}} = \mathbf{x} + \mathbf{u},$$

then $d\widehat{x}_i = dx_i + du_i$ and we can write

$$\begin{aligned}
\widehat{dl}^2 &= (dx_i + du_i)(dx_i + du_i) \\
&= \left(dx_i + \frac{\partial u_i}{\partial x_j} dx_j\right)\left(dx_i + \frac{\partial u_i}{\partial x_l} dx_l\right) \\
&= dx_i\, dx_i + \frac{\partial u_i}{\partial x_l} dx_i\, dx_l + \frac{\partial u_i}{\partial x_j} dx_i\, dx_j + \frac{\partial u_i}{\partial x_j}\frac{\partial u_i}{\partial x_l} dx_j\, dx_l \\
&= dl^2 + \left(\frac{\partial u_i}{\partial x_j} + \frac{\partial u_j}{\partial x_i} + \frac{\partial u_k}{\partial x_i}\frac{\partial u_k}{\partial x_j}\right) dx_i\, dx_j.
\end{aligned}$$

To obtain the last equality we have relabeled carefully the dummy indices and substituted $dl^2 = dx_i\, dx_i$. This expression gives the change experienced by an infinitesimal length element after a deformation in terms of the reference coordinates $\mathbf{x}$ and the displacement $\mathbf{u}$. It can be written in the compact form

$$\widehat{dl}^2 = dl^2 + 2\,\mathrm{S}_{ij} dx_i\, dx_j \tag{2.1}$$

by defining the *strain tensor*

$$\mathrm{S}_{ij} := \frac{1}{2}\left(\frac{\partial u_i}{\partial x_j} + \frac{\partial u_j}{\partial x_i} + \frac{\partial u_k}{\partial x_i}\frac{\partial u_k}{\partial x_j}\right). \tag{2.2}$$

As is clear from the definition, the strain tensor is symmetric, and therefore it can be diagonalized, at least locally. This fact has the physical interpretation that, when viewed locally, deformations are the product of independent strains along orthogonal directions which are referred to as the *principal axes* of the tensor. After diagonalization, the values along the diagonal, called the *principal values*, are related to the reaction of the solid to simple extensions along the principal directions.

As can be inferred from (2.1), small displacement gradients imply small deformations, but the converse statement is not necessarily true. This is usually the case for bodies that are considerably thinner in one space dimension relative to the others, such as long rods or thin plates. In most other instances, small displacements imply small displacement gradients and then the term $\dfrac{\partial u_k}{\partial x_i}\dfrac{\partial u_k}{\partial x_j}$ in (2.2) can be neglected yielding the *linearized strain tensor*

$$\varepsilon_{ij} := \frac{1}{2}\left(\frac{\partial u_i}{\partial x_j} + \frac{\partial u_j}{\partial x_i}\right). \tag{2.3}$$

We emphasize that in order for this linearization to be valid, the assumption of small displacements in not enough and the smallness of the displacement gradients has to be taken as an extra hypothesis. In what follows we will always assume that this two conditions hold and will use exclusively the linearized strain tensor, to which we will refer to as simply strain tensor. The previous expression is a component description, every time we refer to the tensor without referencing the components it will be denoted with boldface $\boldsymbol{\varepsilon}$.

We will say that a deformation is an *infinitesimal rigid deformation* if there exists a skew symmetric matrix $\mathbf{M}$ such that $\phi(\mathbf{x}) = \mathbf{M}\mathbf{x} + \mathbf{b}$ for some $\mathbf{b} \in \mathbb{R}^d$ and for every $\mathbf{x} \in \Omega_-$.

The components of the linearized strain tensor can be interpreted as the infinitesimal deformations of a solid undergoing a displacement. The diagonal terms ε_{ii} encode the infinitesimal extension in each coordinate direction Δu_i by unit length Δx_i

$$\frac{\Delta u_i}{\Delta x_i} \approx \frac{\partial u_i}{\partial x_i} = \frac{1}{2}\varepsilon_{ii},$$

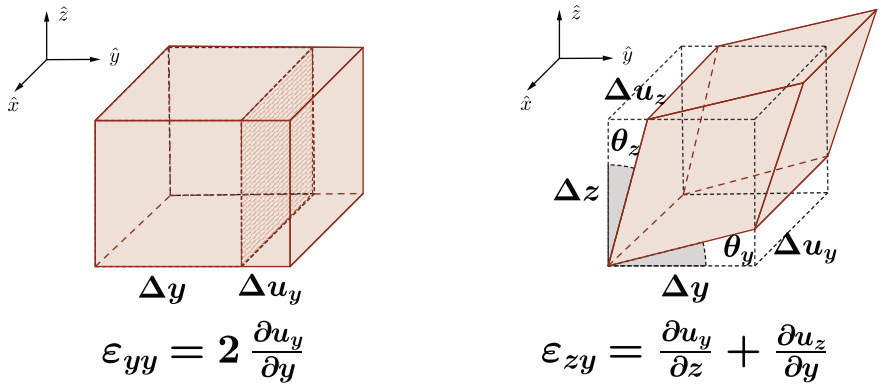

Figure 2.3: The normal strain ε_{yy} is a measure of the infinitesimal extension in the y direction per unit length (left) . The shear strain ε_{zy} measures the total infinitesimal angular deviation induced by a deformation with respect to the rectangular control volume in the planes normal to $\widehat{y}$ and $\widehat{z}$ (right).

known as *uniaxial extension*. On the other hand, the off-diagonal terms ε_{ij} $i \neq j$ contain information on the reaction of the solid to *shear strain*. Consider an infinitesimal rectangular control volume aligned along the coordinate axes as in Figure 2.3. Let θ_i and θ_j denote the infinitesimal angular deviation of the faces of the control volume with respect to the hyperplanes orthogonal to the coordinate axes x_i and x_j, then

$$\theta_i + \theta_j \approx \tan(\theta_i) + \tan(\theta_j) = \frac{\Delta u_i}{\Delta x_j} + \frac{\Delta u_j}{\Delta x_i} \approx \left(\frac{\partial u_i}{\partial x_j} + \frac{\partial u_j}{\partial x_i} \right) = \varepsilon_{ij} \qquad i \neq j.$$

2.5 Korn's Inequalities

The Jacobian matrix of the displacement vector and the strain tensor are strongly related. In fact, the displacement gradient can be split as the sum of the strain tensor $\boldsymbol{\varepsilon}$ and an anti-symmetric part $\boldsymbol{\omega}$

$$\nabla \boldsymbol{\phi} = \boldsymbol{\varepsilon} + \boldsymbol{\omega},$$

where

$$\omega_{ij} := \frac{1}{2} \left(\frac{\partial \phi_i}{\partial x_j} - \frac{\partial \phi_j}{\partial x_i} \right). \tag{2.4}$$

It is then natural to ask under what conditions the L^2 norm of the gradient can be controlled by that of the strain tensor. The following results establish some general conditions under which this can be done and will prove vital in establishing the unique solvability of the Dirichlet and Neumann boundary value problems that will occupy us later on.

Lemma 2.1 (First Korn inequality)**.** *Let $\Omega_- \subset \mathbb{R}^d$, be an open domain. The following inequality holds*

$$\|\nabla \mathbf{u}\|_{\Omega_-} \leq \sqrt{2}\|\boldsymbol{\varepsilon}(\mathbf{u})\|_{\Omega_-}, \qquad \mathbf{u} \in \mathbf{H}^1_0(\Omega_-). \tag{2.5}$$

Proof. Let $\boldsymbol{\phi} \in \boldsymbol{\mathcal{D}}(\Omega_-)$. Decomposing $\nabla \boldsymbol{\phi}$ into its symmetric and anti-symmetric parts –as defined in (2.3) and (2.5)– it is easy to see that

$$\nabla \boldsymbol{\phi} : \nabla \boldsymbol{\phi}^\top = \boldsymbol{\varepsilon}(\boldsymbol{\phi}) : \boldsymbol{\varepsilon}(\boldsymbol{\phi}) - \boldsymbol{\omega}(\boldsymbol{\phi}) : \boldsymbol{\omega}(\boldsymbol{\phi}).$$

On the other hand, using the fact that $\boldsymbol{\phi}$ is infinitely differentiable, some algebraic manipulations show that

$$\nabla \boldsymbol{\phi} : \nabla \boldsymbol{\phi}^\top = \nabla \cdot (\nabla \boldsymbol{\phi}\, \boldsymbol{\phi} - \nabla \cdot \boldsymbol{\phi}\, \boldsymbol{\phi}) + (\nabla \cdot \boldsymbol{\phi}) : (\nabla \cdot \boldsymbol{\phi}).$$

Therefore, integrating over Ω_-, we get

$$\begin{aligned}
\int_{\Omega_-} (\boldsymbol{\varepsilon}(\boldsymbol{\phi}) : \boldsymbol{\varepsilon}(\boldsymbol{\phi}) - \boldsymbol{\omega}(\boldsymbol{\phi}) : \boldsymbol{\omega}(\boldsymbol{\phi})) &= \int_{\Omega_-} (\nabla \cdot (\nabla \boldsymbol{\phi}\, \boldsymbol{\phi} - \nabla \cdot \boldsymbol{\phi}\, \boldsymbol{\phi}) + (\nabla \cdot \boldsymbol{\phi}) : (\nabla \cdot \boldsymbol{\phi})) \\
&= \int_{\Gamma} (\nabla \boldsymbol{\phi}\, \boldsymbol{\phi} - \nabla \cdot \boldsymbol{\phi}\, \boldsymbol{\phi}) \cdot \boldsymbol{\nu} + \int_{\Omega_-} (\nabla \cdot \boldsymbol{\phi}) : (\nabla \cdot \boldsymbol{\phi}) \\
&= \int_{\Omega_-} (\nabla \cdot \boldsymbol{\phi}) : (\nabla \cdot \boldsymbol{\phi}) \\
&\geq 0,
\end{aligned}$$

where an application of the divergence theorem and the fact that $\boldsymbol{\phi}$ is supported away from Γ have been used. This yields $\|\boldsymbol{\omega}(\boldsymbol{\varphi})\|^2_{\Omega} \leq \|\boldsymbol{\varepsilon}(\boldsymbol{\varphi})\|^2_{\Omega_-}$, and as a consequence

$$\|\nabla \boldsymbol{\phi}\|^2_{\Omega_-} = \|\boldsymbol{\varepsilon}(\boldsymbol{\varphi})\|^2_{\Omega_-} + \|\boldsymbol{\omega}(\boldsymbol{\varphi})\|^2_{\Omega_-} \leq 2\|\boldsymbol{\varepsilon}(\boldsymbol{\varphi})\|^2_{\Omega_-}.$$

The result extends to $\mathbf{H}^1_0(\Omega_-)$ by density. □

The proof of the following result, that holds for the case of functions $\mathbf{u} \in H^1(\Omega_-)$, is quite technical and we refer to [46, 25] for the details.

Lemma 2.2 (Second Korn inequality)**.** *Let $\Omega_- \in \mathbb{R}^d$ be open, bounded and with Lipschitz boundary. There exists $C_\Gamma > 0$ depending only on the geometry such that*

$$\|\mathbf{u}\|^2_{1,\Omega_-} \leq C_\Gamma \big(\|\mathbf{u}\|^2_{\Omega_-} + \|\boldsymbol{\varepsilon}(\mathbf{u})\|^2_{\Omega_-} \big), \qquad \mathbf{u} \in \mathbf{H}^1(\Omega_-). \tag{2.6}$$

This result can be stated in many alternative (or slightly more general) ways.

2.6 The Stress Tensor and the Equations of Motion

When subject to a deformation, the constitutive elements of a solid will react exerting forces on each other in an attempt to counter the external agents inducing the deformation and return to its equilibrium configuration. These internal restoring forces are known as *internal stresses* and vanish in the absence of a deformation. In order to describe them, we introduce the *stress tensor*

$$\boldsymbol{\sigma} : \overline{\Omega}_- \longrightarrow \mathbb{R}^{d \times d}$$

which is a second rank tensor whose component σ_{ij} describes, for each $\mathbf{x} \in \overline{\Omega}_-$, the i-th component of the internal stress crossing through a unit surface anchored at $\mathbf{x}$ and normal to the j-th coordinate axis (See Figure 2.4). The projection of the stress tensor onto the normal direction is known as *normal traction* and will be denoted alternatively by

$$\mathbf{t}(\mathbf{u}) := \boldsymbol{\sigma}\, \boldsymbol{\nu}.$$

Integrating the normal traction over the surface Γ we can compute the total flux of stress across Γ, known as traction

$$\mathbf{T} = -\int_\Gamma \boldsymbol{\sigma}\, \boldsymbol{\nu}.$$

The negative sign is merely a convention; it emphasizes the fact that the quantity computed in such a way points towards the outward direction, thus leaving the system.

Consider the vectors $\mathbf{x}, \mathbf{y} \in \mathbb{R}^d$, and the matrix $\mathbf{M} \in \mathbb{R}^{d\times d}$ we will define the *tensor product* $\otimes$ and *wedge product* $\wedge$ respectively by

$$(\mathbf{x}\otimes\mathbf{y})_{ij} := x_i y_j \qquad (\mathbf{x}\otimes\mathbf{M})_{ijk} := x_i M_{jk} \qquad i,j,k = 1,\dots,d.$$
$$(\mathbf{x}\wedge\mathbf{y})_{ij} := x_i y_j - x_j y_i \qquad (\mathbf{x}\wedge\mathbf{M})_{ijk} := x_i M_{jk} - x_j M_{ik} \qquad i,j = 1,\dots,d.$$

Note that the wedge product is twice the anti-symmetric part of the tensor product and thus, for two vectors, has at most $\frac{d^2-d}{2}$ different non-zero components. In the particular case of the wedge product of two vectors in $\mathbb{R}^3$ this reduces to only three independent entries and, by mapping the pairs of indices $(2,3) \to 1, (3,1) \to 2$, and $(1,2) \to 3$ it is possible to identify the independent non-zero terms of the wedge product with the usual components of the cross product in $\mathbb{R}^3$.

If we denote by $\mathbf{f} = (f_1, \dots, f_d) : \Omega_- \to \mathbb{R}^d$ the volumetric density of the external forces, then the total force and torque acting on the solid would be given respectively by

$$\mathbf{F} = \int_{\Omega_-} \mathbf{f}, \qquad \text{and} \qquad \boldsymbol{\tau} = \int_{\Omega_-} \mathbf{x}\wedge\mathbf{f}.$$

When the external forces acting on the solid do not balance with the internal stress, the resulting net force induces is a change in the linear momentum $\boldsymbol{\mathcal{P}}$ of the body given by

$$\frac{d}{dt}\boldsymbol{\mathcal{P}} = \int_{\Omega_-} \rho_\Sigma \ddot{\mathbf{u}},$$

where the dots represent differentiation with respect to time. Hence, from the balance of forces and momentum we get

$$\int_{\Omega_-} f_i + \int_\Gamma \sigma_{ij}\,\nu_j - \int_{\Omega_-} \rho_\Sigma \ddot{u}_i = \int_{\Omega_-} f_i + \int_{\Omega_-} \partial_j \sigma_{ij} + \int_{\Omega_-} \rho_\Sigma \ddot{u}_i = 0.$$

where the second equality is an application of the divergence theorem and ∂_i denotes differentiation with respect to the i-th coordinate. The fact that the integration volume could have been any open subset of Ω_- leads to one of the fundamental equations of the theory of elasticity

$$\nabla\cdot\boldsymbol{\sigma} + \mathbf{f} = \rho_\Sigma \ddot{\mathbf{u}} \quad \text{ in } \Omega_-, \tag{2.7}$$

which is just the mathematical expression of the balance of forces and the change of momentum. Similarly, imposing the balance of torques we get

$$\begin{aligned}\int_{\Omega_-} \rho_\Sigma(x_i\ddot{u}_j - x_j\ddot{u}_i) &= \int_{\Omega_-} (x_i f_j - x_j f_i) + \int_\Gamma (x_i\sigma_{jk} - x_j\sigma_{ik})\nu_k \\ &= \int_{\Omega_-} (x_i f_j - x_j f_i) + \int_{\Omega_-} \partial_k(x_i\sigma_{jk} - x_j\sigma_{ik}) \\ &= \int_{\Omega_-} (x_i f_j - x_j f_i) + \int_{\Omega_-} (\sigma_{ji} - \sigma_{ij} + x_i\partial_k\sigma_{jk} - x_j\partial_k\sigma_{ik}).\end{aligned}$$

One more time, the integrals could have been taken over any arbitrary subset of Ω_- which leads to

$$\mathbf{x} \wedge (\mathbf{f} + \nabla \cdot \boldsymbol{\sigma} - \rho_\Sigma \ddot{\mathbf{u}}) + \boldsymbol{\sigma}^\top - \boldsymbol{\sigma} = 0 \qquad \text{in } \Omega_-.$$

As a consequence of equation (2.7), the term in the parenthesis vanishes and we arrive to the important fact that

$$\boldsymbol{\sigma}^\top = \boldsymbol{\sigma},$$

i.e., the stress tensor is symmetric.

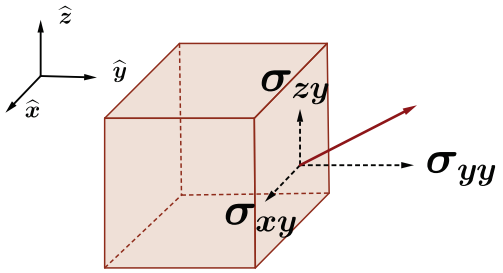

Figure 2.4: The components of the stress tensor measure the flux density force due to the internal restoring forces. At any given point $\mathbf{x}$ the product $\boldsymbol{\sigma}\,\mathbf{v}$ gives the internal stress crossing a unit surface centered at $\mathbf{x}$ and oriented normally with respect to $\mathbf{v}$. The figure shows the x, y, and z components of the flux through the face of the cube normal to the y-axis.

2.7 Hooke's Law and Betti's Formula

The way in which the internal stresses are connected to the external strains applied to a body is known as a *constitutive relation* and depends entirely on the

properties of the body in question. In some cases the stress tensor does not only depend on the internal strains $\boldsymbol{\varepsilon}$ (as will be the case in Chapters 2 and 3) but also on some other physical variables like the electric potential ψ (Chapter 4) or the internal temperature θ (Chapter 5). The particular choice of functional dependence

$$\boldsymbol{\sigma} = F(\boldsymbol{\varepsilon}, \psi, \theta, \ldots)$$

is a question of modeling. Once the functional dependence has been determined it can be substituted in equation (2.5) and the resulting PDE will describe the dynamics of the system in terms of the physical parameters and the external forces. Many different choices, applicable to a wide range of elastic solids have been tried in the literature. Throughout this work explore three particular choices relating linearly the stress tensor to the strain, the strain and the electric potential, and the strain and the temperature.

The simplest constitutive relation between the shear and the stress tensors for a general inhomogeneous and anisotropic material is given by Hooke's Law

$$\boldsymbol{\sigma} = \mathbf{C}\,\boldsymbol{\varepsilon}. \tag{2.8}$$

Here for every $\mathbf{x} \in \Omega_-$ the *elastic stiffness tensor* $\mathbf{C}(\mathbf{x})$ is a fourth order tensor that will be assumed to satisfy the following properties

$$\mathrm{C}_{ijkl} \in L^\infty(\Omega_-)\,, \quad \mathrm{C}_{ijkl} = \mathrm{C}_{jikl} = \mathrm{C}_{klij}, \qquad (i,j,k,l = 1,\ldots,d),$$

and that for any symmetric matrix $\mathbf{M} \in \mathbb{R}^{d\times d}_{sym}$ there exists $c_0 > 0$ such that for almost every $\mathbf{x} \in \Omega_-$

$$c_0\mathbf{M} : \mathbf{M} \leq \mathbf{C}(\mathbf{x})\mathbf{M} : \mathbf{M}.$$

In analogy with the scalar case it will be useful to define the space

$$\mathbf{H}^1_{\Delta^*}(\mathbb{R}^d \setminus \Gamma) := \left\{\mathbf{u} \in \mathbf{H}^1(\mathbb{R}^d \setminus \Gamma) : \nabla \cdot \boldsymbol{\sigma}(\mathbf{u}) \in \mathbf{L}^2(\mathbb{R}^d \setminus \Gamma)\right\}$$

and endow it with the norm

$$\|\mathbf{u}\|^2_{\Delta^*} := \|\mathbf{u}\|^2_{\mathbb{R}^d} + \|\nabla\mathbf{u}\|^2_{\mathbb{R}^d\setminus\Gamma} + \|\nabla\cdot\boldsymbol{\sigma}(\mathbf{u})\|^2_{\mathbb{R}^d\setminus\Gamma}.$$

For functions from this space and under the above assumptions on $\mathbf{C}$, a simple application of the divergence theorem yields the following generalization of Green's identity which we use as a definition of the weak normal traction. Let $\Omega_- \subset \mathbb{R}^d$ be an open domain with Lipschitz boundary Γ and let $\mathbf{u} \in \mathbf{H}^1_{\Delta^*}(\mathbb{R}^d \setminus \Gamma)$, then

$$\langle \boldsymbol{\sigma}(\mathbf{u})\,\boldsymbol{\nu}^{\mp}, \gamma\mathbf{v}\rangle_\Gamma := \pm(\boldsymbol{\sigma}(\mathbf{u}), \boldsymbol{\varepsilon}(\mathbf{v}))_{\Omega_\mp} \pm (\nabla\cdot\boldsymbol{\sigma}(\mathbf{u}), \mathbf{v})_{\Omega_\mp} \qquad \forall \mathbf{v} \in \mathbf{H}^1(\mathbb{R}^d). \tag{2.9}$$

This result, known as Betti's formula, plays the role of an integration by parts formula and will be used extensively.

2.8 Navier-Lamé Equations: Rigid Motions, Pressure, and Shear Waves

For the remaining of this chapter we will consider that the elastic medium is isotropic. Under these conditions (see for instance [47, 77]), the stiffness tensor is diagonal and can be expressed in terms of two independent parameters as

$$\mathrm{C}_{ijkl} = \lambda\delta_{ij}\delta_{kl} + \mu(\delta_{ik}\delta_{jl} + \delta_{il}\delta_{jk}), \tag{2.10}$$

where the Kronecker symbol δ_{ij} denotes the components of the $d \times d$ identity matrix, and the parameters μ and λ (known as the *shear modulus* and *Lamé's second parameter* respectively) are functions in $L^\infty(\Omega_-)$ satisfying almost everywhere in Ω_-

$$\mu > 0 \qquad \text{and} \qquad \lambda + \tfrac{2}{3}\mu > 0.$$

These quantities have physical interpretation: the shear modulus μ is a measure of the medium's resistance to shear strains, while the *bulk modulus* $\mathrm{K} := \lambda + \frac{2}{3}\mu$ measures the resistance to uniform compression. Both of them have units of pressure.

With this assumption, Hooke's law (2.8) reads

$$\sigma_{ij} = 2\mu\varepsilon_{ij} + \lambda\partial_k u_k \delta_{ij},$$

and upon substitution of this expression into the equation of balance of forces (2.7) we obtain the Navier-Lamé equations for the elastic displacement vector $\mathbf{u}$

$$\nabla\cdot(2\mu\boldsymbol{\varepsilon}(\mathbf{u}) + \lambda\nabla\cdot\mathbf{u}\,\mathbf{I}) + \mathbf{f} = \rho_\Sigma\ddot{\mathbf{u}} \qquad \text{in } \Omega_-. \tag{2.11}$$

The case of varying coefficients will be treated in Chapters 4 through 6, but for the time being we will focus on a homogeneous solid for which both λ and μ are constant. We would like to find out if in the absence of external forces ($\mathbf{f} = \mathbf{0}$) equation (2.11) admits traveling wave solutions, i.e. non trivial elastic displacements of the form

$$\mathbf{u}(ct - \mathbf{x} \cdot \mathbf{d}),$$

where c is the constant propagation speed and $\mathbf{d}$ is a unit vector pointing towards the direction in which the wave propagates. Letting

$$\mathbf{u}' := \frac{d\mathbf{u}}{ds}, \qquad s := ct - \mathbf{x} \cdot \mathbf{d},$$

a simple application of the chain rule yields for the components of the elastic displacement

$$\ddot{u}_i = c^2 u_i'' \qquad \text{and} \qquad \partial_j u_i = -d_j u_i'.$$

Substituting these expressions into (2.11), recalling that $\|\mathbf{d}\|^2 = d_i d_i = 1$, and simplifying it follows that the components of the traveling wave must satisfy

$$\mu u_i'' + (\mu + \lambda) d_i d_j u_j'' = \rho_\Sigma c^2 u_i''. \tag{2.12}$$

Multiplying both sides by d_i this implies

$$(2\mu + \lambda - \rho_\Sigma c^2) d_j u_j'' = 0.$$

We must consider three distinct cases:

(a) If $u_j'' = 0$ for all $j = 1, \ldots, d$ we have the simplest instance for which the last equation holds. In this case

$$u_j = a_j(ct - x_k d_k) + b_j$$

for constants $a_j, b_j \in \mathbb{R}$ and hence

$$\mathbf{u} = -(\mathbf{a} \otimes \mathbf{d})\,\mathbf{x} + ct\mathbf{a} + \mathbf{b}$$

is an infinitesimal rigid motion.

(b) If $d_j u_j'' = 0$ and the wave is not a rigid motion then the elastic displacement and the propagation direction are orthogonal and we call the wave a *shear wave*. Moreover, (2.12) becomes

$$\mu u_i'' = \rho_\Sigma c^2 u_i''$$

and since we have excluded rigid motions we must have for the propagation speed

$$c_T := \sqrt{\frac{\mu}{\rho_\Sigma}}. \tag{2.13}$$

The subscript T in the definition stresses the fact that shear waves are transversal.

(c) If $2\mu + \lambda = \rho_\Sigma c^2$, then we define

$$c_L := \sqrt{\frac{\lambda + 2\mu}{\rho_\Sigma}}, \tag{2.14}$$

and (2.12) implies that

$$u_i'' = d_i d_j u_j''.$$

If $\mathbf{u}$ is not a rigid motion, then the last equality implies that the elastic displacement is parallel to the direction of propagation. In this case we call the wave a *pressure wave*; the subscript L on the definition of the wave speed stands for the fact that pressure waves are longitudinal.

2.9 The Resolvent Elastic Equation and its Calderón Calculus

This section uses some non-standard language on vector-valued causal distributions (see Appendix A). When the transient elastic wave equation (2.7) is considered in absence of forcing terms and in the sense of causal tempered distributions $\mathrm{CT}(\mathbf{H}^1_{\Delta^*}(\Omega_\pm))$, its Laplace transform is given by

$$\rho_\Sigma\, s^2\, \mathbf{u} = \nabla \cdot \boldsymbol{\sigma}(\mathbf{u}). \tag{2.15}$$

(We will use the same symbol for the unknown of the time domain and in the Laplace domain, since the treatment will always be done separately.) The time-harmonic wave equation is equation (2.15) with $s = -\imath\omega$, where ω is the frequency. We note that when

(2.15) is posed in an exterior domain like Ω^+ it requires the Kupradze-Sommerfeld radiation condition at infinity (see for instance [3, Section 2.4.3]), but when s takes values in $\mathbb{C}_+ := \{s \in \mathbb{C} : \mathrm{Re}\, s > 0\}$, the radiation condition is substituted by demanding that $\mathbf{u} \in \mathbf{H}^1(\Omega_+)$.

Let us now consider for any $s \in \mathbb{C}_+$, the transmission problem

$$\begin{aligned} \rho_\Sigma\, s^2\, \mathbf{u} &= \nabla \cdot \boldsymbol{\sigma}(\mathbf{u}) \qquad \text{in } \mathbb{R}^2 \setminus \Gamma, \\ [\![\boldsymbol{\gamma}\mathbf{u}]\!] &= \boldsymbol{\psi} \in \mathbf{H}^{1/2}(\Gamma), \\ [\![\boldsymbol{t}\mathbf{u}]\!] &= \boldsymbol{\eta} \in \mathbf{H}^{-1/2}(\Gamma), \end{aligned} \tag{2.16}$$

admits a unique solution in the Sobolev space $\mathbf{H}^1(\mathbb{R}^2 \setminus \Gamma)$, as follows from a simple variational argument. The solution of this problem is a linear function of the densities $\boldsymbol{\psi}$ and $\boldsymbol{\eta}$ and will be written in the form

$$\mathbf{u} = \mathbf{S}(s)\boldsymbol{\eta} - \mathbf{D}(s)\boldsymbol{\psi}. \tag{2.17}$$

The operators $\mathbf{S}(s)$ and $\mathbf{D}(s)$ are respectively called the single and double layer resolvent elastic potentials. For the particular case when $s = -ik$ they reduce to the elastodynamic Single and Double layer potentials. By definition,

$$[\![\boldsymbol{\gamma}\mathbf{S}(s)\boldsymbol{\eta}]\!] = \mathbf{0}, \qquad [\![\boldsymbol{t}\mathbf{S}(s)\boldsymbol{\eta}]\!] = \boldsymbol{\eta}, \qquad [\![\boldsymbol{\gamma}\mathbf{D}(s)\boldsymbol{\psi}]\!] = -\boldsymbol{\psi}, \qquad [\![\boldsymbol{t}\mathbf{D}(s)\boldsymbol{\psi}]\!] = \mathbf{0}, \tag{2.18}$$

for arbitrary densities $\boldsymbol{\eta}$ and $\boldsymbol{\psi}$. We then define the four associated boundary integral operators

$$\mathbf{V}(s)\boldsymbol{\eta} := \{\!\{\boldsymbol{\gamma}\mathbf{S}(s)\boldsymbol{\eta}\}\!\}, \qquad \mathbf{K}^t(s)\boldsymbol{\eta} := \{\!\{\boldsymbol{t}\mathbf{S}(s)\boldsymbol{\eta}\}\!\}, \tag{2.19a}$$

$$\mathbf{K}(s)\boldsymbol{\psi} := \{\!\{\boldsymbol{\gamma}\mathbf{D}(s)\boldsymbol{\psi}\}\!\}, \qquad \mathbf{W}(s)\boldsymbol{\psi} := -\{\!\{\boldsymbol{t}\mathbf{D}(s)\boldsymbol{\psi}\}\!\}. \tag{2.19b}$$

Explicit integral expressions of the potentials and operators (2.17) and (2.19) in two dimensions will be given in Chapter 2. The expressions in three dimensions can be found in [76, 3]. Given (2.18)-(2.19) we can easily derive the jump relations:

$$\boldsymbol{\gamma}^{\pm}\mathbf{S}(s) = \mathbf{V}(s), \qquad \boldsymbol{t}^{\pm}\mathbf{S}(s) = \mp\tfrac{1}{2}\mathbf{I} + \mathbf{K}^t(s), \tag{2.20a}$$

$$\boldsymbol{\gamma}^{\pm}\mathbf{D}(s) = \pm\tfrac{1}{2}\mathbf{I} + \mathbf{K}(s), \qquad \boldsymbol{t}^{\pm}\mathbf{D}(s) = -\mathbf{W}(s). \tag{2.20b}$$

The operators (2.19) receive the following respective names: single layer, transpose double layer, double layer, and hypersingular operators.

2.10 The Resolvent Acoustic Equation and its Calderón Calculus

We now define the acoustic counterpart of the operators of the previous section and some essential properties the will be used constantly on this work, a thorough treatment and explicit expressions of the potentials and operators can be found in [69]. The single and double layer operators associated to the Laplace resolvent equation (the Laplace transform of the wave equation) can be defined as the solution of a transmission problem. For given $(\varphi, \eta) \in H^{1/2}(\Gamma) \times H^{-1/2}(\Gamma)$ and any $s \in \mathbb{C}_+$, the problem of finding $v \in H^1(\mathbb{R}^d \setminus \Gamma)$ satisfying

$$\begin{aligned} \Delta v - (s/c)^2 v = 0 \qquad & \text{in } \mathbb{R}^d \setminus \Gamma, \\ [\![\gamma v]\!] = \varphi, & \\ [\![\partial_\nu v]\!] = \eta, & \end{aligned} \tag{2.21}$$

has a unique solution, which we write in terms of two linear operators, known as the single (S) and double (D) layer potentials

$$v = \mathrm{S}(s/c)\eta - \mathrm{D}(s/c)\varphi. \tag{2.22}$$

These potentials satisfy jump relations completely analogous to those of the elastic operators, namely

$$[\![\gamma \mathrm{S}(s)\eta]\!] = 0, \qquad [\![\partial_\nu \mathrm{S}(s)\eta]\!] = \eta, \qquad [\![\gamma \mathrm{D}(s)\psi]\!] = -\psi, \qquad [\![\partial_\nu \mathrm{D}(s)\psi]\!] = 0. \tag{2.23}$$

Associated to the potentials, we can define four integral operators

$$\mathrm{V}(s) := \{\!\{\gamma \cdot \}\!\}\mathrm{S}(s) = \gamma \mathrm{S}(s), \qquad \mathrm{K}(s) := \{\!\{\gamma \cdot \}\!\}\mathrm{D}(s), \tag{2.24a}$$

$$\mathrm{K}^t(s) := \{\!\{\partial_\nu \cdot \}\!\}\mathrm{S}(s), \qquad \mathrm{W}(s) := -\{\!\{\partial_\nu \cdot \}\!\}\mathrm{D}(s) = -\partial_\nu \mathrm{D}(s). \tag{2.24b}$$

These operators satisfy the limit identities (jump relations)

$$\gamma^{\pm}\mathrm{S}(s) = \mathrm{V}(s), \qquad \partial_\nu \pm \mathrm{S}(s) = \mp \tfrac{1}{2}\mathrm{I} + \mathrm{K}^t(s), \tag{2.25a}$$

$$\gamma^{\pm}\mathrm{D}(s) = \pm \tfrac{1}{2}\mathrm{I} + \mathrm{K}(s), \qquad \partial_\nu^{\pm}\mathrm{D}(s) = -\mathrm{W}(s). \tag{2.25b}$$

Chapter 3

FULL DISCRETIZATION OF THE 2D ELASTODYNAMIC CALDERÓN CALCULUS

In this Chapter we deal with work that was published in the paper *A fully discrete Calderón calculus for the two-dimensional elastic wave equation* [34], done in collaboration with Víctor Domínguez and Francisco-Javier Sayas, concerning the simultaneous discretization of all integral operators that appear in the Calderón projector for the time-harmonic elastic wave equation on a smooth parameterizable curve in the plane. We give experimental evidence that the method proposed is of order three for all computed quantities in the boundary, and also for potential postprocessings. The work is an extension of the `deltaBEM` method developed in [31] for the Helmholtz equation, where a fully discrete Calderón calculus for the acoustic wave equation was developed.

Unlike that case, where a one-parameter family of discretizations was defined, we will give mathematical evidence that for elastodynamics there is a single third-order method of this family. To obtain a fully discrete method for transient problems we take advantage of Lubich's Convolution Quadrature techniques [89, 90, 91].

The chapter is structured as follows. We first provide a short background for reduced quadrature methods for periodic integral equations on smooth plane curves. In Section 3.2 we introduce the main discrete elements (sampling of the curve, mixing matrices) and give a general interpretation of the methods to be defined as non-conforming Petrov-Galerkin methods with very precisely chosen quadrature approximation. In Sections 3.3 and 3.4 we present respectively the discrete layer potentials and integral operators. In Section 3.5 we give mathematical justification of why the shape of the testing devices (that were named "fork" and "ziggurat" in [31]) provides order three

consistency errors for the periodic Hilbert transform, which is the only integral operator that appears in the set of boundary integral equations for elasticity and not for acoustic waves. In Section 3.6 we give a treatment of smooth open arcs using a double cosine sampling of the arc and repeating the same ideas of the previous sections. Finally, in 3.7 we present numerical experiments and convergence studies in the frequency domain, the time domain (using Convolution Quadrature) and for crack problems.

Some background. Let us first give some context to this work. Quadrature methods for periodic integral (and pseudo-differential) equations appeared in the work of Jukka Saranen. In particular, in [111], it was discovered that logarithmic integral equations can be given a very simple treatment providing methods of order two with simple-minded discretization arguments, as long as some parameters were chosen in a particular (and not easy to justify) way. Related references are [112], [119], and [22]. Exploiting these ideas, an equally simple quadrature method of order three for a system of integral equations, that combined the single layer and double layer operators, was given in [33]. A recent article [32] opened new ways by offering an extremely simple form of discretizing the hypersingular operator associated to the Helmholtz equation in a smooth closed curve. As a consequence, there was a chance of creating a full discretization of all operators for the Helmholtz equation [30], using $\mathcal{O}(N^2)$ evaluations of the kernels and obtaining second order approximations for all unknowns in a wide collection of integral equations that could be discretized simultaneously. It was then in [31] where it was discovered that a symmetrization process led to order three discretizations. Consistency error estimates for the second order methods were given in [30], taking advantage of already existing results. The consistency analysis of the order three methods is the subject of current research.

There are two reasons why the extension of the techniques of [31] to the realm of elastic waves is not straightforward. The first of them is the fact that the double layer operator and its adjoint contain a strongly singular operator (a perturbation of the periodic Hilbert transform) that makes the operators of the second kind much more difficult to handle. We show (with experiments and with rigorous mathematical

justification) that the consistency error of our type of discretizations when applied to the periodic Hilbert transform has order three. The second difficult ingredient is the need for a regularized formula (à la Nédélec-Maue) that is compatible with our way of discretizing the other operators. While the regularized formula for static elasticity is easy to find in the literature [103], the dynamic case is much more involved. For instance, in [23] the authors opt for a subtraction technique, where the regularized static hypersingular operator is used and then the difference between the time-harmonic and the static operators is prepared for discretization. Here we will use a formula due to Frangi and Novati [49], which we fully develop so that our results can be easily replicated. For more literature on regularization of hypersingular operators in elastodynamics we refer to [49].

Remark. In this chapter the adjoint double layer operator will be denoted by $\mathbf{J}(s)$ instead of the usual notation $\mathbf{K}^t(s)$. This is due to the fact that the discretization of $\mathbf{K}(s)$ and its adjoint will be done separately, in different discrete spaces and not by transposition.

3.1 Problem Statement

The distributional version of the transmission problem (2.16)

$$\rho_\Sigma\, s^2\, \mathbf{u} = \nabla \cdot \boldsymbol{\sigma}(\mathbf{u}) \quad \text{in } \mathbb{R}^2 \setminus \Gamma, \qquad [\![\boldsymbol{\gamma}\mathbf{u}]\!] = \boldsymbol{\psi}, \qquad [\![\boldsymbol{t}\mathbf{u}]\!] = \boldsymbol{\eta},$$

will be considered for the case when Γ is a smooth 1-periodic parametrized curve and the two parametrized densities $\boldsymbol{\psi}, \boldsymbol{\eta} : \mathbb{R} \to \mathbb{C}^2$ are vector-valued smooth 1-periodic functions. In this chapter we are not going to worry about the construction of well-posed integral equations for different boundary value problems for the elasticity equation (2.15). Instead, following [30]-[31], we will simultaneously discretize the potentials (2.17), the operators (2.19), and the two identity operators in (2.20) in a way that is stable and compatible, so that all these elements can be used to build discrete counterparts of well-posed boundary integral equations for elastic waves.

We will assume that the closed simple curve $\Gamma \subset \mathbb{R}^2$ separating a bounded domain Ω^- from its exterior Ω^+ is given by a smooth, positively oriented, 1-periodic parametrization

$$\mathbf{x} = (x_1, x_2) : \mathbb{R} \to \Gamma$$

satisfying $|\mathbf{x}'(t)| > 0$ for all t. For a given smooth enough vector field $\mathbf{u} : \mathbb{R}^2 \setminus \Gamma \to \mathbb{R}^2$, we will define its parametrized traces (in the style of [75, Section 8.2])

$$\boldsymbol{\gamma}^{\pm}\mathbf{u} := \mathbf{u}^{\pm} \circ \mathbf{x} : \mathbb{R} \to \mathbb{R}^2.$$

The parametrized normal tractions on both sides of Γ are defined by

$$\boldsymbol{t}^{\pm}\mathbf{u} := (\boldsymbol{\sigma}(\mathbf{u}) \circ \mathbf{x})\boldsymbol{\nu} : \mathbb{R} \to \mathbb{R}^2.$$

Note that the choice for a non-normalized normal vector field simplifies a boundary-parametrized version of Betti's formula (2.9)

$$\int_{\Omega^{\pm}} \Big(\boldsymbol{\sigma}(\mathbf{u}) : \nabla \mathbf{v} + (\nabla \cdot \boldsymbol{\sigma}(\mathbf{u})) \cdot \mathbf{v} \Big) = \mp \int_0^1 (\boldsymbol{t}^{\pm}\mathbf{u})(\tau) \cdot (\boldsymbol{\gamma}^{\pm}\mathbf{v})(\tau) \mathrm{d}\tau,$$

where the divergence operator acts row-wise when applied to a matrix-valued function.

3.2 Discrete Elements and Mixing Operators

The curve Γ will be sampled three times, once for the location for densities (sources) and twice for the location of collocation points (targets). The sampling is exactly the same as in [31]. We choose a positive integer N, define $h := 1/N$ and sample midpoints, breakpoints, and normals on the main grid (sources):

$$\mathbf{m}_j := \mathbf{x}(j\,h), \qquad \mathbf{b}_j := \mathbf{x}((j - \tfrac{1}{2})\,h), \qquad \boldsymbol{\nu}_j := h\boldsymbol{\nu}(j\,h). \tag{3.1}$$

This is done for $j \in \mathbb{Z}_N$, that is, the points are indexed modulo N. We then repeat the same process by shifting the uniform grid in parametric spaces $\pm h/6$:

$$\mathbf{m}_i^{\pm} := \mathbf{x}((i \pm \tfrac{1}{6})\,h), \qquad \mathbf{b}_i^{\pm} := \mathbf{x}((i - \tfrac{1}{2} \pm \tfrac{1}{6})\,h), \qquad \boldsymbol{\nu}_i^{\pm} := h\boldsymbol{\nu}((i \pm \tfrac{1}{6}\,h). \tag{3.2}$$

This is all the information that is needed from the parametric curve Γ. Once these elements are sampled, we do not need the parametrization of the curve any longer. It

is important to emphasize that all the following constructions *can be easily extended to multiple scatterers.* The details are given in [31]. As explained in that reference, we only need to create a next-index counter. The choice of the $\pm 1/6$ shifting parameter is justified in [31, Section 4] by an argument that chooses the optimal shifting of a trapezoidal rule applied to periodic logarithmic operators. This idea can be traced back to [111]. In short, if $\log_{\#}(t) := \log(4\sin^2(\pi t))$ is a periodic logarithmic function, then for a smooth enough 1-periodic function ϕ

$$\int_0^1 \log_{\#}(t-\tau)\,\phi(\tau)\mathrm{d}\tau - h\sum_{j=1}^{N}\log_{\#}(t-j\,h)\phi(j\,h) = \mathcal{O}(h^2) \quad \Longleftrightarrow \quad t = (i \pm \tfrac{1}{6})\,h. \tag{3.3}$$

In order to introduce some matrices relevant to the method, we will use the following notation: $\mathrm{TC}(a_1,\ldots,a_N)$ is the Toeplitz Circulant matrix whose first row is the vector $(a_1,\ldots,a_N)$.

We first introduce a block-diagonal matrix with circulant tridiagonal blocks:

$$\mathrm{Q} := \begin{bmatrix} \mathrm{Q}_{\mathrm{sc}} & 0 \\ 0 & \mathrm{Q}_{\mathrm{sc}} \end{bmatrix}, \qquad \mathrm{Q}_{\mathrm{sc}} := \tfrac{1}{24}\,\mathrm{TC}\,(22,1,0,\ldots,0,1)\,. \tag{3.4}$$

The coefficients of the 'scalar' operator Q_{sc} are related to a look-around quadrature formula

$$\int_{-\frac{1}{2}}^{\frac{1}{2}} \phi(t)\mathrm{d}t \approx \frac{1}{24}(\phi(-1) + 22\phi(0) + \phi(1)), \tag{3.5}$$

which has degree of precision three. We also need two matrices that will be used for averaging the information on the two observation grids. Both of them are block diagonal with circulant bidiagonal blocks:

$$\mathrm{P}^{\pm} := \begin{bmatrix} \mathrm{P}^{\pm}_{\mathrm{sc}} & 0 \\ 0 & \mathrm{P}^{\pm}_{\mathrm{sc}} \end{bmatrix}, \qquad \mathrm{P}^{+}_{\mathrm{sc}} := \tfrac{1}{12}\,\mathrm{TC}(5,0,\ldots,0,1), \qquad \mathrm{P}^{-}_{\mathrm{sc}} := (\mathrm{P}^{+}_{\mathrm{sc}})^t. \tag{3.6}$$

The matrices $\mathrm{P}^{\pm}_{\mathrm{sc}}$ are particular cases of a one-parameter dependent construction of numerical schemes in [31]. As we will justify in Section 3.5, this is the right choice of parameters to sample correctly some periodic Hilbert transforms that appear in the double layer operator and its transpose.

In this context, the identity operator will be approximated by the block-diagonal matrix

$$\mathrm{M} := \begin{bmatrix} \mathrm{M}_{\mathrm{sc}} & 0 \\ 0 & \mathrm{M}_{\mathrm{sc}} \end{bmatrix}, \qquad \mathrm{M}_{\mathrm{sc}} := \tfrac{1}{9}\mathrm{TC}(7, 1, 0, \ldots, 0, 1). \tag{3.7}$$

The final matrix to be introduced in this section corresponds to differentiation:

$$\mathrm{D} := \begin{bmatrix} \mathrm{D}_{\mathrm{sc}} & 0 \\ 0 & \mathrm{D}_{\mathrm{sc}} \end{bmatrix}, \qquad \mathrm{D}_{\mathrm{sc}} := \mathrm{TC}(-1, 1, 0, \ldots, 0). \tag{3.8}$$

A formal explanation. After parametrization (see the formulas in Sections 3.3 and 3.4), potentials and integral operators for two-dimensional linear elasticity can be seen as acting on periodic functions and, in the case of the integral operators, outputting periodic functions. In the variational theory for boundary integral equations, traces take values in the Sobolev space $H^{1/2}(\Gamma)$ and normal stresses in its dual $H^{-1/2}(\Gamma)$. These spaces are used as trial spaces and also as test spaces. The main idea behind the methods in [31] (a paper devoted to acoustic waves) is using a *non-conforming* discretization for the spaces $H^{\pm 1/2}$, which are the 1-periodic Sobolev spaces we obtain after parametrizing Γ in $H^{\pm 1/2}(\Gamma)$. Let now δ_t denote the periodic Dirac delta concentrated at the point t, or, better said, the Dirac comb concentrated at $t + \mathbb{Z}$. There are four kinds of elements in the discrete Calderón calculus:

- The unknowns that live in $H^{-1/2}$ are approximated by linear combinations of δ_{jh}.
- Whenever $H^{-1/2}$ plays the role of a test space (i.e., the output of the operator is in $H^{1/2}$), we use a testing device made of symmetric combinations of Dirac deltas in the companion meshes:

  $$\frac{a}{2}(\delta_{(i-1/6)h} + \delta_{(i+1/6)h}) + \frac{1-a}{2}(\delta_{(i-5/6)h} + \delta_{(i+5/6)h}). \tag{3.9}$$

  As we have already mentioned, the choice of moving the grid $\pm 1/6h$ is forced by the need to correctly sample the logarithmic kernel singularities (3.3). By periodicity, the grids displaced $\pm 5/6h$ are the same as those displaced $\mp 1/6h$, and therefore, all Dirac deltas in the testing device (3.9) satisfy the second order condition (3.3). Third order is actually attained thanks to symmetry in (3.9).

- For unknowns in $H^{1/2}$, we use piecewise constant functions, spanned by the periodic characteristic functions defined by $\chi'_j = \delta_{(j-1/2)h} - \delta_{(j+1/2)h}$.

- When $H^{1/2}$ is used as a test space (i.e., the operator has output in $H^{-1/2}$), we test the equation by the piecewise constant functions ξ_i defined by

$$\begin{aligned}\xi'_i &= \frac{a}{2}(\delta_{(i-1/2-1/6)h} + \delta_{(i-1/2+1/6)h}) + \frac{1-a}{2}(\delta_{(i-1/2-5/6)h} + \delta_{(i-1/2+5/6)h}) \\ &\quad -\frac{a}{2}(\delta_{(i+1/2-1/6)h} + \delta_{(i+1/2+1/6)h}) - \frac{1-a}{2}(\delta_{(i+1/2-5/6)h} + \delta_{(i+1/2+5/6)h}).\end{aligned}$$

Whenever a Dirac delta acts on a kernel (as input or as a test), this one is automatically evaluated and there is no need for further approximation. Nevertheless, if a piecewise constant function is used, there are still integrals to be approximated. These are decomposed as combinations of integrals of the kernels on intervals of length h and then approximated using the look-around formula (3.5). As shown in [31], all values of $a \in [1/2, 1]$ give order three methods valid for the acoustic Calderón calculus. The choice $a = 1$ gives the simplest test functions. The choice $a = 5/6$ gives the linear combinations that produce the mixing matrices (3.6). The corresponding testing devices were named the fork and the ziggurat (see Figure 3.1). We will see in Section 3.5 that this choice is the only one that provides order-three discretizations of the Hilbert transform-style operators that appear in elastodynamics and not in scalar waves.

3.3 Layer Potentials

Densities will be discretizations of 1-periodic vector fields. At the discrete level, these will become vectors in $\mathbb{C}^{2N} \equiv \mathbb{C}^N \times \mathbb{C}^N$. In principle, we will think of discrete densities as vectors of $2N$ entries, where the first N entries discretize the first component of the continuous vector field, and are followed by N entries for the second component. Consider then an operator $\mathbb{C}^{2N} \to \mathbb{C}^{2M}$, given through left-multiplication by a $(2M) \times (2N)$ matrix, say A. This matrix can be decomposed in four $M \times N$

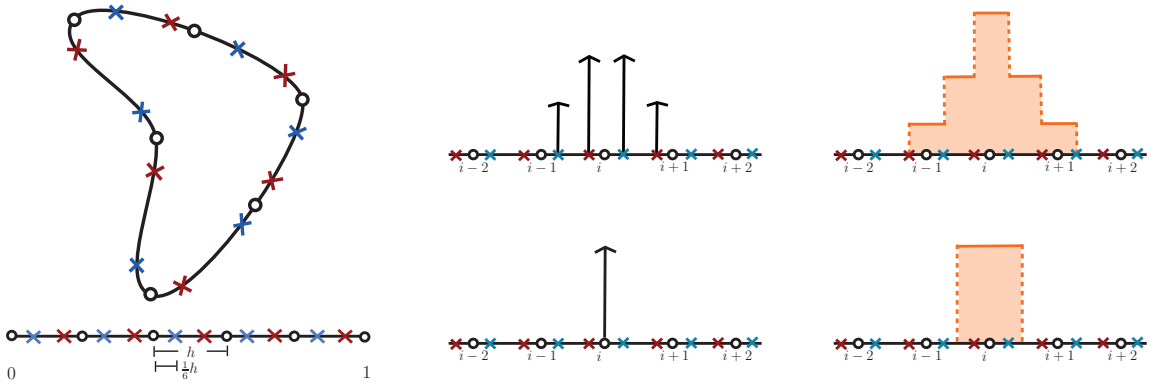

Figure 3.1: Left: A sketch of a sampled geometry and the companion grids on the scatterer (top) and on parametric space (bottom). The collocation points are shown as white dots, while the quadrature points are shown as crosses. Top Row : A sketch of the shapes of the fork and the ziggurat, the main testing devices of the fully discrete Calderón calculus. Bottom Row: The delta and piecewise trial functions for $H^{-1/2}$ and $H^{1/2}$ respectively.

blocks. Alternatively, in can be presented by MN blocks of 2×2 size. Thus, we will write

$$\mathrm{A}_{ij} := \begin{bmatrix} a_{ij} & a_{i,j+N} \\ a_{i+M,j} & a_{i+M,j+N} \end{bmatrix}$$

to make a simpler transition from the continuous expressions to the discrete ones.

In the expression for the fundamental solution of equation (2.15) we use of the definitions of the longitudinal and transversal speeds c_L and c_T given in (2.13), and (2.14) and will further denote

$$\xi := \frac{c_T}{c_L} = \sqrt{\frac{\mu}{\lambda + 2\mu}}.$$

We will make ample use of the modified Bessel function of the second kind and order n, K_n, for non-negative integer n. To translate from the Laplace domain notation to frequency domain notation, recall that $s = -\imath\omega$ and

$$K_n(s) = \frac{\pi\imath}{2} e^{\frac{n\pi\imath}{2}} H_n^{(1)}(\imath s) = \frac{\pi\imath}{2} e^{\frac{n\pi\imath}{2}} H_n^{(1)}(\omega).$$

The following two functions

$$\psi(r) := K_0(r/c_T) + \frac{c_T}{r}\left(K_1(r/c_T) - \xi K_1(r/c_L)\right), \tag{3.10a}$$

$$\chi(r) := K_2(r/c_T) - \xi^2 K_2(r/c_L), \tag{3.10b}$$

and their first derivatives will also be used.

The fundamental solution of the elastic wave equation (2.15) is given by:

$$\boldsymbol{E}(\mathbf{r};s) := \frac{1}{2\pi\mu}\left(\psi(s\,r)\mathbf{I}_2 - \frac{\chi(s\,r)}{r^2}\mathbf{r}\otimes\mathbf{r}\right), \quad r := |\mathbf{r}|, \quad \mathbf{r}\otimes\mathbf{r} := \begin{bmatrix} r_1^2 & r_2 r_1 \\ r_1 r_2 & r_2^2 \end{bmatrix}. \tag{3.11}$$

The parametrized single layer potential is given by

$$\mathbf{S}(s;\mathbf{z})\boldsymbol{\eta} := \int_0^1 \boldsymbol{E}(\mathbf{z}-\mathbf{x}(\tau);s)\boldsymbol{\eta}(\tau)\mathrm{d}\tau, \qquad \mathbf{z}\in\mathbb{R}^2\setminus\Gamma, \tag{3.12}$$

for a (1-periodic) density $\boldsymbol{\eta}:\mathbb{R}\to\mathbb{C}^2$. A discrete density $\boldsymbol{\eta}\in\mathbb{C}^{2N}$ (or, in functional notation, $\boldsymbol{\eta}:\mathbb{Z}_N\to\mathbb{C}^2$) can be presented by pairs of entries

$$\boldsymbol{\eta}_j := \begin{bmatrix} \eta_j \\ \eta_{j+N} \end{bmatrix}.$$

The associated discrete single layer potential is then defined by

$$\mathrm{S}_h(s;\mathbf{z})\boldsymbol{\eta} := \sum_{j=1}^{N} \boldsymbol{E}(\mathbf{z}-\mathbf{m}_j;s)\boldsymbol{\eta}_j \qquad \mathbf{z}\in\mathbb{R}^2\setminus\Gamma. \tag{3.13}$$

The kernel function for the elastic double layer potential

$$\mathbf{D}(s;\mathbf{z})\boldsymbol{\psi} := \int_0^1 \boldsymbol{T}(\mathbf{z}-\mathbf{x}(\tau),\boldsymbol{\nu}(\tau);s)\boldsymbol{\psi}(\tau)\mathrm{d}\tau, \qquad \mathbf{z}\in\mathbb{R}^2\setminus\Gamma, \tag{3.14}$$

is the function

$$\begin{aligned}\boldsymbol{T}(\mathbf{r},\boldsymbol{\nu};s) := & -\frac{s\,\psi'(s\,r)}{2\pi r}\left((\mathbf{r}\cdot\boldsymbol{\nu})\mathbf{I}_2 + \boldsymbol{\nu}\otimes\mathbf{r} + \frac{\lambda}{\mu}\mathbf{r}\otimes\boldsymbol{\nu}\right) \\ & + \frac{1}{2\pi}\chi(s\,r)\left(-\frac{4\mathbf{r}\cdot\boldsymbol{\nu}}{r^4}\mathbf{r}\otimes\mathbf{r} + \frac{1}{r^2}\boldsymbol{\nu}\otimes\mathbf{r} + \frac{\mathbf{r}\cdot\boldsymbol{\nu}}{r^2}\mathbf{I}_2 + \frac{1}{\xi^2 r^2}\mathbf{r}\otimes\boldsymbol{\nu}\right) \\ & + \frac{s}{2\pi}\chi'(s\,r)\left(\frac{2\mathbf{r}\cdot\boldsymbol{\nu}}{r^3}\,\mathbf{r}\otimes\mathbf{r} + \frac{\lambda}{\mu\,r}\mathbf{r}\otimes\boldsymbol{\nu}\right).\end{aligned} \tag{3.15}$$

The discrete double layer operator is thus related to the vector fields $\boldsymbol{T}(\mathbf{z}-\mathbf{m}_j,\boldsymbol{\nu}_j;s)$ but, instead of this kernel being used as in (3.13), it requires to plug the mixing matrix Q of (3.4) between the kernel and the density (recall the arguments given under the title *A formal explanation* in Section 3.2):

$$\mathrm{D}_h(s;\mathbf{z})\boldsymbol{\psi} := \sum_{j=1}^{N} \boldsymbol{T}(\mathbf{z}-\mathbf{m}_j,\boldsymbol{\nu}_j;s)\boldsymbol{\psi}_j^{\text{eff}}, \qquad \boldsymbol{\psi}^{\text{eff}} := \mathrm{Q}\boldsymbol{\psi}. \tag{3.16}$$

Let $\mathbf{u}^{\text{inc}}$ be an incident wave, be it a plane pressure or shear wave, or a cylindrical wave. We first sample it and its associated normal traction on both companion grids, creating four vectors ($\boldsymbol{\beta}_0^{\pm}\in\mathbb{C}^{2N}$ and $\boldsymbol{\beta}_1^{\pm}\in\mathbb{C}^{2N}$) with blocks

$$\boldsymbol{\beta}_{0,i}^{\pm} := \mathbf{u}^{\text{inc}}(\mathbf{m}_i^{\pm}), \qquad \boldsymbol{\beta}_{1,i}^{\pm} := \big(\boldsymbol{\sigma}(\mathbf{u}^{\text{inc}})(\mathbf{m}_i^{\pm})\big)\boldsymbol{\nu}_i^{\pm}. \tag{3.17}$$

The final version of the sampled incident wave involves the mixing operators the Section 3.2:

$$\boldsymbol{\beta}_0 := \mathrm{P}^{+}\boldsymbol{\beta}_0^{+} + \mathrm{P}^{-}\boldsymbol{\beta}_0^{-}, \qquad \boldsymbol{\beta}_1 := \mathrm{Q}(\mathrm{P}^{+}\boldsymbol{\beta}_1^{+} + \mathrm{P}^{-}\boldsymbol{\beta}_1^{-}). \tag{3.18}$$

3.4 Boundary Integral Operators

The parametrized integral expressions for the operators $\mathbf{V}(s)$, $\mathbf{K}(s)$, and $\mathbf{J}(s)$ in (2.19) use the fundamental solution (3.11) and the kernel (3.15):

$$(\mathbf{V}(s)\boldsymbol{\eta})(t) := \int_0^1 \boldsymbol{E}(\mathbf{x}(t)-\mathbf{x}(\tau);s)\boldsymbol{\eta}(\tau)\mathrm{d}\tau, \tag{3.19a}$$

$$(\mathbf{K}(s)\boldsymbol{\psi})(t) := \int_0^1 \boldsymbol{T}(\mathbf{x}(t)-\mathbf{x}(\tau),\boldsymbol{\nu}(\tau);s)\boldsymbol{\psi}(\tau)\mathrm{d}\tau, \tag{3.19b}$$

$$(\mathbf{J}(s)\boldsymbol{\eta})(t) := \int_0^1 \boldsymbol{T}(\mathbf{x}(\tau)-\mathbf{x}(t),\boldsymbol{\nu}(t);s)^t\boldsymbol{\eta}(\tau)\mathrm{d}\tau. \tag{3.19c}$$

Discretization is carried out in two steps. In a first step, two one-sided operators are produced for each operator:

$$\mathrm{V}_{ij}^{\pm}(s) := \boldsymbol{E}(\mathbf{m}_i^{\pm}-\mathbf{m}_j;s), \tag{3.20a}$$

$$\mathrm{K}_{ij}^{\pm}(s) := \boldsymbol{T}(\mathbf{m}_i^{\pm}-\mathbf{m}_j,\boldsymbol{\nu}_j;s) \tag{3.20b}$$

$$\mathrm{J}_{ij}^{\pm}(s) := \boldsymbol{T}(\mathbf{m}_j-\mathbf{m}_i^{\pm},\boldsymbol{\nu}_i^{\pm};s)^t. \tag{3.20c}$$

Then the operators are mixed using the matrices (3.4) and (3.6):

$$\mathrm{V}_h(s) := \mathrm{P}^+\mathrm{V}_h^+(s) + \mathrm{P}^-\mathrm{V}_h^-(s), \tag{3.21a}$$

$$\mathrm{K}_h(s) := (\mathrm{P}^+\mathrm{K}_h^+(s) + \mathrm{P}^-\mathrm{K}_h^-(s))\mathrm{Q}, \tag{3.21b}$$

$$\mathrm{J}_h(s) := \mathrm{Q}(\mathrm{P}^+\mathrm{J}_h^+(s) + \mathrm{P}^-\mathrm{J}_h^-(s)). \tag{3.21c}$$

Here $\mathrm{V}_h^{\pm}(s)$, $\mathrm{K}_h^{\pm}(s)$, and $\mathrm{J}_h^{\pm}(s)$ are the matrices defined in (3.20).

The logic for the placement of Q in the above formulas can be intuited using the non-conforming Petrov-Galerkin interpretation of the method given at the end of Section 3.2 (see also [31]).

The hypersingular operator $\mathbf{W}(s)$ will be discretized after using a decomposition stemming from a regularization formula in [49]. In order to write it concisely we need to introduce some notation. The function

$$G(r) := \frac{1}{2\pi\rho_\Sigma}(K_0(r/c_T) - K_0(r/c_L))$$

plays a key role in the formula. Four functions are derived from it:

$$G_1(r) := \left(\frac{1}{r}\frac{\mathrm{d}}{\mathrm{d}r} + \frac{\mathrm{d}^2}{\mathrm{d}r^2}\right) G(r), \tag{3.22a}$$

$$G_2(r) := \left(\frac{1}{r}\frac{\mathrm{d}}{\mathrm{d}r} + \frac{\mathrm{d}^2}{\mathrm{d}r^2}\right) G_1(r) = \left(\frac{\mathrm{d}^4}{\mathrm{d}r^4} + \frac{2}{r}\frac{\mathrm{d}^3}{\mathrm{d}r^3} - \frac{1}{r^2}\frac{\mathrm{d}}{\mathrm{d}r^2} + \frac{1}{r^3}\frac{\mathrm{d}}{\mathrm{d}r}\right) G(r), \tag{3.22b}$$

$$A(r) := \frac{1}{r^2}G''(r) - \frac{1}{r^3}G'(r) = \frac{1}{r^2}\left(\frac{\mathrm{d}^2}{\mathrm{d}r^2} - \frac{1}{r}\frac{\mathrm{d}}{\mathrm{d}r}\right) G(r), \tag{3.22c}$$

$$B(r) := \frac{1}{r}G'(r) \tag{3.22d}$$

Note that the differential operators in (3.22a) and (3.22b) are the radial part of the two dimensional Laplacian and bi-Laplacian respectively. We will also use the matrix-valued functions

$$\boldsymbol{H}(\mathbf{r}; s) := s^2 A(s\,r)\mathbf{r}\otimes\mathbf{r} + B(s\,r)\boldsymbol{I}_2, \qquad r := |\mathbf{r}|, \tag{3.23a}$$

$$\boldsymbol{M}(\mathbf{r}, \boldsymbol{\nu}, \widetilde{\boldsymbol{\nu}}) := (\widetilde{\boldsymbol{\nu}}\otimes\boldsymbol{\nu})(\mathbf{r}\otimes\mathbf{r}) + (\mathbf{r}\otimes\mathbf{r})(\widetilde{\boldsymbol{\nu}}\otimes\boldsymbol{\nu}), \tag{3.23b}$$

$$M(\mathbf{r}, \boldsymbol{\nu}, \widetilde{\boldsymbol{\nu}}) := (\widetilde{\boldsymbol{\nu}}\otimes\boldsymbol{\nu}) : \mathbf{r}. \tag{3.23c}$$

Translating carefully the formulas in [49], we can write the hypersingular operator for the elastic wave equation in integro-differential (regularized) form

$$(\boldsymbol{W}(s)\boldsymbol{\psi})(t) := -\frac{\mathrm{d}}{\mathrm{d}t}\int_0^1 \boldsymbol{W}_0(\mathbf{x}(t)-\mathbf{x}(\tau);s)\frac{\mathrm{d}}{\mathrm{d}\tau}\boldsymbol{\psi}(\tau)\mathrm{d}\tau + \int_0^1 \boldsymbol{W}_1(\mathbf{x}(t)-\mathbf{x}(\tau),\boldsymbol{\nu}(t),\boldsymbol{\nu}(\tau);s)\boldsymbol{\psi}(\tau)\mathrm{d}\tau, \tag{3.24}$$

where

$$\boldsymbol{W}_0(\mathbf{r};s) := 4\mu^2 G_1(sr) - \boldsymbol{H}(\mathbf{r};s),$$

and

$$\begin{aligned}\boldsymbol{W}_1(\mathbf{r},\boldsymbol{\nu},\widetilde{\boldsymbol{\nu}};s) \;:=\; & \frac{\lambda+2\mu}{\lambda+\mu}s^2\Bigg(\mu G_2(sr)\Big(\lambda\widetilde{\boldsymbol{\nu}}\otimes\boldsymbol{\nu}+\mu\boldsymbol{\nu}\otimes\widetilde{\boldsymbol{\nu}}+\mu(\widetilde{\boldsymbol{\nu}}\cdot\boldsymbol{\nu})\,\boldsymbol{I}_2\Big)\\ & -\frac{1}{c_L^2}\Big(\lambda^2 G_1(sr)\widetilde{\boldsymbol{\nu}}\otimes\boldsymbol{\nu}\\ & \quad + s^2A(sr)\Big(2\lambda\mu\boldsymbol{M}(\mathbf{r},\boldsymbol{\nu},\widetilde{\boldsymbol{\nu}})+\mu^2 M(\mathbf{r},\boldsymbol{\nu},\widetilde{\boldsymbol{\nu}})\boldsymbol{I}_2+\mu^2\boldsymbol{M}(\mathbf{r},\widetilde{\boldsymbol{\nu}},\boldsymbol{\nu})\Big)\\ & \quad + B(sr)\Big(4\lambda\mu\widetilde{\boldsymbol{\nu}}\otimes\boldsymbol{\nu}+\mu^2(\widetilde{\boldsymbol{\nu}}\cdot\boldsymbol{\nu})\boldsymbol{I}_2+\mu^2 s\boldsymbol{\nu}\otimes\widetilde{\boldsymbol{\nu}}\Big)\\ & \quad + \mu^2(\widetilde{\boldsymbol{\nu}}\cdot\boldsymbol{\nu})\boldsymbol{H}(\mathbf{r};s)\Big)\Bigg).\end{aligned}$$

For discretization, we separate the two integral operators that appear in (3.24), building the blocks

$$\mathrm{W}^{\pm}_{ij,0}(s) := \boldsymbol{W}_0(\mathbf{b}_i^{\pm}-\mathbf{b}_j;s), \tag{3.25a}$$

$$\mathrm{W}^{\pm}_{ij,1}(s) := \boldsymbol{W}_1(\mathbf{m}_i^{\pm}-\mathbf{m}_j,\boldsymbol{\nu}_i^{\pm},\boldsymbol{\nu}_j;s), \tag{3.25b}$$

and then mix them using the expression

$$\mathrm{W}_h(s) := \mathrm{D}(\mathrm{P}^{+}\mathrm{W}^{+}_{0,h}(s)+\mathrm{P}^{-}\mathrm{W}^{-}_{0,h}(s))\mathrm{D}^t + \mathrm{Q}(\mathrm{P}^{+}\mathrm{W}^{+}_{1,h}(s)+\mathrm{P}^{-}\mathrm{W}^{-}_{1,h}(s))\mathrm{Q}. \tag{3.26}$$

For the sake of completeness we give here explicit expressions of all the functions that are involved in the definitions of the potentials and integral operators. First of all, we give the derivatives of the functions (3.10):

$$\begin{aligned}\psi'(r) &= -\frac{1}{c_T}K_1(r/c_T)-\frac{2c_T}{r^2}\left(K_1(r/c_T)-\xi K_1(r/c_L)\right)-\frac{1}{r}\left(K_0(r/c_T)-\xi^2K_0(r/c_L)\right),\\ \chi'(r) &= -\frac{1}{2c_T}\left(K_1(r/c_T)+K_3(r/c_T)-\xi^3\left(K_1(r/c_L)+K_3(r/c_L)\right)\right).\end{aligned}$$

The functions (3.22) are combinations of the following derivatives:

$$\begin{aligned}
G'(r) &= \frac{-1}{2\pi\rho_\Sigma c_T}\big(K_1(r/c_T) - \xi K_1(r/c_L)\big),\\
G''(r) &= \frac{1}{4\pi\rho_\Sigma c_T^2}\big(K_0(r/c_T) + K_2(r/c_T) - \xi^2(K_0(r/c_L) + K_2(r/c_L))\big),\\
G'''(r) &= \frac{-1}{8\pi\rho_\Sigma c_T^3}\big(3K_1(r/c_T) + K_3(r/c_T) - \xi^3(3K_1(r/c_L) + K_3(r/c_L))\big),\\
G^{(iv)}(r) &= \frac{1}{2\pi\rho_\Sigma c_T^4}\left(\left(\frac{3c_T^2}{r^2}+1\right)K_2(r/c_T) - \xi^4\left(\frac{3c_L^2}{r^2}+1\right)K_2(r/c_L)\right).
\end{aligned}$$

3.5 Discrete Treatment of Hilbert Transforms

In this section we justify the choice of parameters that are implicit to the definition of the mixing matrices (3.6). We recall that the paper [31] allowed for a one-parameter dependent family of test functions. The choice that produced the fork-and-ziggurat testing elements is the only one that works for the elasticity problem. The main element that appears in the elasticity integral operators **K** and **J** and does not appear in their acoustic counterparts is the periodic Hilbert transform:

$$(H\phi)(t) := \text{p.v.}\int_0^1 \cot(\pi(t-\tau))\phi(\tau)\mathrm{d}\tau. \tag{3.27}$$

(We note that it is customary to multiply this transform by the imaginary unit to relate it to the Hilbert transform on a circle.) For properties of this operator, we refer to [113, Section 5.7]. We will use that the periodic Hilbert transform commutes with differentiation, i.e., $(H\phi)' = H\phi'$, which follows from an easy integration by parts argument. A key result related to trapezoidal approximation of the Hilbert transform is given next. It is an easy consequence of a Lemma 3.3 proved at the end of this section.

Proposition 3.1. *Let $t_j := j\,h$ with $h := 1/N$ and consider the following subspaces of trigonometric polynomials*

$$\mathbb{T}_h := \text{span}\{e_n \,:\, -N/2 \le n < N/2\}, \qquad e_n(t) := \exp(2\pi\imath n t).$$

Then

$$h\sum_{j=1}^{N}\cot(\pi(t-t_j))\phi(t_j) = (H\phi)(t) + \cot(\pi t/h)\phi(t) \qquad \forall\phi\in\mathbb{T}_h. \tag{3.28}$$

Note that both sides of (3.28) blow up when $t/h \in \mathbb{Z}$. We now specialize this formula to $t = t_i^{\pm} := (i \pm \frac{1}{6})h$. For simplicity we will write $\alpha = \cot(\pi/6) = \sqrt{3}$. Using a density argument and Proposition 3.1, it is easy to see that for $\phi \in \mathcal{D} := \{\phi \in \mathcal{C}^\infty(\mathbb{R}) : \phi(1+\cdot) = \phi\}$, we have

$$h\sum_{j=1}^{N} \cot(\pi(t_i^{\pm} - t_j))\phi(t_j) = (H\phi)(t_i^{\pm}) \pm \alpha\phi(t_i^{\pm}) + \mathcal{O}(h^m) \qquad \forall m \in \mathbb{Z}. \tag{3.29}$$

In (3.29) and in the sequel, the Landau symbol will be used with the following precise meaning: $a_i = b_i + \mathcal{O}(h^m)$ denotes the existence of $C > 0$ independent of h such that that $\max_i |a_i - b_i| \le Ch^m$.

Motivated by the quadrature formula (3.5), we introduce the averaging operator

$$\Delta_h\phi := \tfrac{1}{24}\phi(\cdot - h) + \tfrac{11}{12}\phi + \tfrac{1}{24}\phi(\cdot + h),$$

and note that

$$(\Delta_h\phi)(t_j) = \phi(t_j) + \frac{h^2}{24}\phi''(t_j) + \mathcal{O}(h^4) \qquad \forall \phi \in \mathcal{D}. \tag{3.30}$$

Additionally, we consider the space of periodic piecewise constant functions

$$S_h := \{\phi_h : \mathbb{R} \to \mathbb{R} \,:\, \phi_h(1+\cdot) = \phi_h, \quad \phi_h|_{(t_i - h/2, t_i + h/2)} \in \mathbb{P}_0 \quad \forall i\}$$

and the operator $D_h : \mathcal{D} \to S_h$ given by

$$D_h\phi \in S_h, \qquad \widehat{D_h\phi}(\mu) = \widehat{\phi}(\mu), \qquad -N/2 \le \mu < N/2. \tag{3.31}$$

This operator is well defined since periodic piecewise constant functions on a regular grid can be determined by any sequence of N consecutive Fourier coefficients. (This fact seems to be known since at least the 1930s [109], as mentioned in [5].) In particular, this operator has excellent approximation properties in a wide range of negative Sobolev norms (see [4, Theorem 5.1]). In [35, Corollary 3.2] it is proved that

$$(D_h\phi)(t_j) = \phi(t_j) - \frac{h^2}{24}\phi''(t_j) + \mathcal{O}(h^4) \qquad \forall \phi \in \mathcal{D}. \tag{3.32}$$

The following approximations of the periodic Hilbert transform

$$(H_h\phi)(t) := h\sum_{j=1}^{N}\cot(\pi(t-t_j))(\Delta_h\phi)(t_j) \tag{3.33}$$

are relevant for our method, since for $\phi_h \in S_h$, we can write and approximate with (3.5):

$$\begin{aligned}(H\phi_h)(t) &= \sum_{j=1}^{N}\phi_h(t_j)\text{p.v.}\int_{t_j-h/2}^{t_j+h/2}\cot(\pi(t-\tau))\mathrm{d}\tau \\ &\approx h\sum_{j=1}^{N}\phi_h(t_j)(\Delta_h\cot(\pi(t-\cdot)))(t_j) = (H_h\phi_h)(t) \qquad t/h\notin\mathbb{Z}.\end{aligned}$$

This means that using piecewise constant functions as trial functions, and following the idea of using look-around quadrature for integrals over intervals of length h leads naturally to the operator H_h. Note now that

$$\max_j|\cot(\pi(t_i^{\pm}-t_j))| = \mathcal{O}(h^{-1}). \tag{3.34}$$

Therefore

$$\begin{aligned}(H_hD_h\phi)(t_i^{\pm}) =& (H_h\phi)(t_i^{\pm}) - \frac{h^2}{24}(H_h\phi'')(t_i^{\pm}) + \mathcal{O}(h^3) && \text{(by (3.32) and (3.34))}\\ =& h\sum_{j=1}^{N}\cot(\pi(t_i^{\pm}-t_j))\phi(t_j) + \mathcal{O}(h^3) && \text{(by (3.30) and (3.34))}\\ =& (H\phi)(t_i^{\pm}) \pm \alpha\phi(t_i^{\pm}) + \mathcal{O}(h^3), && \text{(by (3.29))}\end{aligned}$$

which, using Taylor expansions, implies that

$$\tfrac{1}{2}(H_hD_h\phi)(t_i^-) + \tfrac{1}{2}(H_hD_h\phi)(t_i^+) = \tfrac{1}{2}(H\phi)(t_i^-) + \tfrac{1}{2}(H\phi)(t_i^+) + \tfrac{1}{6}h\alpha\phi'(t_i) + \mathcal{O}(h^3).$$

Similarly

$$\tfrac{1}{2}(H_hD_h\phi)(t_{i+1}^-) + \tfrac{1}{2}(H_hD_h\phi)(t_{i-1}^+) = \tfrac{1}{2}(H\phi)(t_{i+1}^-) + \tfrac{1}{2}(H\phi)(t_{i-1}^+) - \tfrac{5}{6}h\alpha\phi'(t_i) + \mathcal{O}(h^3).$$

If we then denote (see (3.9))

$$\langle\varphi,\delta_i^\star\rangle := \frac{a}{2}(\varphi(t_i^-)+\varphi(t_i^+)) + \frac{1-a}{2}(\varphi(t_{i-1}^+)+\varphi(t_{i+1}^-)), \tag{3.35}$$

it follows that

$$\langle H_h D_h \phi, \delta_i^\star \rangle = \langle H\phi, \delta_i^\star \rangle + \alpha h \frac{6a-5}{6} \phi'(t_i) + \mathcal{O}(h^3),$$

which shows that $a = 5/6$ is the only choice that provides third order approximation.

In the above we have made use of the following technical results, in which for a given positive integer N we will write $h := 1/N$ and $t_j := j\,h$ for $j \in \mathbb{Z}$. We also let $\log_\# t := \log(4\sin^2(\pi t))$.

Lemma 3.2. *For all N and t*

$$\sum_{j=1}^{N} \log_\#(t - t_j) = \log_\#(t/h), \qquad t/h \notin \mathbb{Z}. \tag{3.36}$$

Proof. We recall the Fourier expansion of the periodic logarithm

$$\log_\# t = \lim_{M\to\infty} \sum_{0\neq n=-M}^{N} \frac{1}{|n|} e_n(t), \qquad e_n(t) := \exp(2\pi\imath n t). \tag{3.37}$$

Also

$$\sum_{j=1}^{N} e_n(t - jh) = e_n(t) \sum_{j=1}^{N} \exp\left(-\frac{2\pi\imath j n}{N}\right) = e_n(t) \begin{cases} N, & \text{if } n/N \in \mathbb{Z}, \\ 0, & \text{otherwise.} \end{cases} \tag{3.38}$$

Combining (3.37) and (3.38) it is easy to see that

$$\begin{aligned} \sum_{j=1}^{N} \log_\#(t - jh) &= \lim_{M\to\infty} \sum_{0\neq n=-M}^{M} \frac{1}{|nN|} N e_{nN}(t) \\ &= \lim_{M\to\infty} \sum_{0\neq n=-M}^{M} \frac{1}{|n|} e_n(t/h) = \log_\#(t/h). \end{aligned}$$

This finishes the proof. □

Lemma 3.3. *For all $N \in \mathbb{Z}$ and $|n| \leq N-1$,*

$$h \sum_{j=1}^{N-1} \cot(\pi(t - t_j)) e_n(t_j) = \text{p.v.} \int_0^1 \cot(\pi(t-\tau)) e_n(\tau) \mathrm{d}\tau + \cot(\pi t/h) e_n(t), \quad t/h \notin \mathbb{Z}.$$

Proof. Differentiating (3.36) we obtain

$$h\sum_{j=1}^{N-1}\cot(\pi(t-t_j)) = \cot(\pi t/h), \qquad t/h \notin \mathbb{Z}, \tag{3.39}$$

which is the case $n = 0$. Consider now the function

$$s_n(\tau;t) := \cot(\pi(t-\tau))(e_n(\tau)-e_n(t)) = e_n(t)\cot(\pi(\tau-t))(1-e_n(\tau-t)).$$

Note now that for $n \geq 1$,

$$\begin{aligned}
\imath\cot(\pi\tau)(1-e_n(\tau)) &= (1+e_1(\tau))\frac{1-e_n(\tau)}{1-e_1(\tau)} \\
&= (1+e_1(\tau))(1+e_1(\tau)+e_2(\tau)+\ldots+e_{n-1}(\tau)) \\
&= 1+2e_1(\tau)+2e_2(\tau)+\ldots+2e_{n-1}(\tau)+e_n(\tau),
\end{aligned}$$

and therefore

$$s_n(\cdot;t) \in \operatorname{span}\{e_m \,:\, 0 \leq m \leq n\} \qquad n \geq 1.$$

By conjugation, it is easy to see then that

$$s_n(\cdot;t) \in \mathbb{T}_{N-1} := \operatorname{span}\{e_m \,:\, |m| \leq N-1\}, \quad |n| \leq N-1. \tag{3.40}$$

It is well known that

$$\int_0^1 \phi(\tau)\mathrm{d}\tau = h\sum_{j=1}^{N}\phi(t_j) \qquad \forall \phi \in \mathbb{T}_{N-1}.$$

Therefore, by (3.40),

$$\begin{aligned}
\text{p.v.}\int_0^1 \cot(\pi(t-\tau))e_n(\tau)\mathrm{d}\tau &= \int_0^1 s_n(\tau;t)\mathrm{d}\tau = h\sum_{j=1}^{N} s_n(t_j;t) \\
&= h\sum_{j=1}^{N}\cot(\pi(t-t_j))e_n(t_j) - e_n(t)h\sum_{j=1}^{N}\cot(\pi(t-t_j)) \\
&= h\sum_{j=1}^{N}\cot(\pi(t-t_j))e_n(t_j) - e_n(t)\cot(\pi t/h),
\end{aligned}$$

where in the last equality we have used (3.39). □

3.6 The Treatment of Open Arcs

In the same spirit as the previous sections, smooth open arcs can be incorporated into the fully discrete Calderón Calculus for elastic waves. The idea is simple: instead of using a traditional cosine change of variable to modify the integral equation into a periodic integral equation, we will use the cosine change of variables to sample geometric features from the open arc and then define the discrete elements (the two layer potentials and the operators V and W) using the same formulas as in the case of closed curves. Note that the operators K and J are not meaningful in the case of open arcs.

Let $\mathbf{x} : [0,1] \to \mathbb{R}^2$ be a regular parametrization of a smooth simple open arc. Let us also consider the 1-periodic even function $\phi : \mathbb{R} \to [0,1]$ given by

$$\phi(t) := \tfrac{1}{2} + \tfrac{1}{2}\cos(\pi(2t-1)).$$

We then define $\mathbf{a}(t) := \mathbf{x}(\phi(t))$ and note that $\mathbf{a}(0) = \mathbf{x}(0) = \mathbf{a}(1)$, $\mathbf{a}(\frac{1}{2}) = \mathbf{x}(1)$, and $\mathbf{a}(1-t) = \mathbf{a}(t)$ for all t. The normal vector field

$$\boldsymbol{\nu}(t) := \mathbf{a}'(t)^{\perp} = -\pi \sin((\pi(2t-1))\, \mathbf{x}'(\phi(t))^{\perp}, \quad \text{where} \quad (c_1, c_2)^{\perp} := (c_2, -c_1),$$

satisfies $\boldsymbol{\nu}(0) = \boldsymbol{\nu}(\frac{1}{2}) = \mathbf{0}$, and $\boldsymbol{\nu}(1-t) = -\boldsymbol{\nu}(t)$ for all t. This means that the normal vector has different signs depending on whether we are moving from the first tip to the second or back. We now choose a positive even integer $N = 2M$, define $h := 1/N = 1/(2M)$, and create the main discrete grid:

$$\mathbf{m}_j := \mathbf{a}((j-\tfrac{1}{2})h), \qquad \mathbf{b}_j := \mathbf{a}((j-1)h), \qquad \boldsymbol{\nu}_j := h\boldsymbol{\nu}((j-\tfrac{1}{2})h), \qquad j \in \mathbb{Z}_N. \tag{3.41}$$

Let us first comment on these formulas. In comparison with (3.1) the breakpoints and midpoints are displaced $\frac{1}{2}h$ in parametric space. Whereas in the case of closed curves this is not relevant, for open arcs it will be essential that the ends of the arc are breakpoints of the discrete grid: $\mathbf{b}_1 = \mathbf{b}_{2M+1} = \mathbf{x}(0)$, $\mathbf{b}_{M+1} = \mathbf{x}(1)$. Also, note that points are sampled twice and we actually have:

$$\mathbf{m}_{N+1-j} = \mathbf{m}_j, \qquad \mathbf{b}_{N+2-j} = \mathbf{b}_j, \qquad \boldsymbol{\nu}_{N+1-j} = -\boldsymbol{\nu}_j.$$

The companion grids are similarly collected from the curve:

$$\mathbf{m}_j^{\pm} := \mathbf{a}((j - \tfrac{1}{2} \pm \tfrac{1}{6})h), \quad \mathbf{b}_j^{\pm} := \mathbf{a}((j - 1 \pm \tfrac{1}{6})h),$$
$$\boldsymbol{\nu}_j^{\pm} := h\boldsymbol{\nu}((j - \tfrac{1}{2} \pm \tfrac{1}{6})h), \quad j \in \mathbb{Z}_N. \tag{3.42}$$

The duplication in the cosine sampling will have some effects in the structure of the discrete Calderón Calculus. Let $\boldsymbol{\xi} \in \mathbb{C}^{2N}$ be a vector with blocks $\boldsymbol{\xi}_j$. We will write $\boldsymbol{\xi} \in \mathbb{C}^{2N}_{\text{even}}$ when $\boldsymbol{\xi}_{N+1-j} = \boldsymbol{\xi}_j$ for all j, and we will write $\boldsymbol{\xi} \in \mathbb{C}^{2N}_{\text{odd}}$ when $\boldsymbol{\xi}_{N+1-j} = -\boldsymbol{\xi}_j$ for all j. Even vectors are those in the nullspace of the matrix

$$\mathrm{H} := \begin{bmatrix} \mathrm{H}_{\text{sc}} & 0 \\ 0 & \mathrm{H}_{\text{sc}} \end{bmatrix}, \qquad \mathrm{H}_{\text{sc}} := \begin{bmatrix} 1 & & & & & -1 \\ & \ddots & & & \iddots & \\ & & 1 & -1 & & \\ & & -1 & 1 & & \\ & \iddots & & & \ddots & \\ -1 & & & & & 1 \end{bmatrix}, \tag{3.43}$$

while odd vectors are in the nullspace of the matrix $|\mathrm{H}|$, obtained by taking the absolute value of the elements of H. Additionally $\mathrm{H}\boldsymbol{\xi} = 2\boldsymbol{\xi}$ if $\boldsymbol{\xi} \in \mathbb{C}^{2N}_{\text{odd}}$ and $|\mathrm{H}|\boldsymbol{\xi} = 2\boldsymbol{\xi}$ if $\boldsymbol{\xi} \in \mathbb{C}^{2N}_{\text{even}}$. Finally if we sample an incident wave on an open arc using (3.17)-(3.18), it is not difficult to prove that

$$\boldsymbol{\beta}_0 \in \mathbb{C}^{2N}_{\text{even}} \qquad \text{and} \qquad \boldsymbol{\beta}_1 \in \mathbb{C}^{2N}_{\text{odd}}.$$

We first study a **Dirichlet crack**. Let Γ be the smooth open curve given in parametric form at the beginning of this section, we look for solutions of $\rho_\Sigma \partial_t^2 \mathbf{u} = \nabla \cdot \boldsymbol{\sigma}(\mathbf{u})$ in $\mathbb{R}^2 \setminus \Gamma$, with the corresponding radiation condition at infinity (see the comments after formula (2.15)), and the Dirichlet condition $\gamma\mathbf{u} + \gamma\mathbf{u}^{\text{inc}} = \mathbf{0}$ on Γ. We assume that the discrete data have already been sampled with (3.41)-(3.42) and that the incident wave has been observed using (3.17)-(3.18), outputting a vector $\boldsymbol{\beta}_0 \in \mathbb{C}^{2N}_{\text{even}}$. We now use the fact that

$$\mathrm{V}_h(s)\boldsymbol{\eta} \in \mathbb{C}^{2N}_{\text{even}} \quad \forall \boldsymbol{\eta} \in \mathbb{C}^{2N}, \quad \text{and} \quad \mathrm{V}_h(s)\boldsymbol{\eta} = \mathbf{0} \quad \forall \boldsymbol{\eta} \in \mathbb{C}^{2N}_{\text{odd}}.$$

(These properties are not difficult to prove.) Therefore, if we solve

$$(\mathrm{V}_h(s) + \mathrm{H})\boldsymbol{\eta} = -\boldsymbol{\beta}_0,$$

we are guaranteed that $\boldsymbol{\eta} \in \mathbb{C}^{2N}_{\text{even}}$. This density is used to build the discrete elastic wavefield $\mathbf{u}_h(\mathbf{z}) = \mathrm{S}_h(s;\mathbf{z})\boldsymbol{\eta}$.

In the case of a **Neumann crack**, we substitute the Dirichlet boundary condition on the open curve Γ by $\boldsymbol{t}(\mathbf{u}) + \boldsymbol{t}(\mathbf{u}^{\text{inc}}) = \mathbf{0}$. Using a similar argument as in the Dirichlet case, we solve the discrete integral equation

$$(\mathrm{W}_h(s) + |\mathrm{H}|)\boldsymbol{\psi} = \boldsymbol{\beta}_1,$$

obtain a unique $\boldsymbol{\psi} \in \mathbb{C}^{2N}_{\text{odd}}$ and input it in a double layer potential representation $\mathbf{u}_h(\mathbf{z}) = \mathrm{D}_h(s;\mathbf{z})\boldsymbol{\psi}$.

3.7 Numerical Experiments

Studies in the frequency domain. In this section we show two numerical experiments, based on different integral equations, for the interior Dirichlet problem. The domain is the ellipse $(\frac{x}{4})^2 + (\frac{y}{3})^2 = 1$ and we choose $\lambda = 5$, $\mu = 3$, and $\rho_\Sigma = 2.5$ as physical parameters. We fix the wave number to be $k = 3$ ($s = -3\imath$ in our Laplace domain based notation) and take data so that the exact solution is the sum of a pressure and a shear wave:

$$\mathbf{u}(\mathbf{z}) := \left(e^{\imath k(\mathbf{z}\cdot\mathbf{d})/c_L} + e^{\imath k(\mathbf{z}\cdot\mathbf{d}^\perp)/c_T}\right)\mathbf{d}, \qquad \mathbf{d} = (\tfrac{1}{\sqrt{2}}, \tfrac{1}{\sqrt{2}}), \qquad \mathbf{d}^\perp = (-\tfrac{1}{\sqrt{2}}, \tfrac{1}{\sqrt{2}}). \quad (3.44)$$

The solution will be observed in ten interior points $\mathbf{z}_i^{\text{obs}}$, $i = 1, \ldots, 10$, randomly chosen in the circle $x^2 + y^2 = 4$. The Dirichlet data is sampled using (3.17)-(3.18) to a vector $\boldsymbol{\beta}_0$. We are going to use a direct formulation, where the discrete elastic wave-field is given by the representation

$$\mathbf{u}_h(\mathbf{z}) = \mathrm{S}_h(s;\mathbf{z})\boldsymbol{\lambda} - \mathrm{D}_h(s;\mathbf{z})\boldsymbol{\varphi}. \quad (3.45)$$

Since we are dealing with the Dirichlet problem, the computation of $\boldsymbol{\varphi}$ is rather straightforward: we just need to solve the sparse linear system (recall (3.7)),

$$\mathrm{M}\boldsymbol{\varphi} = \boldsymbol{\beta}_0, \quad (3.46)$$

which is then postprocessed to create the effective density (see (3.16))

$$\boldsymbol{\varphi}^{\text{eff}} := \mathrm{Q}\boldsymbol{\varphi}. \tag{3.47}$$

The vector $\boldsymbol{\lambda}$ (which approximates the normal traction) will be computed using a first kind discrete integral equation (based on the first integral identity provided by the Calderón projector)

$$\mathrm{V}_h(s)\boldsymbol{\lambda} = (\tfrac{1}{2}\mathrm{M} + \mathrm{K}_h(s))\boldsymbol{\varphi}, \tag{3.48}$$

or a second kind integral equation (based on the second integral identity)

$$(-\tfrac{1}{2}\mathrm{M} + \mathrm{J}_h(s))\boldsymbol{\lambda} = -\mathrm{W}_h(s)\boldsymbol{\varphi}. \tag{3.49}$$

We compute the following errors:

$$E_h^{\mathbf{u}} := \frac{\max_{i=1}^{10} |\mathbf{u}_h(\mathbf{z}_i^{\text{obs}}) - \mathbf{u}(\mathbf{z}_i^{\text{obs}})|}{\max_{i=1}^{10} |\mathbf{u}(\mathbf{z}_i^{\text{obs}})|}, \tag{3.50a}$$

$$E_h^{\boldsymbol{\lambda}} := \frac{\max_{i=1}^{N} |\boldsymbol{\lambda}_i - \boldsymbol{\sigma}(\mathbf{u})(\mathbf{m}_i)\cdot\boldsymbol{\nu}_i|}{\max_{i=1}^{N} |\boldsymbol{\sigma}(\mathbf{u})(\mathbf{m}_i)\cdot\boldsymbol{\nu}_i|}, \tag{3.50b}$$

$$E_h^{\boldsymbol{\varphi}} := \frac{\max_{i=1}^{N} |\boldsymbol{\varphi}_i^{\text{eff}} - \mathbf{u}(\mathbf{m}_i)|}{\max_{i=1}^{N} |\mathbf{u}(\mathbf{m}_i)|}. \tag{3.50c}$$

The expected convergence orders are

$$E_h^{\mathbf{u}} = \mathcal{O}(N^{-3}), \qquad E_h^{\boldsymbol{\lambda}} = \mathcal{O}(N^{-3}), \qquad E_h^{\boldsymbol{\varphi}} = \mathcal{O}(N^{-4}),$$

where it has to be noted that $\boldsymbol{\varphi}$ is not obtained as a solution of an integral equation, but just projected from sampled data, which explains the higher order of convergence. The errors are reported in Tables 3.1 and 3.2 and plotted in Figures 3.2 and 3.3.

Studies in the time domain. In this section we show some tests on how to use the previously devised Calderón calculus for elastic waves in the Laplace/frequency domain to simulate transient waves by using a Convolution Quadrature method. We will be using an order two (BDF2-based) Convolution Quadrature strategy. For a brief introduction to the theoretical aspects of multistep CQ methods applied to wave propagation, and its algorithmic usage we refer to Appendix B.

N	$E_h^{\mathbf{u}}$	e.c.r.	$E_h^{\boldsymbol{\lambda}}$	e.c.r.	$E_h^{\boldsymbol{\phi}}$	e.c.r.
30	1.836	—	2.185	—	5.057×10^{-3}	—
60	3.338×10^{-2}	5.761	2.682×10^{-2}	6.348	1.212×10^{-4}	5.382
120	2.941×10^{-3}	3.542	2.705×10^{-3}	3.309	1.451×10^{-5}	3.063
240	4.352×10^{-4}	2.757	3.224×10^{-4}	3.069	1.011×10^{-6}	3.843
480	5.640×10^{-5}	2.948	3.983×10^{-5}	3.017	6.484×10^{-8}	3.963
960	7.020×10^{-6}	3.006	4.958×10^{-6}	3.006	4.077×10^{-9}	3.991
1920	8.783×10^{-7}	2.998	6.199×10^{-7}	3.000	2.552×10^{-10}	3.998

Table 3.1: Relative errors (3.50) and estimated convergence rates in the frequency domain for $\mathbf{u}$, $\boldsymbol{\lambda}$ and $\boldsymbol{\phi}$ using equation (3.48).

N	$E_h^{\mathbf{u}}$	e.c.r.	$E_h^{\boldsymbol{\lambda}}$	e.c.r.	$E_h^{\boldsymbol{\phi}}$	e.c.r.
30	3.317×10^{-1}	—	5.806×10^{-1}	—	5.057×10^{-3}	—
60	5.785×10^{-2}	2.519	6.836×10^{-2}	3.086	1.212×10^{-4}	5.382
120	7.271×10^{-3}	2.993	7.620×10^{-3}	3.165	1.451×10^{-5}	3.063
240	8.923×10^{-4}	3.026	8.635×10^{-4}	3.142	1.011×10^{-6}	3.843
480	8.087×10^{-5}	3.464	1.030×10^{-5}	3.068	6.484×10^{-8}	3.963
960	1.004×10^{-5}	3.009	1.256×10^{-6}	3.035	4.077×10^{-9}	3.991
1920	1.473×10^{-6}	2.769	1.605×10^{-7}	2.969	2.552×10^{-10}	3.998

Table 3.2: Relative errors (3.50) and estimated convergence rates in the frequency domain for $\mathbf{u}$, $\boldsymbol{\lambda}$ and $\boldsymbol{\phi}$ using equation (3.49).

We use the same geometry and physical parameters as in the experiments of Section 3.7. We solve an interior problem with prescribed Dirichlet (resp. Neumann) boundary condition taken so that the exact solution is the plane pressure wave

$$\mathbf{u}(\mathbf{z},t) = \mathcal{H}(c_L(t-t_0) - \mathbf{z}\cdot\mathbf{d})\sin(2(c_L(t-t_0) - \mathbf{z}\cdot\mathbf{d}))\mathbf{d}, \tag{3.51}$$

with $\mathbf{d} = (1/\sqrt{2}, 1/\sqrt{2})$ and $t_0 = 2.3$. Here

$$\mathcal{H}(t) := t^5(1-5(t-1)+15(t-1)^2-35(t-1)^3+70(t-1)^4-126(t-1)^5)\chi_{[0,1]}(t)+\chi_{[1,\infty)}(t) \tag{3.52}$$

is a smooth version of the Heaviside function. The problem is integrated from 0 to $T = 3$, on a space grid with N points, with M time steps of length T/M: $t_n = n\,T/M$. Relative errors for the solution are computed at the observation points $\mathbf{z}_i^{\text{obs}}$ (those of Section 3.7). In this experiment we fix a space discretization with $n = 500$ points

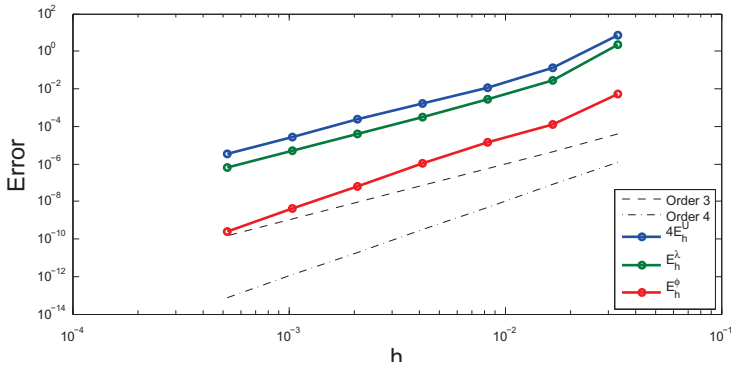

Figure 3.2: Errors corresponding to Table 3.1. The error $E_h^{\mathbf{u}}$ has been rescaled to separate the error graphs.

and refine in the number of time steps M. The results are reported in Table 3.3. The expected order two convergence of CQ is observed until the error due to space discretization dominates. Similar results refining in time and space can be produced in the same way.

M	$E_h^{\mathbf{u}}$ Dirichlet	e.c.r.	$E_h^{\mathbf{u}}$ Neumann	e.c.r.
50	2.828×10^{-1}	—	2.676×10^{-1}	—
100	1.711×10^{-1}	0.725	1.662×10^{-1}	0.686
200	5.181×10^{-2}	1.724	5.205×10^{-2}	1.675
400	1.420×10^{-2}	1.878	1.401×10^{-2}	1.893
800	3.070×10^{-3}	2.199	2.983×10^{-3}	2.232
1600	6.171×10^{-4}	2.313	6.124×10^{-4}	2.284

Table 3.3: Relative errors and estimated convergence rates in the time domain for the displacement at the final time $T = 3$ with Dirichlet and Neumann boundary conditions. The first column shows the number of time steps, 500 discretization points in space were used.

Cracks. We use the half circle $\Gamma = \{x^2 + y^2 = 1\} \cap \{y \geq 0\}$ as the scattering arc. The physical parameters of the surrounding unbounded elastic medium are those of Section 3.7. The incident wave is the pressure part of the function defined in (3.44). The solution is observed at ten random points on a circle of radius 5. Since the exact solution is not know, we use a three grid principle to estimate convergence rates.

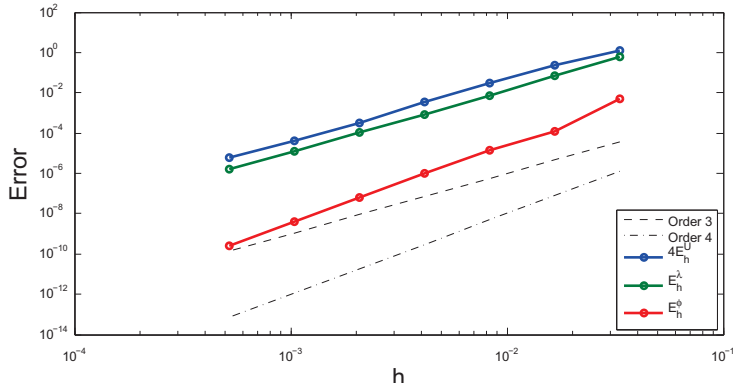

Figure 3.3: Errors corresponding to Table 3.2. The error $E_h^{\mathbf{u}}$ has been rescaled to separate the error graphs.

N	e.c.r. Dirichlet	e.c.r. Neumann
10	—	—
20	—	—
40	3.449	4.446
80	3.120	3.512
160	3.030	3.318
320	3.008	3.010

Table 3.4: Estimated convergence rates in the frequency domain Dirichlet and Neumann cracks. Given the fact that the solution is not known, a three grid principle is used to estimate convergence rates.

Illustrative experiments. We next show the capabilities of the method for the discretization of time domain scattering problems. We will denote by $\mathrm{CQfwd}(\mathrm{A}(s), \eta^n)$ the discrete approximation of the convolution $(\mathcal{L}^{-1}\{\mathrm{A}\} * \eta)(t^n)$ and by $\mathrm{CQeqn}(\mathrm{A}(s), \eta^n)$ the discrete approximation of the convolution with the *inverse* operator $(\mathcal{L}^{-1}\{\mathrm{A}^{-1}\} * \eta)(t^n)$, where $t^n := n\kappa$ (see Appendix B). The first example shows the scattering of an elastic wave by multiple obstacles. The obstacles are three disks with boundaries:

$$(x-1)^2 + (y-1)^2 = 1, \qquad (x-3)^2 + (y-3)^2 = 1, \qquad (x-3.5)^2 + (y-0.4)^2 = 1.$$

For an incident wave $\mathbf{u}^{\mathrm{inc}}(\mathbf{z}, t)$, we use the pressure wave given in (3.51). We look for a causal displacement field satisfying the elastic wave equation (2.11) with boundary

condition $\gamma\mathbf{u}+\gamma\mathbf{u}^{\text{inc}} = \mathbf{0}$ at all times. We use a direct formulation that we next explain in the Laplace domain. Data are sampled in space (with 200 points per obstacle) using (3.17)-(3.18) at equally spaced time-steps of length $k = 28/1200$ and stored in vectors $\boldsymbol{\beta}_0^n$. These data have first to be projected on a space of traces $\boldsymbol{\varphi}^n = -\mathrm{M}^{-1}\boldsymbol{\beta}_0^n$ and then run through a second hand integral operator in order to build the right-hand side of the equations (2.11),

$$\boldsymbol{\xi}^n = -\tfrac{1}{2}\mathrm{M}\boldsymbol{\varphi}^n + \mathrm{CQfwd}(\mathrm{K}_h(s), \boldsymbol{\varphi}^n).$$

(Compare with (3.46) and (3.48) and note the different sign due to the fact that we are solving an exterior problem.) An approximation of the normal stresses is then computed by solving

$$\boldsymbol{\lambda}^n = \mathrm{CQeqn}(\mathrm{V}_h(s), \boldsymbol{\xi}^n).$$

Finally the solution is evaluated at a large number of observation points $\mathbf{z}_i$ using two potentials

$$\mathbf{u}^n(\mathbf{z}_i) = \mathrm{CQfwd}(\mathrm{D}_h(s; \mathbf{z}_i), \boldsymbol{\varphi}^n) - \mathrm{CQfwd}(\mathrm{S}_h(s; \mathbf{z}_i), \boldsymbol{\lambda}^n).$$

Figure 3.4 shows four snapshots of the solution, which is asymptotically reaching the time-harmonic regime. We plot the absolute value of the displacement. The scattered pressure and shear waves can be distinguished by the different speeds of propagation that appear already after the wave hits the first obstacle.

The second example shows the scattering of a pressure wave by a non-convex kite-shaped rigid obstacle. The simulation parameters are the same as those for the previous example, Figure 3.5 shows snapshots of the process.

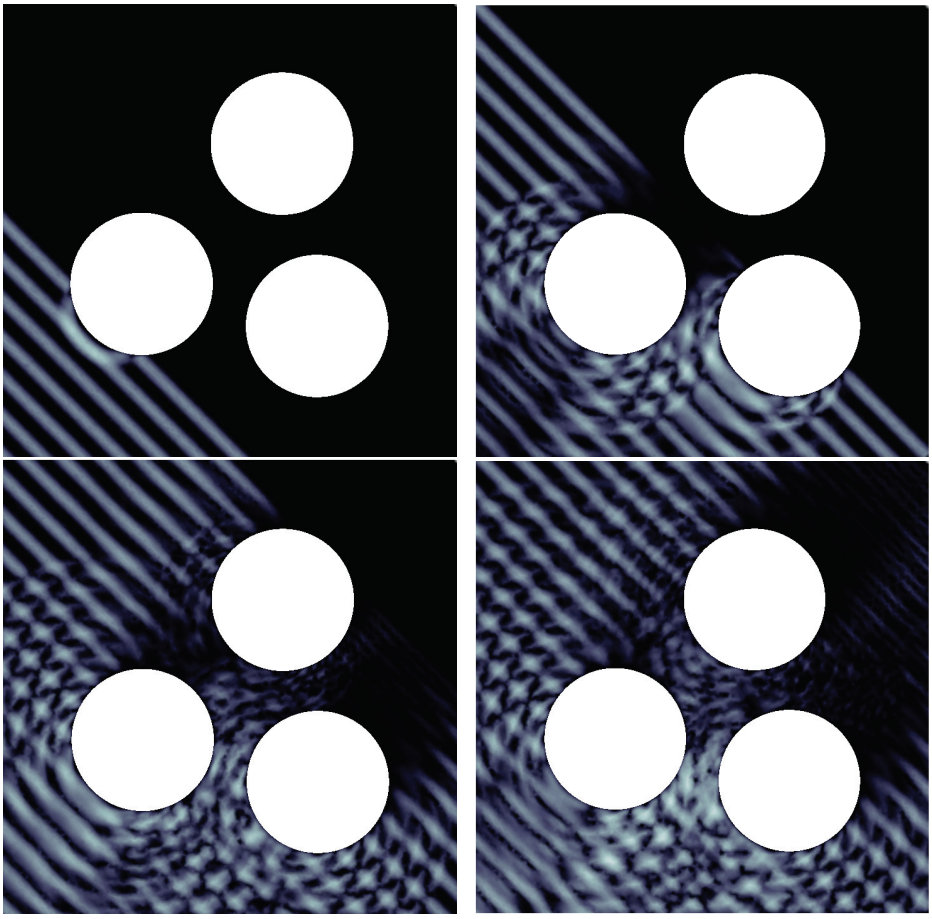

Figure 3.4: Four images of the scattering of a plane pressure wave by three rigid obstacles. The solution transitions to a time-harmonic regime. The absolute value of the displacement field is shown in a gray scale (black is no-displacement).

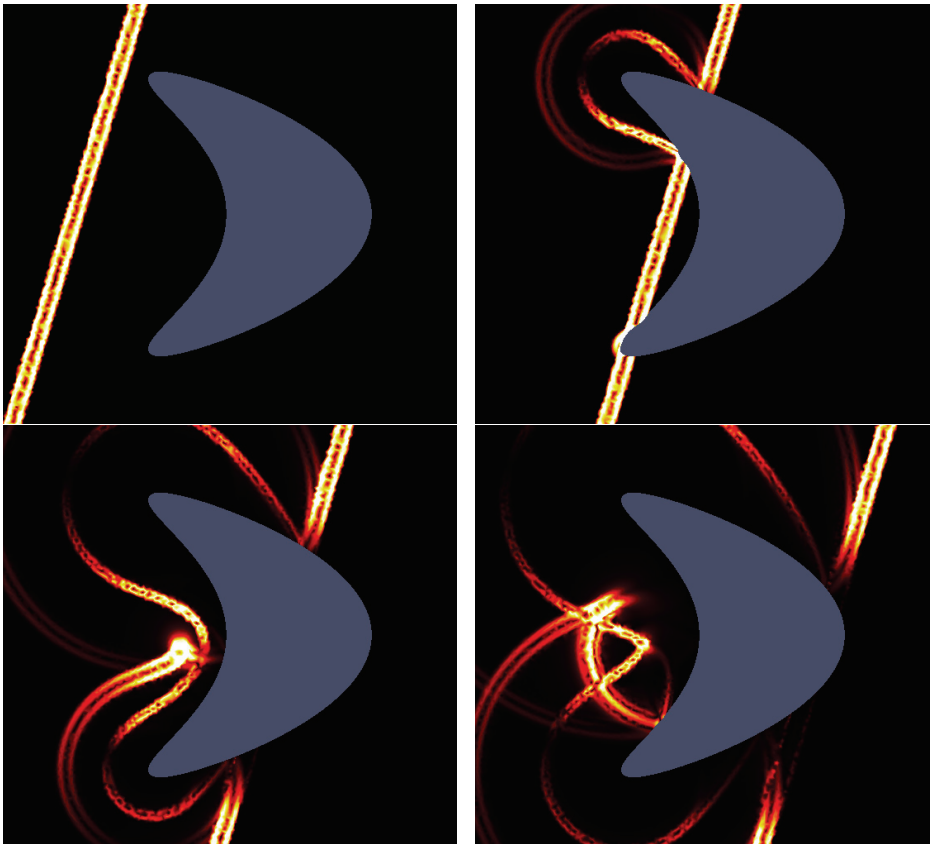

Figure 3.5: Scattering of a plane pressure wave by a kite-shaped obstacle. The absolute value of the displacement field is shown in a heat scale (black is no-displacement).

Chapter 4

ACOUSTIC SCATTERING BY LINEARLY ELASTIC OBSTACLES

This chapter presents the work done in collaboration with George Hsiao and Francisco-Javier Sayas published in the paper *Boundary and coupled boundary-finite element methods for transient wave-structure interaction* [66] regarding the scattering of acoustic waves by a linearly elastic obstacle. The contribution strives to fill the gap in the mathematical analysis of the time domain wave-structure problem for the cases when the scatterer is either a homogeneous isotropic solid or the case of a general inhomogeneous anisotropic linearly elastic body. Despite the fact that each problem requires a formulation which results in a very different numerical discretization, the techniques and tools required to carry out the theoretical study are surprisingly similar.

After a brief survey of the previous related work in Section 4.1 we proceed in Section 4.2 to the study of the pure boundary integral formulation –which arises naturally when dealing with homogeneous acoustic and elastic domains– and leads to a numerical treatment where only Boundary Elements are used for space discretization. Section 4.3 then studies the more general case of an inhomogeneous, anisotropic solid which requires a combined boundary integral/variational treatment where integral equations are used only for the acoustic dynamics. This formulation is naturally suited for a coupled Boundary Element/Finite Element implementation. Finally, Section 4.4 shows numerical experiments and convergence studies for both problems.

Following [82, 115, 9] the analysis is done in the Laplace domain aiming for a Convolution Quadrature treatment similar to that done for the purely acoustic case in [12, 42, 43]. We deal simultaneously with the continuous and discrete cases by posing the problems in a general closed subspace of the appropriate function spaces. Well-posedness is proved in the Laplace domain via an equivalent exotic transmission

problem for which a variational formulation is found. The resulting stability bounds are written carefully in terms of the Laplace parameter s in order to apply results from [116] which give explicit time domain estimates. Error bounds in the time domain are obtained following a similar approach for the semi-discrete problem. Full discretization and convergence estimates are given for the case of BDF2-CQ.

4.1 Background

The study of acoustic/elastic scattering has been a subject of interest in both the mathematical and engineering community for some years now. In the case of time-harmonic regime, the study of the existence and uniqueness of solutions dates back at least to 1986 [57]. The well-posedness of several purely boundary integral formulations was analyzed in [65, 63, 94] by assuming that the scatterer had at least a boundary of class $\mathcal{C}^2$. Later on, in the 2000's, combined boundary integral and variational formulations were proposed in [64, 39] and proven to be well posed also for smooth scatterers. In these works the elastic response is modeled variationally and the unbounded acoustic scattering is treated with either a boundary integral equation or by introducing an artificial boundary where an absorbing condition is imposed. Recently, the more general case of a Lipschitz scatterer was dealt with in [16] within the framework of a variational formulation with a fictitious boundary.

On the computational side, the coupling of Boundary Elements and *hp*-Finite Elements was studied in [27] where the Burton-Miller equation is used to model the acoustic wave-field; the authors provide a posteriori error bounds aiming for an adaptive implementation. The fictitious boundary approach with finite elements has been thoroughly investigated in [97, 51, 52] and a DG-like implementation was carried out recently in [15].

The transient regime, on the other hand, has not enjoyed so much attention –at least in the mathematical community– as its frequency domain cousin. In [44, 45] the problem is posed in a slab-like unbounded domain imposing first order absorbing

boundary conditions, while in [68] well-posedness is established for the coupled boundary integral/variational formulation also in a slab-like region. Within the engineering community, the time domain case has attracted attention at least since 1991. Numerous approaches have been attempted without much theoretical justification but with satisfactory results. To cite some examples, BE/FE coupling with Convolution Quadrature was employed in [41, 108], BE/BE coupling using Newmark time integration was the preferred treatment in [96] and FE/FE coupling with an absorbing boundary condition and Newmark time integration were used in [48]. A comprehensive list of related work can be found in [120].

4.2 Homogeneous Isotropic Solids: BIE Formulation

Within the geometric setting developed in Chapter 2, our problem can be explained as follows: an incident acoustic field v^{inc} traveling in Ω_+ arrives at an obstacle at time $t = 0$ and interacts with a homogeneous isotropic elastic body occupying Ω_-; part of the incident wave is scattered and part of it excites an elastic wave within the obstacle. We are interested in finding the unknown scattered field v and the elastic displacement $\mathbf{u}$ induced by this interaction. These unknown variables satisfy the following system

$$\rho_\Sigma \ddot{\mathbf{u}} = \Delta^* \mathbf{u} \qquad \text{in } \Omega_- \times [0,\infty), \tag{4.1a}$$

$$c^{-2}\ddot{v} = \Delta v \qquad \text{in } \Omega_+ \times [0,\infty), \tag{4.1b}$$

$$-\dot{\mathbf{u}} \cdot \boldsymbol{\nu} = \partial_\nu (v + v^{\text{inc}}) \qquad \text{on } \Gamma \times [0,\infty), \tag{4.1c}$$

$$\mathbf{t}(\mathbf{u}) = -\rho_f (\dot{v} + \dot{v}^{\text{inc}}) \boldsymbol{\nu} \qquad \text{on } \Gamma \times [0,\infty). \tag{4.1d}$$

Here ρ_f and ρ_Σ are the respective constant densities of the fluid and elastic media, and the upper dot denotes differentiation with respect to time. The coupling conditions at Γ can be interpreted physically as follows: (4.1c) expresses the fact that the difference in the normal components of the speed of the fluid and that of the solid at the interface is due to the normal speed of the incident acoustic wave; (4.1d) expresses the condition of equilibrium of pressure at the interface. A derivation of this model can be found in

[70, Section 1.3]. This system is complemented with homogeneous initial conditions for $\mathbf{u}$ and v (and their time derivatives), and a causality condition that can be expressed as: for all $t > 0$, $v \equiv 0$ except in a bounded region (that changes with time).

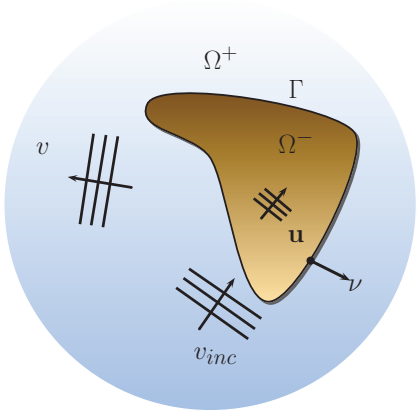

Figure 4.1: A cartoon of the geometric setting: the solid (brown) is surrounded by the unbounded medium (blue).

For the sake of completeness we will now give the weak form of the equations (4.1). Note that all the estimates that we will produce will be developed using the Laplace transformed equations, and it will be only those equations that we will need to deal with rigorously. We look for a pair of causal distributions (the definition of the spaces $\mathrm{CT}(X)$ can be found in Appendix A)

$$(\mathbf{u}, v) \in \mathrm{CT}(\mathbf{H}^1_{\Delta^*}(\mathbb{R}^d \setminus \Gamma) \times H^1_{\Delta}(\mathbb{R}^d \setminus \Gamma)),$$

such that

$$\rho_\Sigma \ddot{\mathbf{u}} = \Delta^* \mathbf{u} \qquad (\text{in } \mathbf{L}^2(\Omega_-)), \tag{4.2a}$$

$$c^{-2} \ddot{v} = \Delta v \qquad (\text{in } L^2(\Omega_+)), \tag{4.2b}$$

$$-\gamma^- \dot{\mathbf{u}} \cdot \boldsymbol{\nu} = \partial^+_\nu v + \alpha_0 \qquad (\text{in } H^{-1/2}(\Gamma)), \tag{4.2c}$$

$$\mathbf{t}^-(\mathbf{u}) = -\rho_f(\gamma^+ \dot{v} + \dot{\beta}_0)\boldsymbol{\nu} \qquad (\text{in } H^{1/2}(\Gamma)). \tag{4.2d}$$

In (4.2), the upper dots are now used for distributional differentiation and the parentheses in the right-hand sides tell where the distributions are compared. Full details

on how to understand wave equations in the sense of vector-valued distributions can be found in [116]. Also, we have used α_0 and β_0 to denote general causal distributions with values in $H^{-1/2}(\Gamma)$ and $H^{1/2}(\Gamma)$ respectively. Existence and uniqueness of solution to (4.2) can be proved with some additional constraints: we have to assume that the data and the solution are Laplace transformable with Laplace transforms defined in a subset of the form $\{s \in \mathbb{C} : \operatorname{Re} s > \sigma_0\}$ for some σ_0.

Let us now consider a slightly different problem. Now $\lambda_0 \in H^{-1/2}(\Gamma)$ and $\phi_0 \in H^{1/2}(\Gamma)$ are data, and we look for $(\mathbf{u}, v) \in \mathbf{H}^1(\Omega_-) \times H^1(\Omega_+)$ such that

$$\rho_\Sigma s^2 \mathbf{u} = \Delta^* \mathbf{u} \qquad \text{in } \Omega_-, \tag{4.3a}$$

$$(s/c)^2 v = \Delta v \qquad \text{in } \Omega_+, \tag{4.3b}$$

$$-s\gamma^- \mathbf{u} \cdot \boldsymbol{\nu} = \partial_\nu^+ v + \lambda_0 \qquad \text{on } \Gamma, \tag{4.3c}$$

$$\mathbf{t}^-(\mathbf{u}) = -\rho_f s(\gamma^+ v + \phi_0)\boldsymbol{\nu} \qquad \text{on } \Gamma. \tag{4.3d}$$

This problem will be studied for all $s \in \mathbb{C}_+ := \{s \in \mathbb{C} : \operatorname{Re} s > 0\}$. The relation between (4.3) and (4.2) is simple: if $\lambda_0 = \mathcal{L}\{\alpha_0\}(s)$ and $\phi_0 = \mathcal{L}\{\beta_0\}(s)$, then the solution of (4.3) is the Laplace transform of the solution of (4.2).

The boundary integral system equivalent to (4.3) is derived by choosing $\boldsymbol{\phi}_\Sigma := \gamma^- \mathbf{u}$ and $\phi_f := \gamma^+ v$ as unknowns, using the representation formulas for v and $\mathbf{u}$ and finally imposing the transmission conditions. The process is quite standard and we will only sketch the main steps. We introduce the matrices of operators

$$\mathbb{L}(s) := \begin{bmatrix} \mathbf{W}(s) + \rho_f s^2 \mathrm{N}^t \mathrm{V}(s/c)\mathrm{N} & \rho_f s(\mathrm{N}^t \mathrm{K}(s/c) - \mathbf{K}^t(s)\mathrm{N}^t) \\ \rho_f s(\mathrm{N}\mathbf{K}(s) - \mathrm{K}^t(s/c)\mathrm{N}) & (\rho_f s)^2 \mathrm{N}\mathbf{V}(s)\mathrm{N}^t + \rho_f \mathrm{W}(s/c) \end{bmatrix}$$

and

$$\mathbb{R}(s) := \begin{bmatrix} -\rho_f s \mathrm{N}^t \mathrm{V}(s/c) & \rho_f s(-\frac{1}{2}\mathbf{I} + \mathbf{K}^t(s))\mathrm{N}^t \\ \rho_f(\frac{1}{2}\mathrm{I} + \mathrm{K}^t(s/c)) & -(\rho_f s)^2 \mathrm{N}\mathbf{V}(s)\mathrm{N}^t \end{bmatrix}.$$

The operator

$$\begin{aligned} \mathrm{N} : \mathbf{H}^{1/2}(\Gamma) &\longrightarrow H^{-1/2}(\Gamma) \\ \boldsymbol{\phi} &\longmapsto \boldsymbol{\phi} \cdot \boldsymbol{\nu} \end{aligned}$$

has been defined in Section 2.1. Denoting

$$\mathbb{H}^{\pm 1/2}(\Gamma) := \mathbf{H}^{\pm 1/2}(\Gamma) \times H^{\pm 1/2}(\Gamma),$$

it is easy to show that by well known properties of the boundary integral operators on Lipschitz domains (see the general theory in [102])

$$\begin{aligned}\mathbb{L}(s) &: \mathbb{H}^{1/2}(\Gamma) \to \mathbb{H}^{-1/2}(\Gamma),\\ \mathbb{R}(s) &: H^{-1/2}(\Gamma) \times H^{1/2}(\Gamma) \to \mathbb{H}^{-1/2}(\Gamma),\end{aligned}$$

are bounded. For the sake of notational simplicity, we will write $\mathbb{L}(s)(\boldsymbol{\phi}, \phi)$, understanding that the vector $(\boldsymbol{\phi}, \phi)$ is first transformed into a column vector and then left-multiplied by $\mathbb{L}(s)$.

Theorem 4.1. *If* $(\mathbf{u}, v)$ *solves* (4.3)*, then* $(\boldsymbol{\phi}_\Sigma, \phi_f) := (\gamma^- \mathbf{u}, \gamma^+ v)$ *satisfies*

$$\mathbb{L}(s)(\boldsymbol{\phi}_\Sigma, \phi_f) = \mathbb{R}(s)(\lambda_0, \phi_0). \tag{4.4}$$

Reciprocally, if $(\boldsymbol{\phi}_\Sigma, \phi_f)$ *is a solution of* (4.4)*, then*

$$\mathbf{u} := -\rho_f s \mathbf{S}(s) \mathrm{N}^t(\phi_0 + \phi_f) - \mathbf{D}(s)\boldsymbol{\phi}_\Sigma, \tag{4.5a}$$

$$v := \mathrm{S}(s/c)(\lambda_0 + s\mathrm{N}\boldsymbol{\phi}_\Sigma) + \mathrm{D}(s/c)\phi_f, \tag{4.5b}$$

define a solution of (4.3).

Proof. If $(\mathbf{u}, v)$ satisfies (4.3a)-(4.3b), then we have the representation formulas

$$\mathbf{u} = \mathbf{S}(s)\mathbf{t}^-(\mathbf{u}) - \mathbf{D}(s)\gamma^-\mathbf{u} \quad \text{and} \quad v = -\mathrm{S}(s/c)\partial_\nu^+ v + \mathrm{D}(s/c)\gamma^+ v, \tag{4.6}$$

and the boundary integral identities (see Sections 2.9 and 2.10)

$$\tfrac{1}{2}\gamma^-\mathbf{u} = \mathbf{V}(s)\mathbf{t}^-(\mathbf{u}) - \mathbf{K}(s)\gamma^-\mathbf{u}, \qquad \tfrac{1}{2}\mathbf{t}^-(\mathbf{u}) = \mathbf{K}^t(s)\mathbf{t}^-(\mathbf{u}) + \mathbf{W}(s)\gamma^-\mathbf{u}, \tag{4.7a}$$

$$\tfrac{1}{2}\gamma^+ v = -\mathrm{V}(s)\partial_\nu^+ v + \mathrm{K}(s)\gamma^+ v, \qquad \tfrac{1}{2}\partial_\nu^+ v = -\mathrm{K}^t(s)\partial_\nu^+ v - \mathrm{W}(s)\gamma^+ v. \tag{4.7b}$$

If we define $(\boldsymbol{\phi}_\Sigma, \phi_f) := (\gamma^-\mathbf{u}, \gamma^+ v)$ the transmission conditions (4.3c)-(4.3d) become

$$\mathbf{t}^-(\mathbf{u}) = -\rho_f s \mathrm{N}^t(\phi_f + \phi_0) \qquad \text{and} \qquad \partial_\nu^+ v = -(s\mathrm{N}\boldsymbol{\phi}_\Sigma + \lambda_0). \tag{4.8}$$

Substituting (4.8) in (4.7) and adding the two equations in (4.7a) and the two in (4.7b) gives the integral equations (4.4).

Reciprocally, let $(\mathbf{u}, v)$ be defined by (4.5) where $(\boldsymbol{\phi}_\Sigma, \phi_f)$ solve (4.4). Since $(\mathbf{u}, v)$ are defined with potentials, it follows that (4.3a) and (4.3b) are satisfied. Applying the limit formulas (4.7) in (4.5), we see that

$$\begin{aligned}
\mathbf{t}^-(\mathbf{u}) + \rho_f s \mathrm{N}^t(\gamma^+ v + \phi_0) =& -\tfrac{1}{2}\rho_f s \mathrm{N}^t(\phi_0 + \phi_f) - \rho_f s \mathbf{K}^t(s)\mathrm{N}^t(\phi_0 + \phi_f) + \mathbf{W}(s)\boldsymbol{\phi}_\Sigma \\
&+ \rho_f s \mathrm{N}^t \mathrm{V}(s/c)(\lambda_0 + s\mathrm{N}\boldsymbol{\phi}_\Sigma) + \rho_f s \mathrm{N}^t(\tfrac{1}{2}\phi_f + \mathrm{K}(s/c)\phi_f) \\
=&(\mathbf{W}(s) + \rho_f s^2 \mathrm{N}^t \mathrm{V}(s/c)\mathrm{N})\boldsymbol{\phi}_\Sigma + \rho_f s(\mathrm{N}^t \mathrm{K}(s/c) - \mathbf{K}^t(s)\mathrm{N}^t)\phi_f \\
&+ \rho_f s \mathrm{N}^t \mathrm{V}(s/c)\lambda_0 + \rho_f s(\tfrac{1}{2}\mathrm{N}^t\phi_0 - \mathbf{K}^t(s)\mathrm{N}^t\phi_0) \\
=&\, 0,
\end{aligned}$$

by the first equation in (4.4). This proves the first transmission condition (4.3c). Similarly (4.3d) is proved using the second equation in (4.4). □

4.2.1 Stability of the Galerkin Semidiscretization in Space

We next consider a Galerkin discretization of the integral equations (4.4). Note that when returning to the time domain (by taking inverse Laplace transforms, see Proposition A.1), this is simply a Galerkin semidiscretization in space of the system of delayed integral equations whose Laplace transform is (4.4). Following [82], the study of solvability for (4.4) is done at the same time as the study of Galerkin stability. We then choose two *closed* subspaces $\mathbf{Y}_h \subset \mathbf{H}^{1/2}(\Gamma)$ and $Y_h \subset H^{1/2}(\Gamma)$. For Galerkin semidiscretization, these spaces are taken to be finite dimensional. In the case of non-discretization (analysis of well-posedness of (4.4)) we just take $\mathbf{Y}_h = \mathbf{H}^{1/2}(\Gamma)$ and $Y_h = H^{1/2}(\Gamma)$.

The Galerkin discretization of (4.4) seeks $(\boldsymbol{\phi}_\Sigma^h, \phi_f^h) \in \mathbf{Y}_h \times Y_h$ satisfying

$$\langle \mathbb{L}(s)(\boldsymbol{\phi}_\Sigma^h, \phi_f^h), (\boldsymbol{\mu}^h, \mu^h)\rangle_\Gamma = \langle \mathbb{R}(s)(\lambda_0, \boldsymbol{\phi}_0), (\boldsymbol{\mu}^h, \mu^h)\rangle_\Gamma \qquad \forall (\boldsymbol{\mu}^h, \mu^h) \in \mathbf{Y}_h \times Y_h. \quad (4.9)$$

The angled bracket is the duality product of $\mathbb{H}^{-1/2}(\Gamma)$ with $\mathbb{H}^{1/2}(\Gamma)$. We can also write (4.9) in the very condensed form

$$\mathbb{L}(s)(\boldsymbol{\phi}_\Sigma^h, \phi_f^h) - \mathbb{R}(s)(\lambda_0, \boldsymbol{\phi}_0) \in \mathbf{Y}_h^\circ \times Y_h^\circ \equiv (\mathbf{Y}_h \times Y_h)^\circ, \tag{4.10}$$

where X° denotes the polar set of X, that is, the set of elements of the dual space that vanish on X. Following the same techniques of [82] we first rewrite the Galerkin equations (4.9) as an exotic transmission problem. Note that in the new transmission problem, the elastic and the acoustic fields are defined on both sides of the boundary.

Proposition 4.2 (Transmission problem for Galerkin equations)**.** *Let* $(\boldsymbol{\phi}_\Sigma^h, \phi_f^h) \in \mathbf{Y}_h \times Y_h$ *satisfy* (4.9) *and let*

$$\mathbf{u}^h := -\rho_f s \mathbf{S}(s) \mathrm{N}^t(\phi_0 + \phi_f^h) - \mathbf{D}(s)\boldsymbol{\phi}_\Sigma^h, \tag{4.11a}$$

$$v^h := \mathrm{S}(s/c)(\lambda_0 + s\mathrm{N}\boldsymbol{\phi}_\Sigma^h) + \mathrm{D}(s/c)\phi_f^h. \tag{4.11b}$$

Then $(\mathbf{u}^h, v^h) \in \mathbf{H}^1(\mathbb{R}^d \setminus \Gamma) \times H^1(\mathbb{R}^d \setminus \Gamma)$ *satisfies:*

$$\Delta^* \mathbf{u}^h - \rho_\Sigma s^2 \mathbf{u}^h = \mathbf{0} \quad \text{in } \mathbb{R}^d \setminus \Gamma, \tag{4.12a}$$

$$\Delta v^h - (s/c)^2 v^h = 0 \quad \text{in } \mathbb{R}^d \setminus \Gamma, \tag{4.12b}$$

$$s\mathrm{N}[\![\gamma \mathbf{u}^h]\!] - [\![\partial_\nu v^h]\!] = -\lambda_0, \tag{4.12c}$$

$$[\![\mathbf{t}(\mathbf{u}^h)]\!] - \rho_f s \mathrm{N}^t [\![\gamma v^h]\!] = -\rho_f s \mathrm{N}^t \phi_0, \tag{4.12d}$$

$$([\![\gamma \mathbf{u}^h]\!], [\![\gamma v^h]\!]) \in \mathbf{Y}_h \times Y_h, \tag{4.12e}$$

$$(s\mathrm{N}\gamma^+ \mathbf{u}^h + \partial_\nu^- v^h, \mathbf{t}^+(\mathbf{u}^h) + \rho_f s \mathrm{N}^t \gamma^- v^h) \in \mathbf{Y}_h^\circ \times Y_h^\circ. \tag{4.12f}$$

Reciprocally, given a solution of (4.12) *the functions*

$$(\boldsymbol{\phi}_\Sigma^h, \phi_f^h) := ([\![\gamma \mathbf{u}^h]\!], -[\![\gamma v^h]\!]) \in \mathbf{Y}_h \times Y_h \tag{4.13}$$

satisfy (4.9).

Proof. It is clear that the functions defined by (4.11) satisfy (4.12a) and (4.12b). Moreover, $[\![\gamma \mathbf{u}^h]\!] = \boldsymbol{\phi}_\Sigma^h$ and $[\![\gamma v^h]\!] = -\phi_f^h$, and therefore (4.12e) is satisfied. At the same time,

$$\begin{aligned} [\![\mathbf{t}(\mathbf{u}^h)]\!] &= -\rho_f s\mathrm{N}^t(\phi_0 + \phi_f^h) = -\rho_f s\mathrm{N}^t(\phi_0 - [\![\gamma v^h]\!]), \\ [\![\partial_\nu v^h]\!] &= \lambda_0 + s\mathrm{N}\boldsymbol{\phi}_\Sigma^h = \lambda_0 + s\mathrm{N}[\![\gamma \mathbf{u}^h]\!], \end{aligned}$$

which proves (4.12c) and (4.12d). Finally, using the jump properties of the potentials, it is easy to verify that

$$(s\mathrm{N}\gamma^+\mathbf{u}^h + \partial_\nu^- v^h, \mathbf{t}^+(\mathbf{u}^h) + \rho_f s\mathrm{N}^t\gamma^- v^h) = \mathbb{L}(s)(\boldsymbol{\phi}_\Sigma^h, \phi_f^h) - \mathbb{R}(s)(\lambda_0, \phi_0), \tag{4.14}$$

which proves (4.12f) (see (4.10)).

Reciprocally, if we are given a solution of (4.12) and we define $(\boldsymbol{\phi}_\Sigma^h, \phi_f^h)$ with (4.13), then by the representation formulas and (4.12c)-(4.12d), it follows that we can write the fields $(\mathbf{u}^h, v^h)$ as in (4.11). We can then use (4.14) again and prove that (4.12f) implies (4.9). □

The next step consists of finding a variational formulation for (4.12). This will be done in the space

$$\mathbb{H}_h := \{(\mathbf{u}^h, v^h) \in \mathbf{H}^1(\mathbb{R}^d \setminus \Gamma) \times H^1(\mathbb{R}^d \setminus \Gamma) \,:\, ([\![\gamma \mathbf{u}^h]\!], [\![\gamma v^h]\!]) \in \mathbf{Y}_h \times Y_h\},$$

which incorporates the only homogeneous essential transmission conditions of (4.12).

Proposition 4.3 (Equivalent variational formulation)**.** *Problem* (4.12) *is equivalent to finding*

$$(\mathbf{u}^h, v^h) \in \mathbb{H}_h \quad s.t. \quad B((\mathbf{u}^h, v^h), (\mathbf{w}, w); s) = \ell((\mathbf{w}, w); s) \qquad \forall (\mathbf{w}, w) \in \mathbb{H}_h, \tag{4.15}$$

where

$$\begin{aligned} B((\mathbf{u},v),(\mathbf{w},w);s) &:= (\boldsymbol{\sigma}(\mathbf{u}),\boldsymbol{\varepsilon}(\mathbf{w}))_{\mathbb{R}^d\setminus\Gamma} + \rho_\Sigma s^2(\mathbf{u},\mathbf{w})_{\mathbb{R}^d} \\ &\quad +\rho_f(\nabla v,\nabla w)_{\mathbb{R}^d\setminus\Gamma} + \rho_f(s/c)^2(v,w)_{\mathbb{R}^d} \\ &\quad +\rho_f s\big(\langle\gamma^+ v,\mathrm{N}\gamma^-\mathbf{w}\rangle_\Gamma - \langle\gamma^- v,\mathrm{N}\gamma^+\mathbf{w}\rangle_\Gamma \\ &\qquad +\langle\mathrm{N}\gamma^+\mathbf{u},\gamma^- w\rangle_\Gamma - \langle\mathrm{N}\gamma^-\mathbf{u},\gamma^+ w\rangle_\Gamma\big), \\ \ell((\mathbf{w},w);s) &:= \rho_f\left(\langle\lambda_0,\gamma^+ w\rangle_\Gamma - s\langle\mathrm{N}^t\phi_0,\gamma^-\mathbf{w}\rangle_\Gamma\right). \end{aligned}$$

Proof. The definition of the normal traction for $\mathbf{u}$ and the normal derivative for v, plus simple algebraic manipulations, show that

$$\begin{aligned} &\rho_f(\Delta v,w)_{\mathbb{R}^d\setminus\Gamma} + \rho_f(\nabla v,\nabla w)_{\mathbb{R}^d\setminus\Gamma} + (\Delta^*\mathbf{u},\mathbf{w})_{\mathbb{R}^d\setminus\Gamma} + (\boldsymbol{\sigma}(\mathbf{u}),\boldsymbol{\varepsilon}(\mathbf{w}))_{\mathbb{R}^d\setminus\Gamma} \\ &\quad =\langle[\![\mathbf{t}(\mathbf{u})]\!],\gamma^-\mathbf{w}\rangle_\Gamma + \langle\mathbf{t}^+(\mathbf{u}),[\![\gamma\mathbf{w}]\!]\rangle_\Gamma + \rho_f\langle\partial^- v,[\![\gamma w]\!]\rangle_\Gamma + \rho_f\langle[\![\partial_\nu v]\!],\gamma^+ w\rangle_\Gamma \\ &\quad =\langle\mathbf{t}^+(\mathbf{u}) + \rho_f s\mathrm{N}^t\gamma^- v,[\![\gamma\mathbf{w}]\!]\rangle_\Gamma + \rho_f\langle\partial_\nu^- v + s\mathrm{N}\gamma^+\mathbf{u},[\![\gamma w]\!]\rangle_\Gamma \\ &\qquad + \langle[\![\mathbf{t}(\mathbf{u})]\!] - \rho_f s\mathrm{N}^t[\![\gamma v]\!],\gamma^-\mathbf{w}\rangle_\Gamma + \rho_f\langle[\![\partial_\nu v]\!] - s\mathrm{N}[\![\gamma\mathbf{u}]\!],\gamma^+ w\rangle_\Gamma \\ &\qquad + \rho_f s\left(\langle\mathrm{N}^t\gamma^- v,\gamma^+\mathbf{w}\rangle_\Gamma - \langle\mathrm{N}^t\gamma^+ v,\gamma^-\mathbf{w}\rangle_\Gamma + \langle\mathrm{N}\gamma^-\mathbf{u},\gamma^+ w\rangle_\Gamma - \langle\mathrm{N}\gamma^+\mathbf{u},\gamma^- w\rangle_\Gamma\right), \end{aligned}$$

or, equivalently,

$$\begin{aligned} &B((\mathbf{u},v),(\mathbf{w},w);s) + (\Delta^*\mathbf{u} - \rho_\Sigma s^2\mathbf{u},\mathbf{w})_{\mathbb{R}^d\setminus\Gamma} + \rho_f(\Delta v - (s/c)^2 v,w)_{\mathbb{R}^d\setminus\Gamma} \\ &\qquad =\langle\mathbf{t}^+(\mathbf{u}) + \rho_f s\mathrm{N}^t\gamma^- v,[\![\gamma\mathbf{w}]\!]\rangle_\Gamma + \rho_f\langle\partial_\nu^- v + s\mathrm{N}\gamma^+\mathbf{u},[\![\gamma w]\!]\rangle_\Gamma \\ &\qquad\quad - \rho_f\langle s\mathrm{N}[\![\gamma\mathbf{u}]\!] - [\![\partial_\nu v]\!],\gamma^+ w\rangle_\Gamma + \langle[\![\mathbf{t}(\mathbf{u})]\!] - \rho_f s\mathrm{N}^t[\![\gamma v]\!],\gamma^-\mathbf{w}\rangle_\Gamma. \end{aligned} \tag{4.16}$$

From here it is clear that a solution of (4.12) satisfies (4.15). Reciprocally, if we have a solution of (4.15), testing with smooth functions with compact support in $\mathbb{R}^d\setminus\Gamma$, we can easily recover equations (4.12a) and (4.12b). Therefore, by (4.16) it follows that

$$\begin{aligned} &-\rho_f\langle s\mathrm{N}[\![\gamma\mathbf{u}^h]\!] - [\![\partial_\nu v^h]\!] + \lambda_0,\gamma^+ w\rangle_\Gamma + \langle[\![\mathbf{t}(\mathbf{u}^h)]\!] - \rho_f s\mathrm{N}^t([\![\gamma v^h]\!] + \phi_0),\gamma^-\mathbf{w}\rangle_\Gamma \\ &\qquad +\langle\mathbf{t}^+(\mathbf{u}^h) + \rho_f s\mathrm{N}^t\gamma^- v^h,[\![\gamma\mathbf{w}]\!]\rangle_\Gamma + \rho_f\langle\partial_\nu^- v^h + s\mathrm{N}\gamma^+\mathbf{u}^h,[\![\gamma w]\!]\rangle_\Gamma = 0 \end{aligned}$$

for all $(\mathbf{w}, w) \in \mathbb{H}_h$. The transmission conditions (4.12c), (4.12d), and (4.12f) follow from the simple observation that the map

$$\begin{aligned} \mathbb{H}_h &\longrightarrow H^{1/2}(\Gamma) \times \mathbf{H}^{1/2}(\Gamma) \times \mathbf{Y}_h \times Y_h \\ (\mathbf{w}, w) &\longmapsto (\gamma^+ w, \gamma^- \mathbf{w}, [\![\gamma \mathbf{w}]\!], [\![\gamma w]\!]) \end{aligned}$$

is surjective. □

The third step in the analysis is the proof of well-posedness of the variational problem (4.15). Following [82], we define the energy norm

$$|\!|\!| (\mathbf{u}, v) |\!|\!|_{|s|}^2 := (\boldsymbol{\sigma}(\mathbf{u}), \boldsymbol{\varepsilon}(\overline{\mathbf{u}}))_{\mathbb{R}^d \setminus \Gamma} + \| s \sqrt{\rho_\Sigma} \mathbf{u} \|_{\mathbb{R}^d}^2 + \rho_f \| \nabla v \|_{\mathbb{R}^d \setminus \Gamma}^2 + \rho_f c^{-2} \| s\, v \|_{\mathbb{R}^d}^2.$$

We will also write $\sigma := \operatorname{Re} s > 0$ (for all $s \in \mathbb{C}_+$) and $\underline{\sigma} := \min\{\sigma, 1\}$. To shorten some of the forthcoming expressions, we will denote:

$$\begin{aligned} \| (\mathbf{u}, v) \|_{1, \mathbb{R}^d \setminus \Gamma}^2 &:= (\boldsymbol{\sigma}(\mathbf{u}), \boldsymbol{\varepsilon}(\overline{\mathbf{u}}))_{\mathbb{R}^d \setminus \Gamma}^2 + \| \sqrt{\rho_\Sigma} \mathbf{u} \|_{\mathbb{R}^d}^2 + \rho_f \| \nabla v \|_{\mathbb{R}^d \setminus \Gamma}^2 + \rho_f c^{-2} \| v \|_{\mathbb{R}^d}^2, \\ \| (\boldsymbol{\phi}, \phi) \|_{1/2, \Gamma}^2 &:= \| \boldsymbol{\phi} \|_{1/2, \Gamma}^2 + \| \phi \|_{1/2, \Gamma}^2, \\ \| (\lambda, \varphi) \|_{-1/2, 1/2, \Gamma}^2 &:= \| \lambda \|_{-1/2, \Gamma}^2 + \| \varphi \|_{1/2, \Gamma}^2. \end{aligned}$$

Note that the energy norm and the first of the above norms are related by

$$\underline{\sigma} \| (\mathbf{u}, v) \|_{1, \mathbb{R}^d \setminus \Gamma} \leq |\!|\!| (\mathbf{u}, v) |\!|\!|_{|s|} \leq \frac{|s|}{\underline{\sigma}} \| (\mathbf{u}, v) \|_{1, \mathbb{R}^d \setminus \Gamma}. \tag{4.17}$$

Finally, the expression *independent of h* will be used to mean independent of the choice of the spaces $\mathbf{Y}_h$ and Y_h.

Proposition 4.4 (Well-posedness)**.** *Problem* (4.15) *is uniquely solvable for any*

$$(\lambda_0, \phi_0) \in H^{-1/2}(\Gamma) \times H^{1/2}(\Gamma) \quad \text{and} \quad s \in \mathbb{C}_+.$$

Moreover, there exists $C > 0$, independent of h, such that

$$|\!|\!| (\mathbf{u}^h, v^h) |\!|\!|_{|s|} \leq C \frac{|s|}{\underline{\sigma}\, \sigma} \| (\lambda_0, s \phi_0) \|_{-1/2, 1/2, \Gamma}. \tag{4.18}$$

Proof. A simple computation shows that

$$\text{Re } (\overline{s}B((\mathbf{u},v),(\overline{\mathbf{u}},\overline{v});s)) = \sigma|||(\mathbf{u},v)|||^2_{|s|}, \tag{4.19}$$

and that

$$|\ell((\mathbf{u},v);s)| \le C\rho_f \|(\lambda_0, s\phi_0)\|_{-1/2,1/2,\Gamma} \|(\mathbf{u},v)\|_{1,\mathbb{R}^d\setminus\Gamma}, \tag{4.20}$$

which proves well-posedness of (4.15) by the Lax-Milgram lemma. The estimate (4.18) is a direct consequence of (4.19) and (4.20), using (4.17) to relate the norms. □

The final step wraps up the analysis by collecting information from the previous results.

Corollary 4.5. *Equations* (4.9) *are uniquely solvable for all* $s \in \mathbb{C}_+$ *and any choice of the closed spaces* $\mathbf{Y}_h$ *and* Y_h*. Moreover, if* $(\mathbf{u}^h, v^h)$ *are defined using* (4.11) *from the solution of* (4.9)*, the following bounds hold with* $C > 0$ *independent of* h*:*

$$\|(\mathbf{u}^h, v^h)\|_{1,\mathbb{R}^d\setminus\Gamma} \le C\frac{|s|}{\underline{\sigma}^2\sigma}\|(\lambda_0, s\phi_0)\|_{-1/2,1/2,\Gamma}, \tag{4.21a}$$

$$\|(\boldsymbol{\phi}^h_\Sigma, \phi^h_f)\|_{1/2,\Gamma} \le C\frac{|s|}{\underline{\sigma}^2\sigma}\|(\lambda_0, s\phi_0)\|_{-1/2,1/2,\Gamma}. \tag{4.21b}$$

Proof. Propositions 4.2 and 4.3 relate the discrete integral system (4.9) to the variational problem (4.15), which is shown to be uniquely solvable in Proposition 4.4. The estimate (4.21a) follows from (4.18) and (4.17). Finally, the bound (4.21b) follows from (4.21a) and (4.13). □

We end this section by noting that Corollary 4.5 implies the unique solvability of the semidiscrete equations that are obtained by taking the inverse Laplace transform of (4.9). They can also be translated into a time domain estimate that bounds norms of the solution in terms of bounds for the data (Proposition 4.12 below).

4.2.2 The Effect of Galerkin Semidiscretization

In this section we analyze the effect of space semidiscretization, that is, we estimate the difference between the solution of (4.4) and (4.9). The analysis follows

a very similar pattern to the one displayed in Section 4.2.1. We start by writing the error equations:

$$\mathbb{L}(s)(\boldsymbol{\phi}_\Sigma^h - \boldsymbol{\phi}_\Sigma, \phi_f^h - \phi_f) \in \mathbf{Y}_h^\circ \times Y_h^\circ. \tag{4.22}$$

We will develop the analysis in terms of the variables

$$\mathbf{e}^h := \mathbf{u}^h - u \quad \text{and} \quad e^h := v^h - v,$$

from which the error of the boundary unknowns can be recovered:

$$(\boldsymbol{\phi}_\Sigma^h - \boldsymbol{\phi}_\Sigma, \phi_f^h - \phi_f) = (\llbracket \gamma \mathbf{e}^h \rrbracket, -\llbracket \gamma e^h \rrbracket). \tag{4.23}$$

The potential representation for $(\mathbf{e}^h, e^h)$ is obtained by subtracting (4.5) from (4.11)

$$\mathbf{e}^h = -\rho_f s \mathbf{S}(s) \mathrm{N}^t(\phi_f^h - \phi_f) - \mathbf{D}(s)(\boldsymbol{\phi}_\Sigma^h - \boldsymbol{\phi}_\Sigma), \tag{4.24a}$$

$$e^h = s\mathrm{S}(s/c)\mathrm{N}(\boldsymbol{\phi}_\Sigma^h - \boldsymbol{\phi}_\Sigma) + \mathrm{D}(s/c)(\phi_f^h - \phi_f). \tag{4.24b}$$

The proofs of the following results are quite similar to those of Propositions 4.2, 4.3, and 4.4. We will only point out the main differences.

Proposition 4.6. *The error potentials $\mathbf{e}^h := \mathbf{u}^h - u$ and $e^h := v^h - v$ satisfy:*

$$\Delta^* \mathbf{e}^h - \rho_\Sigma s^2 \mathbf{e}^h = \mathbf{0} \qquad \text{in } \mathbb{R}^d \setminus \Gamma, \tag{4.25a}$$

$$\Delta e^h - (s/c)^2 e^h = 0 \qquad \text{in } \mathbb{R}^d \setminus \Gamma, \tag{4.25b}$$

$$s\mathrm{N}\llbracket \gamma \mathbf{e}^h \rrbracket - \llbracket \partial_\nu e^h \rrbracket = 0, \tag{4.25c}$$

$$\llbracket \mathbf{t}(\mathbf{e}^h) \rrbracket - \rho_f s \mathrm{N}^t \llbracket \gamma e^h \rrbracket = 0, \tag{4.25d}$$

$$(\llbracket \gamma \mathbf{e}^h \rrbracket, \llbracket \gamma e^h \rrbracket) + (\boldsymbol{\phi}_\Sigma, -\phi_f) \in \mathbf{Y}_h \times Y_h, \tag{4.25e}$$

$$(s\mathrm{N}\gamma^+ \mathbf{e}^h + \partial_\nu^- e^h, \mathbf{t}^+(\mathbf{e}^h) + \rho_f s \mathrm{N}^t \gamma^- e^h) \in \mathbf{Y}_h^\circ \times Y_h^\circ. \tag{4.25f}$$

Reciprocally, given a solution of (4.25), the quantities defined in (4.23) satisfy (4.22).

Proposition 4.7. *Problem (4.25) is equivalent to the variational problem: find*

$$(\mathbf{e}^h, e^h) \in \mathbf{H}^1(\mathbb{R}^d \setminus \Gamma) \times H^1(\mathbb{R}^d \setminus \Gamma)$$

such that

$$([\![\gamma \mathbf{e}^h]\!] + \boldsymbol{\phi}_\Sigma, [\![\gamma e^h]\!] - \phi_f) \in \mathbf{Y}_h \times Y_h, \tag{4.26a}$$

$$B((\mathbf{e}^h, e^h), (\mathbf{w}, w); s) = 0 \qquad \forall (\mathbf{w}, w) \in \mathbb{H}_h. \tag{4.26b}$$

We note that, in comparison with (4.15), problem (4.26) has homogeneous right-hand side but incorporates a side restriction (4.26a). This compares with how the conditions (4.12c)-(4.12d) have become homogeneous in (4.25c)-(4.25d), while the homogeneous condition (4.12e) is now non-homogeneous (4.25e).

Proposition 4.8. *Problem* (4.26) *is uniquely solvable for any* $(\boldsymbol{\phi}_\Sigma, \phi_f) \in \mathbb{H}^{1/2}(\Gamma)$ *and* $s \in \mathbb{C}_+$. *Moreover, there exists* $C > 0$ *independent of* h *such that*

$$|\!|\!|(\mathbf{e}^h, e^h)|\!|\!|_{|s|} \leq C \frac{|s|^2}{\sigma \underline{\sigma}} \|(\boldsymbol{\phi}_\Sigma, \phi_f)\|_{1/2,\Gamma}. \tag{4.27}$$

Proof. Using the definition of the bilinear form B (see Proposition 4.3) and (4.17), we can easily bound

$$\begin{aligned} |B((\mathbf{u}, v), (\mathbf{w}, w); s)| &\leq |\!|\!|(\mathbf{u}, v)|\!|\!|_{|s|} |\!|\!|(\mathbf{w}, w)|\!|\!|_{|s|} + C|s| \, \|(\mathbf{u}, v)\|_{1,\mathbb{R}^d\setminus\Gamma} \|(\mathbf{w}, w)\|_{1,\mathbb{R}^d\setminus\Gamma} \\ &\leq C \frac{|s|}{\underline{\sigma}} \|(\mathbf{u}, v)\|_{1,\mathbb{R}^d\setminus\Gamma} |\!|\!|(\mathbf{w}, w)|\!|\!|_{|s|}. \end{aligned} \tag{4.28}$$

Take now $(\mathbf{w}, w) \in \mathbf{H}^1(\mathbb{R}^d \setminus \Gamma) \times H^1(\mathbb{R}^d \setminus \Gamma)$ such that

$$[\![\gamma \mathbf{w}]\!] = \boldsymbol{\phi}_\Sigma, \quad [\![\gamma w]\!] = -\phi_f, \quad \|(\mathbf{w}, w)\|_{1,\mathbb{R}^d\setminus\Gamma} \leq C \|(\boldsymbol{\phi}_\Sigma, \phi_f)\|_{1/2,\Gamma}. \tag{4.29}$$

By the energy identity (4.19), the fact that $(\mathbf{e}^h + \mathbf{w}, e^h + w) \in \mathbb{H}_h$, and (4.28), it follows that

$$\begin{aligned} |\!|\!|(\mathbf{e}^h + \mathbf{w}, e^h + w)|\!|\!|^2_{|s|} &\leq \frac{|s|}{\sigma} |B((\mathbf{e}^h + \mathbf{w}, e^h + w), (\mathbf{e}^h + \mathbf{w}, e^h + w); s)| \\ &= \frac{|s|}{\sigma} |B((\mathbf{w}, w), (\mathbf{e}^h + \mathbf{w}, e^h + w); s)| \\ &\leq C \frac{|s|^2}{\sigma \underline{\sigma}} \|(\mathbf{w}, w)\|_{1,\mathbb{R}^d\setminus\Gamma} |\!|\!|(\mathbf{e}^h + \mathbf{w}, e^h + w)|\!|\!|_{|s|}. \end{aligned}$$

Therefore, using (4.17)

$$|\!|\!|(\mathbf{e}^h, e^h)|\!|\!|_{|s|} \leq C \frac{|s|^2}{\sigma \underline{\sigma}} \|(\mathbf{w}, w)\|_{1,\mathbb{R}^d\setminus\Gamma},$$

and the result follows from (4.29). For readers who are acquainted with this kind of Laplace domain estimates, let us clarify that the use of the optimal $|s|$-dependent lifting of Bamberger-HaDuong [6, Lemma 1] (see also [116, Proposition 2.5.1]), instead of the plain lifting used in (4.29), does not improve the estimate. This is principally due to the s factor in the boundary terms of the bilinear form B (see (4.28)). □

Corollary 4.9. *Let $(\boldsymbol{\phi}_\Sigma, \phi_f)$ and $(\boldsymbol{\phi}_\Sigma^h, \phi_f^h)$ be the respective solutions of (4.4) and (4.9). Let then $(\mathbf{u}, v)$ and $(\mathbf{u}^h, v^h)$ be defined through (4.5) and (4.11) respectively. Then there exists $C > 0$ independent of h such that*

$$\begin{aligned}\|(\mathbf{u}^h - \mathbf{u}, v^h - v)\|_{1,\mathbb{R}^d\setminus\Gamma} &\leq C\frac{|s|^2}{\sigma\underline{\sigma}^2}\|(\boldsymbol{\phi}_\Sigma, \phi_f)\|_{1/2,\Gamma},\\ \|(\boldsymbol{\phi}_\Sigma^h - \boldsymbol{\phi}_\Sigma, \phi_f^h - \phi_f)\|_{1/2,\Gamma} &\leq C\frac{|s|^2}{\sigma\underline{\sigma}^2}\|(\boldsymbol{\phi}_\Sigma, \phi_f)\|_{1/2,\Gamma}.\end{aligned}$$

Proof. The result is a direct consequence of Propositions 4.6, 4.7, and 4.8. □

Using the results obtained in the previous two subsections it is possible to establish error estimates in the time domain. Data will be taken in the Sobolev spaces

$$W_+^k(H^{\pm1/2}(\Gamma)) := \{\xi \in \mathcal{C}^{k-1}(\mathbb{R}; H^{\pm1/2}(\Gamma)) : \xi \equiv 0 \text{ in } (-\infty, 0), \xi^{(k)} \in L^1(\mathbb{R}; H^{\pm1/2}(\Gamma))\},$$

for $k \geq 1$. A straightforward application of the inversion theorem of the Laplace transform [37, Theorem 7.1] (see also Proposition A.1) starting with the bounds of Corollary 4.5 yields the following:

Corollary 4.10. *If the data of the problem satisfy*

$$\lambda_0 \in W_+^3(H^{-1/2}(\Gamma)) \quad \text{and} \quad \phi_0 \in W_+^4(H^{1/2}(\Gamma)),$$

then $(\boldsymbol{\phi}_\Sigma, \phi_f)$ and $(\mathbf{u}^h, v^h)$ are continuous causal functions of time and for all $t \geq 0$

$$\|(\boldsymbol{\phi}_\Sigma, \phi_f)(t)\|_{1/2,\Gamma} \leq \frac{D_1 t^2}{t+1}\max\{1, t^2\}\int_0^t \|\mathcal{P}_3(\lambda_0, \dot{\phi}_0)(\tau)\|_{-1/2,1/2,\Gamma}\, d\tau,$$

$$\|(\mathbf{u}^h, v^h)(t)\|_{1,\mathbb{R}^d\setminus\Gamma} \leq \frac{D_2 t^2}{t+1}\max\{1, t^2\}\int_0^t \|\mathcal{P}_3(\lambda_0, \dot{\phi}_0)(\tau)\|_{-1/2,1/2,\Gamma}\, d\tau,$$

where D_1 and D_2 depend only on Γ and

$$(\mathcal{P}_k f)(t) := \sum_{l=0}^{k} \binom{k}{l} f^{(l)}(t).$$

In a similar fashion, a combined application of Proposition A.1 and Corollary 4.9, provides the following estimate for the errors of semidiscretization in time. Note that we are allowed to insert the best approximation operators in the right-hand side of the bound of Corollary 4.11 because the error produced by trying to compute the exact solution and the difference of the exact solution with its best approximation is the same.

Corollary 4.11. *If the exact solution of (4.4) satisfies*

$$(\boldsymbol{\phi}_\Sigma, \phi_f) \in W_+^4(\mathbf{H}^{1/2}(\Gamma)) \times W_+^4(H^{1/2}(\Gamma)),$$

then

$$(\mathbf{e}^h, e^h) := (\mathbf{u} - \mathbf{u}^h, v - v^h) \in \mathcal{C}(\mathbb{R}, \mathbf{H}^1(\mathbb{R}^d \setminus \Gamma) \times H^1(\mathbb{R}^d \setminus \Gamma)),$$

and for all $t \geq 0$ we have the bound

$$\|(\mathbf{e}^h, e^h)(t)\|_{1,\mathbb{R}^d\setminus\Gamma} \leq \frac{Dt^2}{t+1} \max\{1, t^2\} \int_0^t \|\mathcal{P}_4(\boldsymbol{\phi}_\Sigma - \boldsymbol{\Pi}_h \boldsymbol{\phi}_\Sigma, \phi_f - \Pi_h \phi_f)(\tau)\|_{1/2,\Gamma}\, d\tau,$$

where $\boldsymbol{\Pi}_h$ and Π_h are the best approximation operators in $\mathbf{Y}_h$ and Y_h, and D depends only on Γ.

4.2.3 Full Discretization with BDF2-CQ

A fully discrete method can be obtained by using any of the many Convolution Quadrature schemes (See Appendix B). We next give an estimate for the BDF2-based CQ method, based on the stability bound in the Laplace domain obtained in Propositions 4.4 and B.2 (a slight refinement of one of the main convergence theorems in [91]).

Proposition 4.12. *Let $\ell = 6$ and (λ_0, ϕ_0) be causal problem data such that*

$$\lambda_0 \in W_+^\ell(H^{-1/2}(\Gamma)) \quad \text{and} \quad \phi_0 \in W_+^{\ell+1}(H^{1/2}(\Gamma)),$$

and $(\mathbf{u}_\kappa^h, v_\kappa^h)$ *be the BDF2-based CQ discretization of* $(\mathbf{u}^h, v^h)$*. Then, for* $t \geq 0$

$$\|(\mathbf{u}^h, v^h)(t) - (\mathbf{u}_\kappa^h, v_\kappa^h)(t)\|_{1,\mathbb{R}^d\setminus\Gamma} \leq D\kappa^2(1+t^2)\int_0^t \|(\lambda_0^{(\ell)}, \phi_0^{(\ell+1)})(\tau)\|_{-1/2,1/2,\Gamma}\, d\tau.$$

It is important to note that the high-order regularity $\ell = 6$ is only required to achieve optimal convergence of order κ^2. For problem data with regularity as low as $\ell = 3$, reduced convergence of order $\kappa^{3/2}$ is achieved (see [116]).

4.3 Coupling BEM-FEM for General Linear Elastic Materials

Going back to the system of equations (4.3), an alternate approach aiming for a finite element solution of the elastic wavefield and a boundary element solution of the acoustic wavefield is to use a direct boundary integral representation of the acoustic wave while keeping the partial differential equation for the elastic displacement in variational form. This approach is particularly well suited for the case of variable elastic density and Lamé coefficients, and also for heterogeneous anisotropic materials. We will still use the Hooke's Law (2.8) relating stress and strain and will require the stiffness tensor $\mathbf{C}$ to satisfy all the assumptions made on Section 2.7.

The derivation of the model employs standard arguments of boundary integral equations and is presented with careful detail in [68], with the resulting equivalent system being

$$\rho_\Sigma s^2 \mathbf{u} - \Delta^* \mathbf{u} = 0 \qquad \text{in } \Omega_-, \tag{4.30a}$$

$$\mathbf{t}^-(\mathbf{u}) + \rho_f s \mathrm{N}^t \phi = -\rho_f s \mathrm{N}^t \phi_0 \qquad \text{on } \Gamma, \tag{4.30b}$$

$$\mathrm{V}(s/c)\lambda + \left(\tfrac{1}{2}\mathrm{I} - \mathrm{K}(s/c)\right)\phi = 0 \qquad \text{on } \Gamma, \tag{4.30c}$$

$$\left(-\tfrac{1}{2}\mathrm{I} + \mathrm{K}^t(s/c)\right)\lambda + \mathrm{W}(s/c)\phi - s\mathrm{N}\gamma\mathbf{u} = \lambda_0 \qquad \text{on } \Gamma. \tag{4.30d}$$

For notational convenience, we introduce the interior elastodynamic bilinear form in the Laplace domain

$$a(\mathbf{u}, \mathbf{w}; s) := (\boldsymbol{\sigma}(\mathbf{u}), \boldsymbol{\varepsilon}(\mathbf{w}))_{\Omega_-} + s^2(\rho_\Sigma \mathbf{u}, \mathbf{w})_{\Omega_-},$$

so that the variational formulation of (4.30a)-(4.30b) reads

$$a(\mathbf{u}, \mathbf{w}; s) + s\langle \rho_f(\phi + \phi_0), \gamma\mathbf{w}\cdot\boldsymbol{\nu}\rangle_\Gamma = 0 \quad \forall \mathbf{w} \in \mathbf{H}^1(\Omega_-).$$

We note that the operator $\mathrm{N}\gamma\mathbf{w} = \gamma\mathbf{w}\cdot\boldsymbol{\nu}$ appears in this weak formulation, while N^t will not be used any longer in this section. Since the language of this section is less heavy on the side of operators, we will keep the explicit form of the combined operator $\mathrm{N}\gamma$ as a trace operator dotted with the normal vector field.

4.3.1 Galerkin Semidiscretization in Space

Just as in Section 4.2.1, the solvability and stability of (4.30) are studied simultaneously. In order to do so, we define the closed subspaces

$$\mathbf{V}_h \subset \mathbf{H}^1(\Omega_-), \quad X_h \subset H^{-1/2}(\Gamma), \quad Y_h \subset H^{1/2}(\Gamma).$$

The following result establishes the connection between the discrete counterpart of problem (4.30) and a non-standard transmission problem. Note that the 'Finite Element' form is a discretization of the interior Navier-Lamé equation, and therefore, the elastic operator has been discretized, as opposed to what happens with the 'Boundary Element' counterpart, where only transmission conditions are discretized.

Proposition 4.13 (Transmission problem for Galerkin equations)**.** *If*

$$(\mathbf{u}^h,\, \phi^h,\, \lambda^h) \,\in\, \mathbf{V}_h \times Y_h \times X_h$$

satisfies the Galerkin equations

$$a(\mathbf{u}^h, \mathbf{w}; s) + s\langle \rho_f(\phi^h + \phi_0), \gamma\mathbf{w}\cdot\boldsymbol{\nu}\rangle_\Gamma = 0 \qquad \forall \mathbf{w} \in \mathbf{V}_h, \tag{4.31a}$$

$$-s\gamma\mathbf{u}^h\cdot\boldsymbol{\nu} + \mathrm{W}(s/c)\phi^h + \left(-\tfrac{1}{2}\mathrm{I} + \mathrm{K}^t(s/c)\right)\lambda^h - \lambda_0 \,\in\, Y_h^\circ, \tag{4.31b}$$

$$\left(\tfrac{1}{2}\mathrm{I} - \mathrm{K}(s/c)\right)\phi^h + \mathrm{V}(s/c)\lambda^h \,\in\, X_h^\circ, \tag{4.31c}$$

and

$$v^h := \mathrm{D}(s/c)\phi^h - \mathrm{S}(s/c)\lambda^h, \tag{4.32}$$

then the pair $(\mathbf{u}^h, v^h) \in \mathbf{V}_h \times H^1(\mathbb{R}^d \setminus \Gamma)$ *satisfies the transmission problem*

$$a(\mathbf{u}^h, \mathbf{w}; s) + s\langle \rho_f(-[\![\gamma v^h]\!] + \phi_0), \gamma \mathbf{w} \cdot \boldsymbol{\nu}\rangle_\Gamma = 0 \qquad \forall \mathbf{w} \in \mathbf{V}_h, \tag{4.33a}$$

$$-\Delta v^h + (s/c)^2 v^h = 0 \qquad \text{in } \mathbb{R}^d \setminus \Gamma, \tag{4.33b}$$

$$[\![\gamma v^h]\!] \in Y_h, \tag{4.33c}$$

$$[\![\partial_\nu v^h]\!] \in X_h, \tag{4.33d}$$

$$s\gamma \mathbf{u}^h \cdot \boldsymbol{\nu} + \partial_\nu^+ v^h + \lambda_0 \in Y_h^\circ, \tag{4.33e}$$

$$\gamma^- v^h \in X_h^\circ. \tag{4.33f}$$

Conversely, given a solution of (4.33)*, the triplet*

$$(\mathbf{u}^h, \phi^h, \lambda^h) := (\mathbf{u}^h, -[\![\gamma v^h]\!], -[\![\partial_\nu v^h]\!]) \in \mathbf{V}_h \times Y_h \times X_h \tag{4.34}$$

satisfies (4.31)*.*

Proof. Equations (4.33b), (4.33c), and (4.33d) are simple consequences of the definition of v^h and the jump relations of the double and single layer potentials. Moreover, using the definition of v^h and the identities (2.25)

$$\partial_\nu^- \mathrm{S}(s) = \tfrac{1}{2}\mathrm{I} + \mathrm{K}^t(s)\,, \qquad \gamma^- \mathrm{D}(s) = -\tfrac{1}{2}\mathrm{I} + \mathrm{K}(s),$$

it is easy to verify that (4.33e) and (4.33f) are just restatements of (4.31b) and (4.31c).

To prove the converse, note that (4.33b) and the definition of (ϕ^h, λ^h) in (4.34) imply the integral representation (4.32). Then (4.31b) is equivalent to (4.33e) and (4.31c) is equivalent to (4.33f). □

Proposition 4.14 (Equivalent variational formulation)**.** *Consider the space*

$$V_h := \{v \in H^1(\mathbb{R}^d \setminus \Gamma) : [\![\gamma v]\!] \in Y_h\,,\ \gamma^- v \in X_h^\circ\}.$$

The problem (4.33) *is equivalent to finding* $(\mathbf{u}^h, v^h) \in \mathbf{V}_h \times V_h$ *such that*

$$\mathcal{A}\left((\mathbf{u}^h, v^h), (\mathbf{w}, w); s\right) = f\left((\mathbf{w}, w); s\right) \quad \forall (\mathbf{w}, w) \in \mathbf{V}_h \times V_h, \tag{4.35}$$

where

$$\begin{aligned}\mathcal{A}\left((\mathbf{u},v),(\mathbf{w},w);s\right) &:= \left(\boldsymbol{\sigma}(\mathbf{u}),\boldsymbol{\varepsilon}(\mathbf{w})\right)_{\Omega_-} + s^2\left(\rho_\Sigma\mathbf{u},\mathbf{w}\right)_{\Omega_-}\\ &\quad + \rho_f\left(\nabla v,\nabla w\right)_{\mathbb{R}^d\setminus\Gamma} + \rho_f(s/c)^2\left(v,w\right)_{\mathbb{R}^d\setminus\Gamma}\\ &\quad + \rho_f s\langle\gamma\mathbf{u}\cdot\boldsymbol{\nu},[\![\gamma w]\!]\rangle_\Gamma - \rho_f s\langle[\![\gamma v]\!],\gamma\mathbf{w}\cdot\boldsymbol{\nu}\rangle_\Gamma,\\ f\left((\mathbf{w},w);s\right) &:= -\rho_f s\langle\phi_0,\gamma\mathbf{w}\cdot\boldsymbol{\nu}\rangle_\Gamma - \rho_f\langle\lambda_0,[\![\gamma w]\!]\rangle_\Gamma.\end{aligned}$$

Proof. Let $(\mathbf{u}^h,v^h)$ be a solution pair for (4.33). Then, for all $w\in V_h$,

$$\begin{aligned}\langle\partial_\nu^+ v^h,[\![\gamma w]\!]\rangle_\Gamma &= \langle\partial_\nu^- v^h,\gamma^- w\rangle_\Gamma - \langle\partial_\nu^+ v^h,\gamma^+ w\rangle_\Gamma - \langle[\![\partial_\nu v^h]\!],\gamma^- w\rangle_\Gamma\\ &= \left(\nabla v^h,\nabla w\right)_{\mathbb{R}^d\setminus\Gamma} + (s/c)^2(v^h,w)_{\mathbb{R}^d},\end{aligned}$$

after applying (4.33b) and (4.33f). Therefore, testing (4.33e) with $[\![\gamma w]\!]$ for $w\in V_h$, and substituting the above, it follows that

$$(s/c)^2(v^h,w)_{\mathbb{R}^d} + \left(\nabla v^h,\nabla w\right)_{\mathbb{R}^d\setminus\Gamma} + s\langle\gamma\mathbf{u}^h\cdot\boldsymbol{\nu},[\![\gamma w]\!]\rangle_\Gamma = -\langle\lambda_0,[\![\gamma w]\!]\rangle_\Gamma \quad \forall w\in V_h. \tag{4.36}$$

However, the pair of equations (4.33a) and (4.36) are equivalent to (4.35).

To prove the converse statement, note that we need to show that a solution of (4.36) satisfies (4.33b), (4.33d), and (4.33e). Equation (4.36) applied to a general compactly supported $w\in\mathcal{C}^\infty(\mathbb{R}^d\setminus\Gamma)$ is the distributional form of (4.33b). Therefore, (4.36) (after integration by parts) implies

$$\langle\partial_\nu^- v^h,\gamma^- w\rangle_\Gamma - \langle\partial_\nu^+ v^h,\gamma^+ w\rangle_\Gamma + \langle s\gamma\mathbf{u}^h\cdot\boldsymbol{\nu}+\lambda_0,[\![\gamma w]\!]\rangle_\Gamma = 0 \quad \forall w\in V_h,$$

which, after some simple algebra, is shown to be equivalent to

$$\langle\partial_\nu^+ v^h + s\gamma\mathbf{u}^h\cdot\boldsymbol{\nu}+\lambda_0,[\![\gamma w]\!]\rangle_\Gamma + \langle[\![\partial_\nu v^h]\!],\gamma^- w\rangle_\Gamma = 0 \qquad \forall w\in V_h. \tag{4.37}$$

However, the operator $V_h\ni w\longmapsto([\![\gamma w]\!],\gamma^- w)\in Y_h\times X_h^\circ$ is surjective, and therefore (4.37) is equivalent to (4.33d) and (4.33e). □

For the analysis of (4.35), we need to redefine the energy norm

$$|\!|\!|(\mathbf{u},v)|\!|\!|_{|s|}^2 := \left(\boldsymbol{\sigma}(\mathbf{u}),\boldsymbol{\varepsilon}(\overline{\mathbf{u}})\right)_{\Omega_-} + \|s\sqrt{\rho_\Sigma}\mathbf{u}\|_{\Omega_-}^2 + \rho_f\|\nabla v\|_{\mathbb{R}^d\setminus\Gamma}^2 + \rho_f\|(s/c)\,v\|_{\mathbb{R}^d}^2,$$

due to the fact that the elastic field is not handled with a potential representation and, therefore, it does not extend to the other side of the interface. Note that $|\!|\!| \cdot |\!|\!|_1$ is equivalent to the $\mathbf{H}^1(\Omega_-) \times H^1(\mathbb{R}^d \setminus \Gamma)$ norm and that, similarly to (4.17),

$$\underline{\sigma}|\!|\!|(\mathbf{u}, v)|\!|\!|_1 \leq |\!|\!|(\mathbf{u}, v)|\!|\!|_{|s|} \leq \frac{|s|}{\underline{\sigma}}|\!|\!|(\mathbf{u}, v)|\!|\!|_1. \tag{4.38}$$

Proposition 4.15 (Well-posedness)**.** *Problem* (4.35) *is uniquely solvable for any*

$$(\phi_0, \lambda_0) \in H^{1/2}(\Gamma) \times H^{-1/2}(\Gamma) \quad \text{and} \quad s \in \mathbb{C}_+.$$

Moreover, there exist $C_1, C_2 > 0$*, independent of* h*, such that*

$$|\!|\!|(\mathbf{u}^h, v^h)|\!|\!|_1 + \|\phi^h\|_{1/2,\Gamma} \leq C_1 \frac{|s|}{\sigma \underline{\sigma}^2} \|(s\phi_0, \lambda_0)\|_{1/2,-1/2,\Gamma}, \tag{4.39}$$

$$\|\lambda^h\|_{-1/2,\Gamma} \leq C_2 \frac{|s|^{3/2}}{\sigma \underline{\sigma}^{3/2}} \|(s\phi_0, \lambda_0)\|_{1/2,-1/2,\Gamma}. \tag{4.40}$$

Proof. It is straightforward to verify that

$$\mathrm{Re}\left(\overline{s}\mathcal{A}\left((\mathbf{u}, v), (\overline{\mathbf{u}}, \overline{v}); s\right)\right) = \sigma |\!|\!|(\mathbf{u}, v)|\!|\!|_{|s|}^2, \tag{4.41}$$

and

$$|f\left((\mathbf{w}, w); s\right)| \leq C \|(s\phi_0, \lambda_0)\|_{1/2,-1/2,\Gamma} |\!|\!|(\mathbf{w}, w)|\!|\!|_1,$$

where the constant depends only on ρ_f and Γ. Hence, by (4.38) and the Lax-Milgram lemma, we have unique solvability of (4.35) and the following bound in the energy norm:

$$|\!|\!|(\mathbf{u}^h, v^h)|\!|\!|_{|s|} \leq C \frac{|s|}{\sigma \underline{\sigma}} \|(s\phi_0, \lambda_0)\|_{1/2,-1/2,\Gamma}. \tag{4.42}$$

The estimate (4.39) can be easily derived from (4.42) and (4.38) and the fact that $\phi^h = -[\![\gamma v^h]\!]$. Finally, recalling that $\lambda^h = -[\![\partial_\nu v^h]\!]$ and using [82, Lemma 15], namely if $\Delta v - s^2 v = 0$ in an open set $\mathcal{O}$ with Lipschitz boundary, then

$$\|\partial_\nu v\|_{-1/2,\partial\mathcal{O}} \leq C \left(\frac{|s|}{\underline{\sigma}}\right)^{1/2} (\|sv\|_{\mathcal{O}} + \|\nabla v\|_{\mathcal{O}}), \tag{4.43}$$

it can be shown that (4.40) follows from (4.39). □

4.3.2 Semidiscretization Error

We now study the difference between the solutions to the exact problem and their finite dimensional approximations. It is important to stress that $\mathbf{u}^h - \mathbf{u} \notin \mathbf{V}_h$, and therefore we will not be able to write a transmission problem for the error $\mathbf{u}^h - \mathbf{u}$ in the style of (4.33). Instead, we will work with the difference

$$\mathbf{e}^h := \mathbf{u}^h - \mathbf{P}_h\mathbf{u},$$

where $\mathbf{P}_h : \mathbf{H}^1(\Omega_-) \to \mathbf{V}_h$ is an elliptic projection that will be defined below. We first need to introduce the finite dimensional space of infinitesimal rigid motions

$$\mathbf{M} := \left\{ \mathbf{m} \in \mathbf{H}^1(\Omega_-) : (\boldsymbol{\sigma}(\mathbf{m}), \boldsymbol{\varepsilon}(\mathbf{m}))_{\Omega_-} = 0 \right\}.$$

From now on we will assume that $\mathbf{M} \subset \mathbf{V}_h$. The operator $\mathbf{P}_h$ is given by the solution of the problem

$$(\boldsymbol{\sigma}(\mathbf{P}_h\mathbf{u}), \boldsymbol{\varepsilon}(\mathbf{w}))_{\Omega_-} = (\boldsymbol{\sigma}(\mathbf{u}), \boldsymbol{\varepsilon}(\mathbf{w}))_{\Omega_-} \quad \forall \mathbf{w} \in \mathbf{V}_h, \tag{4.44a}$$

$$(\mathbf{P}_h\mathbf{u}, \mathbf{m})_{\Omega_-} = (\mathbf{u}, \mathbf{m})_{\Omega_-} \quad \forall \mathbf{m} \in \mathbf{M}. \tag{4.44b}$$

Using Korn's inequality it is easy to show that $\mathbf{P}_h$ is well defined and that the approximation error $\|\mathbf{u} - \mathbf{P}_h\mathbf{u}\|_{1,\Omega_-}$ is equivalent to the $\mathbf{H}^1(\Omega_-)$-best approximation on $\mathbf{V}_h$. In order to shorten notation, we will write $\mathbf{r}^h := \mathbf{P}_h\mathbf{u} - \mathbf{u}$.

The triplet $(\mathbf{e}^h, \phi^h, \lambda^h) \in \mathbf{V}_h \times Y_h \times X_h$ satisfies the following error equations:

$$a(\mathbf{e}^h, \mathbf{w}; s) + s^2 \left(\rho_\Sigma \mathbf{r}^h, \mathbf{w}\right)_{\Omega_-} + \rho_f s \langle (\phi^h - \phi), \gamma\mathbf{w} \cdot \boldsymbol{\nu} \rangle_\Gamma = 0 \quad \forall \mathbf{w} \in \mathbf{V}_h \tag{4.45a}$$

$$-s\gamma(\mathbf{e}^h + \mathbf{r}^h) \cdot \boldsymbol{\nu} + \mathrm{W}(s/c)(\phi^h - \phi) - \left(\tfrac{1}{2}\mathrm{I} - \mathrm{K}^t(s/c)\right)(\lambda^h - \lambda) \in Y_h^\circ, \tag{4.45b}$$

$$\left(\tfrac{1}{2}\mathrm{I} - \mathrm{K}(s/c)\right)(\phi^h - \phi) + \mathrm{V}(s/c)(\lambda^h - \lambda) \in X_h^\circ. \tag{4.45c}$$

For this system there is a corresponding non-standard transmission problem as the following proposition shows.

Proposition 4.16. *If* $(\mathbf{e}^h, \lambda^h, \phi^h)$ *satisfies* (4.45) *and we define*

$$e^h := \mathrm{D}(s/c)(\phi^h - \phi) - \mathrm{S}(s/c)(\lambda^h - \lambda),$$

then the pair then $(\mathbf{e}^h, e^h)$ *is a solution of the transmission problem*

$$a(\mathbf{e}^h, \mathbf{w}; s) - s\langle \rho_f [\![\gamma e^h]\!], \gamma \mathbf{w} \cdot \boldsymbol{\nu} \rangle_\Gamma = -\, s^2 \left(\rho_\Sigma \mathbf{r}^h, \mathbf{w}\right)_{\Omega_-} \qquad \forall \mathbf{w} \in \mathbf{V}_h, \tag{4.46a}$$

$$-\Delta e^h + (s/c)^2 e^h = 0 \qquad \text{in } \mathbb{R}^d \setminus \Gamma, \tag{4.46b}$$

$$[\![\gamma e^h]\!] - \phi \in Y_h, \tag{4.46c}$$

$$[\![\partial_\nu e^h]\!] - \lambda \in X_h, \tag{4.46d}$$

$$s\gamma(\mathbf{e}^h + \mathbf{r}^h) \cdot \boldsymbol{\nu} + \partial_\nu^+ e^h \in Y_h^\circ, \tag{4.46e}$$

$$\gamma^- e^h \in X_h^\circ. \tag{4.46f}$$

Conversely, if $(\mathbf{e}^h, e^h)$ *is a solution of* (4.46) *then*

$$(\mathbf{e}^h, \phi^h, \lambda^h) := (\mathbf{e}^h, \phi - [\![\gamma e^h]\!], \lambda - [\![\partial_\nu e^h]\!]),$$

solves (4.45).

Proof. Starting with a solution of (4.45), we see that (4.46b) is a consequence of the definition of e^h, while (4.46a) follows readily from (4.45a), noting that $([\![\gamma e^h]\!], [\![\partial_\nu e^h]\!]) = (\phi - \phi^h, \lambda - \lambda^h)$. The equations (4.46c) and (4.46d) can also be verified from the last observation, since $Y_h \times X_h \ni (\phi^h, \lambda^h) = (\phi - [\![\gamma e^h]\!], \lambda - [\![\partial_\nu e^h]\!])$. Finally, using

$$\partial_\nu^-(\mathrm{S}(s)\lambda) = (\tfrac{1}{2}\mathrm{I} + \mathrm{K}^t(s))\lambda\,, \qquad \gamma^-(\mathrm{D}(s)\phi) = \left(-\tfrac{1}{2}\mathrm{I} + \mathrm{K}(s)\right)\phi,$$

we see that (4.45b) and (4.45c) imply (4.46e) and (4.46f).

The proof of the converse statement is very similar. □

Proposition 4.17. *The system* (4.46) *is equivalent to the variational problem of finding* $(\mathbf{e}^h, e^h) \in \mathbf{H}^1(\Omega_-) \times H^1(\mathbb{R}^d \setminus \Gamma)$ *such that*

$$(\gamma^- e^h, [\![\gamma e^h]\!] - \phi) \in X_h^\circ \times Y_h, \tag{4.47a}$$

$$\mathcal{A}((\mathbf{e}^h, e^h), (\mathbf{w}, w); s) = b\,((\mathbf{w}, w); s) \qquad \forall (\mathbf{w}, w) \in \mathbf{V}_h \times V_h, \tag{4.47b}$$

where the bilinear form $\mathcal{A}$ is defined in the statement of Proposition 4.14 and

$$b\left((\mathbf{w},w);s\right) := \rho_f\langle\lambda,\gamma^- w\rangle_\Gamma + s\rho_f\langle\gamma\mathbf{r}^h\cdot\boldsymbol{\nu},[\![\gamma w]\!]\rangle_\Gamma - s^2\left(\rho_\Sigma\mathbf{r}^h,\mathbf{w}\right)_{\Omega_-}.$$

Proof. The proof is very similar to the one of Proposition 4.14. Details are omitted. □

Proposition 4.18. *Problem (4.47) is uniquely solvable for any*

$$(\mathbf{u},\phi,\lambda)\in\mathbf{H}^1(\Omega_-)\times H^{1/2}(\Gamma)\times H^{-1/2}(\Gamma),\qquad \textit{and}\qquad s\in\mathbb{C}_+.$$

Moreover, there exist constants $C_1,C_2>0$ independent of h such that

$$|\!|\!|(\mathbf{e}^h,e^h)|\!|\!|_1+\|\phi-\phi^h\|_{1/2,\Gamma}\leq C_1\frac{|s|}{\sigma\underline{\sigma}^2}\Big(\|(s\,\phi,\lambda)\|_{1/2,-1/2,\Gamma}+\|s\mathbf{r}^h\|_{1,\Omega_-}+\|s^2\mathbf{r}^h\|_{\Omega_-}\Big),\tag{4.48}$$

$$\|\lambda-\lambda^h\|_{1/2,\Gamma}\leq C_2\frac{|s|^{3/2}}{\sigma\underline{\sigma}^{3/2}}\Big(\|(s\,\phi,\lambda)\|_{1/2,-1/2,\Gamma}+\|s\mathbf{r}^h\|_{1,\Omega_-}+\|s^2\mathbf{r}^h\|_{\Omega_-}\Big).\tag{4.49}$$

Proof. The existence and uniqueness of the solution to (4.47) is proven in a way analogous to that used in Proposition 4.15. We will next prove a bound in the energy norm

$$|\!|\!|(\mathbf{e}^h,e^h)|\!|\!|_{|s|}\leq C_1\frac{|s|}{\sigma\underline{\sigma}}\Big(\|(s\,\phi,\lambda)\|_{1/2,-1/2,\Gamma}+\|s\mathbf{r}^h\|_{1,\Omega_-}+\|s^2\mathbf{r}^h\|_{\Omega_-}\Big).\tag{4.50}$$

The estimate (4.48) follows from (4.50) and (4.38). In order to get to (4.49) we make use of (4.50), the fact that $\lambda-\lambda^h=[\![\partial_\nu e^h]\!]$, and (4.43).

To prove (4.50) we proceed as follows. We first obtain an upper bound for the bilinear form

$$|\mathcal{A}((\mathbf{u},v),(\mathbf{w},w);s)|\leq C\frac{|s|}{\underline{\sigma}}|\!|\!|(\mathbf{u},v)|\!|\!|_1|\!|\!|(\mathbf{w},w)|\!|\!|_{|s|},\tag{4.51}$$

by the same argument that was used in Proposition 4.8. Also

$$|b\left((\mathbf{w},w);s\right)|\leq\frac{C}{\underline{\sigma}}\left(\|\lambda\|_{-1/2,\Gamma}+\|s\mathbf{r}^h\|_{1,\Omega_-}+\|s^2\mathbf{r}^h\|_{\Omega_-}\right)|\!|\!|(\mathbf{w},w)|\!|\!|_{|s|}.\tag{4.52}$$

The constants in (4.51) and (4.52) depend only on the geometry. Now, for $\phi\in H^{1/2}(\Gamma)$, pick a lifting $w_\phi\in H^1(\mathbb{R}^d\setminus\Gamma)$ such that $\gamma^+w_\phi=\phi$, $\gamma^-w_\phi=0$, and

$$\|w_\phi\|_{1,\mathbb{R}^d\setminus\Gamma}\leq C\|\phi\|_{1/2,\Gamma}.\tag{4.53}$$

Since $(\mathbf{e}^h, e^h + w_\phi) \in \mathbf{V}_h \times V_h$ we can use (4.41), (4.47b), (4.51), and (4.52) (i.e., coercivity, the variational equation, and boundedness of the bilinear form and right-hand side) to estimate

$$\begin{aligned}
|\!|\!|(\mathbf{e}^h, e^h + w_\phi)|\!|\!|_{|s|}^2 &\leq \frac{|s|}{\sigma} |\mathcal{A}\left((\mathbf{e}^h, e^h + w_\phi), (\mathbf{e}^h, e^h + w_\phi); s\right)| \\
&= \frac{|s|}{\sigma} |b\left((\mathbf{e}^h, e^h + w_\phi); s\right) + \mathcal{A}\left((\mathbf{0}, w_\phi), (\mathbf{e}^h, e^h + w_\phi); s\right)| \\
&\leq C \frac{|s|}{\sigma \underline{\sigma}} |\!|\!|(\mathbf{e}^h, e^h + w_\phi)|\!|\!|_{|s|} \\
&\quad \times \left(|s| \|w_\phi\|_{1,\mathbb{R}^d \setminus \Gamma} + \|\lambda\|_{-1/2,\Gamma} + \|s\mathbf{r}^h\|_{1,\Omega_-} + \|s^2 \mathbf{r}^h\|_{\Omega_-}\right).
\end{aligned}$$

This bound, together with

$$|\!|\!|(\mathbf{0}, \omega_\phi)|\!|\!|_{|s|} \leq \frac{C}{\underline{\sigma}} \|s\,\phi\|_{1/2,\Gamma}$$

(see (4.38) and (4.53)) prove (4.50). □

4.3.3 Estimates in the Time Domain

Using the bounds for the error operators derived in the previous section, we can prove explicit time domain estimates. Just like in the BEM/BEM case, we can use Proposition A.1 and combine it with the Laplace domain estimates from Propositions 4.15 and 4.18 to obtain the following results.

Corollary 4.19. *Consider causal problem data*

$$\phi_0 \in W_+^4(H^{1/2}(\Gamma)) \quad \text{and} \quad \lambda_0 \in W_+^3(H^{-1/2}(\Gamma)).$$

Then $\mathbf{u}^h, v^h, \phi^h, \lambda^h$ *are continuous causal functions of time and for all* $t \geq 0$

$$\begin{aligned}
|\!|\!|(\mathbf{u}^h, v^h)(t)|\!|\!|_1 + \|\phi^h(t)\|_{1/2,\Gamma} &\leq D_1 \max\{1, t^2\} \frac{t^2}{t+1} \int_0^t \|\mathcal{P}_3(\dot{\phi}_0, \lambda_0)(\tau)\|_{1/2,-1/2,\Gamma}\, d\tau, \\
\|\lambda^h(t)\|_{-1/2,\Gamma} &\leq D_2 \max\{1, t^{3/2}\} \frac{t\sqrt{t}}{\sqrt{t+1}} \int_0^t \|\mathcal{P}_3(\dot{\phi}_0, \lambda_0)(\tau)\|_{1/2,-1/2,\Gamma}\, d\tau,
\end{aligned}$$

where D_1 *and* D_2 *depend only on* Γ.

To abbreviate the following statement, we will use the following shorthand for approximation errors

$$a_h(t) := \int_0^t \left(\|\mathcal{P}_3(\dot{\phi} - \Pi_h^Y \dot{\phi})(\tau)\|_{1/2,\Gamma} + \|\mathcal{P}_3(\lambda - \Pi_h^X \lambda)(\tau)\|_{-1/2,\Gamma} \right) d\tau + \int_0^t \left(\|\mathcal{P}_3(\dot{\mathbf{u}} - \mathbf{P}_h \dot{\mathbf{u}})(\tau)\|_{1,\Omega_-} + \|\mathcal{P}_3(\ddot{\mathbf{u}} - \mathbf{P}_h \ddot{\mathbf{u}})(\tau)\|_{\Omega_-} \right) d\tau,$$

where $\Pi_h^Y : H^{1/2}(\Gamma) \to Y_h$ and $\Pi_h^X : H^{-1/2}(\Gamma) \to X_h$ are orthogonal projections and $\mathbf{P}_h$ is the elliptic elastic projection onto $\mathbf{V}_h$ defined in (4.44).

Corollary 4.20. *If the solution triplet satisfies*

$$(\mathbf{u}, \phi, \lambda) \in W_+^3(\mathbf{H}^1(\Omega_-)) \times W_+^4(H^{1/2}(\Gamma)) \times W_+^3(H^{-1/2}(\Gamma)),$$

then $(\mathbf{e}^h, e^h) \in \mathcal{C}(\mathbb{R}, \mathbf{H}^1(\Omega_-) \times H^1(\mathbb{R}^d \setminus \Gamma))$ *is causal and we have constants* D_1 *and* D_2 *depending only on* Γ *such that for* $t \geq 0$

$$|||(\mathbf{e}^h, e^h)(t)|||_1 + \|(\phi - \phi^h)(t)\|_{1/2,\Gamma} \leq D_1 \max\{1, t^2\} \frac{t^2}{t+1}\, a_h(t),$$
$$\|(\lambda - \lambda^h)(t)\|_{-1/2,\Gamma} \leq D_2 \max\{1, t^{3/2}\} \frac{t^{3/2}}{\sqrt{t+1}}\, a_h(t).$$

4.3.4 Full Discretization with BDF2-CQ

The purely boundary integral formulation treated in the first part of this chapter lent itself naturally to a full discretization using one of the many Convolution Quadrature schemes for the time evolution. For the current variational/boundary integral formulation it would seem that an independent treatment with traditional time-stepping for the Finite Element part and Convolution Quadrature for the discretized boundary integral equations would be the best way to proceed, and for our computational implementation we will proceed in this fashion.

However, it turns out that the separate application of time stepping and CQ to different parts of the system is equivalent to the application of CQ globally, as long as the time stepping method used for the FEM part coincides with the one giving rise to the CQ family used for the implementation (see Proposition B.3). This observation

will allow us to analyze the fully discrete method as if the whole discretization were done with CQ.

We present results for the coupled schemes based on BDF2. In the following section we will show numerical experiments for BDF2-CQ and Trapezoidal Rule-CQ. (We note that the general analysis of Trapezoidal Rule CQ applied to wave propagation problems was done by Lehel Banjai in [8], although it does not give explicit behaviour of bounds with respect to t.) We will use $(\mathbf{u}_\kappa^h, v_\kappa^h)$ to denote the fully discrete approximation of $(\mathbf{u}, v)$ using a CQ method with constant time-step κ. In parallel to the corresponding result in Section 4.2.3 (Proposition 4.12), the next estimate follows from the Laplace domain estimates in Proposition 4.18 and an application of [116, Proposition 4.6.1].

Proposition 4.21. *Let $\ell = 6$ and (ϕ_0, λ_0) be causal problem data such that*

$$(\phi_0, \lambda_0) \in W_+^{\ell+1}(H^{1/2}(\Gamma)) \times W_+^{\ell}(H^{-1/2}(\Gamma)),$$

and let $(\mathbf{u}_\kappa^h, v_\kappa^h)$ be the BDF2-based CQ discretization of $(\mathbf{u}^h, v^h)$. Then, for $t \geq 0$, it holds that

$$|||(\mathbf{u}^h, v^h)(t) - (\mathbf{u}_\kappa^h, v_\kappa^h)(t)|||_1 \leq D\kappa^2(1+t^2) \int_0^t \|(\phi_0^{(\ell+1)}, \lambda_0^{(\ell)})(\tau)\|_{1/2,-1/2,\Gamma}\, d\tau.$$

It is important to note that the high-order regularity $\ell = 6$ is only required to achieve optimal convergence of order κ^2. For problem data with regularity as low as $\ell = 3$, reduced convergence of order $\kappa^{3/2}$ is achieved (see [116, Chapter 4]).

4.4 Numerical Experiments

In this section, we show some experiments for fully discrete methods applied to the BEM and BEM/FEM formulations we have analyzed. For general ideas of what CQ time-discretization means and how it is used, we refer to Appendix B. Algorithms for BEM/FEM applied to acoustic transmission problems are explained in [61].

Boundary integral method. In order to test the convergence properties of the implementation the following synthetic problem was solved in $\mathbb{R}^2$. The interior

elastic domain will be the unit disk $\Omega_- = \{\mathbf{x} : x_1^2 + x_2^2 < 1\}$, and its exterior will be the acoustic domain. If we let

$$\mathcal{H}(t) := t^5(1-5(t-1)+15(t-1)^2-35(t-1)^3+70(t-1)^4-126(t-1)^5)\chi_{[0,1]}(t)+\chi_{[1,\infty)}(t) \quad (4.54)$$

be a $\mathcal{C}^5$ piecewise polynomial approximation to the Heaviside function, then the elastic causal pressure wave

$$\mathbf{u}(\mathbf{x},t) = \mathcal{H}(c_L t - \mathbf{x}\cdot\mathbf{d})\sin\left(3(c_L t - \mathbf{x}\cdot\mathbf{d})\right)\mathbf{d}, \quad \mathbf{d} = \left(\tfrac{1}{\sqrt{2}}, \tfrac{1}{\sqrt{2}}\right), \quad c_L = \sqrt{\frac{2\mu+\lambda}{\rho_\Sigma}},$$

and the cylindrical acoustic wave

$$v(\mathbf{x},t) = \mathcal{L}^{-1}\left\{\imath H_0^{(1)}(\imath s|\mathbf{x}|)\,\mathcal{L}\{\mathcal{H}(t)\sin(2t)\}\right\}$$

solve equations (4.2a) and (4.2b) respectively. Here $\mathcal{L}$ is the Laplace transform. In order for them to satisfy the entire IBVP (4.2), equations (4.2c) and (4.2d) were used to define the boundary data $\alpha_0 := \partial_\nu v^{inc}$ and $\beta_0 := v^{inc}$.

The boundary data was sampled accordingly and the Laplace transformed equivalent system (4.4) was discretized in space with `deltaBEM` (the reader is referred to [34, 31] for further details on the computational aspects of `deltaBEM`), which can be considered as a Galerkin $\mathcal{P}_1$ method with reduced quadrature, while Convolution Quadrature was used for time stepping on increasingly finer space/time discretizations with N space points and the same number of time steps. The approximated solutions were then sampled in 20 random points on the circle of radius $r = .7$ for the elastic wave and $r = 2$ for the acoustic wave and compared against the exact solutions. The maximum difference in the final time

$$E_{h,k}^{v} := \frac{\max_{i=1}^{20}|v(\mathbf{x}_i,t_f) - v^{h,k}(\mathbf{x}_i,t_f)|}{\max_{i=1}^{20}|v(\mathbf{x}_i,t_f)|},$$
$$E_{h,k}^{\mathbf{u}} := \frac{\max_{i=1}^{20}|\mathbf{u}(\mathbf{x}_i,t_f) - \mathbf{u}^{h,k}(\mathbf{x}_i,t_f)|}{\max_{i=1}^{20}|\mathbf{u}(\mathbf{x}_i,t_f)|},$$

is used as the error measure. Trapezoidal Rule CQ and BDF2-CQ were both implemented and compared. Tables 4.1 and 4.2 summarize the results, while convergence

N	$E^{\mathbf{u}}_{h,k}$	e.c.r.	$E^{v}_{h,k}$	e.c.r.
20	0.5202	—	3.1119	—
40	0.1068	2.2837	1.8104	0.7815
80	0.0289	1.8864	0.4133	2.1310
160	0.0113	1.3556	0.1242	1.7342
320	0.0041	1.4753	0.0307	2.0187
640	0.0012	1.7503	0.0066	2.2228

Table 4.1: Relative errors and estimated convergence rates in the time domain for the BDF2 Convolution Quadrature with lowest order Galerkin discretization (with reduced quadrature): N represents the number of space discretization points (elements) and timesteps. The errors are measured at the final time $T = 1.5$.

N	$E^{\mathbf{u}}_{h,k}$	e.c.r.	$E^{v}_{h,k}$	e.c.r.
20	1.1536	—	5.0725	—
40	0.2517	2.1964	0.9693	2.3876
80	0.0680	1.8879	0.2968	1.7077
160	0.0199	1.7711	0.0847	1.8081
320	0.0053	1.9207	0.0191	2.1525
640	0.0013	2.0377	0.0040	2.2597

Table 4.2: Relative errors and estimated convergence rates in the time domain for the Trapezoidal Rule Convolution Quadrature with the same space discretization as in Table 4.1: N represents the number of space discretization points and timesteps. The errors are measured at the final time $T = 1.5$.

plots can be seen in Figure 4.2. The values $\lambda = 9$, $\mu = 15$, $\rho_\Sigma = 1.5$, $\rho_f = 1$ and $c = \sqrt{5}$ were used, and the final time was $T = 1.5$.

Coupled boundary-field method. The FEM-BEM discretization of the bilinear form $\mathcal{A}$ in (4.35) (the transfer function for the time domain operator we are discretizing) is a matrix of the form:

$$\mathrm{A}(s) := \begin{pmatrix} \mathrm{S} + s^2\mathrm{M} & -s\rho_f \mathrm{R} \\ s\rho_f \mathrm{R}^t & \rho_f \mathrm{BEM}(s) \end{pmatrix}.$$

Here S and M are the sparse FEM elastic stiffness and mass matrices. The BEM block

$$\mathrm{BEM}(s) := \begin{pmatrix} \mathrm{V}(s) & -\left(-\frac{1}{2}\mathrm{I} + \mathrm{K}(s)\right) \\ \left(-\frac{1}{2}\mathrm{I} + \mathrm{K}(s)\right)^t & \mathrm{W}(s) \end{pmatrix}$$

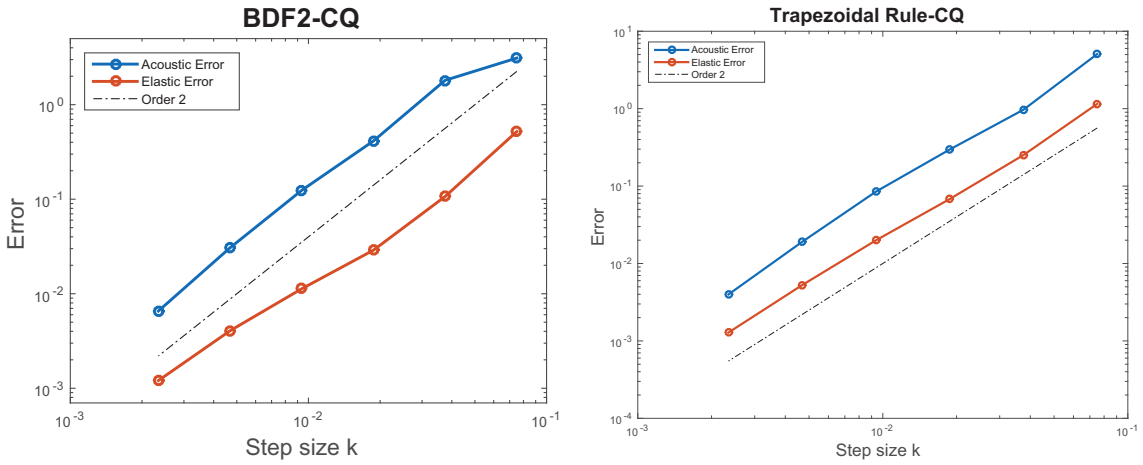

Figure 4.2: Relative errors for the BDF2 and TR implementations of CQ. The maximum difference between the approximate and exact solutions on the sampled points.

includes Galerkin discretizations of all integral operators of the Calderón projector and the matrix I contains the $L^2(\Gamma)$ inner products of pairs of basis functions in $Y_h \times X_h$. Finally the rectangular matrix R has the form $\begin{pmatrix} \mathbf{0} & \mathrm{T} \end{pmatrix}$, where T contains the $L^2(\Gamma)$ inner products of elements of the normal components of basis functions of $\mathbf{V}_h$ by basis functions of Y_h. As explained in [61] for a purely acoustic problem, there are several strategies to implement a fully implicit CQ-FEM-BEM coupled scheme: (a) apply CQ to the monolithic operator $\mathrm{A}(s)$ using a parallel strategy [13, 14], which amounts to solving systems with associated matrix $\mathrm{A}(s_j)$ for many complex frequencies s_j; (b) use time stepping, which requires solving a system with matrix $\mathrm{A}(\frac{3}{2\kappa})$ on each time step, and computing the memory terms for the integral equation part; (c) use the parallel strategy of [13] on the Schur complement $\rho_f \mathrm{BEM}(s) + s^2\rho_f^2 \mathrm{R}^t(\mathrm{S} + s^2\mathrm{M})^{-1}\mathrm{R}$, which amounts to condensing the FEM solves on the boundary interface and formally working on a pure boundary problem. The numerical experiments have been performed using this third strategy.

The previous coupling scheme was implemented using Galerkin Boundary Elements (using hierarchical polynomial bases and well known quadrature techniques

based on Duffy transformations [114]) for the acoustic wave field and Lagrangian Finite Elements for the interior elastic wavefield. The convergence studies were carried out for polynomial degrees $k = 1$ and $k = 2$ using the rectangle $[1, 3] \times [1, 2]$ as the elastic domain, which was triangulated using Matlab-produced unstructured meshes. Known solutions were imposed for the interior and exterior problems; a plane pressure wave on the interior

$$\mathbf{u} = \psi(c_L t - \mathbf{x} \cdot \mathbf{d})\, \mathbf{d}, \qquad \psi(t) := \mathcal{H}(t) \sin(2t), \qquad c_L := \sqrt{\frac{\lambda + 2\mu}{\rho_\Sigma}},$$

and a cylindrical acoustic wave on the exterior

$$v = \mathcal{L}^{-1} \left\{ \tfrac{i}{4} H_0^{(1)}(3|\mathbf{x} - \mathbf{x}_0|)\, \mathcal{L}\{\varphi(t)\} \right\}, \qquad \varphi(t) := \mathcal{H}(t) \sin(3t)$$

where $\mathbf{x}_0 = (1.5, 1.5)$ is the location of the source of the cylindrical wave, $\mathcal{H}(t)$ is the smoothened Heaviside function defined in (4.54), and $\lambda = 2$, $\mu = 3$ and $\rho_\Sigma = 5$.

These two functions satisfy equations (4.3a) and (4.3b). In order to force them to solve the problem in question, the boundary data was manufactured using (4.3c) and (4.3d) as the definitions for (λ_0, ϕ_0). The relevant information was sampled from the known solution, combined according to (4.3c) and (4.3b) and the resulting pair (λ_0, ϕ_0) was then fed to the discrete system as boundary data.

The experiment was run with succesive refinements on both the time step size and on the FEM and BEM grids. For the sake of comparison, both BDF2 and Trapezoidal Rule time discretizations were used. The errors were measured for the final time, for the finite element solution $E^{\mathbf{u}}_{h,k,L^2}$ in the $L^2(\Omega_-)$ norm and $E^{\mathbf{u}}_{h,k,H^1}$ in the $H^1(\Omega_-)$ norm. For the acoustic wavefield the discrete solution was postprocessed, sampled and compared to the exact solution in 20 random points in the acoustic domain, with the -normalized- maximum discrepancy $E^{v}_{h,k}$ being considered as the error. The results are shown in Tables 4.3 to 4.6 and Figures 4.3 and 4.4.

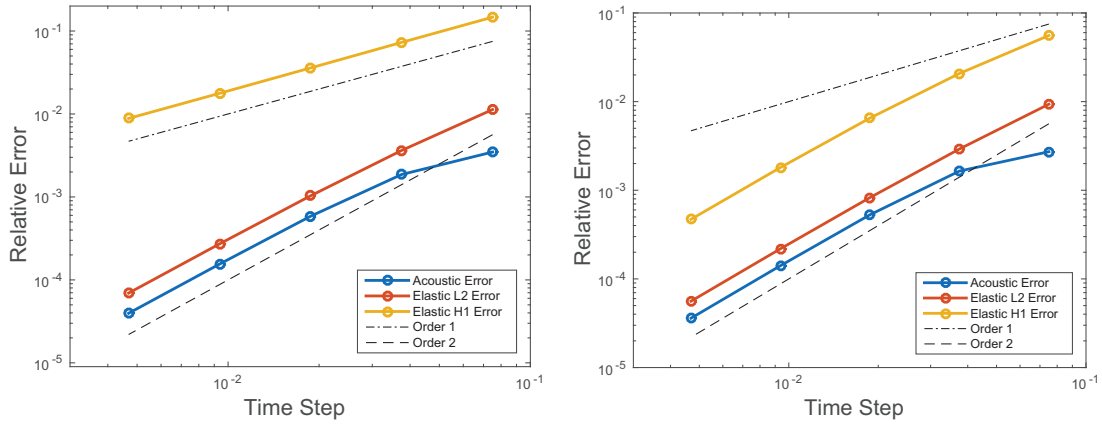

Figure 4.3: Convergence studies for the coupled FEM/BEM scheme with BDF2-based time evolution. On the left, space discretization is done with $\mathcal{P}_1$ elements were used for the finite element solution and $\mathcal{P}_1/\mathcal{P}_0$ elements for the boundary element solution. On the right the polynomial degree is increased to $\mathcal{P}_2$ for the FEM part and $\mathcal{P}_2/\mathcal{P}_1$ for the BEM part.

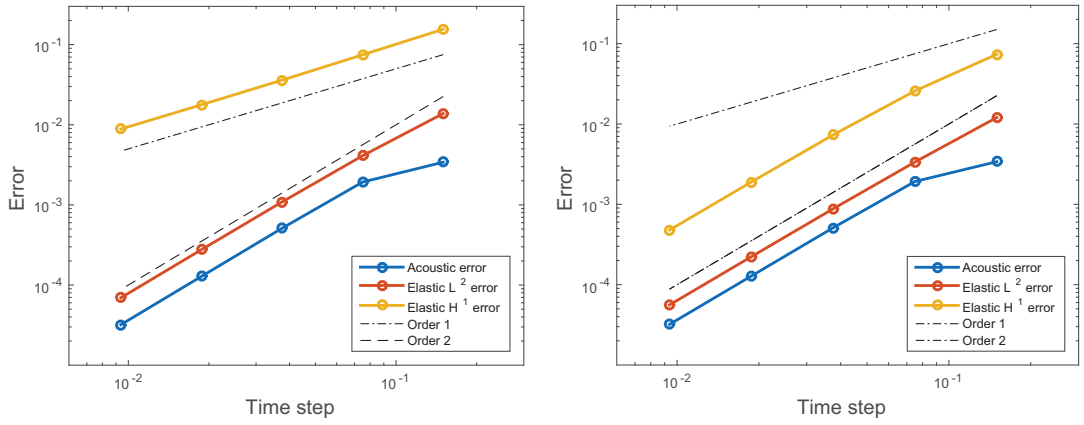

Figure 4.4: Convergence studies for the Trapezoidal Rule-based time evolution. Simultaneous space/time refinements were done. Left: $\mathcal{P}_1$ elements were used for the finite element solution and $\mathcal{P}_1/\mathcal{P}_0$ elements for the boundary element solution. Right: $\mathcal{P}_2$ elements were used for the finite element solution and $\mathcal{P}_2/\mathcal{P}_1$ elements for the boundary element solution.

M/N	$E^v_{h,k}$	e.c.r.	$E^{\mathbf{u}}_{h,k,L^2}$	e.c.r.	$E^{\mathbf{u}}_{h,k,H^1}$	e.c.r.
20/1	3.478 E-3	—	1.131 E-2	—	1.469 E-1	—
40/2	1.864 E-3	0.900	3.632 E-3	1.639	7.290 E-2	1.011
80/3	5.856 E-4	1.670	1.032 E-3	1.815	3.591 E-2	1.022
160/4	1.552 E-4	1.915	2.719 E-4	1.925	1.775 E-2	1.016
320/5	3.960 E-5	1.971	6.937 E-5	1.971	8.843 E-3	1.006

Table 4.3: Relative errors and estimated convergence rates in the time domain for the BDF2 Convolution Quadrature. Space discretization was done with $\mathcal{P}_1$ elements for the FEM part and $\mathcal{P}_1/\mathcal{P}_0$ for the BEM part. M is the number of timesteps, N defines the refinement level of the mesh $h = 0.52 \times 2^{-N}$. Final time $T = 1.5$.

M/N	$E^v_{h,k}$	e.c.r.	$E^{\mathbf{u}}_{h,k,L^2}$	e.c.r.	$E^{\mathbf{u}}_{h,k,H^1}$	e.c.r.
20/1	2.722 E-3	—	9.354 E-3	—	5.572 E-2	—
40/2	1.646 E-3	0.726	2.920 E-3	1.679	2.077 E-3	1.424
80/3	5.289 E-4	1.638	8.266 E-4	1.821	6.523 E-3	1.671
160/4	1.410 E-4	1.907	2.188 E-4	1.917	1.807 E-3	1.852
320/5	3.604 E-5	1.968	5.605 E-5	1.965	4.702 E-4	1.943

Table 4.4: Relative errors and estimated convergence rates in the time domain for the BDF2 Convolution Quadrature. The table shows the case where $\mathcal{P}_2$ is used for the FEM part and $\mathcal{P}_2/\mathcal{P}_1$ for the BEM part. M is the number of timesteps, the mesh parameter is given in terms of N by $h = 0.52 \times 2^{-N}$. Final time $T = 1.5$.

M/N	$E^v_{h,k}$	e.c.r.	$E^{\mathbf{u}}_{h,k,L^2}$	e.c.r.	$E^{\mathbf{u}}_{h,k,H^1}$	e.c.r.
10/1	3.412 E-3	—	1.382 E-2	—	1.555 E-1	—
20/2	1.929 E-3	0.823	4.112 E-3	1.749	7.467 E-2	1.058
40/3	5.113 E-4	1.915	1.088 E-3	1.917	3.604 E-2	1.051
80/4	1.281 E-4	1.996	2.763 E-4	1.978	1.776 E-2	1.021
160/5	3.202 E-5	2.000	6.935 E-5	1.994	8.843 E-3	1.006

Table 4.5: Relative errors and estimated convergence rates in the time domain for the Trapezoidal Rule Convolution Quadrature with $\mathcal{P}_1/\mathcal{P}_0$ boundary elements and $\mathcal{P}_1$ finite elements. $h = 0.52 \times 2^{-N}$ is the maximum lenght of the triangulation and M is the number of timesteps. Final time $T = 1.5$.

M/N	$E^{v}_{h,k}$	e.c.r.	$E^{\mathbf{u}}_{h,k,L^2}$	e.c.r.	$E^{\mathbf{u}}_{h,k,H^1}$	e.c.r.
10/1	3.395 E-3	—	1.205 E-2	—	7.369 E-2	—
20/2	1.925 E-3	0.819	3.364 E-3	1.841	2.581 E-2	1.513
40/3	5.108 E-4	1.912	8.799 E-4	1.935	7.316 E-3	1.819
80/4	1.281 E-4	1.996	2.223 E-4	1.981	1.896 E-3	1.948
160/5	3.201 E-5	2.000	5.591 E-5	1.995	4.783 E-4	1.987

Table 4.6: Relative errors and estimated convergence rates in the time domain for the Trapezoidal Rule Convolution Quadrature with $\mathcal{P}_2/\mathcal{P}_1$ boundary elements and $\mathcal{P}_2$ finite elements. $h = 0.52 \times 2^{-N}$ is the maximum lenght of the triangulation and M is the number of timesteps. Final time $T = 1.5$.

Chapter 5

ACOUSTIC SCATTERING BY PIEZOELECTRIC OBSTACLES

This chapter extends the analysis tools developed in the previous chapter to the study of the interaction between an acoustic wave and a piezoelectric elastic obstacle and reflects the work in the paper *Boundary-Finite Element discretization of time dependent acoustic scattering by elastic obstacles with piezoelectric behavior* written in collaboration with Francisco-Javier Sayas [110].

The chapter is structured as follows. After a brief review of previous work on this area, the general problem is presented in Section 2, where the time domain PDE model and the geometry are introduced along with the required notation and assumptions on physical parameters. Section 3 introduces the Laplace-transformed problem. Using standard BIE techniques we derive an equivalent integro-differential system and pose it variationally. The error equations satisfied by the resulting Galerkin space semi-discretization and the required elliptic projector are then presented. The core of the analysis is done in Section 4, where a slightly more general discrete system – encompassing both the discrete-in-space problem and the error equations– is shown to be uniquely solvable by studying the variational formulation of an equivalent transmission problem; stability bounds are obtained in terms of the Laplace parameter s. The main results in the time domain are presented in Section 5, where the estimates obtained in the previous section are translated into the time domain and the system is fully discretized with BDF2-based Convolution Quadrature; for sufficiently smooth problem data second-order-in-time convergence is proven. Section 6 is dedicated to numerical experiments, some remarks pertaining the implementation of CQ and the coupling of boundary and finite elements are followed by experiments confirming convergence for the methods based in BDF2 and Trapezoidal Rule.

5.1 Background

The study of the interaction between acoustic waves and elastic structures has been subject of much work in recent decades. Many of the recent modeling and computational efforts have been driven by the need to develop and improve techniques for vibration control and reduction. Passive techniques rely on the use of sound absorbing materials that dissipate the energy of the acoustic wave and have been successfully used to damp high-frequency vibrations. On the other hand, active techniques employing piezoelectric materials exploit the adaptability of the piezoelectric solid to react to the vibrations in order to cancel them. Active materials are used to provide extra control in the low frequency range.

In the frequency domain, works like [28, 29] have derived mathematical models and variational formulations suitable for numerical treatment of the process, their approach uses an effective load to model the action of the incident acoustic wave on the piezoelectric material and is geared towards a finite element solution of all the unknowns involved in the problem. In the time domain, [2] is a classic reference for finite element simulation of waves in piezoelectrics, and a thorough review of the work done on this area up until the early 2000's can be found in [17]. The propagation of plane waves waves in layered piezoelectric media has been addressed recently in [107, 125], using analytical methods to study the reflection and transmission of plane waves at the interface of media with different material coefficients. Within the context of dynamic crack propagation in piezoelectric solids, finite element formulations have been explored in [40, 104], while Boundary Integral Equations (BIE) have been treated in [106, 78, 53]. Time domain BIE's for a purely piezoelectric problem have been used in recent works like [50, 126], where a Nyström approach is followed for the space discretization and Convolution Quadrature is used in time. In both cases the model concerns only the propagation of the wave inside the piezoelectric material and no interaction with an acoustic wave is considered.

The present Chapter describes, discretizes, and analyzes the complete interaction problem, considering an acoustic wave that impinges upon a piezoelectric scatterer

inducing an elastic wave within the piezoelectric obstacle and a scattered acoustic wave traveling in a homogeneous unbounded domain. The system of PDE's used to model the problem combines the acoustic/elastic coupling conditions presented in [66] for wave structure interaction, with the PDE's used in [29] to describe the time evolution of the relevant variables. Aiming for a Finite Element discretization of the elastic and electric variables and a boundary element treatment of the acoustic wave, the system is translated into an integro-differential problem in the Laplace domain, the analysis is carried out following the techniques systematized in [82] and originated in the seminal work [6]. Galerkin discretization in space is used for all the variables, while Convolution Quadrature combined with time stepping are used for the time evolution.

We prove that the resulting fully discrete problem is well posed and determine stability and error bounds with explicit time dependence for the time discretization based on second order backwards differentiation formulas (BDF2). A similar study with the backward Euler method is easy to obtain, while a Trapezoidal Rule CQ method is also available [8], but knowledge of the behavior of constants with respect to time is not known at current time.

5.2 Problem Statement

Constitutive relations. In the interior domain Ω_- the problem variables will be the elastic displacement field $\mathbf{u}$ and the electric potential ψ

$$\mathbf{u} : \Omega_- \times [0,\infty) \longrightarrow \mathbb{R}^d, \qquad \psi : \Omega_- \times [0,\infty) \longrightarrow \mathbb{R}.$$

We will use the following constitutive relations [121] to define the piezoelectric stress tensor $\boldsymbol{\sigma}$ and the electric displacement vector $\mathbf{D}$

$$\boldsymbol{\sigma} := \mathbf{C}\boldsymbol{\varepsilon}(\mathbf{u}) + \mathbf{e}\nabla\psi\,, \qquad \mathbf{D} := \mathbf{e}^t\boldsymbol{\varepsilon}(\mathbf{u}) - \boldsymbol{\epsilon}\nabla\psi. \tag{5.1}$$

In the above definition $\boldsymbol{\varepsilon}(\mathbf{u})$ and $\mathbf{C}$ are the linearized elastic strain tensor and the stiffness tensor defined on (2.3) and (2.8). The piezoelectric tensor $\mathbf{e}$ and dielectric

tensor $\boldsymbol{\epsilon}$ encode the electric properties of the material. For a real symmetric matrix $\mathbf{M} \in \mathbb{R}^{d\times d}_{sym}$ and for a vector, $\mathbf{d} \in \mathbb{R}^d$ we define

$$
\begin{aligned}
(\mathbf{e}(\mathbf{x})\mathbf{d})_{ij} &:= \sum_k \mathbf{e}_{kij}\mathbf{d}_k\,, \\
(\mathbf{e}^t(\mathbf{x})\mathbf{M})_k &:= \sum_{ij} \mathbf{e}_{kij}\mathbf{M}_{ij}\,, \\
(\boldsymbol{\epsilon}(\mathbf{x})\mathbf{d})_i &:= \sum_j \boldsymbol{\epsilon}_{ij}(\mathbf{x})\mathbf{d}_j.
\end{aligned}
$$

Due to physical considerations, these tensors exhibit the following symmetries [79]:

$$
\mathbf{e}_{lij} = \mathbf{e}_{lji}\,, \qquad \boldsymbol{\epsilon}_{il} = \boldsymbol{\epsilon}_{li}. \tag{5.2}
$$

As we did earlier with the stiffness tensor, we will require that the components of $\mathbf{e}$ and $\boldsymbol{\epsilon}$ belong to $L^\infty(\Omega_-)$ and that for any $\mathbf{d} \in \mathbb{R}^d$ there exists a positive constant d_0 such that for almost every $\mathbf{x} \in \Omega_-$

$$
\boldsymbol{\epsilon}(\mathbf{x})\mathbf{d}\cdot\mathbf{d} \geq d_0\,\mathbf{d}\cdot\mathbf{d}.
$$

The presence of an electric field inside of the scatterer will require one more geometric assumption on the boundary Γ which now will be partitioned in two non-overlapping parts where Dirichlet and Neumann boundary conditions for the electric potential will be imposed. The two subdomains Γ_D and Γ_N will be open relative to Γ and such that $\Gamma = \overline{\Gamma}_D \cup \overline{\Gamma}_N$ and $\Gamma_D \neq \varnothing$. A schematic of the physical setup is shown in Figure 5.1.

The PDE model. Under all the above considerations, and recalling the definitions (5.1), the interaction between the incident acoustic wave and the piezoelectric scatterer is governed by the following system of PDE's:

$$c^{-2}\ddot{v} = \Delta v \qquad \text{in } \Omega_+ \times [0,\infty), \tag{5.3a}$$

$$\rho_\Sigma \ddot{\mathbf{u}} = \nabla \cdot \boldsymbol{\sigma} \qquad \text{in } \Omega_- \times [0,\infty), \tag{5.3b}$$

$$\nabla \cdot \mathbf{D} = 0 \qquad \text{in } \Omega_- \times [0,\infty), \tag{5.3c}$$

$$\dot{\mathbf{u}} \cdot \boldsymbol{\nu} + \partial_\nu v = -\alpha_d \qquad \text{on } \Gamma \times [0,\infty), \tag{5.3d}$$

$$\boldsymbol{\sigma}\,\boldsymbol{\nu} + \rho_f \dot{v}\boldsymbol{\nu} = -\rho_f \dot{\beta}_d \boldsymbol{\nu} \qquad \text{on } \Gamma \times [0,\infty), \tag{5.3e}$$

$$\mathbf{D} \cdot \boldsymbol{\nu} = \eta_d \qquad \text{on } \Gamma_N \times [0,\infty), \tag{5.3f}$$

$$\psi = \mu_d \qquad \text{on } \Gamma_D \times [0,\infty), \tag{5.3g}$$

with homogeneous initial conditions for v, $\dot{v}$, $\mathbf{u}$, and $\dot{\mathbf{u}}$. See, for instance, [70] for the coupling of elastic and acoustic interactions, in [71] the authors provide mathematical justification for the use of a quasi-static piezoelectric approximation employed by [29], where an effective load vector is used to represent the acoustic interaction.

The problem data is

$$\alpha_d := \partial_\nu v^{inc}|_\Gamma : \Gamma \times [0,\infty) \longrightarrow \mathbb{R}, \qquad \eta_d : \Gamma_N \times [0,\infty) \longrightarrow \mathbb{R},$$
$$\beta_d := \quad v^{inc}|_\Gamma : \Gamma \times [0,\infty) \longrightarrow \mathbb{R}, \qquad \mu_d : \Gamma_D \times [0,\infty) \longrightarrow \mathbb{R}.$$

This system can be given a rigorous form using causal distributions taking values in Sobolev spaces as in [66, 82], etc. For the time being we will deal only with the Laplace transform of this system and will come back to the time domain only at the time of giving stability and error estimates.

5.3 A Laplace Domain Semidiscrete Problem

For $(\mathbf{u}, \psi) \in \mathbf{H}^1(\Omega_-) \times H^1(\Omega_-)$ such that $\nabla \cdot \boldsymbol{\sigma}(\mathbf{u}, \psi) \in \mathbf{L}^2(\Omega_-)$ we define the weak interior traction field in analogy to the purely elastic normal stress with the formula

$$\langle \boldsymbol{\sigma}\boldsymbol{\nu}, \gamma \mathbf{w} \rangle_\Gamma := (\mathbf{C}\boldsymbol{\varepsilon}(\mathbf{u}), \boldsymbol{\varepsilon}(\mathbf{w}))_{\Omega_-} + (\mathbf{e}\nabla\psi, \boldsymbol{\varepsilon}(\mathbf{w}))_{\Omega_-} + (\nabla \cdot \boldsymbol{\sigma}, \mathbf{w})_{\Omega_-} \qquad \forall \mathbf{w} \in \mathbf{H}^1(\Omega_-).$$

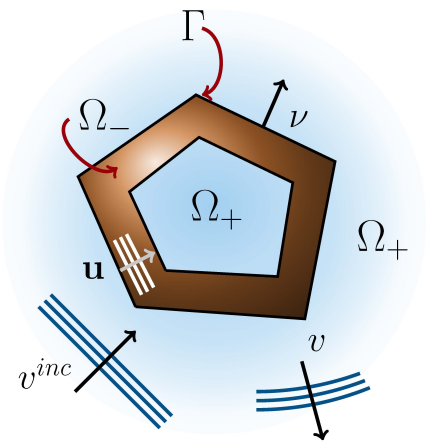

Figure 5.1: Scheme of the scattering geometry. The problem unknowns are the scattered acoustic wave v (defined in the unbounded region Ω_+), the induced elastic wave $\mathbf{u}$, and the electric potential ψ (both defined inside the obstacle Ω_-).The total elastic boundary Γ is the disjoint union of the electric Dirichlet boundary Γ_D, and the electric Neumann boundary Γ_N which are both open relative to Γ. The normal vectors $\boldsymbol{\nu}$ are exterior to the elastic domain and point towards the acoustic domain Ω_+.

In a similar fashion, for $(\mathbf{u}, \psi) \in \mathbf{H}^1(\Omega_-) \times H^1(\Omega_-)$ such that $\nabla \cdot \mathbf{D}(\mathbf{u}, \psi) \in L^2(\Omega_-)$, the weak normal electric displacement will be defined by

$$\langle \mathbf{D} \cdot \boldsymbol{\nu}, \gamma w \rangle_\Gamma := (\boldsymbol{\varepsilon}(\mathbf{u}), \mathbf{e}\nabla w)_{\Omega_-} - (\boldsymbol{\epsilon}\nabla\psi, \nabla w)_{\Omega_-} + (\nabla \cdot \mathbf{D}, w)_{\Omega_-} \qquad \forall w \in H^1(\Omega_-).$$

These are, respectively, elements of the dual spaces $\mathbf{H}^{-1/2}(\Gamma)$ and $H^{-1/2}(\Gamma)$. To deal with the Dirichlet and Neumann conditions for the electric potential, we need additional notation. The restriction to the Dirichlet boundary of the trace of a function $u \in H^1(\Omega_-)$ will be denoted by $\gamma_D u := \gamma u|_{\Gamma_D}$ and we define the function spaces

$$H^{1/2}(\Gamma_D) := \left\{\gamma_D u : u \in H^1(\Omega_-)\right\}, \qquad H^1_D(\Omega_-) := \left\{u \in H^1(\Omega_-) : \gamma_D u = 0\right\},$$
$$\widetilde{H}^{1/2}(\Gamma_N) := \left\{\gamma u|_{\Gamma_N} : u \in H^1_D(\Omega_-)\right\}, \qquad H^{-1/2}(\Gamma_N) := \left(\widetilde{H}^{1/2}(\Gamma_N)\right)'.$$

The angled bracket $\langle \cdot, \cdot \rangle_{\Gamma_N}$ should be understood as the duality pairing of $H^{-1/2}(\Gamma_N)$ with $\widetilde{H}^{1/2}(\Gamma_N)$.

Laplace domain "dynamic" problem. From this point on, we will only consider the problem in the Laplace domain and we will use the same symbol to

represent a function and its Laplace transform without ambiguity. Let $s \in \mathbb{C}_+ := \{s \in \mathbb{C} : \operatorname{Re} s > 0\}$ and let

$$(\alpha_d, \beta_d, \eta_d, \mu_d) \in H^{-1/2}(\Gamma) \times H^{1/2}(\Gamma) \times H^{-1/2}(\Gamma_N) \times H^{1/2}(\Gamma_D)$$

be problem data. We look for $(v, \mathbf{u}, \psi) \in H^1(\Omega_+) \times \mathbf{H}^1(\Omega_-) \times H^1(\Omega_-)$ such that

$$(s/c)^2 v - \Delta v = 0 \qquad \text{in } \Omega_+, \tag{5.4a}$$

$$\rho_\Sigma s^2 \mathbf{u} - \nabla \cdot \boldsymbol{\sigma} = \mathbf{0} \qquad \text{in } \Omega_-, \tag{5.4b}$$

$$\nabla \cdot \mathbf{D} = 0 \qquad \text{in } \Omega_-, \tag{5.4c}$$

$$s\gamma \mathbf{u} \cdot \boldsymbol{\nu} + \partial_\nu^+ v = -\alpha_d \qquad \text{on } \Gamma, \tag{5.4d}$$

$$\boldsymbol{\sigma}\boldsymbol{\nu} + \rho_f s \gamma^+ v \boldsymbol{\nu} = -\rho_f s \beta_d \boldsymbol{\nu} \qquad \text{on } \Gamma, \tag{5.4e}$$

$$\mathbf{D} \cdot \boldsymbol{\nu} = \eta_d \qquad \text{on } \Gamma_N, \tag{5.4f}$$

$$\gamma \psi = \mu_d \qquad \text{on } \Gamma_D, \tag{5.4g}$$

where $\boldsymbol{\sigma}$ and $\mathbf{D}$ are defined by (5.1).

A coupled integro-differential system. If $(v, \mathbf{u}, \psi)$ is a solution of (5.4), then v can be represented as

$$v = \mathrm{D}(s/c)\phi - \mathrm{S}(s/c)\lambda, \tag{5.5}$$

where $\phi := \gamma^+ v$ and $\lambda := \partial_\nu^+ v$. Note that this representation can be extended to Ω_-, yielding $v \equiv 0$ in Ω_-. Therefore if we use the limit identities (2.25) to write $\gamma^- v$, we arrive at

$$\mathrm{V}(s/c)\lambda - \left(-\tfrac{1}{2}\mathrm{I} + \mathrm{K}(s/c)\right)\phi = 0 \qquad \text{on } \Gamma. \tag{5.6a}$$

Additionally, (5.4d) and (2.25) imply

$$\left(-\tfrac{1}{2}\mathrm{I} + \mathrm{K}^t(s/c)\right)\lambda + \mathrm{W}(s/c)\phi - s\gamma \mathbf{u} \cdot \boldsymbol{\nu} = \alpha_d \qquad \text{on } \Gamma. \tag{5.6b}$$

Finally, (5.4e) can be written in terms of ϕ

$$\boldsymbol{\sigma}\boldsymbol{\nu} + \rho_f s \phi \boldsymbol{\nu} = -\rho_f s \beta_d \boldsymbol{\nu} \qquad \text{on } \Gamma. \tag{5.6c}$$

Reciprocally, if the integro-differential equations (5.6a) through (5.6c) are satisfied, if $(\mathbf{u}, \psi, \lambda, \phi)$ satisfies (5.4b), (5.4c), (5.4f), and (5.4g), and we define v with the representation formula (5.5), it follows that $\lambda = \partial_\nu^+ v$, $\phi = \gamma^+ v$, and we recover the system (5.4).

A variational formulation. We next define the elastodynamic bilinear form

$$b(\mathbf{u}, \mathbf{w}; s) := (\mathbf{C}\boldsymbol{\varepsilon}(\mathbf{u}), \boldsymbol{\varepsilon}(\mathbf{w}))_{\Omega_-} + s^2(\rho_\Sigma \mathbf{u}, \mathbf{w})_{\Omega_-}, \tag{5.7a}$$

and the coupled elastic-electric bilinear form

$$\begin{aligned}\mathcal{B}((\mathbf{u}, \psi), (\mathbf{w}, \varphi); s) :=& b(\mathbf{u}, \mathbf{w}; s) + (\mathbf{e}\nabla\psi, \boldsymbol{\varepsilon}(\mathbf{w}))_{\Omega_-} \\ &- (\boldsymbol{\varepsilon}(\mathbf{u}), \mathbf{e}\nabla\varphi)_{\Omega_-} + (\boldsymbol{\epsilon}\nabla\psi, \nabla\varphi)_{\Omega_-},\end{aligned} \tag{5.7b}$$

which is bounded in $\mathbf{H}^1(\Omega_-) \times H^1(\Omega_-)$. We also collect all the integral operators in (5.6a)-(5.6b) in a single matrix of operators

$$\mathbb{D}(s) := \begin{bmatrix} \mathrm{V}(s) & +\frac{1}{2}\mathrm{I} - \mathrm{K}(s) \\ -\frac{1}{2}\mathrm{I} + \mathrm{K}^t(s) & \mathrm{W}(s) \end{bmatrix} : H^{-1/2}(\Gamma) \times H^{1/2}(\Gamma) \to H^{1/2}(\Gamma) \times H^{-1/2}(\Gamma). \tag{5.7c}$$

For the sake of notational simplicity, we will write $\mathbb{D}(s)(\lambda, \phi)$ for the action of $\mathbb{D}(s)$ on the column vector $(\lambda, \phi)^t$. We now present the continuous variational formulation of the problem which reads:

Given data

$$(\alpha_d, \beta_d, \eta_d, \mu_d) \in H^{-1/2}(\Gamma) \times H^{1/2}(\Gamma) \times H^{-1/2}(\Gamma_N) \times H^{1/2}(\Gamma_D),$$

find

$$(\mathbf{u}, \psi, \lambda, \phi) \in \mathbf{H}^1(\Omega_-) \times H^1(\Omega_-) \times H^{-1/2}(\Gamma) \times H^{1/2}(\Gamma)$$

such that

$$\gamma_D \psi = \mu_d, \tag{5.8a}$$

and for all $(\mathbf{w}, \varphi) \in \mathbf{H}^1(\Omega_-) \times H^1(\Omega_-)$ and $(\xi, \chi) \in H^{-1/2}(\Gamma) \times H^{1/2}(\Gamma)$

$$\mathcal{B}((\mathbf{u}, \psi), (\mathbf{w}, \varphi); s) + \rho_f s \langle \phi, \gamma\mathbf{w} \cdot \boldsymbol{\nu} \rangle_\Gamma = -\rho_f s \langle \beta_d, \gamma\mathbf{w} \cdot \boldsymbol{\nu} \rangle_\Gamma + \langle \eta_d, \gamma\varphi \rangle_{\Gamma_N}, \tag{5.8b}$$

$$-s\langle \gamma\mathbf{u} \cdot \boldsymbol{\nu}, \chi \rangle_\Gamma + \langle \mathbb{D}(s/c)(\lambda, \phi), (\xi, \chi) \rangle_\Gamma = \langle \alpha_d, \chi \rangle_\Gamma. \tag{5.8c}$$

Discrete formulation. In order to discretize the system (5.8) a few definitions are in order. We consider finite dimensional subspaces

$$\mathbf{V}_h \subseteq \mathbf{H}^1(\Omega_-), \qquad V_h \subseteq H^1(\Omega_-), \qquad V_{h,D} := V_h \cap H^1_D(\Omega_-),$$
$$X_h \subseteq H^{-1/2}(\Gamma), \qquad Y_h \subseteq H^{1/2}(\Gamma).$$

(Following [82], the theoretical treatment of the s-dependent discrete problem only uses that these spaces are closed. This has the advantage of simultaneously providing a well-posedness analysis of the continuous problem.) It will be assumed that the set

$$\mathbf{M} := \big\{\mathbf{m} \in \mathbf{H}^1(\Omega_-) : \boldsymbol{\varepsilon}(\mathbf{m}) = \mathbf{0} \quad \forall \mathbf{w} \in \mathbf{H}^1(\Omega_-)\big\}$$

of elastic rigid motions is always contained in $\mathbf{V}_h$. In the discrete case, the Dirichlet boundary condition will be approximated in the space $\gamma_D V_h := \big\{\gamma_D v^h : v^h \in V_h\big\}$. With all this in mind, we can now pose the discrete counterpart of (5.8).

Given problem data

$$(\alpha_d, \beta_d, \eta_d, \mu_d^h) \in H^{-1/2}(\Gamma) \times H^{1/2}(\Gamma) \times H^{-1/2}(\Gamma_N) \times \gamma_D V_h,$$

find $(\mathbf{u}^h, \psi^h, \lambda^h, \phi^h) \in \mathbf{V}_h \times V_h \times Y_h \times X_h$ such that

$$\gamma_D \psi^h = \mu_d^h, \tag{5.9a}$$

and for all $(\mathbf{w}, \varphi) \in \mathbf{V}_h \times V_{h,D}$ and $(\xi, \chi) \in X_h \times Y_h$

$$\mathcal{B}((\mathbf{u}^h, \psi^h), (\mathbf{w}, \varphi); s) + \rho_f s \langle \phi^h, \gamma\mathbf{w} \cdot \boldsymbol{\nu}\rangle_\Gamma = -\rho_f s \langle \beta_d, \gamma\mathbf{w} \cdot \boldsymbol{\nu}\rangle_\Gamma + \langle \eta_d, \gamma\varphi\rangle_{\Gamma_N}, \tag{5.9b}$$

$$-s\langle \gamma\mathbf{u}^h \cdot \boldsymbol{\nu}, \chi\rangle_\Gamma + \langle \mathbb{D}(s/c)(\lambda^h, \phi^h), (\xi, \chi)\rangle_\Gamma = \langle \alpha_d, \chi\rangle_\Gamma. \tag{5.9c}$$

A shorthand form of (5.9c) can be given using polar sets as done in the previous chapter in the form

$$-(0, s\gamma\mathbf{u}^h \cdot \boldsymbol{\nu}) + \mathbb{D}(s/c)(\lambda^h, \phi^h) - (0, \alpha_d) \in X_h^\circ \times Y_h^\circ \equiv (X_h \times Y_h)^\circ.$$

Trace liftings. By definition, the restriction of the trace to the Dirichlet boundary

$$\gamma_D : H^1(\Omega_-) \longrightarrow H^{1/2}(\Gamma_D)$$

is a surjective operator, and so is

$$\gamma_{h,D} := \gamma_D|_{V_h} : V_h \longrightarrow \gamma_D V_h.$$

Note that there exists a bounded right-inverse of γ_D (or lifting) which will be denoted by $\gamma_D^\dagger$. For the discrete counterpart, *the existence of a right-inverse of* $\gamma_{h,D}$ *that is bounded uniformly in* h *will be assumed* (see [36]) and will be denoted $\gamma_{h,D}^\dagger$.

An elliptic projector. A projection operator will be required in order to project the solid-electric component of the exact solution on the discrete space. Given $(\mathbf{u}, \psi, \mu_d^h) \in \mathbf{H}^1(\Omega_-) \times H_D^1(\Omega_-) \times \gamma_D V_h$ we will write $(\mathbf{P}_h\mathbf{u}, \mathrm{P}_h\psi) \in \mathbf{V}_h \times V_{h,D}$ to denote the pair satisfying

$$\gamma_D \mathrm{P}_h \psi = \mu_d^h, \tag{5.10a}$$

the discrete variational equation

$$\mathcal{B}((\mathbf{P}_h\mathbf{u}, \mathrm{P}_h\psi), (\mathbf{w}, \varphi); 0) = \mathcal{B}((\mathbf{u}, \psi), (\mathbf{w}, \varphi); 0) \qquad \forall (\mathbf{w}, \varphi) \in \mathbf{V}_h \times V_{h,D}, \tag{5.10b}$$

and the 'grounding condition'

$$(\mathbf{P}_h\mathbf{u}, \mathbf{m})_{\Omega_-} = (\mathbf{u}, \mathbf{m})_{\Omega_-} \qquad \forall \mathbf{m} \in \mathbf{M}. \tag{5.10c}$$

Note that the bilinear form in (5.10) does not contain the s-dependent term (we have set $s = 0$), which is the kinetic part of the elastic-electric bilinear form $\mathcal{B}$. Note also that both $\mathbf{P}_h u$ and $\mathrm{P}_h\psi$ depend on $(\mathbf{u}, \psi)$ as well as on the discrete data μ_d^h. We will keep the simplified (and somewhat misleading) notation for the sake of simplicity. The next lemma shows that this elliptic projection is quasioptimal.

Lemma 5.1. *Problem* (5.10) *is uniquely solvable and there exists* $C > 0$ *such that*

$$\begin{aligned}\|\mathbf{u} - \mathbf{P}_h\mathbf{u}\|_{1,\Omega_-} + \|\psi - \mathrm{P}_h\psi\|_{1,\Omega_-} \leq C\Big(&\inf_{\mathbf{w}\in\mathbf{V}_h} \|\mathbf{u} - \mathbf{w}\|_{1,\Omega_-} + \inf_{\varphi\in V_h} \|\psi - \varphi\|_{1,\Omega_-} \\ &+ \|\gamma_D\psi - \mu_d^h\|_{1/2,\Gamma}\Big).\end{aligned}$$

Proof. The bilinear form $\mathcal{B}(\cdot,\cdot;0)$ is coercive in the space

$$\{\mathbf{u} \in \mathbf{H}^1(\Omega_-) : (\mathbf{u}, \mathbf{m})_{\Omega_-} = 0 \quad \forall \mathbf{m} \in \mathbf{M}\} \times H_D^1(\Omega_-),$$

as follows from the second Korn and Poincaré-Friedrichs inequalities, since $\Gamma_D \neq \varnothing$. If $\{\mathbf{m}_i : i = 1, \ldots, N_d\}$ is a basis for the space $\mathbf{M}$, then a simple compactness argument shows that the bilinear form

$$\mathcal{B}((\mathbf{u}, \psi), (\mathbf{w}, \varphi); 0) + \sum_{i=1}^{N_d} (\mathbf{u}, \mathbf{m}_i)_{\Omega_-} (\mathbf{w}, \mathbf{m}_i)_{\Omega_-}$$

is coercive in $H^1(\Omega_-) \times H^1_D(\Omega_-)$. Therefore, when $\mu^h_D = 0$, it is simple to see that (5.10) is just a Galerkin discretizations in $\mathbf{V}_h \times V_{h,D}$ of a coercive problem, and therefore a Céa estimate holds. The consideration of non-homogeneous boundary conditions, leading to an estimate like the one on the statement of the Lemma, can be approached using standard arguments based on the hypothesis of the existence of an h-uniform lifting of $\gamma_{h,D}$ (see [36]). □

Error equations. The error will be analyzed using the variables

$$\mathbf{e}^h_{\mathbf{u}} := \mathbf{P}_h \mathbf{u} - \mathbf{u}^h, \qquad e^h_\psi := \mathrm{P}_h \psi - \psi^h,$$
$$e^h_\lambda := \lambda - \lambda^h, \qquad e^h_\phi := \phi - \phi^h,$$

which satisfy

$$\gamma_D e^\psi_h = 0, \tag{5.11a}$$

and for all $(\mathbf{w}, \varphi) \in \mathbf{V}_h \times V_{h,D}$

$$\mathcal{B}((\mathbf{e}^h_{\mathbf{u}}, e^h_\psi), (\mathbf{w}, \varphi); s) + \rho_f s \langle e^h_\phi, \gamma \mathbf{w} \cdot \boldsymbol{\nu} \rangle_\Gamma - s^2 (\rho_\Sigma (\mathbf{P}_h \mathbf{u} - \mathbf{u}), \mathbf{w})_{\Omega_-} = 0, \tag{5.11b}$$

$$-(0, s\gamma \mathbf{e}^h_{\mathbf{u}} \cdot \boldsymbol{\nu}) + \mathbb{D}(s/c)(e^h_\lambda, e^h_\phi) - (0, s\gamma (\mathbf{P}_h \mathbf{u} - \mathbf{u}) \cdot \boldsymbol{\nu}) \in X^\circ_h \times Y^\circ_h, \tag{5.11c}$$

$$(e^h_\lambda - \lambda, e^h_\phi - \phi) \ \in \ X_h \times Y_h. \tag{5.11d}$$

5.4 Laplace Domain Analysis

We consider a slightly more general problem from which both stability and error estimates for (5.9) will be obtained. Data are

$$(\alpha_d, \beta_d, \eta_d, \mu^h_d) \in H^{-1/2}(\Gamma) \times H^{1/2}(\Gamma) \times H^{-1/2}(\Gamma_N) \times \gamma_D V_h, \tag{5.12a}$$

and

$$(\boldsymbol{\theta}_d, \theta_d, \lambda_d, \phi_d) \in \mathbf{H}^1(\Omega_-) \times L^2(\Gamma) \times H^{-1/2}(\Gamma) \times H^{1/2}(\Gamma), \tag{5.12b}$$

and we look for

$$(\widehat{\mathbf{u}}^h, \widehat{\psi}^h) \in \mathbf{V}_h \times V_{h,D} \quad \text{and} \quad (\widehat{\lambda}^h, \widehat{\phi}^h) \in H^{-1/2}(\Gamma) \times H^{1/2}(\Gamma)$$

such that

$$\gamma_D \widehat{\psi}^h = \mu_d^h, \tag{5.13a}$$

$$\begin{aligned} \mathcal{B}((\widehat{\mathbf{u}}^h, \widehat{\psi}^h), (\mathbf{w}, \varphi); s) + \rho_f s \langle \widehat{\phi}^h, \gamma \mathbf{w} \cdot \boldsymbol{\nu} \rangle_\Gamma = & -\rho_f s \langle \beta_d, \gamma \mathbf{w} \cdot \boldsymbol{\nu} \rangle_\Gamma + \langle \eta_d, \gamma \varphi \rangle_{\Gamma_N} \\ & + s^2 (\rho_\Sigma \boldsymbol{\theta}_d, \mathbf{w})_{\Omega_-} \\ & \forall\, (\mathbf{w}, \varphi) \in \mathbf{V}_h \times V_{h,D}, \end{aligned} \tag{5.13b}$$

$$-(0, s\gamma \widehat{\mathbf{u}}^h \cdot \boldsymbol{\nu}) + \mathbb{D}(s/c)(\widehat{\lambda}^h, \widehat{\phi}^h) - (0, \alpha_d + s\theta_d) \in X_h^\circ \times Y_h^\circ, \tag{5.13c}$$

$$(\widehat{\lambda}^h, \widehat{\phi}^h) - (\lambda_d, \phi_d) \in X_h \times Y_h. \tag{5.13d}$$

Note that if the first group of data (5.12a) is set to be zero and we take

$$(\boldsymbol{\theta}_d, \theta_d, \lambda_d, \phi_d) = (\mathbf{P}_h \mathbf{u} - \mathbf{u}, \gamma(\mathbf{P}_h \mathbf{u} - \mathbf{u}) \cdot \boldsymbol{\nu}, \lambda, \phi),$$

the system (5.13) reduces to the error equations (5.11), while if the second group of data (5.12b) is identically zero then the discrete equations (5.9) are recovered.

Two equivalent problems. Using the Galerkin equations (5.13) as the starting point, the analysis will proceed as in [82] by finding an equivalent transmission problem that can then be studied variationally. Solvability will then be established for the variational formulation and the stability constants will be obtained from the variational problem as well.

Proposition 5.2 (Transmission problem)**.** *If* $(\widehat{\mathbf{u}}^h, \widehat{\psi}^h, \widehat{\lambda}^h, \widehat{\phi}^h)$ *solves* (5.13)*, and*

$$\widehat{v}^h := \mathrm{D}(s/c)\widehat{\phi}^h - \mathrm{S}(s/c)\widehat{\lambda}^h, \tag{5.14}$$

then $(\widehat{v}^h, \widehat{\mathbf{u}}^h, \widehat{\psi}^h) \in H^1(\mathbb{R}^d \setminus \Gamma) \times \mathbf{V}_h \times V_{h,D}$ *satisfies*

$$-\Delta \widehat{v}^h + (s/c)^2 \widehat{v}^h = 0 \qquad \text{in } \mathbb{R}^d \setminus \Gamma, \tag{5.15a}$$

$$\gamma_D \widehat{\psi}^h = \mu_d^h \qquad \text{on } \Gamma, \tag{5.15b}$$

$$\begin{aligned} \mathcal{B}((\widehat{\mathbf{u}}^h, \widehat{\psi}^h), (\mathbf{w}, \varphi); s) - \rho_f s \langle [\![\gamma \widehat{v}^h]\!], \gamma \mathbf{w} \cdot \boldsymbol{\nu} \rangle_\Gamma = & -\rho_f s \langle \beta_d, \gamma \mathbf{w} \cdot \boldsymbol{\nu} \rangle_\Gamma + \langle \eta_d, \gamma \varphi \rangle_{\Gamma_N} \\ & + s^2 (\rho_\Sigma \boldsymbol{\theta}_d, \mathbf{w})_{\Omega_-} \\ & \forall\, (\mathbf{w}, \varphi) \in \mathbf{V}_h \times V_{h,D}, \end{aligned} \tag{5.15c}$$

$$-(0, s\gamma \widehat{\mathbf{u}}^h \cdot \boldsymbol{\nu}) + (\gamma^- \widehat{v}^h, \partial_\nu^+ \widehat{v}^h) - (0, \alpha_d + s\theta_d) \in X_h^\circ \times Y_h^\circ, \tag{5.15d}$$

$$([\![\partial_\nu \widehat{v}^h]\!] + \lambda_d, [\![\gamma \widehat{v}^h]\!] + \phi_d) \in X_h \times Y_h. \tag{5.15e}$$

Conversely, given a solution triplet $(\widehat{v}^h, \widehat{\mathbf{u}}^h, \widehat{\psi}^h)$ *to* (5.15) *and defining*

$$\widehat{\lambda}^h := -[\![\partial_\nu \widehat{v}^h]\!], \qquad \widehat{\phi}^h := -[\![\gamma \widehat{v}^h]\!],$$

the functions $(\widehat{\mathbf{u}}^h, \widehat{\psi}^h, \widehat{\lambda}^h, \widehat{\phi}^h)$ *solve* (5.13).

Proof. Given a solution of (5.13) and defining $\widehat{v}^h$ as in (5.14), it follows from the properties of the layer potentials that (5.15a) is satisfied. Another consequence of this definition is that $[\![\gamma \widehat{v}^h]\!] = -\widehat{\phi}^h$ and $[\![\partial_\nu \widehat{v}^h]\!] = -\widehat{\lambda}^h$, which shows that equations (5.15c) and (5.15e) follow readily from (5.13b) and (5.13d) by substitution of the above terms. Moreover, using the identities (4.7b) to compute $\gamma^- \widehat{v}^h$ and $\partial_\nu^+ \widehat{v}^h$, it can be seen that (5.13c) and (5.15d) are equivalent.

The proof of the converse is very similar and requires only to observe that (5.15a) allows for the layer potential representation of the acoustic field

$$\widehat{v}^h = \mathrm{D}(s/c)\gamma^+ \widehat{v}^h - \mathrm{S}(s/c)\partial_\nu^+ \widehat{v}^h.$$

Thus, defining $\widehat{\lambda}^h$ and $\widehat{\phi}^h$ as in the statement all the above arguments can be repeated to show that equations (5.13) hold. □

The system (5.15) can now be treated variationally. To do this we introduce the space

$$V_h^* := \left\{ w \in H^1(\mathbb{R}^d \setminus \Gamma) : [\![\gamma w]\!] \in Y_h, \text{ and } \gamma^- w \in X_h^\circ \right\}.$$

The following proposition gives the equivalent variational formulation from which the solvability and stability bounds of the entire problem will be deduced.

Proposition 5.3 (Variational formulation)**.** *Consider the bilinear and linear forms*

$$\begin{aligned}
\mathcal{A}((v,\mathbf{u},\psi),(w,\mathbf{w},\varphi);s) :=\ & (\nabla v,\nabla w)_{\mathbb{R}^d\setminus\Gamma} + (s/c)^2(v,w)_{\mathbb{R}^d\setminus\Gamma} \\
& + \mathcal{B}((\mathbf{u},\psi),(\mathbf{w},\varphi);s) \\
& + \rho_f s\langle\gamma\mathbf{u}\cdot\boldsymbol{\nu},[\![\gamma w]\!]\rangle_\Gamma - \rho_f s\langle[\![\gamma v]\!],\gamma\mathbf{w}\cdot\boldsymbol{\nu}\rangle_\Gamma, \\
\ell\left((w,\mathbf{w},\varphi);s\right) :=\ & -\langle\lambda_d,\gamma^- w\rangle_\Gamma + \langle\alpha_d + s\theta_d,[\![\gamma w]\!]\rangle_\Gamma \\
& + s^2(\rho_\Sigma\boldsymbol{\theta}_d,\mathbf{w})_{\Omega_-} - \rho_f s\langle\beta_d,\gamma\mathbf{w}\cdot\boldsymbol{\nu}\rangle_\Gamma \\
& + \langle\eta_d,\gamma\varphi\rangle_{\Gamma_N}.
\end{aligned}$$

The system (5.15) *is equivalent to the problem of finding*

$$(\widehat{v}^h,\widehat{\mathbf{u}}^h,\widehat{\psi}^h)\in H^1(\mathbb{R}^d\setminus\Gamma)\times\mathbf{V}_h\times V_{h,D}$$

such that

$$\gamma_D\widehat{\psi}^h = \mu_d^h, \tag{5.16a}$$

$$([\![\gamma\widehat{v}^h]\!]+\phi_d,\gamma^-\widehat{v}^h)\in Y_h\times X_h^\circ, \tag{5.16b}$$

$$\mathcal{A}((\widehat{v}^h,\widehat{\mathbf{u}}^h,\widehat{\psi}^h),(w,\mathbf{w},\varphi);s) = \ell\left((w,\mathbf{w},\varphi);s\right)\quad\forall(w,\mathbf{w},\varphi)\in V_h^*\times\mathbf{V}_h\times V_{h,D}. \tag{5.16c}$$

Proof. Given a solution $(\widehat{v}^h,\widehat{\mathbf{u}}^h,\widehat{\psi}^h)$ to (5.15) we note that (5.16b) is equivalent to the first component of (5.15d) and the second component of (5.15e). Moreover, testing $\partial_\nu^+\widehat{v}$ with $[\![\gamma w]\!]$ for $w\in V_h^*$, we obtain

$$\begin{aligned}
\langle\partial_\nu^+\widehat{v}^h,[\![\gamma w]\!]\rangle_\Gamma &= \langle\partial_\nu^-\widehat{v}^h,\gamma^- w\rangle_\Gamma - \langle\partial_\nu^+\widehat{v}^h,\gamma^+ w\rangle_\Gamma - \langle[\![\partial_\nu\widehat{v}^h]\!],\gamma^- w\rangle_\Gamma \\
&= (\nabla\widehat{v}^h,\nabla w)_{\mathbb{R}^d\setminus\Gamma} + (\Delta\widehat{v}^h,w)_{\mathbb{R}^d\setminus\Gamma} - \langle[\![\partial_\nu\widehat{v}^h]\!],\gamma^- w\rangle_\Gamma \\
&= (\nabla\widehat{v}^h,\nabla w)_{\mathbb{R}^d\setminus\Gamma} + (s/c)^2(\widehat{v}^h,w)_{\mathbb{R}^d\setminus\Gamma} - \langle[\![\partial_\nu\widehat{v}^h]\!]+\lambda_d,\gamma^- w\rangle_\Gamma + \langle\lambda_d,\gamma^- w\rangle_\Gamma \\
&= (\nabla\widehat{v}^h,\nabla w)_{\mathbb{R}^d\setminus\Gamma} + (s/c)^2(\widehat{v}^h,w)_{\mathbb{R}^d\setminus\Gamma} + \langle\lambda_d,\gamma^- w\rangle_\Gamma,
\end{aligned} \tag{5.17}$$

where we have used the definition of the weak normal derivative $\partial_\nu^{\pm}\widehat{v}^h$ in conjunction with equations (5.15a), (5.15d) and the first component of (5.15e). Therefore, for $w \in V_h^*$ it follows from the second component of (5.15e) and (5.17) that

$$(\nabla\widehat{v}^h, \nabla w)_{\mathbb{R}^d\setminus\Gamma} + (s/c)^2(\widehat{v}^h, w)_{\mathbb{R}^d\setminus\Gamma} + \langle\lambda_d, \gamma^- w\rangle_\Gamma + \langle s\gamma\widehat{\mathbf{u}}^h\cdot\boldsymbol{\nu} + \alpha_d + s\theta_d, [\![\gamma w]\!]\rangle_\Gamma = 0.$$

The combined application of this last expression with equation (5.15c) is equivalent to (5.16c).

To verify the converse statement, we expand the bilinear form in (5.16c) and rewrite it in terms of the interior/exterior normal derivatives of $\widehat{v}^h$ and its Laplacian to show that

$$\begin{aligned}
0 = {} & (\Delta\widehat{v}^h, w)_{\Omega_-} - (s/c)^2(\widehat{v}^h, w)_{\Omega_-} \\
& + \mathcal{B}((\widehat{\mathbf{u}}^h, \widehat{\psi}^h), (\mathbf{w}, \varphi); s) - s^2(\rho_\Sigma\boldsymbol{\theta}_d, \mathbf{w})_{\Omega_-} - \rho_f s\langle[\![\gamma\widehat{v}^h]\!] + \beta_d, \gamma\mathbf{w}\cdot\boldsymbol{\nu}\rangle_\Gamma - \langle\eta_d, \gamma\varphi\rangle_{\Gamma_N} \\
& + \langle\rho_f s\gamma\widehat{\mathbf{u}}^h\cdot\boldsymbol{\nu} + \alpha_d + s\theta_d, [\![\gamma w]\!]\rangle_\Gamma \\
& + \langle[\![\partial_\nu\widehat{v}^h]\!] + \lambda_d, \gamma^- w\rangle_\Gamma.
\end{aligned}$$

Once the equation is rewritten in this form, it is enough to notice that the mapping

$$\begin{aligned}
V_h^* \times \mathbf{V}_h \times V_{h,D} &\longrightarrow V_h^* \times \mathbf{V}_h \times V_{h,D} \times X_h^\circ \times Y_h \\
(w, \mathbf{w}, \varphi) &\longmapsto (w, \mathbf{w}, \varphi, \gamma^- w, [\![\gamma w]\!])
\end{aligned}$$

is surjective to conclude that every line of the above expression must vanish independently, which implies –line by line– equations (5.15a), (5.15c), the second component of (5.15d), and the first component of (5.15e). The boundary condition (5.15b) is given and the remaining two components of (5.15d) and (5.15e) are imposed strongly by the choice of function spaces. □

Well-posedness and stability. For $s \in \mathbb{C}_+$ we write as usual

$$\sigma := \operatorname{Re} s > 0\,, \qquad \underline{\sigma} := \min\{\sigma, 1\}.$$

To shorten some of the forthcoming expressions, we will denote:

$$\begin{aligned}\|(v,\mathbf{u},\psi)\|_1^2 :=& \rho_f\|\nabla v\|^2_{\mathbb{R}^d\setminus\Gamma} + \rho_f c^{-2}\|v\|^2_{\mathbb{R}^d}\\ &+ (\mathbf{C}\boldsymbol{\varepsilon}(\mathbf{u}),\boldsymbol{\varepsilon}(\overline{\mathbf{u}}))_{\Omega_-} + (\rho_\Sigma\mathbf{u},\overline{\mathbf{u}})_{\Omega_-} + (\boldsymbol{\epsilon}\nabla\psi,\nabla\overline{\psi})_{\Omega_-}.\end{aligned}$$

Following the program laid out in [82], we define the energy norm

$$\begin{aligned}|\!|\!|(v,\mathbf{u},\psi)|\!|\!|^2_{|s|} :=& \rho_f\|\nabla v\|^2_{\mathbb{R}^d\setminus\Gamma} + \rho_f c^{-2}\|sv\|^2_{\mathbb{R}^d}\\ &+ (\mathbf{C}\boldsymbol{\varepsilon}(\mathbf{u}),\boldsymbol{\varepsilon}(\overline{\mathbf{u}}))_{\Omega_-} + \|s\sqrt{\rho_\Sigma}\mathbf{u}\|^2_{\Omega_-} + (\boldsymbol{\epsilon}\nabla\psi,\nabla\overline{\psi})_{\Omega_-},\end{aligned}$$

which includes kinetic and potential contributions from the acoustic and elastic fields, and the potential energy from the dielectric field. Notice that, since $\Gamma_D \neq \varnothing$, this defines a norm in $V_h^* \times \mathbf{V}_h \times V_{h,D}$. A simple computation shows that

$$\underline{\sigma}\|(v,\mathbf{u},\psi)\|_1 \leq |\!|\!|(v,\mathbf{u},\psi)|\!|\!|_{|s|} \leq \frac{|s|}{\underline{\sigma}}\|(v,\mathbf{u},\psi)\|_1. \tag{5.18}$$

Proposition 5.4 (Well-posedness)**.** *Problem* (5.16) *is uniquely solvable for any*

$$\begin{aligned}&(\alpha_d,\beta_d,\eta_d,\mu_d^h) \in H^{-1/2}(\Gamma)\times H^{1/2}(\Gamma)\times H^{-1/2}(\Gamma_N)\times\gamma_D V_h,\\ &(\boldsymbol{\theta}_d,\theta_d,\lambda_d,\phi_d) \in \mathbf{H}^1(\Omega_-)\times L^2(\Gamma)\times H^{-1/2}(\Gamma)\times H^{1/2}(\Gamma),\end{aligned}$$

and $s\in\mathbb{C}_+$*. Moreover, there exists* $C>0$ *independent of* h *and* s *such that*

$$\|(\widehat{v}^h,\widehat{\mathbf{u}}^h,\widehat{\psi}^h)\|_1 + \|\widehat{\phi}^h\|_{1/2,\Gamma} \leq C\frac{|s|}{\sigma\underline{\sigma}^2}A(\text{data},s), \tag{5.19a}$$

$$\|\widehat{\lambda}^h\|_{-1/2,\Gamma} \leq C\frac{|s|^{3/2}}{\sigma\underline{\sigma}^{3/2}}A(\text{data},s), \tag{5.19b}$$

where

$$\begin{aligned}A(\text{data},s) :=& \|\alpha_d\|_{-1/2,\Gamma} + \|s\beta_d\|_{1/2,\Gamma} + \|\eta_d\|_{-1/2,\Gamma} + \|s\mu_d^h\|_{1/2,\Gamma}\\ &+ \|s^2\boldsymbol{\theta}_d\|_{\Omega_-} + \|s\theta_d\|_\Gamma + \|\lambda_d\|_{-1/2,\Gamma} + \|s\phi_d\|_{1/2,\Gamma}.\end{aligned}$$

Proof. It is easy to check that

$$\left|\operatorname{Re}\overline{s}\mathcal{A}\left((v,\mathbf{u},\psi),\overline{(v,\mathbf{u},\psi)};s\right)\right| = \sigma|\!|\!|(v,\mathbf{u},\psi)|\!|\!|^2_{|s|}.$$

This observation implies the existence and uniqueness of the solution by the Lax-Milgram lemma. In order to prove the stability bounds we first note that

$$|\mathcal{A}\left((v,\mathbf{u},\psi),(w,\mathbf{w},\varphi);s\right)| \leq C_1 \frac{|s|}{\underline{\sigma}} |\!|\!| (w,\mathbf{w},\varphi) |\!|\!|_{|s|} \|(v,\mathbf{u},\psi)\|_1, \tag{5.20}$$

$$\begin{aligned} |\ell\left((w,\mathbf{w},\varphi);s\right)| \leq \frac{C_2}{\underline{\sigma}} |\!|\!| (w,\mathbf{w},\varphi) |\!|\!|_{|s|} \Big(& \|\alpha_d\|_{-1/2,\Gamma} + \|s\beta_d\|_{1/2,\Gamma} + \|\eta_d\|_{-1/2,\Gamma} \\ & + \|s^2\boldsymbol{\theta}_d\|_{\Omega_-} + \|s\theta_d\|_\Gamma + \|\lambda_d\|_{-1/2,\Gamma} \Big), \end{aligned} \tag{5.21}$$

where C_1 and C_2 depend only on the geometry, and in the second inequality we have employed (5.18) to bound the energy norm. Next, we pick liftings of the boundary data $\gamma^\dagger \phi_d \in H^1(\mathbb{R}^d \setminus \Gamma)$ and $\gamma^\dagger_{h,D}\mu_d^h \in V_h$ such that

$$\gamma^- \gamma^\dagger \phi_d = 0\,, \qquad -\gamma^+\gamma^\dagger\phi_d = \phi_d\,, \qquad \|\gamma^\dagger\phi_d\|_{1,\Omega_-} \leq C\|\phi_d\|_{1/2,\Gamma}, \tag{5.22a}$$

$$\gamma\gamma^\dagger_{h,D}\mu_d^h = \mu_d^h\,, \qquad \|\gamma^\dagger_{h,D}\mu_d^h\|_{1,\Omega_-} \leq C\|\mu_d^h\|_{1/2,\Gamma}. \tag{5.22b}$$

Since $\widehat{v}^h + \gamma^\dagger\phi_d \in V_h^*$ and $\widehat{\psi}^h + \gamma^\dagger_{h,D}\mu_d^h \in V_{h,D}$, we can use (5.16c) to show that

$$\begin{aligned} & |\!|\!| (\widehat{v}^h + \gamma^\dagger\phi_d, \widehat{\mathbf{u}}^h, \widehat{\psi}^h + \gamma^\dagger_{h,D}\mu_d^h) |\!|\!|_{|s|}^2 \\ & \quad \leq \frac{|s|}{\sigma} \left| \mathcal{A}((\widehat{v}^h + \gamma^\dagger\phi_d, \widehat{\mathbf{u}}^h, \widehat{\psi}^h + \gamma^\dagger_{h,D}\mu_d^h), (\widehat{v}^h + \gamma^\dagger\phi_d, \widehat{\mathbf{u}}^h, \widehat{\psi}^h + \gamma^\dagger_{h,D}\mu_d^h); s) \right| \\ & \quad = \frac{|s|}{\sigma} \Big| \ell((\widehat{v}^h + \gamma^\dagger\phi_d, \widehat{\mathbf{u}}^h, \widehat{\psi}^h + \gamma^\dagger_{h,D}\mu_d^h); s) \\ & \qquad\qquad + \mathcal{A}((\gamma^\dagger\phi_d, \mathbf{0}, \gamma^\dagger_{h,D}\mu_d^h), (\widehat{v}^h + \gamma^\dagger\phi_d, \widehat{\mathbf{u}}^h, \widehat{\psi}^h + \gamma^\dagger_{h,D}\mu_d^h); s) \Big| \\ & \quad \leq \frac{|s|}{\sigma} |\!|\!| (\widehat{v}^h + \gamma^\dagger\phi_d, \widehat{\mathbf{u}}^h, \widehat{\psi}^h + \gamma^\dagger_{h,D}\mu_d^h) |\!|\!|_{|s|} \\ & \qquad \times \left(\frac{C_2}{\underline{\sigma}} \Big(\|\alpha_d\|_{-1/2,\Gamma} + \|s\beta_d\|_{1/2,\Gamma} + \|\eta_d\|_{-1/2,\Gamma} + \|s^2\boldsymbol{\theta}_d\|_{\Omega_-} \right. \\ & \qquad\qquad \left. + \|s\theta_d\|_\Gamma + \|\lambda_d\|_{-1/2,\Gamma} \Big) + C_1 \frac{|s|}{\underline{\sigma}} \Big) \|\gamma^\dagger\phi_d\|_{1,\Omega_-} + \|\gamma^\dagger_{h,D}\mu_d^h\|_{1,\Omega_-} \Big) \Big) \\ & \quad \leq C \frac{|s|}{\sigma\underline{\sigma}} |\!|\!| (\widehat{v}^h + \gamma^\dagger\phi_d, \widehat{\mathbf{u}}^h, \widehat{\psi}^h + \gamma^\dagger_{h,D}\mu_d^h) |\!|\!|_{|s|} A(\text{data}, s), \end{aligned}$$

where (5.20), (5.21), and (5.22a) have been used. This implies

$$|\!|\!|(\widehat{v}^h + \gamma^\dagger \phi_d, \widehat{\mathbf{u}}^h, \widehat{\psi}^h + \gamma^\dagger_{h,D}\mu^h_d)|\!|\!|_{|s|} \leq C\frac{|s|}{\sigma\underline{\sigma}}A(\text{data}, s). \tag{5.23}$$

The inequality (5.19a) follows from (5.23) with an application of (5.18). The estimate (5.19b) can be derived from (5.23) by recalling that $\widehat{\lambda}^h = -[\![\partial_\nu \widehat{v}^h]\!]$ and applying [82, Lemma 15] which states that, if $\Delta v - s^2 v = 0$ in an open set $\mathcal{O}$ with Lipschitz boundary, then

$$\|\partial_\nu v\|_{-1/2,\partial\mathcal{O}} \leq C\left(\frac{|s|}{\underline{\sigma}}\right)^{1/2}(\|sv\|_{\mathcal{O}} + \|\nabla v\|_{\mathcal{O}}). \tag{5.24}$$

This finishes the proof. (See Proposition 4.15 which uses a similar argument.) □

5.5 Time Domain Estimates

Just as we did in Section 4.2.1, for the time domain estimates, data and solutions will be assumed to be in spaces of the form

$$W^k_+(\mathrm{X}) := \{\xi \in \mathcal{C}^{k-1}(\mathbb{R};\mathrm{X}) \,:\, \xi \equiv 0 \text{ in } (-\infty, 0), \xi^{(k)} \in L^1(\mathbb{R};\mathrm{X})\},$$

for $k \geq 1$. We will also use the linear differential operator (cf. Appendix A.)

$$(\mathcal{P}_k f)(t) := \sum_{l=0}^{k}\binom{k}{l} f^{(l)}(t).$$

The stability bounds and semi-discrete error estimates obtained in the previous section can be translated into the following time domain results. Taking the second group of data (5.12b) to be identically zero and setting

$$(\boldsymbol{\theta}_d, \theta_d, \lambda_d, \phi_d) = (\mathbf{P}_h\mathbf{u} - \mathbf{u}, \gamma(\mathbf{P}_h\mathbf{u} - \mathbf{u})\cdot\boldsymbol{\nu}, \lambda, \phi),$$

an application of [37, Theorem 7.1] combined with Proposition 5.4 yields the following result

Corollary 5.5 (Stability in the time domain)**.** *For causal problem data*

$$(\alpha_d, \beta_d, \eta_d, \mu^h_d) \in W^3_+(H^{-1/2}(\Gamma)) \times W^4_+(H^{1/2}(\Gamma)) \times W^3_+(H^{-1/2}(\Gamma)) \times W^4_+(H^{1/2}(\Gamma))$$

then the solutions of (5.13) $\lambda^h, \phi^h, \mathbf{u}^h$ *and* ψ^h *are continuous causal functions of time and there exist constants* $D_1, D_2 > 0$ *such that, for* $t \geq 0$*:*

$$\|(v^h, \mathbf{u}^h, \psi^h)(t)\|_1 + \|\phi^h(t)\|_{1/2,\Gamma} \leq \frac{D_1 t^2}{t+1} \max\{1, t^2\} \int_0^t \|\mathcal{P}_3(\dot{\alpha}_d, \beta_d, \eta_d, \dot{\mu}_d^h)(\tau)\|_{\pm 1/2,\Gamma}\, d\tau,$$
$$\|\lambda^h(t)\|_{-1/2,\Gamma} \leq \frac{D_2 t^{3/2}}{\sqrt{t+1}} \max\{1, t^{3/2}\} \int_0^t \|\mathcal{P}_3(\dot{\alpha}_d, \beta_d, \eta_d, \dot{\mu}_d^h)(\tau)\|_{\pm 1/2,\Gamma}\, d\tau,$$

where D_1 *and* D_2 *depend only on* Γ*.*

We introduce the approximation error

$$a_h(t) := \int_0^t \left(\|\mathcal{P}_3(\dot{\phi} - \Pi_h^Y \dot{\phi})(\tau)\|_{1/2,\Gamma} + \|\mathcal{P}_3(\lambda - \Pi_h^X \lambda)(\tau)\|_{-1/2,\Gamma} \right) d\tau$$
$$+ \int_0^t \left(\|\mathcal{P}_3(\ddot{\mathbf{u}} - \mathbf{P}_h \ddot{\mathbf{u}})(\tau)\|_{\Omega_-} + \|\mathcal{P}_3(\dot{\mathbf{u}} - \mathbf{P}_h \dot{\mathbf{u}})(\tau)\|_{1,\Omega_-} \right) d\tau,$$

where Π_h^Y and Π_h^X are the orthogonal projections onto Y_h and X_h respectively, and $\mathbf{P}_h$ is part of the elliptic projector defined in (5.10). Note that $\mathbf{P}_h \mathbf{u}$ depends on $\mathbf{u}$, ψ, and μ_d^h and that Lemma 5.1 states that

$$\|\mathbf{u} - \mathbf{P}_h \mathbf{u}\|_{1,\Omega_-} \leq C\big(\|\mathbf{u} - \Pi_{\mathbf{V}}^h \mathbf{u}\|_{1,\Omega_-} + \|\psi - \Pi_V^h \psi\|_{1,\Omega_-} + \|\mu_d - \mu_d^h\|_{1/2,\Gamma}\big),$$

where $\Pi_h^{\mathbf{V}}$ and Π_h^V are the respective H^1 best approximation operators on $\mathbf{V}_h$ and V_h. Taking the data (5.12a) as in Proposition 5.4 and applying [37, Theorem 7.1] we can prove the following result

Corollary 5.6 (Semi-discrete error)**.** *If the solution* $(\lambda, \phi, \mathbf{u}, \psi)$ *is such that*

$$\lambda \in W_+^3(H^{-1/2}(\Gamma)), \qquad \phi \in W_+^4(H^{1/2}(\Gamma)),$$
$$\mathbf{u} \in W_+^5(\mathbf{H}^1(\Omega_-)) \cap W_+^4(\mathbf{L}^2(\Omega_-)), \qquad \psi \in W_+^5(H^1(\Omega_-)) \cap W_+^4(L^2(\Omega_-)),$$

then, for every $t \geq 0$

$$\|(\mathbf{e}_v^h, \mathbf{e}_{\mathbf{u}}^h, e_\psi^h)(t)\|_1 + \|e_\phi^h(t)\|_{1/2,\Gamma} \leq \frac{D_1 t^2}{t+1} \max\{1, t^2\} a_h(t),$$
$$\|(e_\lambda^h)(t)\|_{1/2,\Gamma} \leq \frac{D_2 t^{3/2}}{\sqrt{t+1}} \max\{1, t^{3/2}\} a_h(t),$$

where $D_1, D_2 > 0$ depend only on Γ,

$$e_v^h := \mathcal{D}_c * (\phi - \phi^h) - \mathcal{S}_c * (\lambda - \lambda^h) = v - \mathcal{D}_c * \phi^h + \mathcal{S}_c * \lambda^h.$$

Here $\mathcal{D}_c$ and $\mathcal{S}_c$ are the operator-valued causal distributions whose Laplace transforms are $\mathrm{D}(s/c)$ and $\mathrm{S}(s/c)$, and $*$ is the symbol for distributional convolution in the time variable.

Just as in the previous chapter, we will make use of a resut that will allow us to carry out all the time domain analysis using CQ based tools even if our computational implementation involves traditional time stepping for the finite element discretization. As is shown in [82, Proposition 12], [61] as long as the time stepping method used for the FEM part coincides with the one giving rise to the CQ algorithm in use this split treatment of different parts of a system is equivalent to the application of CQ globally.

The approximation error between the fully discrete solution $(v_\kappa^h, \mathbf{u}_\kappa^h, \psi_\kappa^h)$ obtained using BDF2-CQ with a time step size κ and the semi-discrete approximation $(v^h, \mathbf{u}^h, \psi^h)$ can be estimated from Propostion 5.4 using [116, Proposition 4.6.1] (a slight variant of a result in [91]).

Corollary 5.7. *Let $\ell = 6$ and $(\alpha_d, \beta_d, \eta_d, \mu_d^h)$ be causal problem data satisfying*

$$(\alpha_d, \beta_d, \eta_d, \mu_d^h) \in W_+^{\ell+1}(H^{1/2}(\Gamma)) \times W_+^{\ell}(H^{-1/2}(\Gamma)) \times W_+^{\ell}(H^{-1/2}(\Gamma)) \times W_+^{\ell}(H^{1/2}(\Gamma)).$$

For $t \geq 0$, the difference between the semi-discrete solution and fully discrete solution obtained using BDF2-based Convolution Quadrature is bounded like

$$\|(v^h, \mathbf{u}^h, \psi^h)(t) - (v_\kappa^h, \mathbf{u}_\kappa^h, \psi_\kappa^h)(t)\|_1 \leq D(1+t^2)\kappa^2 \int_0^t \|(\dot{\alpha}_d, \beta_d, \eta_0, \mu_0^h)^{(\ell)}(\tau)\|_\Gamma \, d\tau,$$

where D depends only on Γ. Reduced convergence of order 2/3 is achieved for $\ell = 3$.

5.6 Numerical Experiments

In order to test the convergence results proven in the previous section, the formulation was implemented using standard Lagrangian finite elements for the elastic

and electric fields and Galerkin boundary elements for the acoustic field. We take $\mathbf{V}_h$ and V_h to be continuous $\mathcal{P}_k$ finite elements on a triangular mesh of Ω_-. On the inherited mesh on Γ, we consider the space X_h of discontinuous piecewise $\mathcal{P}_{k-1}$ and the space Y_h of continuous piecewise $\mathcal{P}_k$ functions.

About the implementation. One of the advantages of the formulation we propose is that it lends itself to a highly modular implementation, in the sense that pre-existing FEM code for piezoelectricity and BEM code for acoustics can be used to solve the coupled problem in the frequency domain without any modification. The only requirement is the addition of a "discrete trace" which translates boundary FEM degrees of freedom into BEM degrees of freedom. Formally, the structure of the discrete system (5.8) can be represented as

$$\begin{bmatrix} \mathbf{FEM}(s) & s\rho_f(\mathrm{N}\Gamma)_h^t \\ -s\rho_f(\mathrm{N}\Gamma)_h & \rho_f\mathbf{BEM}(s) \end{bmatrix} \begin{bmatrix} \begin{bmatrix} \mathbf{u}^h \\ \psi^h \end{bmatrix} \\ \begin{bmatrix} \lambda^h \\ \phi^h \end{bmatrix} \end{bmatrix} = \begin{bmatrix} \begin{bmatrix} -s\rho_f\Gamma_h^t\beta^h \\ \eta^h \end{bmatrix} \\ \begin{bmatrix} 0 \\ \rho_f\alpha^h \end{bmatrix} \end{bmatrix},$$

where: (a) the finite element block $\mathbf{FEM}(s)$ contains sparse s-independent elastic stiffness, material mass, piezoelectric, and electric stiffness-like matrices, the material mass matrix being multiplied by s^2 (see (5.7a) and (5.7b)); (b) the boundary element block $\mathbf{BEM}(s)$ contains Galerkin discretizations of the operators of the Calderón projector (see (5.7c)); (c) the sparse matrix $(\mathrm{N}\Gamma)_h$ corresponds to the discretization of the bilinear form $\mathbf{V}_h \times Y_h \ni (\mathbf{u}^h, \chi^h) \mapsto \langle \mathbf{u}^h \cdot \boldsymbol{\nu}, \chi^h \rangle_\Gamma$ with added zero blocks for the interactions of all other spaces. We note that the trace space for $\mathbf{V}_h$ is a vector-valued version of Y_h, which means that, apart from rearrangements of degrees of freedom (and possible changes of local polynomial bases), the only matrix connecting the BEM and FEM codes is simple to implement.

In a similar way, the transition from Laplace domain to time domain can be done modularly, either by implementing a CQ routine that inverts the full operator matrix, or a time stepping routine where s is replaced with a discrete approximation of the differentiation operator, or using a Schur complement strategy as was first suggested

in [13] and outlined in [61] for a purely acoustic system or as in [66] for a coupled acoustic/elastic problem. The latter approach, which results in a decoupling of the boundary integral part of the system, is well suited for parallelization and was the chosen strategy for the following numerical experiments.

Geometric setup and physical parameters. In all the convergence studies (frequency and time domain), the rectangle

$$\Omega_- := (1,\, 3) \times (1,\, 2) \subset \mathbb{R}^2$$

was used as the piezoelectric domain. The double-indices used in our general presentation of tensor in the piezoelectric domains will be reduced to a single index using the simple convention:

$$(1,1) \leftrightarrow 1 \qquad (2,2) \leftrightarrow 2 \qquad (1,2) \leftrightarrow 3.$$

(By symmetry, the pair (2,1) can be avoided in the tensor representations.) We choose the following constant Lamé parameters, mass density, and acoustic speed of sound:

$$\lambda = 2, \quad \mu = 3, \quad \rho_\Sigma = 5, \quad c = 1. \tag{5.25a}$$

We will use Young's modulus and Poisson's ratio

$$E := \frac{2\mu(1+\lambda)}{2\mu+\lambda}, \qquad \nu := \frac{\lambda}{2\mu+\lambda} \tag{5.25b}$$

to express the entries of the elastic compliance tensor $\mathbf{C}$

$$\mathbf{C}_{11} = \mathbf{C}_{22} = \frac{E}{1-\nu^2}, \quad \mathbf{C}_{33} = \frac{E}{2(1+\nu)}, \quad \mathbf{C}_{12} = \frac{E\nu}{1-\nu^2}, \quad \mathbf{C}_{13} = \mathbf{C}_{23} = 0. \tag{5.25c}$$

For the piezoelectric tensor $\mathbf{e}$ the values used were

$$\mathbf{e}_{11} = \mathbf{e}_{22} = \mathbf{e}_{33} = 1, \quad \mathbf{e}_{12} = \mathbf{e}_{13} = \mathbf{e}_{23} = 5, \tag{5.25d}$$

while for the dielectric tensor $\boldsymbol{\epsilon}$ the entries were

$$\boldsymbol{\epsilon}_{11} = \boldsymbol{\epsilon}_{22} = 4, \quad \boldsymbol{\epsilon}_{12} = 1. \tag{5.25e}$$

We take $\Gamma_D = \Gamma$ and $\Gamma_N = \varnothing$.

Convergence studies in the frequency domain. The elastic plane pressure wave

$$\mathbf{u}(\mathbf{x}) = e^{-sc_L\mathbf{x}\cdot\mathbf{d}}\mathbf{d}, \quad \mathbf{d} = \left(\tfrac{1}{\sqrt{2}}, \tfrac{1}{\sqrt{2}}\right), \quad c_L = \sqrt{\frac{2\mu+\lambda}{\rho_\Sigma}}$$

with $s = -2.5\imath$ was imposed as a solution alongside the electric field

$$\psi(\mathbf{x}) = x_1^3 + x_1^3x_2 - 3x_1x_2^2 - \tfrac{1}{3}x_2^3.$$

In the acoustic domain, the cylindrical acoustic wave

$$v(\mathbf{x}) = \tfrac{\imath}{4}H_0^{(1)}(\imath s|\mathbf{x}-\mathbf{x}_0|), \qquad \mathbf{x}_0 = (2, 1.5) \in \Omega_-$$

was used. Right-hand sides are added to equations (5.4b) and (5.4c)

$$\nabla\cdot\boldsymbol{\sigma} = \rho_\Sigma s^2\mathbf{u} + f_1 \qquad \nabla\cdot\mathbf{D} = f_2$$

so that $(\mathbf{u}, \psi)$ is a solution. Boundary data for ψ and transmission data in (5.4d)-(5.4e) are built so that the equations are satisfied.

The experiment was ran using $k = 1, 2$ for the $\mathcal{P}_k$ finite elements and $\mathcal{P}_k/\mathcal{P}_{k-1}$ boundary elements. The acoustic wave was sampled in twenty random points in the exterior of the piezoelectric domain and compared to the exact solution, using the maximum discrepancy as the measure of the acoustic error E_h^v. For the elastic and electric unknowns both $L^2(\Omega_-)$ and $H^1(\Omega_-)$ errors were computed. Tables 5.1 and 5.2 as well as Figure 5.2 show the outcome of the convergence tests.

$k=1$			$L^2(\Omega_-)$				$H^1(\Omega_-)$			
h	E_h^v	e.c.r.	$E_h^{\mathbf{u}}$	e.c.r.	E_h^{ψ}	e.c.r.	$E_h^{\mathbf{u}}$	e.c.r.	E_h^{ψ}	e.c.r.
0.2	7.110 E-2	—	1.167 E-1	—	4.140 E-2	—	7.835 E-1	—	1.718	—
0.1	1.760 E-2	2.014	3.146 E-2	1.891	1.047 E-2	1.984	2.646 E-1	1.566	8.544 E-1	1.007
0.05	4.615 E-3	1.931	8.138 E-3	1.951	2.632 E-3	1.991	9.372 E-2	1.497	4.263 E-1	1.003
0.025	1.171 E-3	1.978	2.059 E-3	1.983	6.599 E-4	1.996	3.734 E-2	1.327	2.130 E-1	1.001

Table 5.1: Relative errors and estimated convergence rates in the time frequency domain with $\mathcal{P}_1$ finite elements and $\mathcal{P}_1/\mathcal{P}_0$ boundary elements. h represents the maximum length of the panels used to discretize the boundary.

$k=2$			$L^2(\Omega_-)$				$H^1(\Omega_-)$			
h	E_h^v	e.c.r.	$E_h^{\mathbf{u}}$	e.c.r.	E_h^{ψ}	e.c.r.	$E_h^{\mathbf{u}}$	e.c.r.	E_h^{ψ}	e.c.r.
0.2	5.545 E-5	—	3.542 E-4	—	3.927 E-4	—	1.350 E-2	—	1.805 E-2	—
0.1	4.161 E-6	3.736	3.949 E-5	3.024	4.872 E-5	3.024	3.083 E-3	2.130	4.450 E-3	2.020
0.05	3.146 E-7	3.725	4.555 E-6	3.116	5.991 E-6	3.010	7.153 E-4	2.108	1.105 E-3	2.009
0.025	2.379 E-8	3.725	5.455 E-7	3.062	7.463 E-7	3.005	1.710 E-4	2.064	2.753 E-4	2.005

Table 5.2: Relative errors and estimated convergence rates in the time frequency domain with $\mathcal{P}_2$ finite elements and $\mathcal{P}_2/\mathcal{P}_1$ boundary elements. h represents the maximum length of the panels used to discretize the boundary.

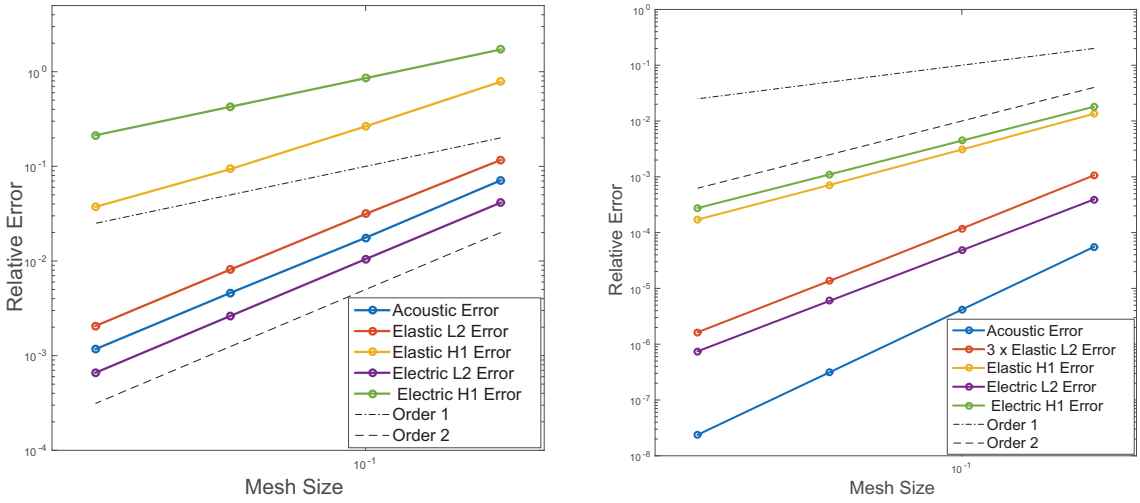

Figure 5.2: Convergence studies for the frequency domain problem are shown for $\mathcal{P}_1/\mathcal{P}_0$ boundary elements and $\mathcal{P}_1$ finite elements (left) and $\mathcal{P}_2/\mathcal{P}_1$ boundary elements and $\mathcal{P}_2$ finite elements (right).

Convergence studies in the time domain

Experiments were carried out using matching time stepping (for the FEM part) and CQ (for the BEM part) based on both Trapezoidal Rule and BDF2 for time evolution. The fully discrete method based on the trapezoidal rule can analyzed in the same way as BDF2, using results from [8]. Note that the only difference is the lack of knowledge of how the error constants depend on the time variable.

Just as in the frequency domain case, the rectangle

$$\Omega_- := (1,\, 3) \times (1,\, 2) \subset \mathbb{R}^2$$

was used as the piezoelectric domain where the elastic plane pressure wave

$$\mathbf{u}(\mathbf{x},t) = \mathcal{H}(c_L t - \mathbf{x}\cdot\mathbf{d})\sin\left(3(c_L t - \mathbf{x}\cdot\mathbf{d})\right)\mathbf{d}, \quad \mathbf{d} = \left(\tfrac{1}{\sqrt{2}}, \tfrac{1}{\sqrt{2}}\right), \quad c_L = \sqrt{\frac{2\mu+\lambda}{\rho_\Sigma}},$$

and the causal electric field

$$\psi(\mathbf{x},t) = \mathcal{H}(t)(x_1^3 + x_1^3 x_2 - 3x_1 x_2^2 - \tfrac{1}{3}x_2^3),$$

were imposed. In the acoustic domain, the cylindrical acoustic wave

$$v(\mathbf{x},t) = \mathcal{L}^{-1}\left\{\imath H_0^{(1)}(\imath s|\mathbf{x}-\mathbf{x}_0|)\,\mathcal{L}\{\mathcal{H}(t)\sin(2t)\}\right\},$$

centered at $\mathbf{x}_0 = (2, 1.5)$, was imposed. In all cases $\mathcal{H}$ is the piecewise polynomial approximation to Heaviside's step function given in (4.54).

Analogously to the frequency domain experiments, right-hand sides were added so that $(\mathbf{u}, \psi)$ are solutions to the system and the appropriate Dirichlet data was sampled at the boundary using Equations (5.3d). (5.3e), and (5.3g) to define the boundary data.

The experiment was ran using $k = 1, 2$ for the $\mathcal{P}_k$ finite elements and $\mathcal{P}_k/\mathcal{P}_{k-1}$ boundary elements. The time step and mesh size were refined simultaneously and the final time was $t = 1.5$. All errors are measured at the final time: $E^v_{h,\kappa}$ measures the maximum error on twenty randomly chosen points in the exterior domain, while elastic and electric fields errors are measured in the $L^2(\Omega_-)$ and $H^1(\Omega_-)$ norms. Tables 5.3 and 5.4 along with Figure 5.3 show the outcome of the convergence tests.

A sample simulation

As an example, we consider the interaction between the acoustic plain wave

$$v^{inc} = 3\chi_{[0,0.3]}(\tau)(88\tau)\sin(88\tau), \quad \tau := t - \mathbf{r}\cdot\mathbf{d}, \quad \mathbf{r} := (x, y), \quad \mathbf{d} := (1, 5)/\sqrt{26},$$

and a pentagonal piezoelectric scatterer with mass density given by

$$\rho_\Sigma = 5 + 25e^{-100r^2} \qquad r := |\mathbf{r}|.$$

$k=1$			$L^2(\Omega_-)$				$H^1(\Omega_-)$			
h/κ	$E^v_{h,\kappa}$	e.c.r.	$E^{\mathbf{u}}_{h,\kappa}$	e.c.r.	$E^{\psi}_{h,\kappa}$	e.c.r.	$E^{\mathbf{u}}_{h,\kappa}$	e.c.r.	$E^{\psi}_{h,\kappa}$	e.c.r.
2 E-1/7.5 E-2	2.054 E-2	—	6.363 E-2	—	4.179 E-2	—	5.714 E-1	—	1.702	—
1 E-1/3.75 E-2	7.864 E-3	1.385	1.726 E-2	1.882	1.034 E-2	2.015	2.067 E-1	1.467	8.515 E-1	0.999
5 E-2/1.875 E-2	1.831 E-3	2.102	4.537 E-3	1.928	2.590 E-3	1.997	8.600 E-2	1.265	4.258 E-1	1.000
2.5 E-2/9.375 E-3	4.485 E-4	2.030	1.159 E-3	1.969	6.485 E-4	1.997	3.912 E-2	1.136	2.129 E-1	1.000

Table 5.3: Relative errors and estimated convergence rates in the time domain for the Trapezoidal Rule Convolution Quadrature with $\mathcal{P}_1$ finite elements and $\mathcal{P}_1/\mathcal{P}_0$ boundary elements: h represents the maximum length of the panels used to discretize the boundary, κ is the size of the timesteps. The errors are measured at the final time $T = 1.5$.

$k=2$			$L^2(\Omega_-)$				$H^1(\Omega_-)$			
h/κ	$E^v_{h,\kappa}$	e.c.r.	$E^{\mathbf{u}}_{h,\kappa}$	e.c.r.	$E^{\psi}_{h,\kappa}$	e.c.r.	$E^{\mathbf{u}}_{h,\kappa}$	e.c.r.	$E^{\psi}_{h,\kappa}$	e.c.r.
2 E-1/7.5 E-2	3.422 E-2	—	4.627 E-2	—	1.544 E-2	—	6.323 E-1	—	1.495 E-1	—
1 E-1/3.75 E-2	2.329 E-2	0.555	1.242 E-2	1.898	3.722 E-3	2.052	1.821 E-1	1.795	3.260 E-2	2.197
5 E-2/1.875 E-2	5.836 E-3	1.997	3.128 E-3	1.989	9.194 E-4	2.017	4.607 E-2	1.983	7.735 E-3	2.076
2.5 E-2/9.375 E-3	1.444 E-3	2.015	7.826 E-4	1.999	2.288 E-4	2.007	1.151 E-2	2.001	1.907 E-3	2.020

Table 5.4: Relative errors and estimated convergence rates in the time domain for the Trapezoidal Rule Convolution Quadrature with $\mathcal{P}_2$ finite elements and $\mathcal{P}_2/\mathcal{P}_1$ boundary elements: h represents the maximum length of the panels used to discretize the boundary, κ is the size of the timesteps. The errors are measured at the final time $T = 1.5$.

The remaining physical parameters of the solid were taken to be those defined by (5.25) and the entire solid/fluid interface was taken as Dirichlet boundary, where a grounding potential $\psi \equiv 0$ was imposed as boundary condition for all times. The simulation was carried out using $\mathcal{P}_2$ Lagrangian finite elements and $\mathcal{P}_2/\mathcal{P}_1$ continuous/discontinuous Galerkin boundary elements with Trapezoidal Rule-based time discretization using a time step $\kappa = 0.005$. Figures 5.5 to 5.7 show snapshots of the process at different times.

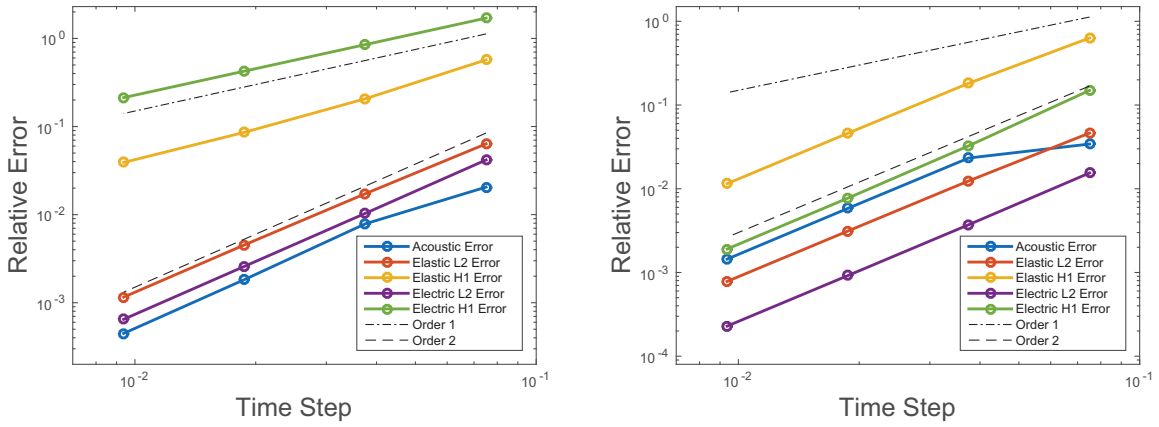

Figure 5.3: Convergence studies for the Trapezoidal Rule-based time stepping in the case of $\mathcal{P}_1/\mathcal{P}_0$ boundary elements and $\mathcal{P}_1$ finite elements (left) and $\mathcal{P}_2/\mathcal{P}_1$ boundary elements and $\mathcal{P}_2$ finite elements (right).

$k=1$			$L^2(\Omega_-)$				$H^1(\Omega_-)$			
h/κ	$E^v_{h,\kappa}$	e.c.r.	$E^{\mathbf{u}}_{h,\kappa}$	e.c.r.	$E^{\psi}_{h,\kappa}$	e.c.r.	$E^{\mathbf{u}}_{h,\kappa}$	e.c.r.	$E^{\psi}_{h,\kappa}$	e.c.r.
2 E-1/7.5 E-2	2.805 E-2	—	9.448 E-2	—	4.772 E-2	—	7.683 E-1	—	1.709	—
1 E-1/3.75 E-2	2.543 E-2	0.141	3.401 E-2	1.474	1.377 E-2	1.793	3.931 E-1	0.967	8.546 E-1	1.000
5 E-2/1.875 E-2	1.571 E-2	0.694	1.010 E-2	1.749	3.689 E-3	1.900	1.513 E-1	1.378	4.264 E-1	1.003
2.5 E-2/9.375 E-3	4.650 E-3	1.757	2.655 E-3	1.930	9.379 E-4	1.975	5.231 E-2	1.532	2.130 E-1	1.001

Table 5.5: Relative errors and estimated convergence rates in the time domain for the BDF2-based Convolution Quadrature with $\mathcal{P}_1$ finite elements and $\mathcal{P}_1/\mathcal{P}_0$ boundary elements: h represents the maximum length of the panels used to discretize the boundary, κ is the size of the timesteps. The errors are measured at the final time $T = 1.5$.

$k=2$			$L^2(\Omega_-)$				$H^1(\Omega_-)$			
h/κ	$E^v_{h,\kappa}$	e.c.r.	$E^{\mathbf{u}}_{h,\kappa}$	e.c.r.	$E^{\psi}_{h,\kappa}$	e.c.r.	$E^{\mathbf{u}}_{h,\kappa}$	e.c.r.	$E^{\psi}_{h,\kappa}$	e.c.r.
2 E-1/7.5 E-2	2.959 E-2	—	9.368 E-2	—	2.999 E-2	—	8.178 E-1	—	2.287 E-1	—
1 E-1/3.75 E-2	3.047 E-2	-0.041	3.884 E-2	1.270	1.247 E-2	1.265	4.699 E-1	0.799	1.097 E-1	1.059
5 E-2/1.875 E-2	1.958 E-2	0.638	1.186 E-2	1.712	3.566 E-3	1.806	1.664 E-1	1.498	3.084 E-3	1.832
2.5 E-2/9.375 E-3	5.680 E-3	1.785	3.099 E-3	1.936	9.102 E-4	1.970	4.511 E-2	1.883	7.617 E-3	2.018

Table 5.6: Relative errors and estimated convergence rates in the time domain for the BDF2-based Convolution Quadrature with $\mathcal{P}_2$ finite elements and $\mathcal{P}_2/\mathcal{P}_1$ boundary elements: h represents the maximum length of the panels used to discretize the boundary, κ is the size of the timesteps. The errors are measured at the final time $T = 1.5$.

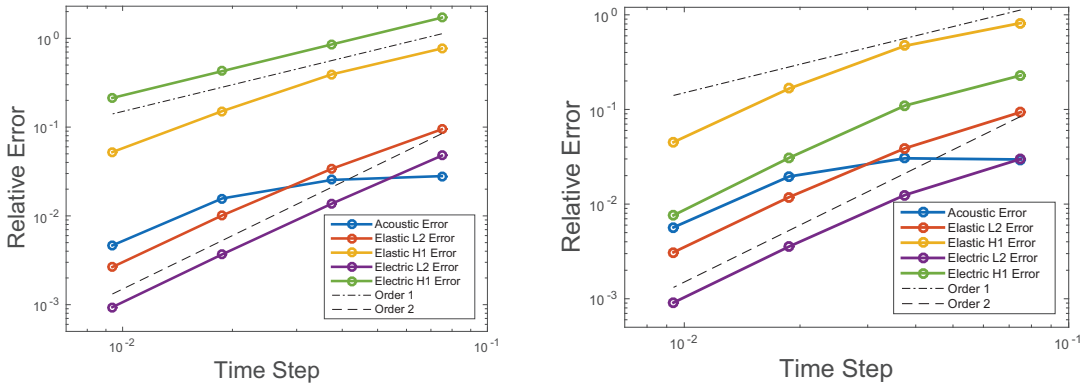

Figure 5.4: Convergence studies for the BDF2-based time stepping in the case of $\mathcal{P}_1/\mathcal{P}_0$ boundary elements and $\mathcal{P}_1$ finite elements (left) and $\mathcal{P}_2/\mathcal{P}_1$ boundary elements and $\mathcal{P}_2$ finite elements (right).

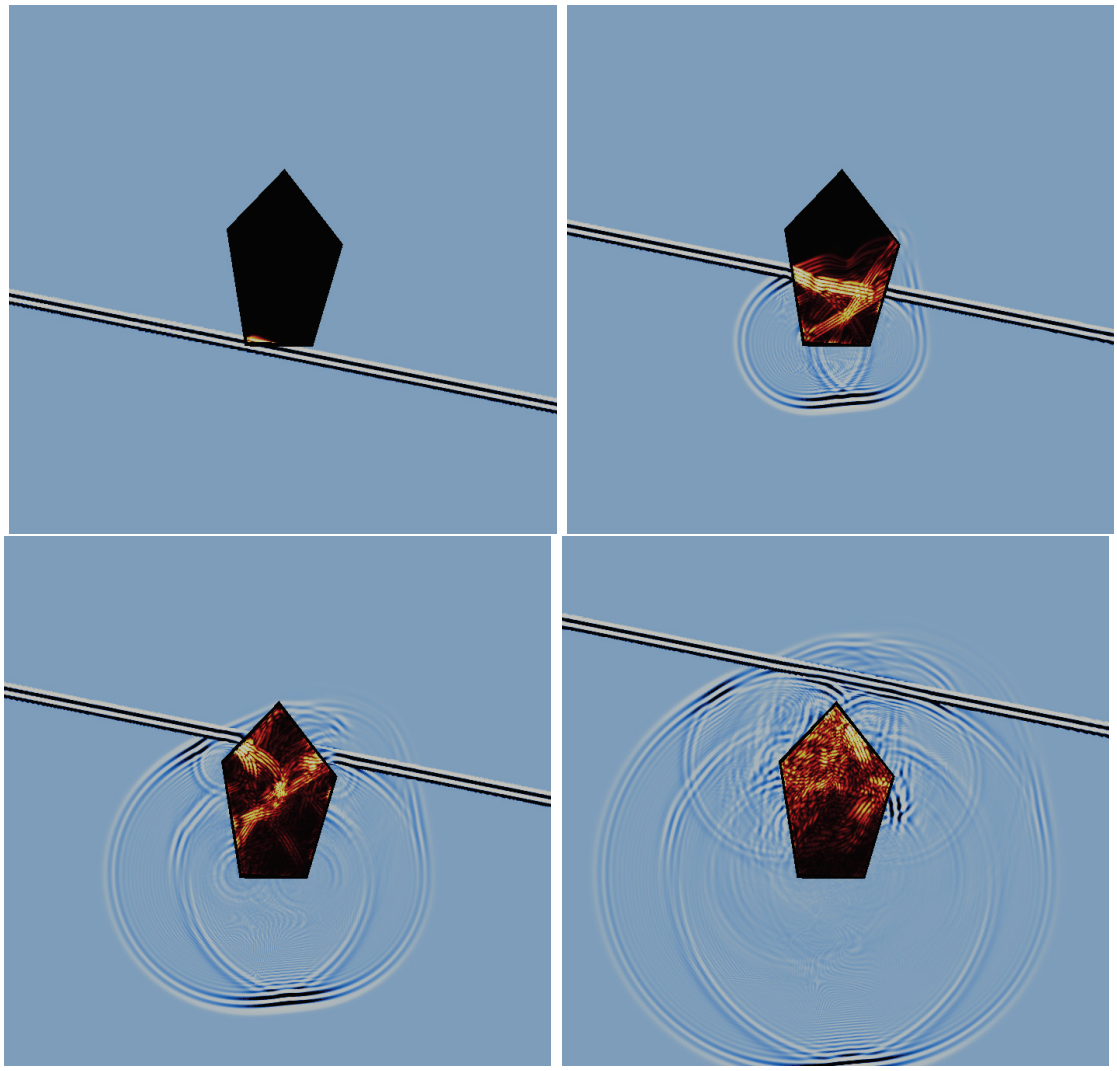

Figure 5.5: The total acoustic wave shown at times $t = 0.175, 0.7, 1.225, 1.75$.

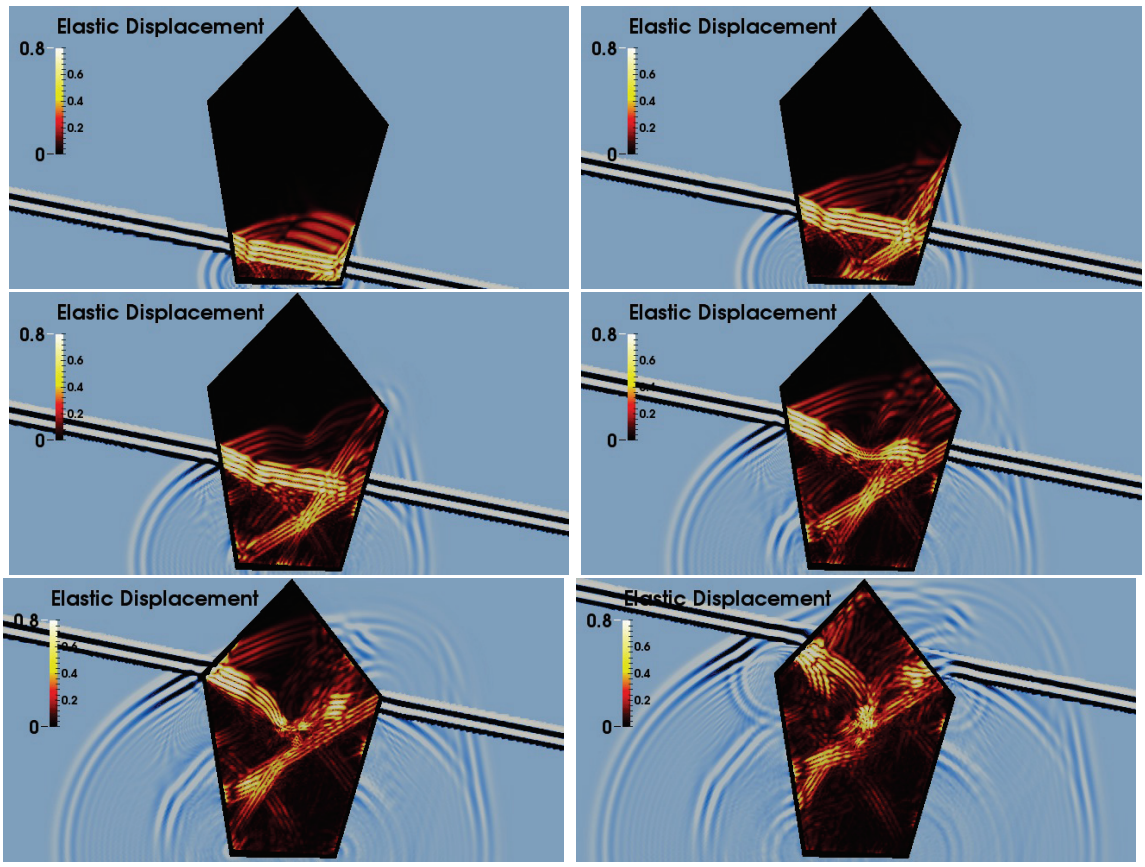

Figure 5.6: Close up of the norm of the elastic displacement at times $t = 0.35, 0.525, 0.7, 0.875, 1.05, 1.225$.

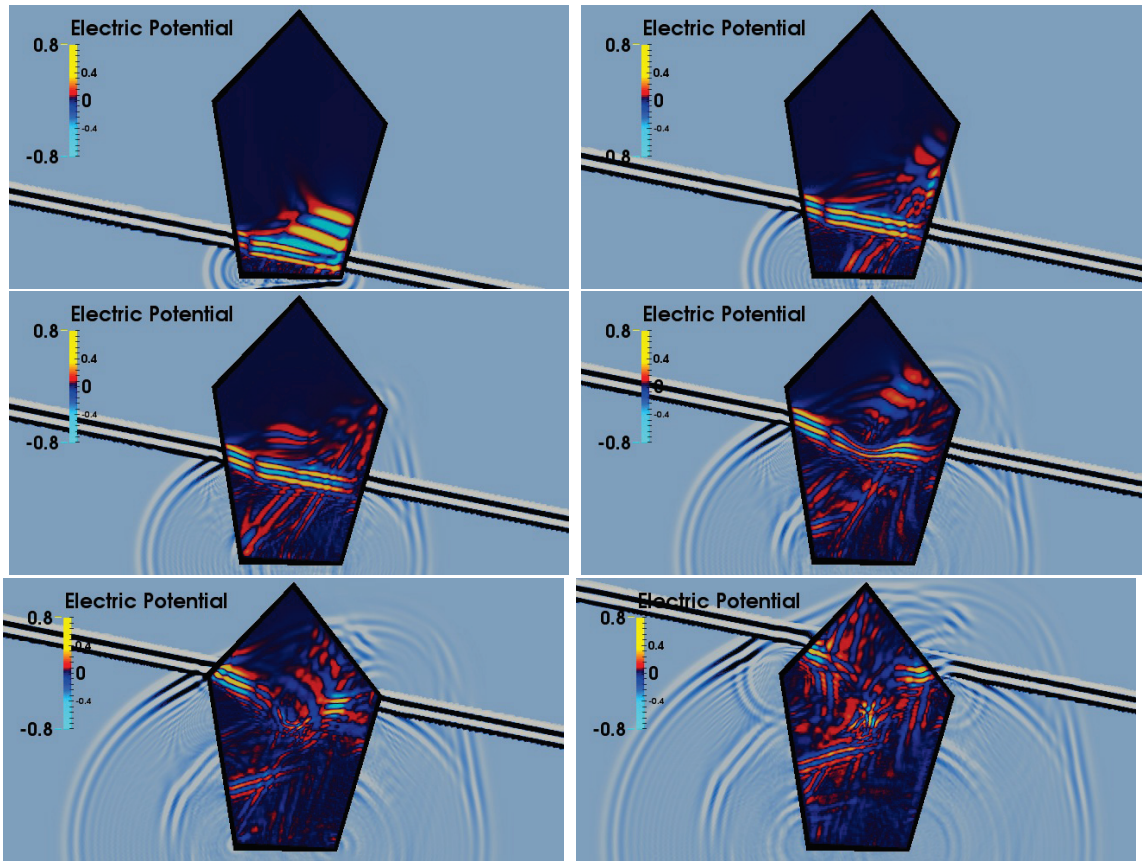

Figure 5.7: Close up of the electric potential at times $t = 0.35, 0.525, 0.7, 0.875, 1.05, 1.225$.

Chapter 6

ACOUSTIC SCATTERING BY THERMOELASTIC OBSTACLES

This chapter includes work in progress in collaboration with George Hsiao, Franciso-Javier Sayas and Richard Weinacht for the paper *A time-depended wave-thermoelastic solid interaction* [67]. The interaction of acoustic waves with elastic bodies is revisited, but this time taking into account the thermodynamics of elastic deformation. These results in the introduction of a new problem unknown, the temperature difference between the reference configuration and the deformed configuration. The resulting system of PDE's couples two hyperbolic equations with one parabolic equation describing the evolution of the thermal field.

From the physical perspective, considering the thermodynamical aspects of elastic deformation when deriving the equations of linear elasticity is a very natural thing to do. In fact, the constitutive relation connecting the elastic stress and strain with the temperature gradients induced in a deformed solid dates back to 1837 in the pioneering work of Duhamel [38] on thermoelastic materials thus predating the study of the piezoelectric effect –that wasn't discovered experimentally until 1881 by Pierre and Jacques Curie and formalized mathematically by Tiersten in 1969 (as cited in [100]).

Kupradze's encyclopedic work [76] can be considered the standard reference for a modern mathematical treatment of the purely thermoelastic problem and [62] is an up to date treatise of thermoelasticity. More recent works [105, 123] revisit the matrix of fundamental solutions for the dynamic equations of thermoelasticity or provide generalized Kirchhoff-type formulas for thermoelastic solids [72, 73] .

In the case of the scattering of thermoelastic waves, major theoretical contributions have been made by Cakoni and Dassios in works like [18] where the unique

solvability of a boundary integral formulation is established or [26] where the interaction of elastic and thermoelastic waves is explored for homogeneous materials. The study of time-harmonic interaction between a scalar field and a thermoelastic solid has been the subject of works like [86] where the interface is taken to be a plane, or [85, 74] where time-harmonic scattering by bounded obstacles is considered.

The problem is introduced in Section 6.1, along with the physical assumptions and the constitutive relation under consideration leading to the time domain system of governing equations. We then move on to Section 6.2 where we introduce the Laplace domain system and the equivalent integro-differential problem that will be formulated variationally for discretization. The closing section 6.4 shows convergence estimates for test problems in both frequency and time domains with BDF2 and Trapezoidal Rule CQ, providing evidence that the approximation is stable and of second order globally. Time domain illustrative experiments using the proposed formulation are included.

6.1 Formulation of the Problem

The problem in question is the time-dependent scattering of an acoustic wave by a thermoelastic solid, which can be simply described as follows: a given acoustic wave v^{inc} propagates in a fluid domain of infinite extent Ω_+ in which a bounded thermoelastic body, described by a Lipschitz bounded domain Ω_-, is immersed. The boundary of the solid, Γ is considered to be Lipschitz continuous and is split in two disjoint parts $\Gamma = \overline{\Gamma}_D \cup \overline{\Gamma}_N$ where thermal Dirichlet and Neumann boundary conditions are imposed.

Under the assumption of irrotational, isotropic flow of a homogeneous inviscid and compressible fluid, the velocity and pressure fields can be represented by a scalar velocity potential v. The problem is then to determine the scattered velocity potential in the fluid domain as well as the deformation of the solid $\mathbf{u}$ and the variation of the temperature in the obstacle with respect to an equilibrium temperature θ_0 which will be denoted by θ and will be assumed to be small $|\theta/\theta_0| << 1$.

Constitutive relations. Consider a thermoelastic solid in an undeformed reference configuration and at thermal equilibrium at temperature θ_0. Under the action

of external forces the body will be subject to internal stresses that will induce local variations of temperature. Reciprocally, if a heat source induces a change in temperature, the body will react by dilating or contracting and this will create internal stresses and deformations. In the classical linear theory [77, 84], the coupling between the mechanic strain and the thermic gradient is modelled by the Duhamel-Neumann law which defines the *thermoelastic stress* $\boldsymbol{\sigma}(\mathbf{u}, \theta)$ and the *thermoelastic heat flux* $\mathbf{F}(\mathbf{u}, \theta)$ (also known as free energy)

$$\boldsymbol{\sigma} := \mathbf{C}\boldsymbol{\varepsilon}(\mathbf{u}) - \boldsymbol{\zeta}\theta\,, \tag{6.1a}$$

$$\mathbf{F} := -\boldsymbol{\eta}\,\dot{\mathbf{u}} + \boldsymbol{\kappa}\nabla\theta. \tag{6.1b}$$

Here the upper dot represents differentiation with respect to time, $\mathbf{C}$ is the *elastic stiffness tensor* defined in (2.8), $\boldsymbol{\kappa}$ is the *thermal conductivity tensor*, which from physical principles [55] is required to be non-singular, symmetric and positive definite, $\boldsymbol{\zeta}$ is the *thermal expansion tensor* which is symmetric, and is related to the tensor $\boldsymbol{\eta}$ by the relation

$$\boldsymbol{\eta} = \theta_0 \boldsymbol{\kappa}^{-1} \boldsymbol{\zeta}. \tag{6.2}$$

In addition of the above physical requirements, we will assume that the components of $\boldsymbol{\kappa}$, $\boldsymbol{\zeta}$, and $\boldsymbol{\eta}$ are all functions in $L^\infty(\Omega_-)$.

The governing equations. Under the above assumptions and definitions and in the absence of external forces or heat sources, the governing equations of the interaction between the scattered acoustic wave v, the elastic displacement field $\mathbf{u}$ and

temperature field θ are

$$\rho_\Sigma \ddot{\mathbf{u}} = \nabla \cdot (\mathbf{C}\boldsymbol{\varepsilon}(\mathbf{u}) - \boldsymbol{\zeta}\theta) \qquad \text{in } \Omega_- \times (0,\infty), \tag{6.3a}$$

$$\dot{\theta} = \nabla \cdot (-\boldsymbol{\eta}\,\dot{\mathbf{u}} + \boldsymbol{\kappa}\nabla\theta) \qquad \text{in } \Omega_- \times (0,\infty), \tag{6.3b}$$

$$c^{-2}\ddot{v} = \Delta v \qquad \text{in } \Omega_+ \times (0,\infty), \tag{6.3c}$$

$$\dot{\mathbf{u}} \cdot \nu + \partial_\nu v = -\partial_\nu v^{inc} \qquad \text{on } \Gamma \times (0,\infty), \tag{6.3d}$$

$$(\mathbf{C}\boldsymbol{\varepsilon}(\mathbf{u}) - \boldsymbol{\zeta}\theta)\,\boldsymbol{\nu} + \rho_f \dot{v}\,\boldsymbol{\nu} = -\rho_f \dot{v}^{inc}\boldsymbol{\nu} \qquad \text{on } \Gamma \times (0,\infty), \tag{6.3e}$$

$$(-\boldsymbol{\eta}\,\dot{\mathbf{u}} + \boldsymbol{\kappa}\nabla\theta) \cdot \boldsymbol{\nu} = 0 \qquad \text{on } \Gamma_N \times (0,\infty), \tag{6.3f}$$

$$\theta = h \qquad \text{on } \Gamma_D \times (0,\infty), \tag{6.3g}$$

where c is the speed of sound in the fluid and ρ_f is the constant fluid density. The system is closed by requesting the causality of all the unknowns, which yields with homogeneous initial conditions for $\mathbf{u}$, $\dot{\mathbf{u}}$, v, $\dot{v}$, and θ and should be understood in the sense of time domain causal tempered distributions defined in Appendix B.

Regarding the transmission boundary conditions we remark that equation (6.3d) is the statement of the equilibrium of pressure at the solid fluid interface (the combined elastic stress, thermal stress and total acoustic pressure field add up to zero), and equation (6.3e) encodes the continuity of the velocity fields in the normal direction, so that no vacuum is created at the interface.

6.2 Continuous Problem in the Laplace Domain

From this point on we will deal exclusively with the Laplace-transformed version of (6.3) and will abuse notation by using the same symbol for the functions $\mathbf{u}$, θ, and v and their Laplace domain counterparts.

After transformation, the thermoelastic stress and heat flux are given by

$$\boldsymbol{\sigma} := \mathbf{C}\boldsymbol{\varepsilon}(\mathbf{u}) - \boldsymbol{\zeta}\theta\,, \qquad \mathbf{F} := -s\boldsymbol{\eta}\,\mathbf{u} + \boldsymbol{\kappa}\nabla\theta. \tag{6.4}$$

For $(\mathbf{u},\theta) \in \mathbf{H}^1(\Omega_-) \times H^1(\Omega_-)$ such that $(\nabla\cdot\boldsymbol{\sigma}, \nabla\cdot\mathbf{F}) \in \mathbf{L}^2(\Omega_-) \times L^2(\Omega_-)$ we can define weakly the normal components of the stress and the flux by

$$\langle \boldsymbol{\sigma}\,\boldsymbol{\nu}, \gamma\mathbf{w}\rangle_\Gamma := (\boldsymbol{\varepsilon}(\mathbf{u}), \boldsymbol{\varepsilon}(\mathbf{w}))_{\Omega_-} - (\boldsymbol{\zeta}\theta, \nabla\mathbf{w})_{\Omega_-} + (\nabla\cdot\boldsymbol{\sigma}, \mathbf{w})_{\Omega_-} \qquad \forall\,\mathbf{w} \in \mathbf{H}^1(\Omega_-), \tag{6.5a}$$

$$\langle \mathbf{F}\cdot\boldsymbol{\nu}, \gamma w\rangle_\Gamma := -(s\boldsymbol{\eta}\,\mathbf{u}, \nabla w)_{\Omega_-} + (\boldsymbol{\kappa}\nabla\theta, \nabla w)_{\Omega_-} + (\nabla\cdot\mathbf{F}, w)_{\Omega_-} \quad \forall\, w \in H^1(\Omega_-). \tag{6.5b}$$

These weak normal fluxes are elements of the dual spaces $\mathbf{H}^{-1/2}(\Gamma)$ and $H^{-1/2}(\Gamma)$ respectively. In order to deal with the boundary conditions we will define the spaces

$$\begin{aligned} H^{1/2}(\Gamma_D) &:= \{\gamma_D u : u \in H^1(\Omega_-)\}, \quad H^1_D(\Omega_-) \quad := \{u \in H^1(\Omega_-) : \gamma_D u = 0\}, \\ \widetilde{H}^{1/2}(\Gamma_N) &:= \{\gamma_N u : u \in H^1_D(\Omega_-)\}, \quad H^{-1/2}(\Gamma_N) := \Big(\widetilde{H}^{1/2}(\Gamma_N)\Big)'. \end{aligned}$$

In these definitions the traces at the Dirichlet and Neumann boundaries are the restrictions

$$\gamma_D u := \gamma u|_{\Gamma_D}, \qquad \gamma_N u := \gamma u|_{\Gamma_N},$$

and the brackets $\langle\cdot,\cdot\rangle_\Gamma$ are used to denote the duality pairing of $H^{-1/2}(\Gamma_N)$ with $\widetilde{H}^{1/2}(\Gamma_N)$.

Two equivalent systems. The Laplace domain problem that we will study is then that of, given problem data

$$(\alpha_d, \beta_d, \eta_d, \mu_d) \in H^{-1/2}(\Gamma) \times H^{1/2}(\Gamma) \times H^{-1/2}(\Gamma_N) \times H^{1/2}(\Gamma_D),$$

finding $(\mathbf{u},\theta,v) \in \mathbf{H}^1(\Omega_-) \times H^1(\Omega_-) \times H^1(\Omega_+)$ satisfying the equations

$$s^2\rho_\Sigma\mathbf{u} - \nabla\cdot(\mathbf{C}\boldsymbol{\varepsilon}(\mathbf{u}) - \boldsymbol{\zeta}\theta) = \mathbf{0} \qquad \text{in } \Omega_-, \tag{6.6a}$$

$$s\theta - \nabla\cdot(-s\boldsymbol{\eta}\,\mathbf{u} + \boldsymbol{\kappa}\nabla\theta) = 0 \qquad \text{in } \Omega_-, \tag{6.6b}$$

$$(s/c)^2 v - \Delta v = 0 \qquad \text{in } \Omega_+, \tag{6.6c}$$

$$s\gamma\mathbf{u}\cdot\boldsymbol{\nu} + \partial^+_\nu v = -\alpha_d \qquad \text{on } \Gamma, \tag{6.6d}$$

$$(\mathbf{C}\boldsymbol{\varepsilon}(\mathbf{u}) - \boldsymbol{\zeta}\theta)\,\boldsymbol{\nu} + \rho_f s\gamma^+ v\,\boldsymbol{\nu} = -\rho_f s\beta_d\boldsymbol{\nu} \qquad \text{on } \Gamma, \tag{6.6e}$$

$$(-s\boldsymbol{\eta}\,\mathbf{u} + \boldsymbol{\kappa}\nabla\theta)\cdot\boldsymbol{\nu} = \eta_d \qquad \text{on } \Gamma_N, \tag{6.6f}$$

$$\gamma\theta = \mu_d \qquad \text{on } \Gamma_D. \tag{6.6g}$$

This system can be stated in an equivalent integro differential form using the Calderón calculus for the acoustic resolvent equation. Since v satisfies the wave equation (6.6c) we can represent it in terms of a combination of double and single layer potentials

$$v = \mathrm{D}(s/c)\phi - \mathrm{S}(s/c)\lambda \tag{6.7}$$

for two unkown densities $(\lambda, \phi) \in H^{-1/2}(\Gamma) \times H^{1/2}(\Gamma)$. This representation can be extended by zero to Ω_- by requiring that $\gamma^- v = 0$. The last condition in combination with the jump identities of the layer potentials implies that $[\![\gamma v]\!] = \gamma^+ v = \phi$, therefore (6.6e) can be written in terms of ϕ yielding

$$\boldsymbol{\sigma}\,\boldsymbol{\nu} + \rho_f s\phi\,\boldsymbol{\nu} = -\rho_f s\beta_d \boldsymbol{\nu} \qquad \text{on } \Gamma.$$

Moreover, the requirement that the interior trace of the acoustic wave must vanish can be written using (2.25) in the form

$$\mathrm{V}(s/c)\lambda - (-\tfrac{1}{2}\mathrm{I} + \mathrm{K}(s/c))\phi = 0 \qquad \text{on } \Gamma.$$

In a similar fashion, the potential representation of v and the limit identities (2.25) can be combined with the boundary condition (6.6d) yielding

$$(-\tfrac{1}{2}\mathrm{I} + \mathrm{K}^t(s/c))\lambda + \mathrm{W}(s/c)\phi - s\gamma\mathbf{u}\cdot\boldsymbol{\nu} = \alpha_d \qquad \text{on } \Gamma.$$

Therefore a solution triplet $(\mathbf{u}, \theta, v)$ of the system (6.6) determines the solution

$$(\mathbf{u}, \theta, \lambda, \phi) \in \mathbf{H}^1(\Omega_-) \times H^1(\Omega_-) \times H^{-1/2}(\Gamma) \times H^{1/2}(\Gamma)$$

of the integro-differential system

$$
\begin{aligned}
s^2\rho_\Sigma \mathbf{u} - \nabla\cdot(\mathbf{C}\boldsymbol{\varepsilon}(\mathbf{u}) - \boldsymbol{\zeta}\theta) &= \mathbf{0} && \text{in } \Omega_-, && (6.8a)\\
s\theta - \nabla\cdot(-s\boldsymbol{\eta}\,\mathbf{u} + \boldsymbol{\kappa}\nabla\theta) &= 0 && \text{in } \Omega_-, && (6.8b)\\
\mathrm{V}(s/c)\lambda - (-\tfrac{1}{2}\mathrm{I} + \mathrm{K}(s/c))\phi &= 0 && \text{on } \Gamma, && (6.8c)\\
(-\tfrac{1}{2}\mathrm{I} + \mathrm{K}^t(s/c))\lambda + \mathrm{W}(s/c)\phi - s\gamma\mathbf{u}\cdot\boldsymbol{\nu} &= \alpha_d && \text{on } \Gamma, && (6.8d)\\
(\mathbf{C}\boldsymbol{\varepsilon}(\mathbf{u}) - \boldsymbol{\zeta}\theta)\,\boldsymbol{\nu} + \rho_f s\gamma^+ v\,\boldsymbol{\nu} &= -\rho_f s\beta_d\boldsymbol{\nu} && \text{on } \Gamma, && (6.8e)\\
(-s\boldsymbol{\eta}\,\mathbf{u} + \boldsymbol{\kappa}\nabla\theta)\cdot\boldsymbol{\nu} &= \eta_d && \text{on } \Gamma_N, && (6.8f)\\
\gamma\theta &= \mu_d && \text{on } \Gamma_D. && (6.8g)
\end{aligned}
$$

Reciprocally, given a solution $(\mathbf{u}, \theta, \lambda, \phi)$ to the above system (6.8), we can define v using the integral representation (6.7) and use the properies of the layer potentials and their limit identities (2.25) to show that with this definition the triplet $(\mathbf{u}, \theta, v)$ satisfies the PDE system (6.6).

A variational formulation. The integral operators appearing on equations (6.8c) and (6.8d) can be expressed succintly in matrix form by defining

$$
\mathbb{D}(s) := \begin{bmatrix} \mathrm{V}(s) & +\tfrac{1}{2}\mathrm{I} - \mathrm{K}(s) \\ -\tfrac{1}{2}\mathrm{I} + \mathrm{K}^t(s/c) & \mathrm{W}(s) \end{bmatrix} : H^{-1/2}(\Gamma)\times H^{1/2}(\Gamma) \to H^{1/2}(\Gamma)\times H^{-1/2}(\Gamma). \tag{6.9}
$$

The action $\mathbb{D}(s)(\lambda,\phi)$ should be understood as the action of $\mathbb{D}(s)$ on the column vector $(\lambda,\phi)^t$. The integro-differential system (6.8) can be formulated variationally through Galerkin testing. In order to do that we define the thermoelastic bilinear form

$$
\begin{aligned}
\mathrm{B}\left((\mathbf{u},\theta),(\mathbf{w},w);s\right) := {} & s^2(\rho_\Sigma\mathbf{u},\mathbf{w})_{\Omega_-} + (\mathbf{C}\boldsymbol{\varepsilon}(\mathbf{u}),\boldsymbol{\varepsilon}(\mathbf{w}))_{\Omega_-} \\
& + s(\theta,w)_{\Omega_-} + (\boldsymbol{\kappa}\nabla\theta,\nabla w)_{\Omega_-} \\
& - s(\boldsymbol{\eta}\mathbf{u},\nabla w)_{\Omega_-} - (\boldsymbol{\zeta}\theta,\boldsymbol{\varepsilon}(\mathbf{w}))_{\Omega_-},
\end{aligned} \tag{6.10}
$$

which is easily shown to be bounded in $\mathbf{H}^1(\Omega_-)\times H^1(\Omega_-)$. The system (6.8) is equivalent to the variational problem of, given data

$$
(\alpha_d,\beta_d,\eta_d,\mu_d) \in H^{-1/2}(\Gamma)\times H^{1/2}(\Gamma)\times H^{-1/2}(\Gamma_N)\times H^{1/2}(\Gamma_D),
$$

finding

$$(\mathbf{u}, \theta, \lambda, \phi) \in \mathbf{H}^1(\Omega_-) \times H^1(\Omega_-) \times H^{-1/2}(\Gamma) \times H^{1/2}(\Gamma)$$

such that the following are satisfied

$$\gamma\theta = \mu_d \qquad \text{on } \Gamma_D, \tag{6.11a}$$

$$\mathrm{B}\left((\mathbf{u}, \theta), (\mathbf{w}, w); s\right) + s\rho_f \langle \gamma\mathbf{w} \cdot \boldsymbol{\nu}, \phi \rangle_\Gamma = -s\rho_f \langle \gamma\mathbf{w} \cdot \boldsymbol{\nu}, \beta_d \rangle_\Gamma + \langle \eta_d, \gamma w \rangle_{\Gamma_N}, \tag{6.11b}$$

$$-s\langle \gamma\mathbf{u} \cdot \boldsymbol{\nu}, \chi \rangle_\Gamma + \langle \mathbb{D}(s/c)(\lambda, \phi), (\xi, \chi) \rangle_\Gamma = \langle \alpha_d, \chi \rangle_\Gamma, \tag{6.11c}$$

for every $(\mathbf{w}, w, \xi, \chi) \in \mathbf{H}^1(\Omega_-) \times H^1(\Omega_-) \times H^{-1/2}(\Gamma) \times H^{1/2}(\Gamma)$.

6.3 Laplace Domain Semidiscretization

We now proceed to discretize the variational formulation (6.11). In order to do so, we will consider the finite dimensional subspaces

$$\mathbf{V}_h \subseteq \mathbf{H}^1(\Omega_-), \quad V_h \subseteq H^1(\Omega_-), \quad V_{h,D} := V_h \cap H^1_D(\Omega_-),$$
$$X_h \subseteq H^{-1/2}(\Gamma), \quad Y_h \subseteq H^{1/2}(\Gamma).$$

Following the analysis from Chapter 5, we will further assume that the space of elastic rigid motions

$$\mathbf{M} := \left\{ \mathbf{m} \in \mathbf{H}^1(\Omega_-) : \boldsymbol{\varepsilon}(\mathbf{m}) = \mathbf{0} \quad \forall \mathbf{w} \in \mathbf{H}^1(\Omega_-) \right\}$$

is contained in the finite element space $\mathbf{V}_h$. Finally, to approximate the Dirichlet boundary condition for θ in the discrete case we will use the discrete space of traces

$$\gamma_D V_h := \{ \gamma_D v^h : v^h \in V_h \}.$$

The discrete version of (6.11) reads: given data

$$(\alpha_d, \beta_d, \eta_d, \mu_d^h) \in H^{-1/2}(\Gamma) \times H^{1/2}(\Gamma) \times H^{-1/2}(\Gamma_N) \times \gamma_D V_h,$$

find

$$(\mathbf{u}^h, \theta^h, \lambda^h, \phi^h) \in \mathbf{V}_h \times V_h \times X_h \times Y_h$$

such that the following are satisfied

$$\gamma\theta^h = \mu_d^h \qquad \text{on } \Gamma_D, \tag{6.12a}$$

$$\mathrm{B}\left((\mathbf{u}^h,\theta^h),(\mathbf{w},w);s\right)+s\rho_f\langle\gamma\mathbf{w}\cdot\boldsymbol{\nu},\phi^h\rangle_\Gamma=\langle\eta_d,\gamma w\rangle_{\Gamma_N}-s\rho_f\langle\gamma\mathbf{w}\cdot\boldsymbol{\nu},\beta_d\rangle_\Gamma, \tag{6.12b}$$

$$-s\langle\gamma\mathbf{u}^h\cdot\boldsymbol{\nu},\chi\rangle_\Gamma+\langle\mathbb{D}(s/c)(\lambda^h,\phi^h),(\xi,\chi)\rangle_\Gamma=\langle\alpha_d,\chi\rangle_\Gamma, \tag{6.12c}$$

for every $(\mathbf{w},w,\xi,\chi)\in\mathbf{V}_h\times V_{h,D}\times X_h\times Y_h$.

Remark. The study of the well-posedness of (6.8) (or equivalently (6.11)) and the discrete problem (6.12) are the aim of current work. At this time some preliminary results for the case when $\boldsymbol{\zeta}$ and $\boldsymbol{\eta}$ are constant diagonal matrices have been proven [67].

6.4 Numerical Experiments

Computational considerations. In order to test numerically the formulations of the previous section, convergence studies were performed in both frequency and time domains. The interior domain Ω_- where the thermoelastic equations were imposed was the general polygon depicted in Figure 6.1. The domain was generated and meshed using Matlab's pdetool and the refinements were done using the refinement capabilities of the pde toolbox.

The linear system arising from the discretization has a very similar structure to that from the Chapter 5 and can be depicted by the block matrix

$$\begin{bmatrix} \mathbf{FEM}(s) & s\rho_f(\mathrm{N}\Gamma)_h^t \\ -s(\mathrm{N}\Gamma)_h & \mathbf{BEM}(s) \end{bmatrix} \begin{bmatrix} \begin{bmatrix} \mathbf{u}^h \\ \theta^h \end{bmatrix} \\ \begin{bmatrix} \lambda^h \\ \phi^h \end{bmatrix} \end{bmatrix} = \begin{bmatrix} \begin{bmatrix} -s\rho_f\Gamma_h^t\beta^h \\ \eta^h \end{bmatrix} \\ \begin{bmatrix} 0 \\ \alpha^h \end{bmatrix} \end{bmatrix}.$$

The main difference is that the sparse Finite Element block

$$\begin{aligned}\mathbf{FEM}(s) := \; & s^2\begin{bmatrix} (\rho_\Sigma\mathbf{u}_j,\boldsymbol{\varphi}_i)_{\Omega_-} & 0 \\ 0 & 0 \end{bmatrix} + s\begin{bmatrix} 0 & 0 \\ -(\boldsymbol{\eta}\mathbf{u}_j,\nabla\varphi_i)_{\Omega_-} & (\theta_j,\varphi_i)_{\Omega_-} \end{bmatrix} \\ & + \begin{bmatrix} (\mathbf{C}\boldsymbol{\varepsilon}(\mathbf{u}_j),\boldsymbol{\varepsilon}(\boldsymbol{\varphi}_i))_{\Omega_-} & -(\boldsymbol{\zeta}\theta_j,\boldsymbol{\varepsilon}(\boldsymbol{\varphi}_i))_{\Omega_-} \\ 0 & (\boldsymbol{\kappa}\nabla\theta_j,\nabla\varphi_i)_{\Omega_-} \end{bmatrix}\end{aligned}$$

now contains first order terms in both space and time. The boundary element block $\mathbf{BEM}(s)$ contains the Galerkin discretization of the operators of the acoustic Calderón calculus and the coupling trace matrix $(\mathrm{N}\Gamma)_h$ is the discretization of the bilinear form arising from the duality pairing $\langle \mathbf{u}^h \cdot \boldsymbol{\nu}, \chi^h \rangle_\Gamma$.

Physical parameters. The following values of the physical parameters are functions only of space and were used equally for both series of experiments, they are chosen for validation and expository purposes only and do not correspond with any relevant physical material. For the entries of the tensors we make use of the symmetries and of Voigt's notation to shorten the subscripts.

1. Density of the elastic solid and Lamé parameters

$$\rho_\Sigma = 5 + \sin(x)\sin(y), \qquad \lambda = 2, \qquad \mu = 3. \tag{6.13}$$

2. The entries of the elastic stiffness tensor can be written compactly in terms of Young's modulus E and Poisson's ratio ν

$$E := \frac{2\mu(1+\lambda)}{2\mu+\lambda}, \qquad \nu := \frac{\lambda}{2\mu+\lambda}. \tag{6.14}$$

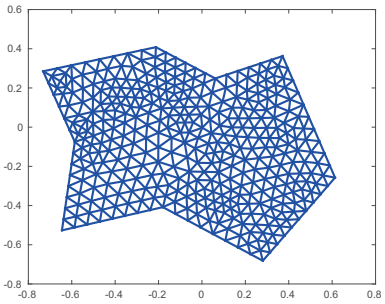

Figure 6.1: Interior geometry used in the numerical experiments for both frequency and time domain studies. The domain was generated and meshed using Matlab's pdetool and refined uniformly using pde tool's refinement capabilities.

3. Elastic stiffness tensor $\mathbf{C}$:

$$\begin{aligned}
\mathbf{C}_1 &\leftrightarrow \mathbf{C}_{1111} = \frac{E}{1-\nu^2},\\
\mathbf{C}_2 &\leftrightarrow \mathbf{C}_{2222} = \frac{E}{1-\nu^2},\\
\mathbf{C}_3 &\leftrightarrow \mathbf{C}_{1212} = \mathbf{C}_{2121} = \frac{E}{1-\nu^2},\\
\mathbf{C}_4 &\leftrightarrow \mathbf{C}_{2212} = \mathbf{C}_{2221} = \mathbf{C}_{1222} = \mathbf{C}_{2122} = \frac{E\nu}{1-\nu^2},\\
\mathbf{C}_5 &\leftrightarrow \mathbf{C}_{1112} = \mathbf{C}_{1121} = \mathbf{C}_{1211} = \mathbf{C}_{2111} = 0,\\
\mathbf{C}_6 &\leftrightarrow \mathbf{C}_{1122} = \mathbf{C}_{2211} = 0.
\end{aligned} \tag{6.15}$$

4. Thermal expansion tensor $\boldsymbol{\zeta}$:

$$\boldsymbol{\zeta}_1 \leftrightarrow \boldsymbol{\zeta}_{11} = \sin(x) + \cos(y), \quad \boldsymbol{\zeta}_2 \leftrightarrow \boldsymbol{\zeta}_{22} = -\sin(y), \quad \boldsymbol{\zeta}_3 \leftrightarrow \boldsymbol{\zeta}_{12} = \boldsymbol{\zeta}_{21} = \cos(x). \tag{6.16}$$

5. Thermal diffusivity tensor $\boldsymbol{\kappa}$:

$$\boldsymbol{\kappa}_1 \leftrightarrow \boldsymbol{\kappa}_{11} = 10 + x^2, \quad \boldsymbol{\kappa}_2 \leftrightarrow \boldsymbol{\kappa}_{22} = 10 + y, \quad \boldsymbol{\kappa}_3 \leftrightarrow \boldsymbol{\kappa}_{12} = \boldsymbol{\kappa}_{21} = 0. \tag{6.17}$$

6. The reference temperature was chosen to be $\theta_0 = 1$ and the tensor $\boldsymbol{\eta}$ was determined through the relation (6.2).

Convergence studies in the frequency domain. We first verify the results in the frequency domain. We proceed by the method of manufactured solutions using the functions

$$\mathbf{u} := (x^3 + xy + y^3, \sin(x)\cos(y)), \qquad \theta := \sin^2(\pi x)\sin^2(y), \tag{6.18a}$$

$$v := \tfrac{i}{4} H_0^{(1)}(isr), \qquad r = \sqrt{x^2 + y^2}, \tag{6.18b}$$

together with the parameters defined in (6.13) through (6.17). Right-hand side load vectors were constructed accordingly and boundary conditions were sampled using (6.6c) through (6.6g) so that (6.18) solve the system (6.5) with the manufactured right-hand sides.

$k=1$			$L^2(\Omega_-)$				$H^1(\Omega_-)$			
h	E_h^v	e.c.r.	$E_h^{\mathbf{u}}$	e.c.r.	$E_{h,\kappa}^{\theta}$	e.c.r.	$E_h^{\mathbf{u}}$	e.c.r.	E_h^{θ}	e.c.r.
1 E-1	1.787 E-2	—	3.999 E-2	—	2.015 E-3	—	2.011 E-1	—	7.430 E-2	—
5.016 E-2	7.292 E-3	1.293	1.675 E-2	1.255	6.397 E-4	1.656	8.733 E-2	1.203	3.746 E-2	0.988
2.508 E-2	2.272 E-3	1.683	5.344 E-3	1.648	1.837 E-4	1.799	3.297 E-2	1.405	1.876 E-2	0.976
1.254 E-2	6.099 E-4	1.897	1.447 E-3	1.885	4.824 E-5	1.929	1.314 E-2	1.327	9.383 E-3	0.996
6.27 E-3	1.556 E-4	1.971	3.703 E-4	1.966	1.223 E-4	1.980	5.961 E-3	1.141	4.692 E-3	1.000

Table 6.1: The experiments were ran using $\mathcal{P}_k$ Lagrangian finite elements and $\mathcal{P}_k/\mathcal{P}_{k-1}$ boundary elements. This table shows the relative errors and estimated convergence rates in the frequency domain for $k=1$. The maximum length of the panels used to discretize the boundary is denoted by h.

$k=2$			$L^2(\Omega_-)$				$H^1(\Omega_-)$			
h	E_h^v	e.c.r.	$E_h^{\mathbf{u}}$	e.c.r.	$E_{h,\kappa}^{\theta}$	e.c.r.	$E_h^{\mathbf{u}}$	e.c.r.	E_h^{θ}	e.c.r.
1 E-1	7.926 E-5	—	1.284 E-4	—	9.742 E-5	—	3.514 E-3	—	6.446 E-3	—
5.016 E-2	6.676 E-6	3.570	1.181 E-5	3.442	1.214 E-5	3.004	8.708 E-4	2.013	1.630 E-3	1.983
2.508 E-2	5.590 E-7	3.578	1.207 E-6	3.290	1.517 E-6	3.000	2.172 E-4	2.003	4.093 E-4	1.993
1.254 E-2	4.630 E-8	3.594	1.331 E-7	3.181	1.897 E-7	2.999	5.426 E-5	2.001	5.426 E-5	1.997
6.27 E-3	3.793 E-9	3.609	1.550 E-8	3.103	2.373 E-8	2.999	1.356 E-8	2.001	2.566 E-5	1.999

Table 6.2: The experiments were ran using $\mathcal{P}_k$ Lagrangian finite elements and $\mathcal{P}_k/\mathcal{P}_{k-1}$ boundary elements. This table shows the relative errors and estimated convergence rates in the frequency domain for $k=2$. The maximum length of the panels used to discretize the boundary is denoted by h.

Lagrangian $\mathcal{P}_k$ finite elements were used for the elastic and thermal unknowns, while Galerkin $\mathcal{P}_k/\mathcal{P}_{k-1}$ continuous/discontinuous Boundary Elements were used for the acoustic potential v. Tables 6.1 to 6.3 and Figure 6.2 show the results of the time harmonic experiment with $s = 2.8i$ and succesive refinements of the grid shown in Figure 6.1 for polynomial degrees $k = 1, 2$, and 3.

Convergence studies in the time domain. In a way analogous to the previous section, the numerical experiments were carried out using the physical parameters and coefficients given in (6.13) through (6.17) and with manufactured solutions using the functions

$$\mathbf{u} := \mathrm{T}(t)(x^3 + xy + y^3, \sin(x)\cos(y)), \qquad \theta := \mathrm{T}(t)\sin^2(\pi x)\sin^2(y), \tag{6.19a}$$

$$v := \mathcal{L}^{-1}\left\{ iH_0^{(1)}(isr)\,\mathcal{L}\{\mathcal{H}(t)\sin(3t)\}\right\}, \qquad r := \sqrt{x^2+y^2}, \tag{6.19b}$$

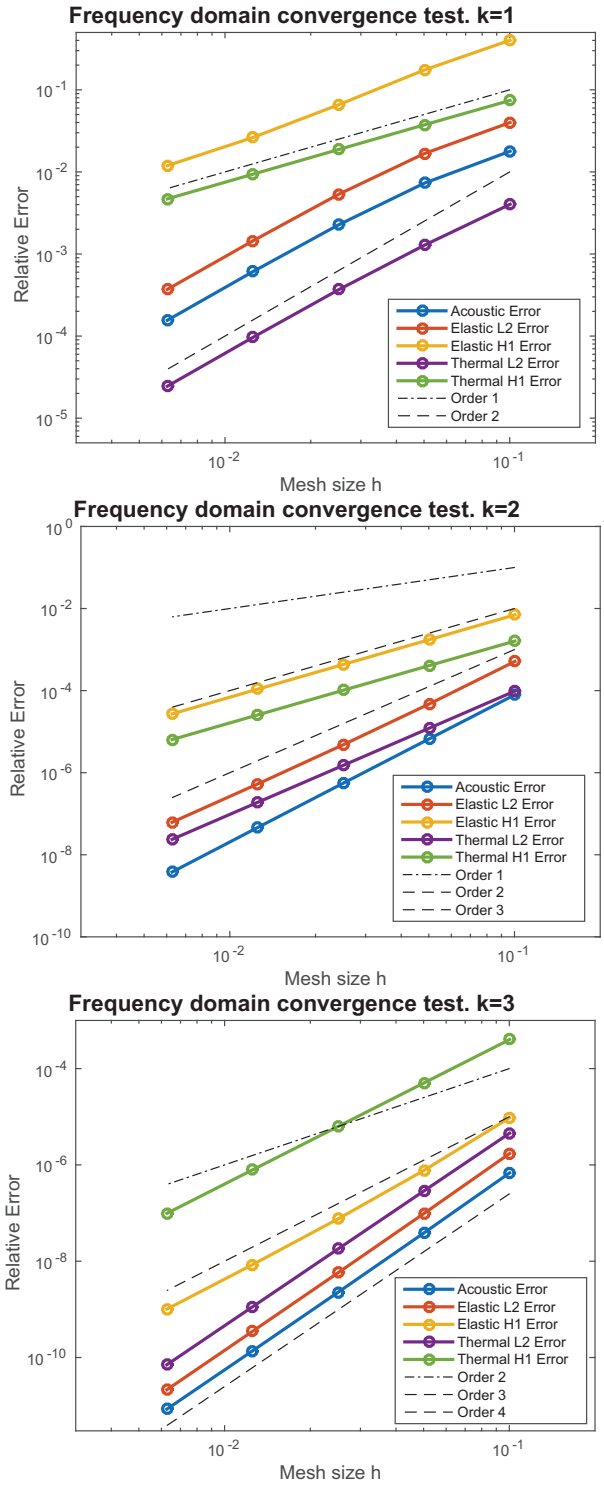

Figure 6.2: Convergence studies in the frequency domain for polynomial degrees $k = 1, 2$, and 3. The mesh was refined uniformly on every succesive iteration.

,

$k=3$			$L^2(\Omega_-)$				$H^1(\Omega_-)$			
h	E_h^v	e.c.r.	$E_h^{\mathbf{u}}$	e.c.r.	$E_{h,\kappa}^{\theta}$	e.c.r.	$E_h^{\mathbf{u}}$	e.c.r.	E_h^{θ}	e.c.r.
1 E-1	6.847 E-7	—	1.726 E-6	—	4.564 E-6	—	9.540 E-6	—	4.018 E-4	—
5.016 E-2	3.869 E-8	4.145	9.804 E-8	4.138	2.886 E-7	3.983	7.701 E-7	3.631	5.044 E-5	2.994
2.508 E-2	2.279 E-9	4.085	5.794 E-9	4.081	1.810 E-8	3.995	7.600 E-8	3.341	6.312 E-6	2.998
1.254 E-2	1.375 E-10	4.051	3.502 E-10	4.048	1.132 E-9	3.999	8.504 E-9	3.160	7.892 E-7	3.000
6.27 E-3	8.468 E-12	4.021	2.141 E-11	4.032	7.076 E-11	4.000	1.011 E-9	3.072	9.866 E-8	3.000

Table 6.3: The experiments were ran using $\mathcal{P}_k$ Lagrangian finite elements and $\mathcal{P}_k/\mathcal{P}_{k-1}$ boundary elements. This table shows the relative errors and estimated convergence rates in the frequency domain for $k=3$. The maximum length of the panels used to discretize the boundary is denoted by h.

where $\mathcal{L}\{\cdot\}$ is the Laplace transform, the time factor $\mathrm{T}(t)$ is given by

$$\mathrm{T} := \mathcal{H}(t)(t^2+2t), \tag{6.19c}$$

and $\mathcal{H}(t)$ is the $\mathcal{C}^5$ approximation to Heaviside's step function (4.54)

The experiments were carried out using the same geometry as in the frequency domain with a fixed spatial mesh, namely the second level of refinement used for the frequency domain experiments. Starting with 40 time steps for time discretization and polynomial degree $k=1$ for space discretization, the number of time steps was doubled and the polynomial degree increased by one in every succesive refinement. The $L^2(\Omega_-)$ and $H^1(\Omega_-)$ errors were measured for a final time $t=1.5$.

The performance of BDF2 and Trapezoidal Rule Convolution Quadrature was compared, Table 6.4 shows the error and estimated convergence rates for BDF2 based time stepping, while Table 6.5 shows the results of the experiment using Trapezoidal Rule. The convergence graphs of the experiments is shown in Figure 6.3.

Examples. We now present a couple of illustrative examples simulation the interaction of an incident acoustic wave with thermoelastic obstacles. The first example shows the interaction between the plane wave

$$v^{inc} = 3\chi_{[0,0.3]}(88\tau)\sin(88\tau), \quad \tau := t - \mathbf{r}\cdot\mathbf{d}, \quad \mathbf{r} := (x,y), \quad \mathbf{d} := (1,5)/\sqrt{26},$$

and a pentagonal scatterer with mass density given by $\rho_\Sigma = 15 + 40e^{-49\,r^2}$ where $r := \sqrt{x^2+y^2}$.

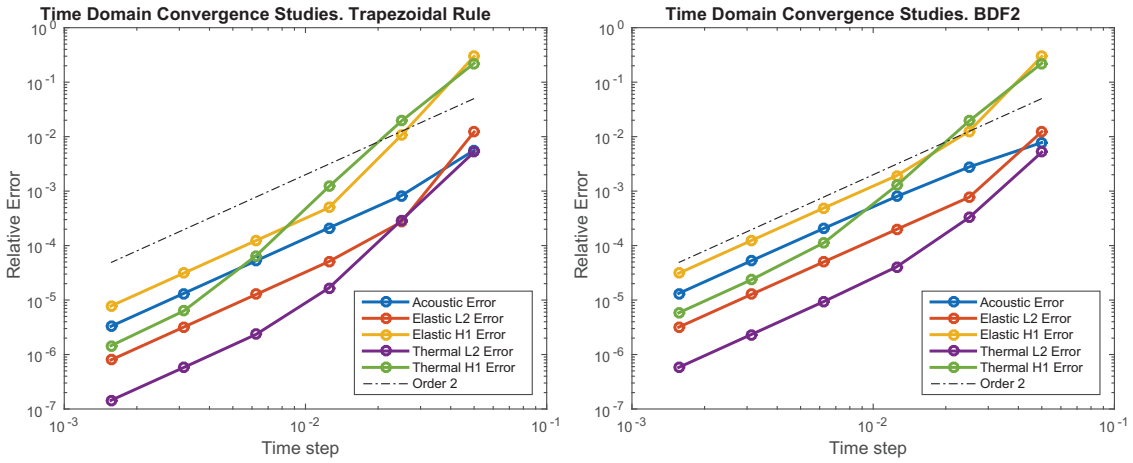

Figure 6.3: Time domain convergence studies for Trapezoidal Rule (Left) and BDF2 (Right) based convolution quadrature. In every refinement the number of time steps was boubled and the polynomial degree of the spatial discretization increased by one.

BDF2			$L^2(\Omega_-)$				$H^1(\Omega_-)$			
κ/Ndof	E_h^v	e.c.r.	$E_h^{\mathbf{u}}$	e.c.r.	$E_{h,\kappa}^{\theta}$	e.c.r.	$E_h^{\mathbf{u}}$	e.c.r.	E_h^{θ}	e.c.r.
3.75 E-2 / 108	7.793 E-3	—	1.231 E-2	—	5.184 E-3	—	2.975 E-1	—	2.222 E-1	—
1.875 E-2 / 394	2.775 E-3	1.489	7.725 E-4	3.994	3.275 E-4	3.984	1.258 E-2	4.563	1.940 E-2	3.518
9.375 E-3 / 859	7.955 E-4	1.803	1.980 E-4	1.964	4.061 E-5	3.012	1.916 E-3	2.715	1.265 E-3	3.938
4.687 E-3 / 1503	2.072 E-4	1.941	5.035 E-5	1.975	9.408 E-6	2.110	4.905 E-4	1.966	1.125 E-4	3.489
2.344 E-3 / 2326	5.258 E-5	1.978	1.267 E-5	1.991	2.329 E-6	2.014	1.236 E-4	1.988	2.355 E-5	2.259
1.172 E-3 / 3328	1.323 E-5	1.991	3.175 E-6	1.996	5.795 E-7	2.007	3.100 E-5	1.995	5.825 E-6	2.015

Table 6.4: Time domain convergence results for BDF2-based CQ. The experiments were ran with a fixed mesh using $\mathcal{P}_k$ Lagrangian finite elements and $\mathcal{P}_k/\mathcal{P}_{k-1}$ boundary elements. In every successive refinement level the size of the time step was halved and the polynomial degree of the space refinement increased by one. The table shows the relative errors and estimated convergence rates measured for a final time $t = 1.5$.

Trapezoidal Rule			$L^2(\Omega_-)$				$H^1(\Omega_-)$			
κ/Ndof	E_h^v	e.c.r.	$E_h^{\mathbf{u}}$	e.c.r.	$E_{h,\kappa}^{\theta}$	e.c.r.	$E_h^{\mathbf{u}}$	e.c.r.	E_h^{θ}	e.c.r.
3.75 E-2 / 108	5.620 E-3	—	1.218 E-2	—	5.213 E-3	—	2.976 E-1	—	2.221 E-1	—
1.875 E-2 / 394	8.283 E-4	2.762	2.713 E-4	5.489	2.934 E-4	4.151	1.064 E-2	4.805	1.934 E-2	3.522
9.375 E-3 / 859	2.107 E-4	1.975	5.085 E-5	2.416	1.660 E-5	4.144	4.958 E-4	4.424	1.209 E-3	4.000
4.687 E-3 / 1503	5.278 E-5	1.997	1.272 E-5	1.999	2.349 E-6	2.821	1.242 E-4	1.997	6.549 E-5	4.206
2.344 E-3 / 2326	1.320 E-5	1.996	3.184 E-6	1.999	5.770 E-7	2.026	3.107 E-5	1.999	6.286 E-6	3.381
1.172 E-3 / 3328	3.300 E-6	2.000	7.956 E-7	2.000	1.442 E-7	2.001	7.770 E-6	2.000	1.451 E-6	2.115

Table 6.5: Time domain convergence results for Trapezoidal Rule-based CQ. The experiments were ran with a fixed mesh using $\mathcal{P}_k$ Lagrangian finite elements and $\mathcal{P}_k/\mathcal{P}_{k-1}$ boundary elements. In every successive refinement level the size of the time step was halved and the polynomial degree of the space refinement increased by one. The table shows the relative errors and estimated convergence rates measured for a final time $t = 1.5$.

The values of the stiffness $\mathbf{C}$, thermic diffusivity $\boldsymbol{\kappa}$, thermoelastic expansion tensors $\boldsymbol{\zeta}$ and $\boldsymbol{\eta}$ were the same as those used for the convergence experiments in the previous paragraphs and given in equations (6.14)-(6.17). The simulation used $\mathcal{P}_2$ Lagrangian finite elements on a grid with mesh parameter $h = 7 \times 10^{-3}$ and 36096 elements. The inherited boundary element grid had 496 panels and a grid parameter of $h = 9.1 \times 10^{-3}$, and $\mathcal{P}_2/\mathcal{P}_1$ continuous/discontinuous Galerkin boundary elements were used. Trapezoidal rule-based discretization was applied in time with a relatively coarse time step $\kappa = 1 \times 10^{-2}$. Some snapshots of the simulation are shown in Figures 6.4-6.6.

The second example is a trapping geometry with density $\rho_\Sigma = 20 + |x| + |y|$ and physical parameters given by (6.14)-(6.17). For this example $\mathcal{P}_5$ Lagrangian elements were used on a grid with 2992 elements and mesh parameter $h = 1.72 \times 10^{-2}$, the acoustic equations were discretized with $\mathcal{P}_5/\mathcal{P}_4$ continuous/discontinuous Galerkin boundary elements on a mesh with 236 panels and mesh parameter $h = 2.5 \times 10^{-2}$. For time discretization trapezoidal rule-bvased CQ was used with a time step size of $\kappa = 2 \times \times 10^{-3}$. Figures 6.7-6.9 show snapshots of the acoustic, elastic and temperature fields.

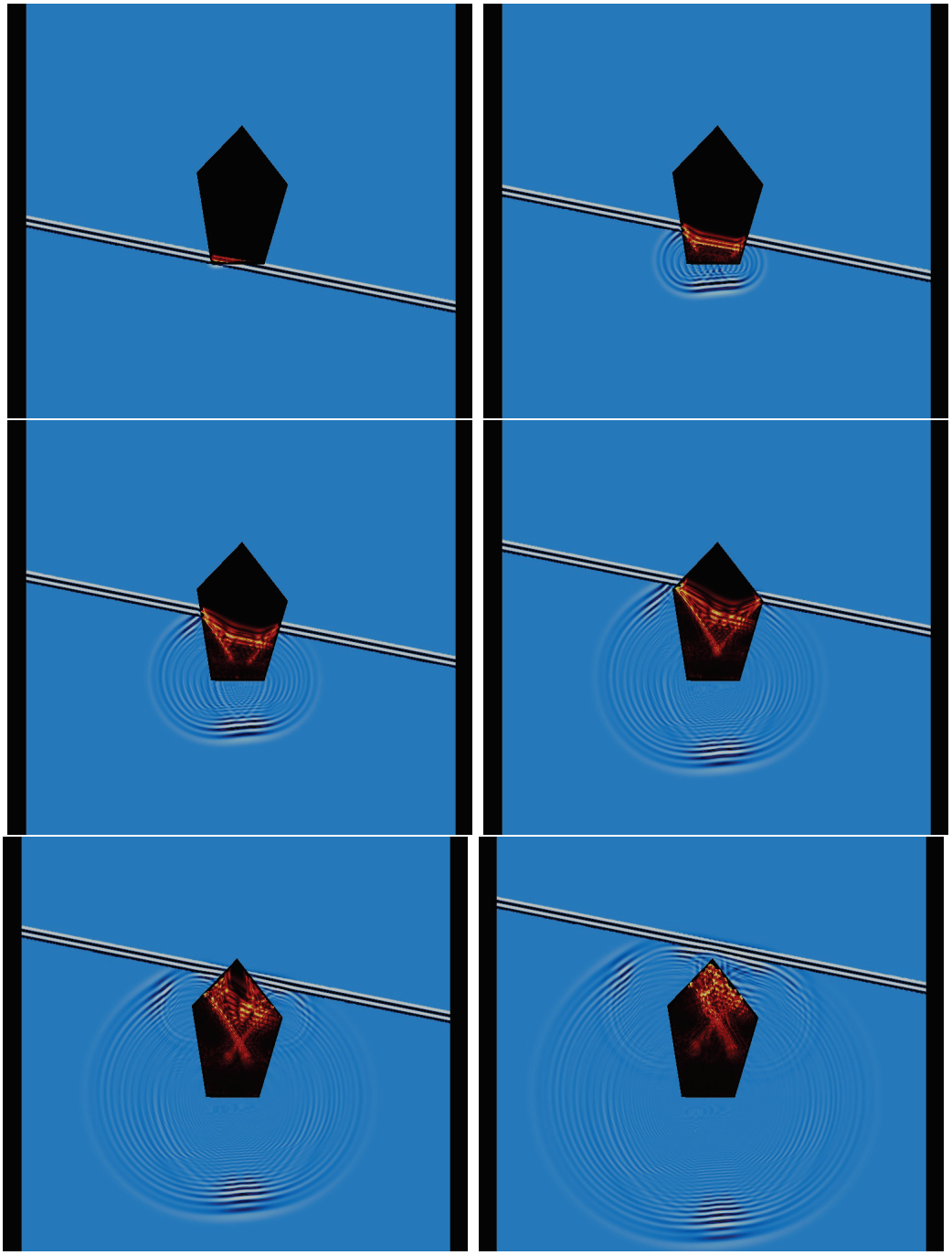

Figure 6.4: Snapshots of the total acoustic field at times $t = 0.25, 0.6, 0.95, 1.3, 1.65, 2$. The interior domain shows the norm of the elastic displacement.

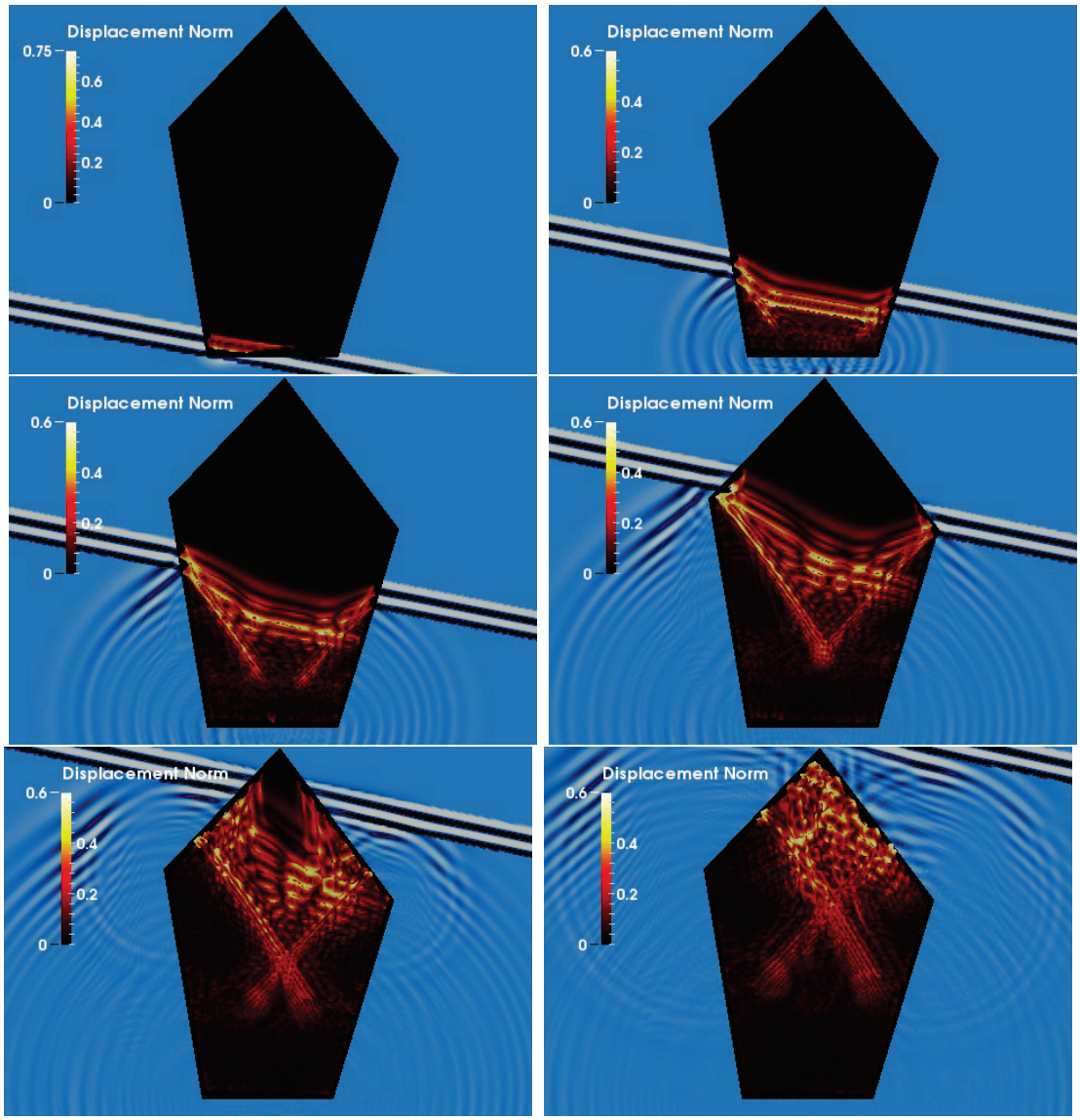

Figure 6.5: Close up of the norm of the elastic displacement for times $t = 0.25, 0.6, 0.95, 1.3, 1.65, 2$. Black represents no displacement.

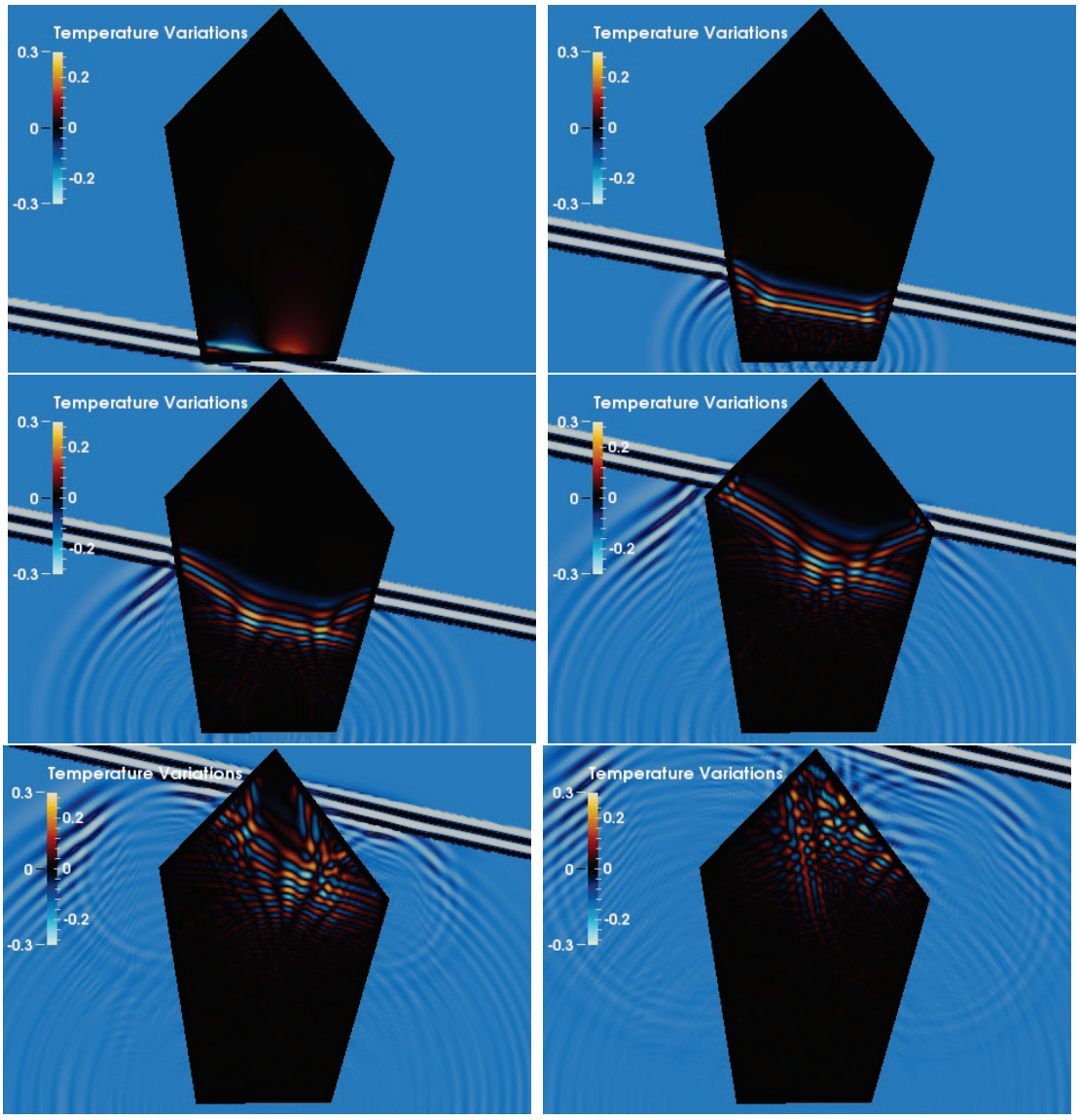

Figure 6.6: Close up of the norm of the temperature variations with respect to the reference configuration for times $t = 0.25, 0.6, 0.95, 1.3, 1.65, 2$. Black represents zero, whereas shades of red and blue represent positive and negative variations respectively.

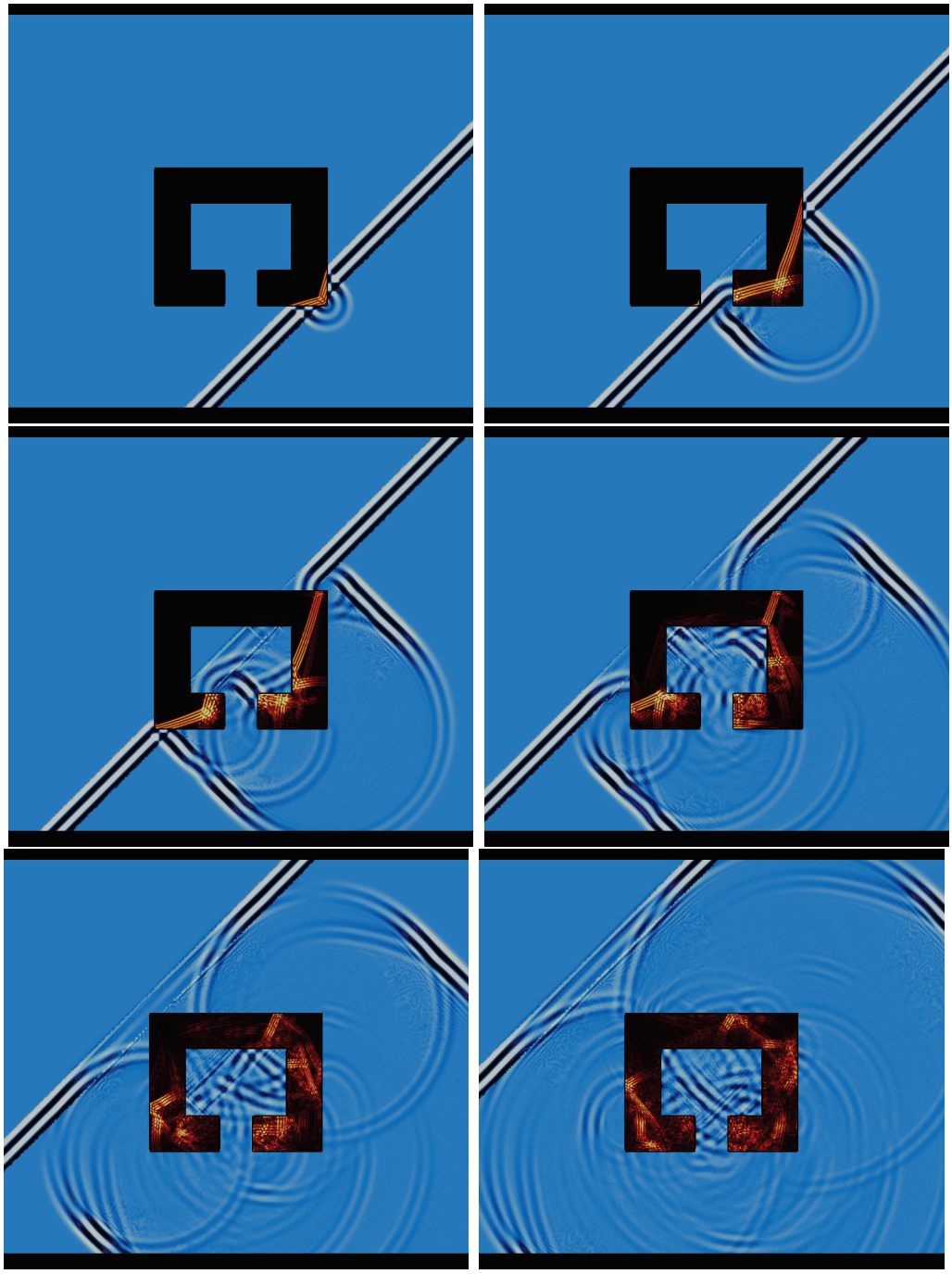

Figure 6.7: Snapshots of the total acoustic field at times $t = 0.3, 0.6, 0.9, 1.2, 1.5, 1.8$. The interior domain shows the norm of the elastic displacement.

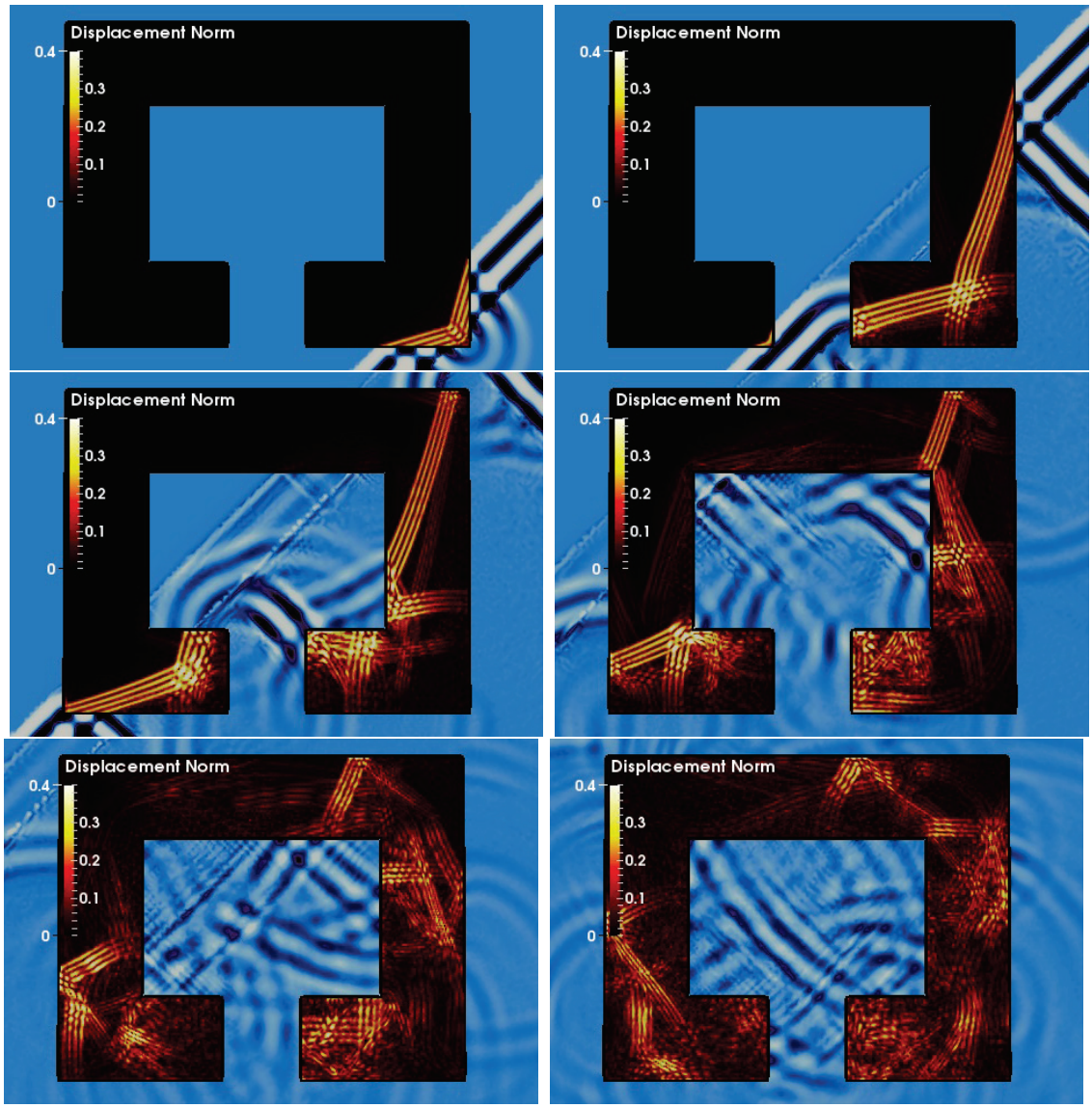

Figure 6.8: Close up of the norm of the elastic displacement for times $t = 0.3, 0.6, 0.9, 1.2, 1.5, 1.8$. Black represents no displacement.

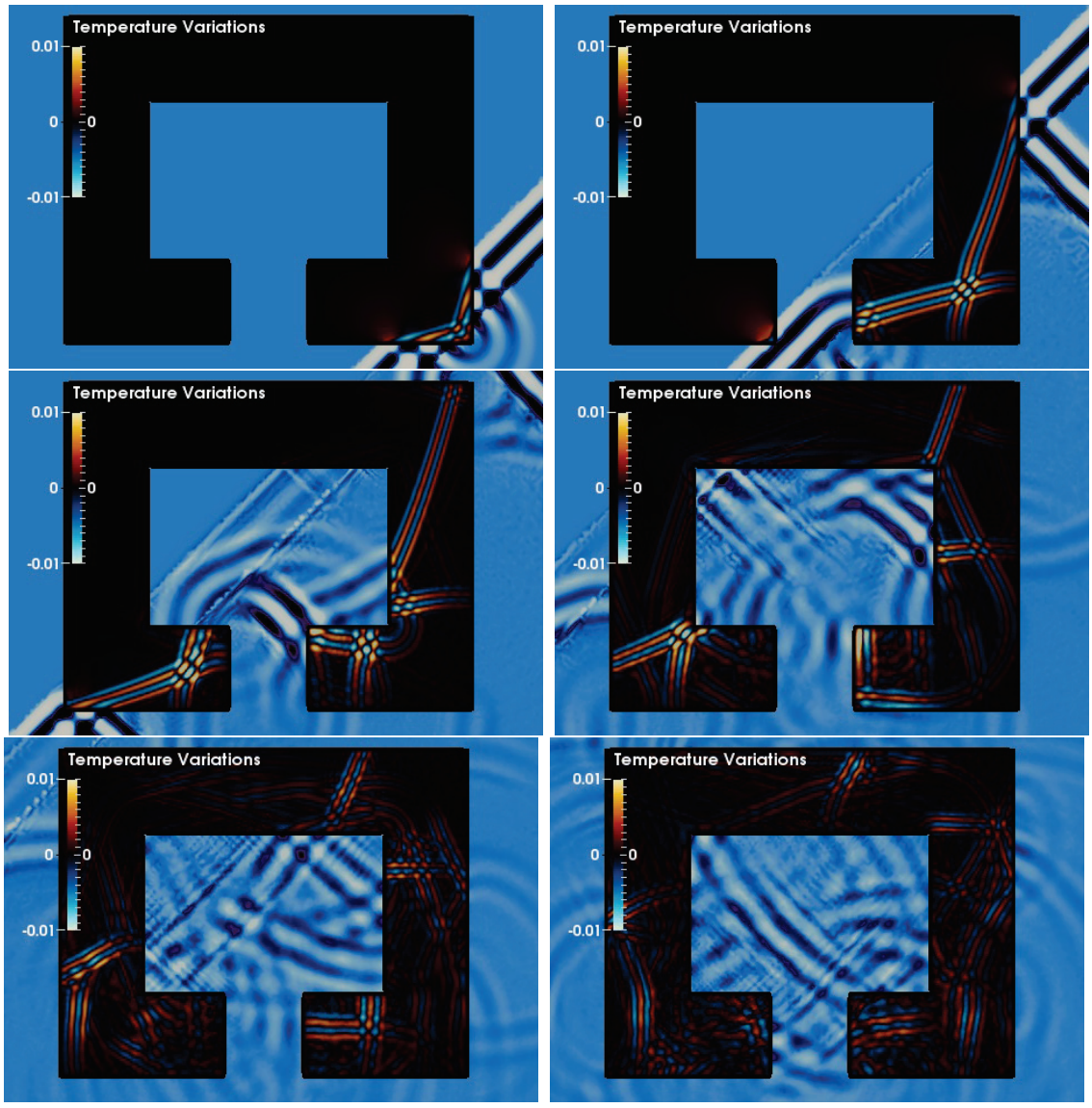

Figure 6.9: Close up of the norm of the temperature variations with respect to the reference configuration for times $t = 0.3, 0.6, 0.9, 1.2, 1.5, 1.8$. Black represents zero, whereas shades of red and blue represent positive and negative variations respectively.

Chapter 7

CONCLUSIONS

We have presented an array of formulations to describe and simulate the transient propagation of elastic waves through media with different elastic properties. In order to deal with homogeneous, inhomogeneous, and unbounded media advantageously, the formulations proposed combine the use of boundary integral equations in the homogeneous regions with that of variational forms in the inhomogeneous parts of the domain. As a result we have analyzed problems involving only boundary integral equations (BIEs) as well those involving combined integro-differential systems. The systems studied range from single hyperbolic equations (as in Chapter 3) from coupled systems of the form hyperbolic-hyperbolic (wave-structure interaction Chapter 4), hyperbolic-hyperbolic-elliptic (scattering by piezoelectric obstacles on Chapter 5) and hyperbolic-hyperbolic-parabolic (when the thermodynamics of the deformation is considered as in Chapter 6).

Following the fundamental works of Bamberger and Ha-Duong [6, 7], and Laliena and Sayas [82], our approach to treat the time dependence of the problems involves the passage through the Laplace domain where the well-posedness of the semidiscrete resolvent problem is established. The resulting estimates can then be used to establish time domain bounds of the fully discretized problem. This novel method of analysis for time domain problems has recently been developed into a unified framework by Francisco-Javier Sayas and thoroughly presented in [116].

Christian Lubich's Convolution quadrature is used all throughout for time discretization. In the current work we have only considered CQ schemes based on second order multistep methods, but a whole wealth different options are available amongst which high order Runge-Kutta methods seem to be the most promising [92, 10, 11]. A

comprehensive, and readable, introduction to the ideas and algorithms behind CQ and the computational implementations used for this work can be found in [60]. Our stance with respect to CQ in this work has been that of a user but the topic is on itself an exciting and active field of research; some of the latest developments include the study of fast and memory efficient algorithms, adaptive and non-uniform time-stepping and the thorough analysis of Runge-Kutta schemes, application to electromagnetic problems, hybrid CQ/Galerkin approaches, etc [87, 9, 88, 24, 124].

For space discretization of the resulting boundary integral equations we have explored techniques from both the Nyström and Galerkin families. On the former side, the thesis studies the discretization of the integral operators associated to the 2-dimensional elastodynamic equation. We proposed an efficient Nyström-like technique yielding third order accuracy by employing a combination of reduced order quadrature (as laid out in [111]) with symmetrization of the companion grids and regularization of the hypersingular operator in the spirit of `deltaBEM` [31]. On the latter, a great deal of this work has explored the discretization of integro-differential equations whose numerical treatment leads to the coupling of Galerkin boundary elements with finite elements.

The analysis and discretization techniques developed here provide a guide to the study of similar problems in multi-physics wave propagation. Many interesting questions remain to be studied in the realm of wave-structure interactions. Our analysis of the acoustic scattering by thermoelastic obstacles remains in progress; the use of a pure BIE approach to deal with homogeneous materials (not included on this work) has been completed [67] but the question is still subject of ongoing research for the general materials considered numerically on the closing chapter. Attempting a similar approach for the study of interactions with poroelastic materials would seem to be natural as well.

Another very interesting path to further develop the current work is the use of alternative analysis tools that sidestep the passage through the Laplace domain. Despite the fact of constituting a very powerful and elegant framework in which time

domain problems of this class can be analyzed with relative ease and simplicity, the journey through the Laplace domain is not a lossless process. The stability bounds and the regularity requirements for problem data obtained with this framework are not sharp. As has been recently shown in [59] for the acoustic wave equation, approaching the PDEs from the abstract point of view of dynamical systems in Banach spaces and applying results from functional calculus and semi-group theory results in sharper stability estimates and reduced regularity requirements for problem data. The application and extension of the techniques developed in that paper to the equations of wave-structure interaction studied in this thesis promises to yield improved results.

Last but not least, the development of `deltaBEM` methods for three dimensional integral equations and their implementation is yet another open problem. The development of an effective symmetrization scheme analogous to the usage of staggered grids in the plane and the analysis of the consistency and accuracy properties of such a scheme remains a challenge, but one well worth tackling. The possibility of attaining increased order of accuracy with the use of lowest order approximants and quadrature rules, and the resulting decrease in the size of linear systems involved in the process would seem to make it a viable approach to 3D problems.

The intellectual journey through each and every subject touched upon this work has been an exciting and instructive personal process, full of discoveries learning experiences. Interesting and challenging problems remain to be addressed in all the subjects touched upon in this work, but hopefully our contribution will constitute a solid starting point for those interested in further developing the results presented in this work. Rather than being a conclusion, I think of this work as the starting point for further mathematical explorations in the years to come.

BIBLIOGRAPHY

[1] R. Adams and J. Fournier. *Sobolev Spaces*. Pure and Applied Mathematics. Elsevier Science, 2003.

[2] H. Allik and T. J. R. Hughes. Finite element method for piezoelectric vibration. *Internat. J. Numer. Methods Engrg.*, 2(2):151–157, 1970.

[3] H. Ammari, H. Kang, and H. Lee. *Layer potential techniques in spectral analysis*, volume 153 of *Mathematical Surveys and Monographs*. American Mathematical Society, Providence, RI, 2009.

[4] D. N. Arnold. A spline-trigonometric Galerkin method and an exponentially convergent boundary integral method. *Math. Comp.*, 41(164):383–397, 1983.

[5] D. N. Arnold and W. L. Wendland. The convergence of spline collocation for strongly elliptic equations on curves. *Numer. Math.*, 47(3):317–341, 1985.

[6] A. Bamberger and T. H. Duong. Formulation variationnelle espace-temps pour le calcul par potentiel retardé de la diffraction d'une onde acoustique. I. *Math. Methods Appl. Sci.*, 8(3):405–435, 1986.

[7] A. Bamberger and T. H. Duong. Formulation variationnelle pour le calcul de la diffraction d'une onde acoustique par une surface rigide. *Math. Methods Appl. Sci.*, 8(4):598–608, 1986.

[8] L. Banjai. Multistep and multistage convolution quadrature for the wave equation: algorithms and experiments. *SIAM J. Sci. Comput.*, 32(5):2964–2994, 2010.

[9] L. Banjai, A. R. Laliena, and F.-J. Sayas. Fully discrete Kirchhoff formulas with CQ-BEM. *IMA J. Numer. Anal.*, 35(2):859–884, 2015.

[10] L. Banjai and C. Lubich. An error analysis of Runge-Kutta convolution quadrature. *BIT*, 51(3):483–496, 2011.

[11] L. Banjai, C. Lubich, and J. M. Melenk. Runge-Kutta convolution quadrature for operators arising in wave propagation. *Numer. Math.*, 119(1):1–20, 2011.

[12] L. Banjai, C. Lubich, and F.-J. Sayas. Stable numerical coupling of exterior and interior problems for the wave equation. *Numer. Math.*, 129(4):611–646, 2015.

[13] L. Banjai and S. Sauter. Rapid solution of the wave equation in unbounded domains. *SIAM J. Numer. Anal.*, 47(1):227–249, 2008/09.

[14] L. Banjai and M. Schanz. Wave propagation problems treated with convolution quadrature and BEM. In *Fast boundary element methods in engineering and industrial applications*, volume 63 of *Lect. Notes Appl. Comput. Mech.*, pages 145–184. Springer, Heidelberg, 2012.

[15] H. Barucq, R. Djellouli, and E. Estecahandy. Efficient DG-like formulation equipped with curved boundary edges for solving elasto-acoustic scattering problems. *Internat. J. Numer. Methods Engrg.*, 98(10):747–780, 2014.

[16] H. Barucq, R. Djellouli, and E. Estecahandy. On the existence and the uniqueness of the solution of a fluid-structure interaction scattering problem. *J. Math. Anal. Appl.*, 412(2):571–588, 2014.

[17] A. Benjeddou. Advances in piezoelectric finite element modeling of adaptive structural elements: a survey. *Computers & Structures*, 76(1–3):347 – 363, 2000.

[18] F. Cakoni. Boundary integral method for thermoelastic screen scattering problem in $\mathbb{R}^3$. *Mathematical Methods in the Applied Sciences*, 23(5):441–466, 2000.

[19] F. Cakoni and G. Dassios. The coated thermoelastic body within a low-frequency elastodynamic field. *Internat. J. Engrg. Sci.*, 36(15):1815–1838, 1998.

[20] F. Cakoni and G. Dassios. The Atkinson-Wilcox theorem in thermoelasticity. *Quart. Appl. Math.*, 57(4):771–795, 1999.

[21] M. P. Calvo, E. Cuesta, and C. Palencia. Runge-Kutta convolution quadrature methods for well-posed equations with memory. *Numer. Math.*, 107(4):589–614, 2007.

[22] R. Celorrio, V. Domínguez, and F.-J. Sayas. Periodic Dirac delta distributions in the boundary element method. *Adv. Comput. Math.*, 17(3):211–236, 2002.

[23] R. Chapko, R. Kress, and L. Mönch. On the numerical solution of a hypersingular integral equation for elastic scattering from a planar crack. *IMA J. Numer. Anal.*, 20(4):601–619, 2000.

[24] Q. Chen, P. Monk, X. Wang, and D. Weile. Analysis of convolution quadrature applied to the time-domain electric field integral equation. *Commun. Comput. Phys.*, 11(2):383–399, 2012.

[25] P. G. Ciarlet. On Korn's inequality. *Chinese Annals of Mathematics, Series B*, 31(5):607–618, 2010.

[26] G. Dassios and V. Kostopoulos. Scattering of elastic waves by a small thermoelastic body. *International Journal of Engineering Science*, 32(10):1593 – 1603, 1994.

[27] L. Demkowicz and J. T. Oden. Application of *hp*-adaptive BE/FE methods to elastic scattering. *Comput. Methods Appl. Mech. Engrg.*, 133(3-4):287–317, 1996.

[28] J.-F. Deü, W. Larbi, and R. Ohayon. Piezoelectric structural acoustic problems: Symmetric variational formulations and finite element results. *Comput. Methods Appl. Mech. Engrg.*, 197(19–20):1715 – 1724, 2008. Computational Methods in Fluid–Structure Interaction.

[29] J.-F. Deü, W. Larbi, and R. Ohayon. Variational formulations of interior structural-acoustic vibration problems. In G. Sandberg and R. Ohayon, editors, *Computational Aspects of Structural Acoustics and Vibration*, volume 505 of *CISM International Centre for Mechanical Sciences*, pages 1–21. Springer Vienna, 2009.

[30] V. Domínguez, S. Lu, and F.-J. Sayas. A fully discrete Calderón calculus for two dimensional time harmonic waves. *Int. J. Numer. Anal. Model.*, 11(2):332–345, 2014.

[31] V. Domínguez, S. L. Lu, and F.-J. Sayas. A Nyström flavored Calderón calculus of order three for two dimensional waves, time-harmonic and transient. *Comput. Math. Appl.*, 67(1):217–236, 2014.

[32] V. Domínguez, S. L. Lu, and F.-J. Sayas. A nyström method for the two dimensional helmholtz hypersingular equation. *Adv. Comput. Math.*, 40(5):1121–1157, 2014.

[33] V. Domínguez, M.-L. Rapún, and F.-J. Sayas. Dirac delta methods for Helmholtz transmission problems. *Adv. Comput. Math.*, 28(2):119–139, 2008.

[34] V. Domínguez, T. Sánchez-Vizuet, and F.-J. Sayas. A fully discrete Calderón calculus for the two-dimensional elastic wave equation. *Comput. Math. Appl.*, 69(7):620–635, 2015.

[35] V. Domínguez and F.-J. Sayas. Full asymptotics of spline Petrov-Galerkin methods for some periodic pseudodifferential equations. *Adv. Comput. Math.*, 14(1):75–101, 2001.

[36] V. Domínguez and F.-J. Sayas. Stability of discrete liftings. *C. R. Math. Acad. Sci. Paris*, 337(12):805–808, 2003.

[37] V. Domínguez and F.-J. Sayas. Some properties of layer potentials and boundary integral operators for the wave equation. *J. Integral Equations Appl.*, 25(2):253–294, 2013.

[38] J.-M.-C. Duhamel. Second mémoire sur les phénomènes thermo-mécaniques. *J. de l'École Polytechnique*, tome 15(cahier 25):pp. 1—-57, 1837.

[39] J. Elschner, G. C. Hsiao, and A. Rathsfeld. An inverse problem for fluid-solid interaction. *Inverse Probl. Imaging*, 2(1):83–119, 2008.

[40] M. Enderlein, A. Ricoeur, and M. Kuna. Finite element techniques for dynamic crack analysis in piezoelectrics. *International Journal of Fracture*, 134(3-4):191–208, 2005.

[41] O. V. Estorff and H. Antes. On FEM-BEM coupling for fluid-structure interaction analyses in the time domain. *Internat. J. Numer. Methods Engrg.*, 31(6):1151–1168, 1991.

[42] S. Falletta, G. Monegato, and L. Scuderi. Space-time BIE methods for non homogeneous exterior wave equation problems. The Dirichlet case. *IMA J. Numer. Anal.*, 32(1):202–226, 2012.

[43] S. Falletta, G. Monegato, and L. Scuderi. A space-time BIE method for wave equation problems. The (2D) Neumann case. *IMA J. Numer. Anal.*, 34(1):390–434, 2014.

[44] X. Feng. Analysis of finite element methods and domain decomposition algorithms for a fluid-solid interaction problem. *SIAM J. Numer. Anal.*, 38(4):1312–1336, 2000.

[45] X. Feng and Z. Xie. A priori error estimates for a coupled finite element method and mixed finite element method for a fluid-solid interaction problem. *IMA J. Numer. Anal.*, 24(4):671–698, 2004.

[46] G. Fichera. Existence theorems in elasticity. In C. Truesdell, editor, *Linear Theories of Elasticity and Thermoelasticity: Linear and Nonlinear Theories of Rods, Plates, and Shells*, pages 347–389. Springer Berlin Heidelberg, Berlin, Heidelberg, 1973.

[47] G. Fichera. Existence theorems in linear and semi-linear elasticity. *ZAMM - Journal of Applied Mathematics and Mechanics / Zeitschrift für Angewandte Mathematik und Mechanik*, 54(12):24–36, 1974.

[48] B. Flemisch, M. Kaltenbacher, and B. I. Wohlmuth. Elasto-acoustic and acoustic-acoustic coupling on non-matching grids. *Internat. J. Numer. Methods Engrg.*, 67(13):1791–1810, 2006.

[49] A. Frangi. and G. Novati. Regularized symmetric Galerkin BIE formulations in the Laplace transform domain for 2D problems. *Computational Mechanics*, 22(1):50–60, 1998.

[50] F. García-Sánchez, C. Zhang, and A. Sáez. 2-D transient dynamic analysis of cracked piezoelectric solids by a time-domain BEM. *Comput. Methods Appl. Mech. Engrg.*, 197(33–40):3108 – 3121, 2008.

[51] G. N. Gatica, A. Márquez, and S. Meddahi. Analysis of the coupling of Lagrange and Arnold-Falk-Winther finite elements for a fluid-solid interaction problem in three dimensions. *SIAM J. Numer. Anal.*, 50(3):1648–1674, 2012.

[52] G. N. Gatica, A. Márquez, and S. Meddahi. Analysis of an augmented fully-mixed finite element method for a three-dimensional fluid-solid interaction problem. *Int. J. Numer. Anal. Model.*, 11(3):624–656, 2014.

[53] L. Gaul, M. Kögl, F. Moser, and M. Schanz. *Boundary Element Methods for the Dynamic Analysis of Elastic, Viscoelastic, and Piezoelectric Solids*, chapter 25, pages 751–769. John Wiley & Sons, Ltd, 2004.

[54] W. Hackbusch, W. Kress, and S. A. Sauter. Sparse convolution quadrature for time domain boundary integral formulations of the wave equation. *IMA J. Numer. Anal.*, 29(1):158–179, 2009.

[55] D. Hahn and M. Ozisik. *Heat Conduction*. Wiley, 2012.

[56] E. Hairer, C. Lubich, and M. Schlichte. Fast numerical solution of nonlinear Volterra convolution equations. *SIAM J. Sci. Statist. Comput.*, 6(3):532–541, 1985.

[57] M. Hamdi and P. Jean. A mixed functional for the numerical resolution of fluid-structure interaction problems. In G. Comte-Bellot and J. E. F. Williams, editors, *Aero- and Hydro-Acoustics*, IUTAM Symposia, pages 269–276. Springer Berlin Heidelberg, 1986.

[58] D. Haroske and H. Triebel. *Distributions, Sobolev Spaces, Elliptic Equations*. EMS Monographs in Mathematics. European Mathematical Society, 2008.

[59] M. Hassell, T. Qiu, T. Sánchez-Vizuet, and F.-J. Sayas. A new and improved analysis of the time domain boundary integral operators for acoustics. *Submitted*, 2015.

[60] M. Hassell and F.-J. Sayas. *Convolution Quadrature for Wave Simulations*. Springer SEMA-SIMAI Lecture Notes in Mathematics, 2016. To appear.

[61] M. Hassell and F.-J. Sayas. A fully discrete BEM-FEM scheme for transient acoustic waves. *Accepted for publication in Comput. Methods Appl. Mech. Engrg.*, 2016.

[62] R. Hetnarski and M. Eslami. *Thermal Stresses – Advanced Theory and Applications*. Solid Mechanics and Its Applications. Springer Netherlands, 2008.

[63] G. C. Hsiao. On the boundary-field equation methods for fluid-structure interactions. In *Problems and methods in mathematical physics (Chemnitz, 1993)*, volume 134 of *Teubner-Texte Math.*, pages 79–88. Teubner, Stuttgart, 1994.

[64] G. C. Hsiao, R. E. Kleinman, and G. F. Roach. Weak solutions of fluid-solid interaction problems. *Math. Nachr.*, 218:139–163, 2000.

[65] G. C. Hsiao, R. E. Kleinman, and L. S. Schuetz. On variational formulations of boundary value problems for fluid-solid interactions. In *Elastic wave propagation (Galway, 1988)*, volume 35 of *North-Holland Ser. Appl. Math. Mech.*, pages 321–326. North-Holland, Amsterdam, 1989.

[66] G. C. Hsiao, T. Sánchez-Vizuet, and F.-J. Sayas. Boundary and coupled boundary-finite element methods for transient wave-structure interaction. *IMA J. Numer. Anal.*, 2016. doi:10.1093/imanum/drw009.

[67] G. C. Hsiao, T. Sánchez-Vizuet, F.-J. Sayas, and R. Weinacht. A time-depended wave-thermoeastic solid interaction. *In preparation*, 2016.

[68] G. C. Hsiao, F.-J. Sayas, and R. J. Weinacht. Time-dependent fluid-structure interaction. *Math. Method. Appl. Sci.*, 2015.

[69] G. C. Hsiao and W. L. Wendland. *Boundary Integral Equations*. Applied Mathematical Sciences. Springer Berlin Heidelberg, 2008.

[70] F. Ihlenburg. *Finite element analysis of acoustic scattering*, volume 132 of *Applied Mathematical Sciences*. Springer-Verlag, New York, 1998.

[71] S. Imperiale and P. Joly. Mathematical and numerical modelling of piezoelectric sensors. *ESAIM Math. Model. Numer. Anal.*, 46(4):875–909, 2012.

[72] M. Jakubowska. Kirchhoff's formula for thermoelastic solid. *J. Therm. Stresses*, 5(2):127–144, 1982.

[73] M. Jakubowska. Kirchhoff's type formula in thermoelasticity with finite wave speeds. *J. Therm. Stresses*, 7(3-4):259–283, 1984.

[74] L. Jentsch and D. Natroshvili. Interaction between thermoelastic and scalar oscillation fields. *Integral Equations Operator Theory*, 28(3):261–288, 1997.

[75] R. Kress. *Linear integral equations*, volume 82 of *Applied Mathematical Sciences*. Springer, New York, third edition, 2014.

[76] V. Kupradze. *Potential Methods in the Theory of Elasticity*. Israel Program for Scientific Translations, 1965.

[77] V. D. Kupradze and T. V. Burchuladze. The dynamical problems of the theory of elasticity and thermoelasticity. *Journal of Soviet Mathematics*, 7(3):415–500, 1977.

[78] M. Kögl and L. Gaul. A boundary element method for transient piezoelectric analysis. *Engineering Analysis with Boundary Elements*, 24(7–8):591 – 598, 2000.

[79] M. Kögl and L. Gaul. Piezoelectric analysis with FEM and BEM. In A. Suleman, editor, *Smart Structures*, volume 429 of *International Centre for Mechanical Sciences*, pages 120–130. Springer Vienna, 2001.

[80] A. Laliena. *Theoretical and algorithmic aspects of the convolution quadrature method applied to scattering of acoustic waves (Spanish)*. PhD thesis, Universidad de Zaragoza, 2011.

[81] A. R. Laliena and F.-J. Sayas. A distributional version of Kirchhoff's formula. *J. Math. Anal. Appl.*, 359(1):197–208, 2009.

[82] A. R. Laliena and F.-J. Sayas. Theoretical aspects of the application of Convolution Quadrature to scattering of acoustic waves. *Numer. Math.*, 112(4):637–678, 2009.

[83] L. Landau, L. E.M., A. Kosevich, and L. Pitaevskiĭ. *Electrodynamics of Continuous Media*, volume 8 of *Course of theoretical physics*. Pergamon, 2nd ed., rev. and enl edition, 1984.

[84] L. Landau, L. E.M., A. Kosevich, and L. Pitaevskiĭ. *Theory of Elasticity*, volume 7 of *Course of theoretical physics*. Butterworth-Heinemann, 1986.

[85] W. H. Lin and A. Raptis. Thermoviscous effects on acoustic scattering by thermoelastic solid cylinders and spheres. *The Journal of the Acoustical Society of America*, 74(5):1542–1554, 1983.

[86] A. A. Lopat'ev. Effect of thermoelastic scattering in a liquid and solid body on the reflection of harmonic waves from a plane boundary of separation. *Soviet Applied Mechanics*, 15(1):79–82, 1979.

[87] M. Lopez-Fernandez and S. Sauter. Generalized convolution quadrature with variable time stepping. *IMA J. Numer. Anal.*, 33(4):1156–1175, Jan 2013.

[88] M. Lopez-Fernandez and S. Sauter. Generalized convolution quadrature with variable time stepping. part ii: Algorithm and numerical results. *Applied Numerical Mathematics*, 94:88 – 105, 2015.

[89] C. Lubich. Convolution quadrature and discretized operational calculus. I. *Numer. Math.*, 52(2):129–145, 1988.

[90] C. Lubich. Convolution quadrature and discretized operational calculus. II. *Numer. Math.*, 52(4):413–425, 1988.

[91] C. Lubich. On the multistep time discretization of linear initial-boundary value problems and their boundary integral equations. *Numer. Math.*, 67(3):365–389, 1994.

[92] C. Lubich and A. Ostermann. Runge-Kutta methods for parabolic equations and convolution quadrature. *Math. Comp.*, 60(201):105–131, 1993.

[93] C. Lubich and R. Schneider. Time discretization of parabolic boundary integral equations. *Numer. Math.*, 63(4):455–481, 1992.

[94] C. J. Luke and P. A. Martin. Fluid-solid interaction: acoustic scattering by a smooth elastic obstacle. *SIAM J. Appl. Math.*, 55(4):904–922, 1995.

[95] L. Malvern. *Introduction to the mechanics of a continuous medium*. Prentice-Hall series in engineering of the physical sciences. Prentice-Hall, 1969.

[96] W. Mansur and D. Soares Jr. Dynamic analysis of fluid-soil-structure interaction problems by the boundary element method. *J. Comput. Phys.*, 219(2):498 – 512, 2006.

[97] A. Márquez, S. Meddahi, and V. Selgas. A new BEM-FEM coupling strategy for two-dimensional fluid-solid interaction problems. *J. Comput. Phys.*, 199(1):205–220, 2004.

[98] J. Marsden and T. Hughes. *Mathematical Foundations of Elasticity*. Prentice-Hall Personal Computing Series. Prentice-Hall, 1983.

[99] G. A. Maugin. *Continuum mechanics through the twentieth century*, volume 196 of *Solid Mechanics and its Applications*. Springer, Dordrecht, 2013. A concise historical perspective.

[100] G. A. Maugin. *Continuum mechanics through the eighteenth and nineteenth centuries*, volume 214 of *Solid Mechanics and its Applications*. Springer, Cham, 2014. Historical perspectives from John Bernoulli (1727) to Ernst Hellinger (1914).

[101] G. A. Maugin. *Continuum mechanics through the ages—from the Renaissance to the twentieth century*, volume 223 of *Solid Mechanics and its Applications*. Springer, Cham, 2016. From hydraulics to plasticity.

[102] W. McLean. *Strongly elliptic systems and boundary integral equations*. Cambridge University Press, Cambridge, 2000.

[103] J.-C. Nédélec. Integral equations with nonintegrable kernels. *Integral Equations Operator Theory*, 5(4):562–572, 1982.

[104] H. Nguyen-Vinh, I. Bakar, M. Msekh, J.-H. Song, J. Muthu, G. Zi, P. Le, S. Bordas, R. Simpson, S. Natarajan, T. Lahmer, and T. Rabczuk. Extended finite element method for dynamic fracture of piezo-electric materials. *Engineering Fracture Mechanics*, 92:19 – 31, 2012.

[105] N. Ortner and P. Wagner. On the fundamental solution of the operator of dynamic linear thermoelasticity. *J. Math. Anal. Appl.*, 170(2):524–550, 1992.

[106] E. Pan. A BEM analysis of fracture mechanics in 2D anisotropic piezoelectric solids. *Engineering Analysis with Boundary Elements*, 23(1):67 – 76, 1999.

[107] Y. Pang, Y.-S. Wang, J.-X. Liu, and D.-N. Fang. Reflection and refraction of plane waves at the interface between piezoelectric and piezomagnetic media. *International Journal of Engineering Science*, 46(11):1098 – 1110, 2008.

[108] A. Pereira and G. Beer. Fluid-structure interaction by a Duhamel-BEM/FEM coupling. In *Recent advances in boundary element methods*, pages 339–354. Springer, New York, 2009.

[109] L. Quade, W. Collatz. Zur interpolationstheorie der reellen periodischen funktionen. *Verl. der Akademie der Wissenschaften*, 49 S, 1938.

[110] T. Sánchez-Vizuet and F.-J. Sayas. Boundary-finite element discretization of time dependent acoustic scattering by elastic obstacles with piezoelectric behavior. *Submitted*, 2016.

[111] J. Saranen and L. Schroderus. Quadrature methods for strongly elliptic equations of negative order on smooth closed curves. *SIAM J. Numer. Anal.*, 30(6):1769–1795, 1993.

[112] J. Saranen and I. H. Sloan. Quadrature methods for logarithmic-kernel integral equations on closed curves. *IMA J. Numer. Anal.*, 12(2):167–187, 1992.

[113] J. Saranen and G. Vainikko. *Periodic Integral and Pseudodifferential Equations with Numerical Approximation*. Springer Monographs in Mathematics. Springer-Verlag, Berlin, 2002.

[114] S. A. Sauter and C. Schwab. *Boundary element methods*, volume 39 of *Springer Series in Computational Mathematics*. Springer-Verlag, Berlin, 2011.

[115] F.-J. Sayas. Energy estimates for Galerkin semidiscretizations of time domain boundary integral equations. *Numer. Math.*, 124(1):121–149, 2013.

[116] F.-J. Sayas. *Retarded potentials and time domain integral equations: a roadmap*, volume 50 of *Computational Mathematics*. Springer, 2016.

[117] A. Schädle, M. López-Fernández, and C. Lubich. Fast and oblivious convolution quadrature. *SIAM J. Sci. Comput.*, 28(2):421–438 (electronic), 2006.

[118] M. Schanz, T. Rüberg, and L. Kielhorn. Time domain BEM: numerical aspects of collocation and Galerkin formulations. In *Recent advances in boundary element methods*, pages 415–432. Springer, New York, 2009.

[119] I. H. Sloan and B. J. Burn. An unconventional quadrature method for logarithmic-kernel integral equations on closed curves. *J. Integral Equations Appl.*, 4(1):117–151, 1992.

[120] D. Soares Jr. Coupled numerical methods to analyze interacting acoustic-dynamic models by multidomain decomposition techniques. *Math. Probl. Eng.*, 2011(4):1–28, 2011.

[121] H. F. Tiersten. *Linear piezoelectric plate vibrations*. Springer, 1969.

[122] T. Valent. *Boundary value problems of finite elasticity: local theorems on existence, uniqueness, and analytic dependence on data*. Springer tracts in natural philosophy. Springer-Verlag, 1988.

[123] P. Wagner. Fundamental matrix of the system of dynamic linear thermoelasticity. *J. Therm. Stresses*, 17(4):592–565, 1994.

[124] D. S. Weile. Mitigating the dispersion of convolution quadrature approaches to the solution of the time domain integral equations of electromagnetics. In *2014 IEEE Antennas and Propagation Society International Symposium (APSURSI)*. Institute of Electrical & Electronics Engineers (IEEE), jul 2014.

[125] X. Yuan and Z. Zhu. Reflection and refraction of plane waves at interface between two piezoelectric media. *Acta Mechanica*, 223(12):2509–2521, 2012.

[126] P. Zhao, T. Qin, and L. Zhang. A regularized time-domain BIEM for transient elastodynamic crack analysis in piezoelectric solids. *Engineering Analysis with Boundary Elements*, 56:145 – 153, 2015.

Appendix A

VECTOR-VALUED CAUSAL DISTRIBUTIONS AND THEIR LAPLACE TRANSFORMS

The equations we have considered throughout this work should be understood in the sense of vector-valued causal distributions. We briefly define them and their Laplace transform in what follows and give a brief summary of the main results used throughout the text. Further details can be found in [80, 116].

A.1 Causal Tempered Distributions

Let X be a Banach space, $\mathcal{P}$ the space of polynomials with complex coefficients and $\mathcal{S}(\mathbb{R})$ the Schwartz class of rapidly decreasing functions

$$\mathcal{S}(\mathbb{R}) := \left\{\varphi \in \mathcal{C}^\infty(\mathbb{R}) : p\,\varphi^{(q)} \in L^\infty(\mathbb{R})\ \forall\, q \geq 0 \ \text{ and } p \in \mathcal{P}\right\}.$$

When endowed with an appropriate metric, $\mathcal{S}(\mathbb{R})$ is known to be a Fréchet space. If f is a continuous linear map $f : \mathcal{S}(\mathbb{R}) \longrightarrow X$ with the property

$$\langle f, \varphi\rangle = 0 \qquad \forall \varphi \in \mathcal{S}(\mathbb{R}) \text{ such that } \mathit{supp}\,\varphi \subset (-\infty, 0]$$

we will call f a *causal tempered distribution* with values in X and for brevity will write simply $f \in \mathrm{CT}(X)$. Within this context, time differentiation is defined by transposition. Given $f \in \mathrm{CT}(X)$ we define for every $\varphi \in \mathcal{S}(\mathbb{R})$

$$\langle \tfrac{d}{dt} f, \varphi\rangle := -\langle f, \tfrac{d}{dt}\ \varphi\rangle \in \mathrm{CT}(X).$$

Hence, time differentiation maps $\mathrm{CT}(X)$ continuously into itself. The composition of vector-valued causal tempered distributions with steady-state operators can also be

defined in a natural way. Let X and Y be Banach spaces and $f \in \mathrm{CT}(X)$, then for a bounded linear operator $D : X \longrightarrow Y$ we define the distribution $Df \in \mathrm{CT}(Y)$ by

$$\langle Df, \varphi \rangle := D\langle f, \varphi \rangle \qquad \forall \varphi \in \mathcal{S}(\mathbb{R}).$$

Therefore by letting X and Y be given Sobolev spaces and D a steady state partial differential operator the previous definitions give a precise meaning to the distributional version of a time dependent PDE.

A.2 Laplace Transform

For distributions $f \in \mathrm{CT}(X)$ and complex numbers s in the positive half plane

$$\mathbb{C}_+ := \{s \in \mathbb{C} : \mathrm{Re}\, s > 0\}$$

it is possible to define the Laplace transform as the function

$$s \longmapsto \mathcal{L}\{f\}(s) = \mathrm{F}(s) := \langle f, \exp(-s\,\cdot)\rangle.$$

Note that, despite the fact that $t \mapsto \exp(-st)$ does not belong to the Schwartz class, the causality of f ensures that the above duality product is well defined and the definition still makes sense. Alternatively, the definition can be done by a density argument as

$$\mathrm{F}(s) := \lim_{n\to\infty} \langle f, h_n \exp(-s\,\cdot)\rangle,$$

where $\{h_n\}_{n\geq 1}$ is a sequence of smooth approximations to the Heaviside function.

For distributions in $\mathrm{CT}(X)$ and steady state operators $A \in \mathcal{B}(X, Y)$, the following three key properties are easy to verify:

1. $\mathcal{L}\left\{\frac{d}{dt} f\right\} = s\,\mathrm{F}(s)$.
2. If $f \in \mathrm{CT}(X)$ is such that $\mathrm{F}(s) = 0\ \forall\, s \in \mathbb{C}_+$ then $f \equiv 0$.
3. $\mathcal{L}\{Af\}(s) = A\mathrm{F}(s)$.

A.3 Inverse Laplace Transform

Let $\mu \in \mathbb{R}$ and X be a Banach space. We say that an analytic function $F : \mathbb{C}_+ \longrightarrow X$ belongs to the class of symbols $\mathcal{A}(\mu, X)$ if it satisfies

$$\|\mathrm{F}(s)\| \leq C_{\mathrm{F}}(\operatorname{Re} s)|s|^{\mu}$$

for some $\mu \in \mathbb{R}$ and some non-increasing function $C_{\mathrm{F}} : \mathbb{R} \longrightarrow \mathbb{R}$ such that

$$C_{\mathrm{F}}(\sigma) \leq \frac{C}{\sigma^m}, \quad \forall\, \sigma \in (0, 1], \tag{A.1}$$

for some $C > 0$. We will define the $\mathrm{TD}(X)$ as the set of all $f \in \mathrm{CT}(X)$ such that F satisfies the above conditions for some μ and C_{F}. In particular, if $\mathrm{F} \in \mathcal{A}(\mu, X)$ for some $\mu < -1$ then *Mellin's strong inversion formula* can be used to define the inverse Laplace transform of F

$$f(t) := \frac{1}{2\pi i} \int_{\sigma - i\infty}^{\sigma + i\infty} e^{st} \mathrm{F}(s)\, ds.$$

It is possible to show [59, Theorem 2.2] that the operators of the Calderón projector for the Laplace resolvent equation satisfy

$$\begin{aligned}
\mathrm{S} &\in \mathcal{A}(1, \mathcal{B}(H^{-1/2}(\Gamma), H^1(\mathbb{R}^d))), & \mathrm{D} &\in \mathcal{A}(3/2, \mathcal{B}(H^{1/2}(\Gamma), H^1(\mathbb{R}^d \setminus \Gamma))),\\
\mathrm{V} &\in \mathcal{A}(1, \mathcal{B}(H^{-1/2}(\Gamma), H^{1/2}(\Gamma))), & \mathrm{W}^{-1} &\in \mathcal{A}(1, \mathcal{B}(H^{-1/2}(\Gamma), H^{1/2}(\Gamma))),\\
\mathrm{K} &\in \mathcal{A}(3/2, \mathcal{B}(H^{1/2}(\Gamma), H^{1/2}(\Gamma))), & \mathrm{K}^t &\in \mathcal{A}(3/2, \mathcal{B}(H^{-1/2}(\Gamma), H^{-1/2}(\Gamma))),\\
\mathrm{W} &\in \mathcal{A}(2, \mathcal{B}(H^{1/2}(\Gamma), H^{-1/2}(\Gamma))), & \mathrm{V}^{-1} &\in \mathcal{A}(2, \mathcal{B}(H^{1/2}(\Gamma), H^{-1/2}(\Gamma))).
\end{aligned}$$

An analogous result can be proven for the Navier-Lamé operators. The following result [116, Proposition 3.2.2] is used for translating the stability estimates obtained in the Laplace domain into stability and regularity estimates in the time domain

Proposition A.1. *Let* $\mathrm{A} = \mathcal{L}\{a\} \in \mathcal{A}(\mu, \mathcal{B}(X, Y))$ *with* $\mu \geq 0$ *and*

$$k := \lfloor \mu + 2 \rfloor \qquad \epsilon := k - \mu - 1 \in (0, 1].$$

Let $g \in \mathcal{C}^{k-1}(\mathbb{R}, X)$ *be a causal function such that* $g^{(k)} \in L^1(\mathbb{R}, X)$. *Then* $a * g \in \mathcal{C}(\mathbb{R}, Y)$ *is causal and*

$$\|(a * g)(t)\| \leq 2^{\mu} C_{\epsilon}(t) C_A(t^{-1}) \int_0^1 \|\mathcal{P}_k g(\tau)\|\, d\tau,$$

where C_A is the bound of the form (A.1) *associated to* A,

$$C_\epsilon(t) := \frac{1+\epsilon}{\pi\epsilon}\frac{t^\epsilon}{(1+t)^\epsilon}, \qquad \textit{and} \qquad \mathcal{P}_k g(t) := \sum_{\ell=0}^{k} \binom{k}{\ell} g^{(\ell)}(t).$$

Appendix B

CONVOLUTION QUADRATURE

B.1 Some Background

Convolution Quadrature (CQ) was developed by Christian Lubich in the late 80's and early 90's [56, 89, 90, 91] as a way to approximate causal convolutions and convolution equations based on the knowledge of the Laplace transform of the convolution kernel and time domain data.

Since then it has been enriched greatly by works like [117, 21, 54, 8, 10, 11, 12] and –due to its stability properties, the advantage of requiring only Laplace domain fundamental solutions and the possibility to take damping effects into account with relative ease – has become one of the preferred tools for the numerical analysis and simulation of evolutionary problems arising from wave propagation and diffraction. A thorough review of results and properties of CQ applied to boundary integral equations can be found in [14], while [60] gives a detailed explanation of the computational and algorithmic subtleties involved in its implementation.

B.2 CQ as a Black Box

For the purposes of exposition we can present CQ as two blackboxes. In the forward CQ, a sequence of vectors $\boldsymbol{\beta}^n \in \mathbb{R}^{n_1}$ (for $n \geq 0$) is input, a $\mathbb{C}^{n_2 \times n_1}$-valued transfer operator $\mathrm{A}(s)$ is given, and another sequence of vectors $\boldsymbol{\delta}^n \in \mathbb{R}^{n_2}$ is output. We will denote this as

$$\boldsymbol{\delta}^n = \mathrm{CQfwd}(\mathrm{A}(s), \boldsymbol{\beta}^n),$$

with the implicit understanding that a particular time value $\boldsymbol{\delta}^n$ depends on the past of the input $\boldsymbol{\beta}^m$ for $m \leq n$. We note that even if CQ can be understood and implemented

as a time-stepping (marching-on-in-time) method, these small experiments are carried out using an all-times-at-once strategy [14] involving evaluations of the transfer function $\mathrm{A}(s)$ at many different complex frequencies. The second kind of CQ blackbox takes input $\boldsymbol{\beta}^n \in \mathbb{R}^r$, uses a invertible transfer operator $\mathrm{A}(s) \in \mathbb{C}^{r\times r}$, and outputs another sequence $\boldsymbol{\delta}^n \in \mathbb{R}^r$. This convolution equation process is equivalent to the forward process applied to the inverse transfer function

$$\boldsymbol{\delta}^n = \mathrm{CQeqn}(\mathrm{A}(s), \boldsymbol{\beta}^n) = \mathrm{CQfwd}(\mathrm{A}(s)^{-1}, \boldsymbol{\beta}^n),$$

and can be implemented in different ways, either by solving equations related to $\mathrm{A}(s)$ at many complex frequencies or by repeatedly inverting $\mathrm{A}(c_0)$ for a large positive value c_0 (which corresponds to a highly diffusive equation).

B.3 A Formal Explanation

The following informal discussion is meant just to give an idea of the way in which CQ works and to state the main results used throughout this work. For a rigorous explanation the reader is referred to [60]. For some $\sigma > 0$, and causal functions f, g with enough regularity (see A) we can write

$$(f * g)(t) = \frac{1}{2\pi i}\int_{\sigma-i\infty}^{\sigma+i\infty}\int_0^t F(s)e^{s\tau}g(t-\tau)\,d\tau\,ds = \frac{1}{2\pi i}\int_{\sigma-i\infty}^{\sigma+i\infty} F(s)y(t;s)\,ds, \quad \text{(B.1)}$$

where $y(t;s)$ is the unique solution of

$$\dot{y}(t) - sy(t) = g(t), \quad y(0) = 0. \quad \text{(B.2)}$$

This differential equation can be approximately solved by any ODE-solving procedure using time domain information from g. The numerical solution can then be used to approximate the complex contour integral, therefore, in the heart of every CQ implementation lies an ODE solver which determines its analytic and convergence properties and gives rise to different families of CQ algorithms.

We consider briefly the particular case of multi-step backwards differentiation formulas with constant time-step κ. We will denote by z^n the translation operator

$$z^n y(t) := y(t - n\kappa)$$

and by δ, the characteristic function associated to the multi-step method in question. In this context the approximation to the solution of (B.2) can be written -at least formally- in terms of the time domain data $g(t)$ as

$$y(t_n) \approx \left(\frac{\delta(z)}{\kappa} - s\right)^{-1} g(t_{n-m}).$$

We can then substitute this expression into (B.1) yielding

$$\begin{aligned}(f * g)(t_n) &= \frac{1}{2\pi i}\int_{\sigma-i\infty}^{\sigma+i\infty} \mathrm{F}(s) y(t_n; s)\, ds \\ &\approx \frac{1}{2\pi i}\int_{\sigma-i\infty}^{\sigma+i\infty} \mathrm{F}(s)\left(\frac{\delta(z)}{\kappa} - s\right)^{-1} g(t_{n-m})\, ds \\ &= \mathrm{F}\left(\frac{\delta(z)}{\kappa}\right) g(t_{n-m}) \\ &= \sum_{m=0}^{\infty} \omega_m^{\mathrm{F}}(\kappa) z^m\, g(t_n),\end{aligned}$$

where we have made use of Cauchy's integral representation formula and the fact that F is analytic. Therefore, if the first m coefficients $\omega_i^{\mathrm{F}}(\kappa)$ of the power series expansion of $\mathrm{F}\left(\frac{\delta(z)}{\kappa}\right)$ are known, we can approximate

$$(f * g)(t_n) \approx \sum_{m=0}^{n} \omega_m^{\mathrm{F}}(\kappa) z^m\, g(t_n). \tag{B.3}$$

This can be done using once more the analyticity of F and Cauchy's integral formula since

$$\omega_n^{\mathrm{F}}(\kappa) = \frac{1}{2\pi i}\oint_{\gamma} z^{-n-1}\mathrm{F}(\tfrac{1}{\kappa}\delta(z))\, dz,$$

where γ is a closed curve contained in the region of analiticity of F. This integral can be approximated accurately and efficiently choosing the circle

$$\gamma = \{s \in \mathbb{C} : s = Re^{2\pi i\theta},\ \theta \in [0, 1)\}$$

and exploiting the convergence properties of the trapezoidal rule for periodic functions ($z_n = e^{2\pi i/n}$). The trapezoidal rule approximation of the coefficients is

$$\omega_n^{\mathrm{F}}(\kappa) \approx \frac{R^{-n}}{N+1}\sum_{\ell=0}^{N} z_{N+1}^{n\ell}\mathrm{F}\left(\tfrac{1}{\kappa}\delta(Rz_{N+1}^{-\ell})\right).$$

Finally, the final step on the approximation of $(f * g)(t_n)$ involves evaluating discrete convolution (B.3) which can be done efficiently with using a fast Fourier transform.

B.4 Important Theorems and Convergence Estimates

The following proposition, a simplified version of [116][Proposition 4.5.2, Proposition 4.5.4], guarantees that the BDF apporximations

$$\mathrm{F}_\kappa(s) := \mathrm{F}\left(\frac{\delta(e^{-s\kappa})}{\kappa}\right) \approx \mathrm{F}(s)$$

Is indeed a symbol (and thus it is the Laplace transform of a causal tempered distribution) and also gives the rate of convergence in terms of the rate of the multi step method associated to $\delta(z)$.

Proposition B.1. *For $\mathcal{A}(\mu, X)$ with $\mu \geq 0$, F_κ is a symbol of order μ with bounding function independent of κ and $f_\kappa := \mathcal{L}^{-1}\{\mathrm{F}_\kappa(s)\} \in \mathrm{TD}(X)$. Moreover*

$$\|\mathrm{F}(s) - \mathrm{F}_\kappa(s)\| \leq C(\mathrm{F}, \sigma)\kappa^q |s|^{\mu+q+1} \qquad \forall\, s \in \mathbb{C}_+,$$

where q is the degree of the multistep formula associated with δ and $C(\mathrm{F}, \sigma)$ depends only on C_F (see (A.1)) and on $\sigma := \operatorname{Re} s$.

For the results concerning time domain convergence of the approximate convolution $(f_\kappa * g)(t)$ we have used the following result [116][Proposition 4.6.1] for which we define the following Sobolev spaces in time

$$W^\ell_+(\mathbb{R}, X) := \{g \in \mathcal{C}^{\ell-1}(\mathbb{R}, X) :\ g(t) = 0\ \forall t \leq 0 \ \text{ and } \ g^{(\ell)} \in L^1(\mathbb{R}, X)\}.$$

Proposition B.2 (Uniform convergence with L^1 regularity)**.** *Let $\mathrm{F} \in \mathcal{A}(\mu, \mathcal{B}(X, Y))$ with $\mu \geq 0$ and define $D_\mathrm{F}(\sigma) := C_\mathrm{F}(C\underline{\sigma})$. If $g \in W^\ell_+(\mathbb{R}, X)$ for $\ell > \mu + 1$, then*

$$\|(f * g)(t) - (f_\kappa * g)(t)\| \leq D \times error(\kappa) h(t) \int_0^t \|g^{(\ell)}(\tau)\|\, d\tau,$$

where D depends only on μ, ℓ and the degree of the multi step approximation q used to obtain f_κ,

$$error(\kappa) := \kappa^{(\ell-\mu-1)\frac{q}{q+1}} + \delta_{\ell,\mu+q+2}\kappa^q |\log \kappa| + \kappa^q,$$

$\delta_{i,j}$ here is the Kronecker symbol and

$$h(t) := \begin{cases} t^{\ell-\mu} D_\mathrm{F}(t^{-1}) & t \geq 1 \\ D_\mathrm{F}(1) t^{\ell-\mu-q-1} & t \leq 1 \ \text{ and } \ \ell \geq \mu + q + 1 \\ D_\mathrm{F}(1) & t \geq 1\ \mu + 1 < \ell < \mu + q + 1. \end{cases}$$

Optimal convergence of order q is obtained for $\ell > \mu + q + 2$.

Finally, the key resut that will allow us to carry out all the time domain analysis using CQ based tools –even if our computational implementation involves traditional time stepping for the finite element discretization– is that this split treatment of different parts of a system is equivalent to the application of CQ globally, as long as the time stepping method used for the FEM part coincides with the one giving rise to the CQ algorithm in use.

Proposition B.3. *If the CQ method based on*

$$p(z) := \frac{\alpha(z)}{\beta(z)} = \frac{\alpha_0 + \alpha_1 z + \ldots + \alpha_N z^N}{\beta_0 + \beta_1 z + \ldots + \beta_N z^N}$$

to an equation of the form

$$(\delta_0 \otimes A) * g + (\delta' \otimes B) * g = h,$$

where A and B are bounded operators the result is the same as that obtained when applying the multistep method to the implicit differential equation

$$Ag + \frac{d}{dt}(Bg) = h.$$

Appendix C

RIGHTS & PERMISSIONS

ELSEVIER LICENSE
TERMS AND CONDITIONS

Jun 07, 2016

This Agreement between Tonatiuh Sanchez ("You") and Elsevier ("Elsevier") consists of your license details and the terms and conditions provided by Elsevier and Copyright Clearance Center.

License Number	3883961312643
License date	Jun 07, 2016
Licensed Content Publisher	Elsevier
Licensed Content Publication	Computers & Mathematics with Applications
Licensed Content Title	A fully discrete Calderón calculus for the two-dimensional elastic wave equation
Licensed Content Author	Víctor Domínguez,Tonatiuh Sánchez-Vizuet,Francisco-Javier Sayas
Licensed Content Date	April 2015
Licensed Content Volume Number	69
Licensed Content Issue Number	7
Licensed Content Pages	16
Start Page	620
End Page	635
Type of Use	reuse in a thesis/dissertation
Portion	full article
Format	both print and electronic
Are you the author of this Elsevier article?	Yes
Will you be translating?	No
Order reference number	
Title of your thesis/dissertation	Integral and coupled integral-volume methods for transient problems in wave-structure interaction
Expected completion date	Jul 2016
Estimated size (number of pages)	140
Elsevier VAT number	GB 494 6272 12
Requestor Location	Tonatiuh Sanchez-Vizuet 501 Ewing Hall. Dept. Mathematical Sciences. University of Delaware NEWARK, DE 19716 United States

The contents of Chapter 4 is based on a pre-copyedited, author-produced PDF of an article accepted for publication in IMA Journal of Numerical Analysis following peer review. The version of record *Boundary and Coupled Boundary-Finite Element Methods For Transient Wave-Structure Interaction* by George C. Hsiao, Tonatiuh Sánchez-Vizuet and Francisco-Javier Sayas published by IMA Journal of Numerical Analysis, Oxford University Press (DOI: 10.1093/imanum/drw009) is available online at:

`http://imajna.oxfordjournals.org/content/early/2016/05/09/imanum.drw009.full.pdf+html.`